


AN ABSTRACT OF THE THESIS OF

Carlos Francisco Cruz-Fierro for the degree of Doctor of Philosophy in Chemical Engineering presented on April 27, 2005.

Title: Hydrodynamic Effects of Particle Chaining in Liquid-Solid Magnetofluidized Beds: Theory, Experiment, and Simulation.

Redacted for privacy

Abstract approved: _____

 Goran N. Jovanovic

In a fluidized bed of magnetically susceptible particles, the presence of a magnetic field induce the formation of particle chains due to interparticle magnetic forces. The resulting effect is a change in the overall spatial distribution of the particles, transitioning from a random, isotropic distribution to an ordered, anisotropic distribution. For a magnetic field with the same direction as the superficial fluid velocity, the resulting structures offer less resistance to flow, resulting in a decrease of the effective drag coefficient. Thus the bed is less expanded and have lower voidage in the presence of the magnetic field, at a given fluid superficial velocity.

The effect of particle chaining in the particle drag in a liquid-solid fluidized bed is studied. Experimental data is collected on voidage and pressure drop for particle Reynolds number between 75 and 190, and for particle chain separation force to buoyant weight ratio between 0 and 0.58.

A two-parameter equation for the change in drag coefficient with respect to the hydrodynamic and magnetic operating conditions in the bed is obtained. It provides very good agreement with the experimental data.

A proprietary 3-D simulation code implementing a Computational Fluid Dynamics-Discrete Particle Method is developed and tested under the same conditions as the experiments performed. Without the use of any correction in the drag coefficient, the simulation code overestimates the bed expansion by as much as 70%. This error is reduced to or below 10% when the drag coefficient is corrected using the equation here obtained.

© Copyright by Carlos Francisco Cruz-Fierro
April 27, 2005
All Rights Reserved

Hydrodynamic Effects of Particle Chaining in Liquid-Solid
Magnetofluidized Beds: Theory, Experiment, and Simulation

by
Carlos Francisco Cruz-Fierro

A THESIS

submitted to

Oregon State University

in partial fulfillment of
the requirements for the
degree of

Doctor of Philosophy

Presented April 27, 2005

Commencement June 2005

Doctor of Philosophy thesis of Carlos Francisco Cruz-Fierro presented on April 27, 2005.

APPROVED:

Redacted for privacy

Major Professor, representing Chemical Engineering

Redacted for privacy

Head of the Department of Chemical Engineering

Redacted for privacy

Dean of the Graduate School

I understand that my thesis will become part of the permanent collection of Oregon State University libraries. My signature below authorizes release of my thesis to any reader upon request.

Redacted for privacy

Carlos Francisco Cruz-Fierro, Author

ACKNOWLEDGMENTS

Barclay: I made you some fresh tea for the trip, not that replicated stuff.

Janeway: Thank you, for everything. I wouldn't have been able to do this without you.

-- Star Trek Voyager,
"Endgame"

I wish to express my sincere acknowledgment to the people and organizations that contributed to the successful achievement of this research. The economical support was provided by the Mexican Government through Consejo Nacional de Ciencia y Tecnología (CONACyT), and by the National Aeronautics and Space Administration (NASA Grant NAG9-1472).

I also extend my grateful appreciation to the members of my Graduate Committee. It was Dr. Goran Jovanovic, my major advisor, who brought fascinating new concepts into my attention. From him I learned to see the world from a different perspective, always looking for unexplored possibilities. I thank him for allowing me to "give my mind freedom to roam". Also to Dr. Chih-hung Chang, Dr. Joe McGuire, Dr. Ronald Guenther, and Dr. Richard Peterson, for their endless support and encouragement, and to Dr. Jennifer Field, for kindly agreeing to act as Graduate Council Representative.

Warm thanks to the people in this Chemical Engineering Department; you have become a family away from home. In particular, to Pranav Joshi, for being "a clever man, in any time period". Also to other of my closest friends, Giang Ma, Brian Reed, Kevin Harris, Nick Wannenmacher, Prakash Mugdur,

Elham Aslani, Clayton Jeffryes, and Tavi Cruz-Urbe. To Dawn Beveal, Ann Kimerling, Andy Brickman, and Karen Kelly, for their cheerful support through these years, and to current and former members of my lab group, with whom I shared so many experiences.

Sincerely to my friends, professors, and colleagues in Mexico, for they all have contributed to making me the person I am now. I really wish I could mention all of them, but then I would have to remove a couple of chapters... or an appendix, perhaps.

I want to thank two special people whom I never met: Carl Sagan and Gene Roddenberry. It was through Sagan's television series *Cosmos*, that my childhood imagination took a leap to the stars. Something still stirs inside me when I hear that "the cosmos is all that is, or ever was, or ever will be". And Roddenberry's vision of the future of humanity, with the wonderful *Star Trek* characters that he and his successors created, have left an indelible mark in my personality. I aspire to be the change I want to see in the world.

From the depths of my self, I thank my mother. Not only do I owe her my life, as she reminds me from time to time, but the very essence of my human soul. And to my family, who supported and nourished my desire to learn.

And thanks to God, whatever He might be. I find it conceivable that the grandiosity of the universe and its exquisite underlying order come from something beyond our limited understanding. The pursuit of truth, whether scientific, historic, or personal, brings us closer to understanding His order of the universe.

TABLE OF CONTENTS

	<u>Page</u>
Chapter 1 Introduction	1
1.1 Fluidization	1
1.2 Magnetofluidization.....	2
1.3 Computer simulation of fluidized beds.....	5
1.4 Thesis rationale.....	8
1.4.1 Hypothesis.....	8
1.4.2 Objectives	9
Chapter 2 Theoretical background.....	11
2.1 Governing equations of the continuous phase	11
2.1.1 Mass conservation equation	11
2.1.2 Momentum conservation equation	12
2.2 Governing equations of the discrete phase	14
2.2.1 Equations of motion	14
2.2.2 Body forces	15
2.2.3 Drag force	15
2.2.4 Lift forces	20
2.2.5 Viscous torque on particle.....	22
2.2.6 Other fluid-particle interaction forces.....	23
2.2.7 Collision forces.....	24
2.2.8 Interparticle magnetic force	28
2.3 Explanatory dimensionless numbers	33

TABLE OF CONTENTS (Continued)

	<u>Page</u>
Chapter 3 Experimental methodology	38
3.1 Fluidized bed system	38
3.1.1 Bed design	38
3.1.2 Flow system	42
3.2 Magnetic field	45
3.3 Pressure measurement	47
3.3.1 Probe design.....	47
3.3.2 Data acquisition system	49
3.3.3 Probe calibration	50
3.4 Fluidized media	51
3.4.1 Production	52
3.4.2 Characterization	52
Chapter 4 Numerical simulation	56
4.1 Overview of strategy.....	56
4.2 Continuous phase	59
4.2.1 Computational domain.....	60
4.2.2 The SIMPLE algorithm	62
4.2.3 Discretization of the x -momentum equation	63
4.2.4 Discretization of the y -momentum equation.....	67
4.2.5 Discretization of the z -momentum equation	70
4.2.6 Pressure correction	93
4.3 Particle phase	79
4.3.1 Selection of the time step	79
4.3.2 Integration of equations of motion	80

TABLE OF CONTENTS (Continued)

	<u>Page</u>
Chapter 5 Results and analysis	82
5.1 Pressure drop measurements	82
5.2 Model selection	89
5.3 Comparison between model and experimental data.....	93
Chapter 6 Conclusions and recommendations.....	101
6.1 Conclusions.....	101
6.2 Future work	102
References	104
Appendices	107

LIST OF FIGURES

<u>Figure</u>	<u>Page</u>
1.1 Chain formation in a magnetically stabilized fluidized bed.	3
1.2 Difference in flow pattern through random and structured fluidized bed	4
1.3 Three levels of detail in simulation of particulate-fluid systems	7
2.1 Drag coefficient for a single spherical particle	19
2.2 The exponent β of the voidage function	20
2.3 Soft sphere model for particle collisions.....	25
2.4 Attractive and repulsive limits of the interparticle magnetic force	28
2.5 Components of the interparticle magnetic force	29
3.1 Schematic of the experimental apparatus.	39
3.2 Experimental apparatus	40
3.3 Fluidized bed.....	40
3.4 Close up of the calming zones and distributor plate.....	41
3.5 Overflow and recycle	42
3.6 Close up of the flow meters.....	43
3.7 Calibration of the 10 LPM flow meter	43
3.8 Magnetic field along the centerline of the coil	45
3.9 Close up of the pressure transducer	47

LIST OF FIGURES (Continued)

<u>Figure</u>	<u>Page</u>
3.10 Close up of the mounted pressure probe	48
3.11 Visual Designer diagram for pressure data acquisition	49
3.12 Pressure probe calibration data	51
3.13 Sample of the alginate beads used as fluidized media.....	53
4.1 Particle-X fluidization simulation code, general flowchart	57
4.2 Computational domain for momentum transport	61
4.3 Staggered cells for momentum transport and their relationship to the pressure correction cell.....	62
4.4 Control volume for x -momentum discretization	65
4.5 Control volume for y -momentum discretization	68
4.6 Control volume for z -momentum discretization.....	71
4.7 Control volume for pressure correction.....	74
4.8 Momentum balance for pressure correction	75
5.1 Dynamic pressure data for $u_0 = 0.0287$ m/s and $B_0 = 0$	83
5.2 Dynamic pressure data for $u_0 = 0.0287$ m/s and $B_0 = 15.3$ mT	83
5.3 Dynamic pressure data for $u_0 = 0.0287$ m/s and $B_0 = 0$	85
5.4 Dynamic pressure data for $u_0 = 0.0287$ m/s and $B_0 = 15.3$ mT	85

LIST OF FIGURES (Continued)

<u>Figure</u>		<u>Page</u>
5.5	Matrix of scatterplots for preliminary exploratory data analysis	89
5.6	Matrix of scatterplots, transformed variables.....	90
5.7	Experimentally determined drag correction factor and model fit for 4 LPM runs	94
5.8	Experimentally determined drag correction factor and model fit for 5 LPM runs	94
5.9	Experimentally determined drag correction factor and model fit for 6 LPM runs	95
5.10	Experimentally determined drag correction factor and model fit for 7 LPM runs	95
5.11	Experimentally determined drag correction factor and model fit for 8 LPM runs	96
5.12	Experimentally determined drag correction factor and model fit for 9 LPM runs	96
5.13	Experimentally determined drag correction factor and model fit for 10 LPM runs	97
5.14	Experimentally determined drag correction factor and model fit for 14 LPM runs	97
5.15	Agreement between experimental and predicted values of the drag correction factor	98
5.16	Error in bed height as estimated by simulation.....	99

LIST OF TABLES

<u>Table</u>	<u>Page</u>
2.1 Correlations for drag coefficient of single sphere.....	17
2.2 Physical quantities for dimensional analysis	34
3.1 Flow rates used in this study	44
3.2 Magnetic fields used in this study	46
3.3 Composition of the fluidized media	52
4.1 Coefficients of the discretized x-momentum equation.....	66
4.2 Coefficients of the discretized y-momentum equation.....	69
4.3 Coefficients of the discretized z-momentum equation	72
4.4 Coefficients of the discretized pressure correction equation	78
5.1 Experimental estimates of voidage and drag reduction factor	87
5.2 Coefficients of multiple linear regression model.....	91
5.3 Coefficients of multiple linear regression model, simplified model	92
5.4 Coefficients of non-linear regression model	93

LIST OF APPENDICES

<u>Appendix</u>	<u>Page</u>
A	Additional equipment specifications.....108
B	Notes on Particle-X code114
B.1	Discretization of the momentum equations.....114
B.2	Particle-X main program119
B.3	Particle-X global variables126
B.4	Sample input file132
B.5	Sample timeline file134
B.6	Dynamic behavior of the program.....135
C	Notes on Bolitas 2 visualization software142
C.1	Overview142
C.2	List of defined variable identifiers145
D	Additional experimental data148
E	Particle radial distribution analysis177
F	Material Safety Data Sheets.....181
F.1	Sodium Alginate.....181
F.2	Calcium Chloride185
F.3	Ferrite.....189
G	Biographical note.....195

Companion CD with Particle X source code

LIST OF APPENDIX FIGURES

<u>Figure</u>	<u>Page</u>
A.1 Front/back piece of fluidized bed	109
A.2 Side piece of fluidized bed.....	110
A.3 Bottom piece of fluidized bed	111
A.4 Pre-distributor plate and distributor plate	111
A.5 Front/back piece for overflow box.....	112
A.6 Bottom piece for overflow box.....	112
A.7 Front/back piece for overflow box.....	113
A.8 Mounting plate for pressure transducer	113
B.1 Dynamic comparison between experiment and simulation, $t = 0$ s.....	136
B.2 Dynamic comparison between experiment and simulation, $t = 1$ s.....	137
B.3 Dynamic comparison between experiment and simulation, $t = 2$ s.....	137
B.4 Dynamic comparison between experiment and simulation, $t = 3$ s.....	138
B.5 Dynamic comparison between experiment and simulation, $t = 4$ s.....	138
B.6 Dynamic comparison between experiment and simulation, $t = 5$ s.....	139
B.7 Dynamic comparison between experiment and simulation, $t = 6$ s.....	139
B.8 Dynamic comparison between experiment and simulation, $t = 7$ s.....	140

LIST OF APPENDIX FIGURES (Continued)

<u>Figure</u>	<u>Page</u>
B.9 Dynamic comparison between experiment and simulation, $t = 8$ s.....	140
B.10 Dynamic comparison between experiment and simulation, $t = 9$ s.....	141
B.11 Dynamic comparison between experiment and simulation, $t = 10$ s.....	141
C.1 Representative samples of Bolitas output	144
D.1 Dynamic pressure data for $u_0 = 0.0134$ m/s and $B_0 = 0$	148
D.2 Dynamic pressure data for $u_0 = 0.0134$ m/s and $B_0 = 1.28$ mT	148
D.3 Dynamic pressure data for $u_0 = 0.0134$ m/s and $B_0 = 2.56$ mT	149
D.4 Dynamic pressure data for $u_0 = 0.0134$ m/s and $B_0 = 5.11$ mT	149
D.5 Dynamic pressure data for $u_0 = 0.0134$ m/s and $B_0 = 7.67$ mT	150
D.6 Dynamic pressure data for $u_0 = 0.0134$ m/s and $B_0 = 10.2$ mT	150
D.7 Dynamic pressure data for $u_0 = 0.0134$ m/s and $B_0 = 15.3$ mT	151
D.8 Dynamic pressure data for $u_0 = 0.0170$ m/s and $B_0 = 0$	151
D.9 Dynamic pressure data for $u_0 = 0.0170$ m/s and $B_0 = 1.28$ mT	152

LIST OF APPENDIX FIGURES (Continued)

<u>Figure</u>	<u>Page</u>
D.10 Dynamic pressure data for $u_0 = 0.0170$ m/s and $B_0 = 2.56$ mT	152
D.11 Dynamic pressure data for $u_0 = 0.0170$ m/s and $B_0 = 5.11$ mT	153
D.12 Dynamic pressure data for $u_0 = 0.0170$ m/s and $B_0 = 7.67$ mT	153
D.13 Dynamic pressure data for $u_0 = 0.0170$ m/s and $B_0 = 10.2$ mT	154
D.14 Dynamic pressure data for $u_0 = 0.0170$ m/s and $B_0 = 15.3$ mT	154
D.15 Dynamic pressure data for $u_0 = 0.0208$ m/s and $B_0 = 0$	155
D.16 Dynamic pressure data for $u_0 = 0.0208$ m/s and $B_0 = 1.28$ mT	155
D.17 Dynamic pressure data for $u_0 = 0.0208$ m/s and $B_0 = 2.56$ mT	156
D.18 Dynamic pressure data for $u_0 = 0.0208$ m/s and $B_0 = 5.11$ mT	156
D.19 Dynamic pressure data for $u_0 = 0.0208$ m/s and $B_0 = 7.67$ mT	157
D.20 Dynamic pressure data for $u_0 = 0.0208$ m/s and $B_0 = 10.2$ mT	157
D.21 Dynamic pressure data for $u_0 = 0.0208$ m/s and $B_0 = 15.3$ mT	158
D.22 Dynamic pressure data for $u_0 = 0.0247$ m/s and $B_0 = 0$	158

LIST OF APPENDIX FIGURES (Continued)

<u>Figure</u>	<u>Page</u>
D.23 Dynamic pressure data for $u_0 = 0.0247$ m/s and $B_0 = 1.28$ mT	159
D.24 Dynamic pressure data for $u_0 = 0.0247$ m/s and $B_0 = 2.56$ mT	159
D.25 Dynamic pressure data for $u_0 = 0.0247$ m/s and $B_0 = 5.11$ mT	160
D.26 Dynamic pressure data for $u_0 = 0.0247$ m/s and $B_0 = 7.67$ mT	160
D.27 Dynamic pressure data for $u_0 = 0.0247$ m/s and $B_0 = 10.2$ mT	161
D.28 Dynamic pressure data for $u_0 = 0.0247$ m/s and $B_0 = 15.3$ mT	161
D.29 Dynamic pressure data for $u_0 = 0.0287$ m/s and $B_0 = 0$	162
D.30 Dynamic pressure data for $u_0 = 0.0287$ m/s and $B_0 = 1.28$ mT	162
D.31 Dynamic pressure data for $u_0 = 0.0287$ m/s and $B_0 = 2.56$ mT	163
D.32 Dynamic pressure data for $u_0 = 0.0287$ m/s and $B_0 = 5.11$ mT	163
D.33 Dynamic pressure data for $u_0 = 0.0287$ m/s and $B_0 = 7.67$ mT	164
D.34 Dynamic pressure data for $u_0 = 0.0287$ m/s and $B_0 = 10.2$ mT	164
D.35 Dynamic pressure data for $u_0 = 0.0287$ m/s and $B_0 = 15.3$ mT	165

LIST OF APPENDIX FIGURES (Continued)

<u>Figure</u>	<u>Page</u>
D.36 Dynamic pressure data for $u_0 = 0.0328$ m/s and $B_0 = 0$	165
D.37 Dynamic pressure data for $u_0 = 0.0328$ m/s and $B_0 = 1.28$ mT	166
D.38 Dynamic pressure data for $u_0 = 0.0328$ m/s and $B_0 = 2.56$ mT	166
D.39 Dynamic pressure data for $u_0 = 0.0328$ m/s and $B_0 = 5.11$ mT	167
D.40 Dynamic pressure data for $u_0 = 0.0328$ m/s and $B_0 = 7.67$ mT	167
D.41 Dynamic pressure data for $u_0 = 0.0328$ m/s and $B_0 = 10.2$ mT	168
D.42 Dynamic pressure data for $u_0 = 0.0328$ m/s and $B_0 = 15.3$ mT	168
D.43 Dynamic pressure data for $u_0 = 0.0370$ m/s and $B_0 = 0$	169
D.44 Dynamic pressure data for $u_0 = 0.0370$ m/s and $B_0 = 1.28$ mT	169
D.45 Dynamic pressure data for $u_0 = 0.0370$ m/s and $B_0 = 2.56$ mT	170
D.46 Dynamic pressure data for $u_0 = 0.0370$ m/s and $B_0 = 5.11$ mT	170
D.47 Dynamic pressure data for $u_0 = 0.0370$ m/s and $B_0 = 7.67$ mT	171
D.48 Dynamic pressure data for $u_0 = 0.0370$ m/s and $B_0 = 10.2$ mT	171

LIST OF APPENDIX FIGURES (Continued)

<u>Figure</u>	<u>Page</u>
D.49 Dynamic pressure data for $u_0 = 0.0370$ m/s and $B_0 = 15.3$ mT	172
D.50 Dynamic pressure data for $u_0 = 0.0482$ m/s and $B_0 = 0$	172
D.51 Dynamic pressure data for $u_0 = 0.0482$ m/s and $B_0 = 1.28$ mT	173
D.52 Dynamic pressure data for $u_0 = 0.0482$ m/s and $B_0 = 2.56$ mT	173
D.53 Dynamic pressure data for $u_0 = 0.0482$ m/s and $B_0 = 5.11$ mT	174
D.54 Dynamic pressure data for $u_0 = 0.0482$ m/s and $B_0 = 7.67$ mT	174
D.55 Dynamic pressure data for $u_0 = 0.0482$ m/s and $B_0 = 10.2$ mT	175
D.56 Dynamic pressure data for $u_0 = 0.0482$ m/s and $B_0 = 15.3$ mT	175
E.1 Construction of a radial distribution map	178
E.2 Sample radial distribution maps from 8 LPM simulation cases	179

NOTATION AND SYMBOLS

Worf: What is a "Q"?

Yar: It's a letter of the alphabet, as far as I know.

— Star Trek The Next Generation,
"All Good Things..."

Unless otherwise specified, vector quantities are denoted by bold typeface or arrow overhead (e.g. \mathbf{B} , $\vec{\omega}$), unit vectors by a hat (e.g. \hat{r}) and tensors by bold block typeface (e.g. \mathbf{T}). Vector components are denoted by subscripts (e.g. \mathbf{u} has components u_x , u_y , and u_z), and the magnitude of a vector is denoted with italic typeface (e.g. $B \equiv |\mathbf{B}|$).

Symbol	Description	Units
A	Characteristic area	$[\text{m}^2]$
\mathbf{B}	Magnetic field	$[\text{T}]$
\mathbf{B}_0	Externally applied magnetic field	$[\text{T}]$
\mathbf{B}_{dip}	Magnetic field of a dipole	$[\text{T}]$
C_D	Drag coefficient	$[-]$
C_L	Lift coefficient	$[-]$
d_p	Particle diameter	$[\text{m}]$
D_h	Hydraulic diameter	$[\text{m}]$
e	Coefficient of restitution	$[-]$

NOTATION AND SYMBOLS (Continued)

Symbol	Description	Units
\mathbf{F}	Force	[N]
\mathbf{F}_B	External magnetic force	[N]
\mathbf{F}_b	Buoyancy force	[N]
\mathbf{F}_c	Collision force	[N]
$\mathbf{F}_{cn,ij}$	Normal force in collision of particles i and j	[N]
$\mathbf{F}_{ct,ij}$	Tangential force in collision of particles i and j	[N]
\mathbf{F}_D	Drag force	[N]
\mathbf{F}_g	Gravitational force	[N]
\mathbf{F}_{IM}	Interparticle magnetic force	[N]
\mathbf{F}_{ML}	Magnus lift force	[N]
$\mathbf{F}_{SL,0}$	Low Re_ω Saffman lift force	[N]
\mathbf{F}_{SL}	Saffman lift force	[N]
\mathbf{F}_{VM}	Virtual mass force	[N]
\mathbf{f}	Volumetric force density	[N/m ³]
\mathbf{g}	Gravitational field	[m/s ²]
\mathbf{H}	Magnetic H-field (magnetic field strength)	[A/m]
\mathbf{H}_{loc}	Local magnetic H-field	[A/m]

NOTATION AND SYMBOLS (Continued)

Symbol	Description	Units
h	Bed height	[m]
\mathbf{I}	Unit tensor $\begin{bmatrix} 1 & 0 & 0 \\ 0 & 1 & 0 \\ 0 & 0 & 1 \end{bmatrix}$	[-]
I	Electric current	[A]
I_p	Particle inertia moment	[?]
k_n, k_t	Normal and tangential stiffness	[N/m]
$d\vec{\ell}$	Oriented line differential	[m]
\mathbf{M}	Magnetization	[A/m]
\mathbf{m}	Magnetic dipole moment	[A·m ²]
m_p	Mass of the particle	[kg]
$\hat{\mathbf{n}}$	Normal unit vector	[-]
$\mathcal{O}(\)$	Order of magnitude	[-]
P	Pressure	[Pa]
P^*	Guessed pressure	[Pa]
P'	Pressure correction	[Pa]
P_d	Dynamic pressure	[Pa]
Re	Reynolds number $\frac{\rho \langle u \rangle D_h}{\mu}$	[-]

NOTATION AND SYMBOLS (Continued)

Symbol	Description	Units
Re_p	Particle Reynolds number $\frac{\rho_f d_p \mathbf{u} - \mathbf{v} }{\mu_f}$	[-]
Re_ω	Particle rotation Reynolds number $\frac{\rho_f d_p^2 \bar{\omega}_r }{4\mu_f}$	[-]
\mathcal{S}	Surface	[m ²]
$d\bar{\mathcal{S}}$	Differential oriented surface element	[m ²]
\mathbf{T}	Torque on particle	[N·m]
t	Time	[s]
\mathbf{u}	Fluid velocity	[m/s]
$\langle u \rangle$	Average velocity of laminar flow	[m/s]
\mathbf{V}	Relative velocity for collisions	[m/s]
\mathbf{v}	Particle velocity	[m/s]
\mathcal{V}	Volume	[m ³]
$d\mathcal{V}$	Differential volume element	[m ³]
\mathcal{V}_p	Volume of particle	[m ³]
\mathbf{x}	Particle position vector	[m]
β	Voidage function exponent	[-]
γ	Sliding friction coefficient	[-]
δ_n	Normal elastic overlap in collisions	[m]

NOTATION AND SYMBOLS (Continued)

Symbol	Description	Units
$\bar{\delta}_t$	Tangential elastic displacement in collisions	[m]
ε	Void fraction	[-]
η_n, η_t	Normal and tangential damping coefficients	[kg/s]
λ	Pressure factor for pressure correction	[m/Pa·s]
μ_f	Fluid viscosity	[Pa·s]
ρ_f	Fluid density	[kg/m ³]
ρ_p	Particle density	[kg/m ³]
σ	Surface current density	[A/m]
τ	Viscous stress tensor	[N/m ²]
χ	Magnetic susceptibility	[-]
χ_p	Particle magnetic susceptibility	[-]
χ_e	Particle effective magnetic susceptibility $\frac{\chi_p}{1 + \frac{1}{3}\chi_p}$	[-]
$\bar{\Omega}$	Vorticity	[rad/s]
$\bar{\omega}$	Particle angular velocity	[rad/s]
$\bar{\omega}_r$	Particle-fluid relative spin	[rad/s]

NOTATION AND SYMBOLS (Continued)

Symbol	Description	Units
Б (Cyrillic B)	Chain strength parameter $\frac{ \mathbf{F}_{IM,max} }{(\rho_P - \rho_F) g \mathcal{V}_P}$	[-]
Д (Cyrillic D)	Drag reduction factor $\frac{C_{D0} _{B_0}}{C_{D0} _{B_0=0}}$	[-]

Coordinate systems used

	Coordinates	Unit vectors
Cartesian	x, y, z	$\hat{x}, \hat{y}, \hat{z}$
Spherical	r, θ, ϕ	$\hat{r}, \hat{\theta}, \hat{\phi}$

NOTATION AND SYMBOLS (Continued)

Physical constants

	Symbol	Value	Units
Vacuum permeability	μ_0	$4\pi \times 10^{-7}$	N/A ²

Special symbols

Symbol	Description
∇	Gradient operator
$\nabla \cdot$	Divergence operator
$\nabla \times$	Curl operator
$[\]$	Matrix
$ $	Magnitude of a vector; determinate of a matrix
$[[\]]$	Maximum of a set of values

NOTATION AND SYMBOLS (Continued)

Subscripts in discretization equations

Neighboring cells are identified by uppercase subscripts according to the following convention

P	Point	Current (center) cell
W	West	Cell in the x^- side of P
E	East	Cell in the x^+ side of P
S	South	Cell in the y^- side of P
N	North	Cell in the y^+ side of P
B	Back	Cell in the z^- side of P
F	Front	Cell in the z^+ side of P

The corresponding interfaces are denoted with lowercase subscripts, and vertices by triple subscripts indicating which three cells share the vertex.

DEDICATION

Yar: I have been blessed with your friendship and
your love.

— Star Trek The Next Generation,
“Skin of Evil”

To my mother,
Aída,
true source of inspiration and strength.

To my father,
Jorge,
in loving memory.

To my brothers,
Claudio Manuel, Jorge, and Juan Bosco,
and to my sister,
Patricia Aída,
for their support and dear care.

To my dear friends,
so numerous to name them all,
for countless wonderful memories.

Hydrodynamic Effects of Particle Chaining in Liquid-Solid Magnetofluidized Beds: Theory, Experiment, and Simulation

CHAPTER 1

INTRODUCTION

Monk: You've come back to seek the spirits?
Janeway: I don't know what I'm seeking.
Monk: Then I believe you're ready to begin.
— Star Trek Voyager,
"Sacred Ground"

1.1 Fluidization

Fluidization is a contacting unit operation for where solid particles are suspended by an upward stream of fluid (liquid, gas, or both). From a macroscopic point of view, the solid (dispersed) phase behaves as a fluid, hence the name of "fluidization".

Gas-Solid systems can show different fluidization regimes, particularly the formation of bubbles (regions of much lower particulate content). Liquid-Solid systems, on the other hand, are hydrodynamically more stable.

Fluidized beds have been used in variety of applications [12], including

- Mechanical classification of particles by size, density, or shape.
- Washing or leaching of solid particles.

- Seeded crystallization.
- Adsorption and ion exchange.
- Enhancement of electrolysis by fluidized particles.
- Fluidized bed heat exchangers.
- Heterogeneous catalytic reactions, especially hydrocarbon cracking.
- Fluidized bed coal combustion.
- Fluidized bed coal gasification.
- Fluidized bed bioreactors.

1.2 Magnetofluidization

When the solid particles are magnetically susceptible, the behavior of the fluidized bed can be altered by means of an external magnetic field. Some of the first studies of magnetically susceptible fluidized systems were related to the prevention (stabilization) of bubble formation in gas-solid systems [23, 24].

The most important effect of interparticle magnetic forces is the formation of chains and clusters of particles. The particles, magnetized in the direction of the field, attract each other. There is a dynamic equilibrium between the chain-forming effect of interparticle magnetic forces, and the chain-breaking effect of collisions and fluid drag. As result, the solid phase will

usually consist of an ensemble of individual particles, chains, and even clusters of particles, depending on the local conditions of flow and magnetic field strength. Figure 1.1 is an illustrative example of particle chaining.

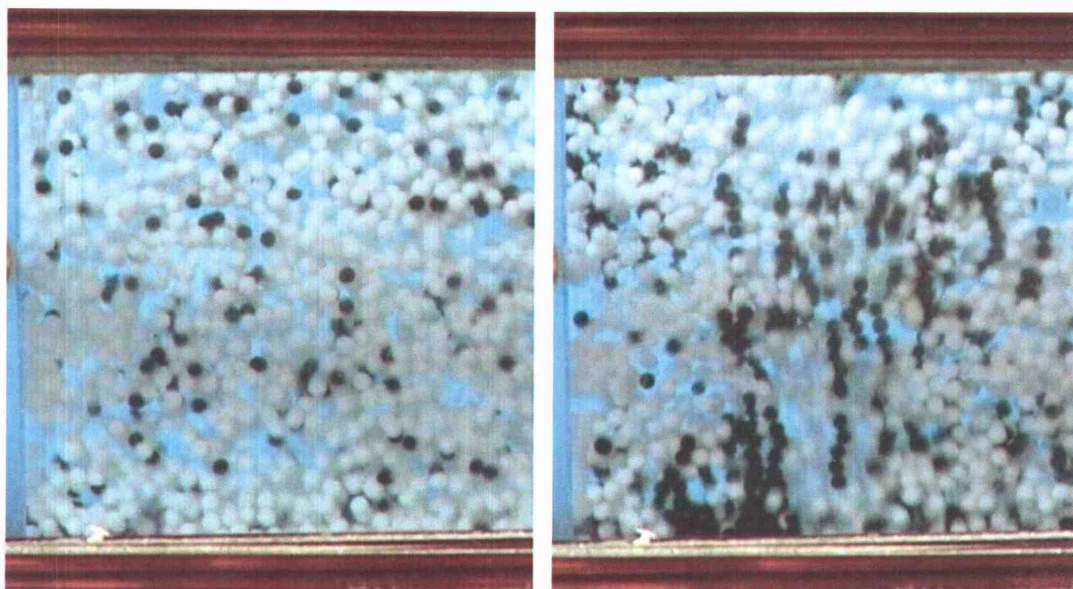


Figure 1.1. Chain formation in a magnetically stabilized fluidized bed. In the absence of field (left) all particles are free and randomly distributed. When the field is applied (right) the magnetically susceptible particles form chains. White, non-magnetic particles were added to enhance contrast.

These structures have a tendency to remain aligned with the applied field. As result, the particles in the chain or cluster will experience significantly different flow fields than the free, randomly distributed, particles in the absence of the field (Figure 1.2).

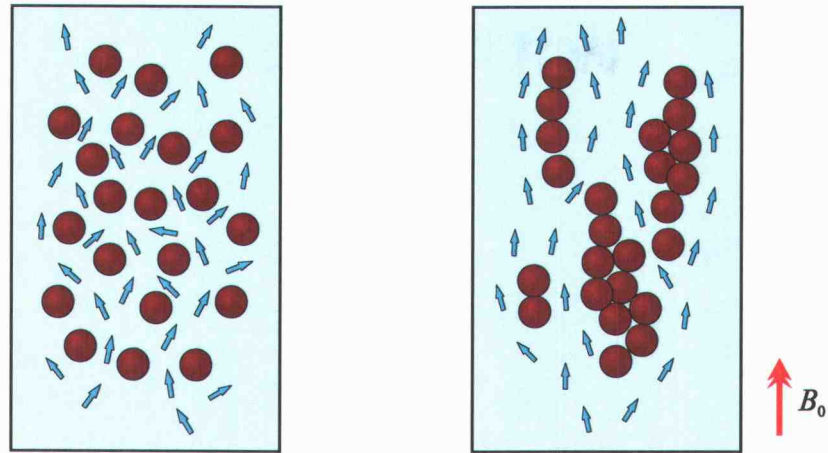


Figure 1.2. Difference in flow pattern through random (left) and structured (right) fluidized bed.

It has been observed that, under constant fluid flow, the bed height decreases with increasing magnetic field [17, 21, 29]. Within a given chain, the upstream particles “protect” the downstream particles from the influence of the incoming fluid. The drag force exerted on these particles is, therefore, reduced. Additionally, the space in-between chains provide a path with less resistance for the fluid. The combined effect causes the bed to begin collapsing. This, in turn, decreases the overall void fraction, thus increasing the fluid interstitial velocity until a new dynamic equilibrium is reached.

In addition to the interparticle magnetic force, an additional force of is present if the particles are in a non-uniform field, attracting the particles towards regions of higher magnetic field. It has been proposed [21, 26] that

this external magnetic force can be used to substitute gravity in low- and zero-gravity environments. NASA is currently funding research in fluidization technology for space applications based on this principle.

1.3 Computer simulation of fluidized beds

The study of fluidized beds has greatly benefited from computer simulations of increasing levels of detail (see Figure 1.3). One of the first models, often called "two-fluid model", considers the solid phase as a continuum-like fluid, interpenetrating the fluidizing continuous media. It is the least computationally intensive model, requiring the simultaneous solution of coupled PDEs of mass and momentum conservation for each of the phases. It does not provide information on the behavior of individual particles, although the effect of interaction forces between the particles can be included in the form of an elastic modulus [26]. In spite of its limitations, this is still the only type of model suitable for 3D simulations of large scale fluidized beds.

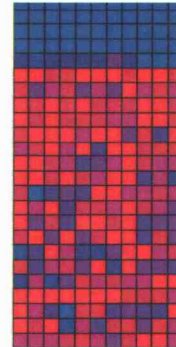
The next level of detail is continuous-semidiscrete, commonly known as CFD-DPM model (Computational Fluid Dynamics – Discrete Particle Method). In this model, each solid particle is individually described by equations of motion. However, the effects of the particles over the fluid, represented by voidage and drag force, are averaged over each fluid cell, which needs to be

large enough to have representative averages (usually containing at least 10 particles). The flow field is then solved as a continuous phase, flowing through a porous region of voidage prescribed by the particles. The advantage of accurate particle tracking is somewhat offset by the less-accurate calculation of the flow field. Nevertheless, the CFD-DPM model has yielded good results, qualitatively and quantitatively in agreement with experimental evidence. Current computational power allows for simulations up to $\mathcal{O}(10^4)$ or even $\mathcal{O}(10^5)$ particles, enough for simulating laboratory-scale fluidized beds.

A more accurate model is a continuous-discrete approach. Here, the fluid flow is resolved in the actual space in between the particles. The treatment of the solid phase, and its interaction with the fluid, is completely discrete. Since the flow field is calculated in the void spaces between the particles, the computational mesh for the fluid phase contains several orders of magnitude more elements. In addition, this fluid mesh needs to be reconstructed at each time step to accommodate the movement of the particles. Due to these high computational requirements, it is still restricted to a very low number of particles, probably not exceeding $\mathcal{O}(100)$ or even as low as $\mathcal{O}(10)$.

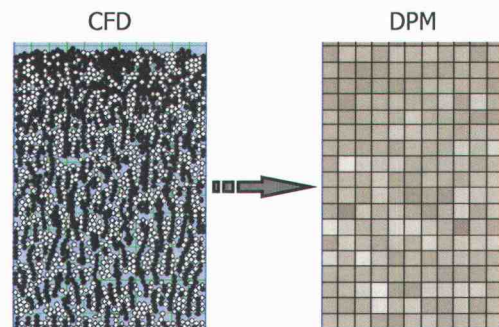
TWO-CONTINUUM

Two interpenetrating fluids.
No information on individual
particles or structures formed.



CONTINUUM-SEMIDISCRETE

Tracking of individual particles.
Identity and structure lost
when obtaining average void
fraction for flow field
calculation.



CONTINUUM-DISCRETE

Tracking of individual particles.
Fluid flow resolved in space
between particles. True flow
field obtained.

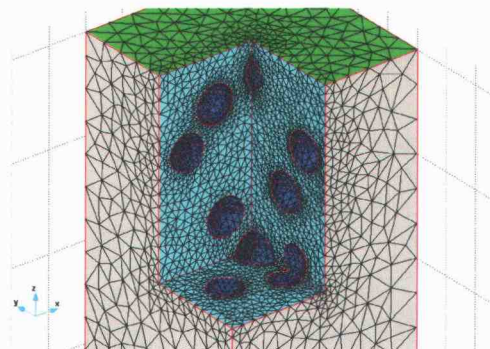


Figure 1.3. Three levels of detail in simulation of particulate-fluid systems.

1.4 Thesis rationale

The CFD-DPM simulation tools currently available do not take into account the effect of the induced bed structure in the drag over particles. This deficiency has been postulated as explanation for the discrepancies between experimental measurements of bed expansion and the corresponding simulations, under the presence of magnetic fields [21].

The code in question gives good agreement with the experimental observations of the fluidized bed in the absence of a magnetic field, but overestimates the bed height when the field is applied. A simulation code cannot become a research and design tool if does not produce realistic data. The need for a correction on the calculated drag was the origin of this research work.

1.4.1 Hypothesis

The following hypothesis is postulated as basis for this research work:

"The effect of the particle structures formed in a liquid-solid magnetofluidized fluidized bed can be accounted for in the

form of a drag correction factor, which is a function of the operating conditions such as flow strength and magnetic field intensity.”

1.4.2 Objectives

In order to test the aforementioned hypothesis, the following objectives are proposed

- Collect pressure drop and bed expansion data at different flow rates using a laboratory-scale magnetofluidized bed, under uniform magnetic field aligned with the main direction of the flow.
- Correlate the average drag coefficient with magnetic field strength and Reynolds number.
- Develop a code for 3D simulation of the fluidized bed, using the continuous-semidiscrete model.
- Confirm the validity of the average drag coefficient by comparing macroscopic parameters of the simulation with the experimental data.

The successful completion of these objectives will yield significant insight on fluid-particle interaction in the non-isotropic conditions of a magnetically assisted fluidized bed. First, the correlation model obtained can be applied to continuum/semi-discrete and two-continuum modeling of

fluidized beds. Second, the simulation code developed will allow further research in this field, especially for conditions not readily available experimentally (such as low- and zero-gravity applications). The outcome would constitute a significant contribution to the field of particle-fluid flows.

CHAPTER 2

THEORETICAL BACKGROUND

The Doctor: The Vulcan brain... a puzzle wrapped inside an
enigma, housed inside a cranium.

— Star Trek Voyager,
“Riddles”

2.1 Governing equations of the continuous phase

The fluid phase is governed by conservation of mass and momentum. The conservation principles are applied in the form of volume-averaged equations involving the local voidage ε . The derivation was presented by Anderson and Jackson [1].

2.1.2 *Mass conservation equation*

For a fluid of constant density, the conservation of mass is expressed in the form of the continuity equation,

$$\frac{\partial \varepsilon}{\partial t} + \nabla \cdot (\varepsilon \mathbf{u}) = 0 \quad (2.1-1)$$

Expanding the divergence term, the continuity equation reads

$$\frac{\partial \varepsilon}{\partial t} + \frac{\partial}{\partial x}(\varepsilon u_x) + \frac{\partial}{\partial y}(\varepsilon u_y) + \frac{\partial}{\partial z}(\varepsilon u_z) = 0 \quad (2.1-2)$$

2.1.2 Momentum conservation equation

The volume-averaged momentum conservation equation for a fluid of constant density is

$$\rho_f \frac{\partial}{\partial t}(\varepsilon \mathbf{u}) + \rho_f \nabla \cdot (\varepsilon \mathbf{u} \mathbf{u}) + \varepsilon \nabla P + \nabla \cdot (\varepsilon \boldsymbol{\tau}) - \varepsilon \rho_f \mathbf{g} - \mathbf{f} = 0 \quad (2.1-3)$$

This vector equation can be separated into x -component,

$$\begin{aligned} \rho_f \frac{\partial}{\partial t}(\varepsilon u_x) + \rho_f \frac{\partial}{\partial x}(\varepsilon u_x u_x) + \rho_f \frac{\partial}{\partial y}(\varepsilon u_x u_y) + \rho_f \frac{\partial}{\partial z}(\varepsilon u_x u_z) + \varepsilon \frac{\partial P}{\partial x} \\ + \frac{\partial}{\partial x}(\varepsilon \tau_{xx}) + \frac{\partial}{\partial y}(\varepsilon \tau_{yx}) + \frac{\partial}{\partial z}(\varepsilon \tau_{zx}) - \varepsilon \rho_f g_x - f_x = 0 \end{aligned} \quad (2.1-4)$$

y -component,

$$\begin{aligned} \rho_f \frac{\partial}{\partial t}(\varepsilon u_y) + \rho_f \frac{\partial}{\partial x}(\varepsilon u_x u_y) + \rho_f \frac{\partial}{\partial y}(\varepsilon u_y u_y) + \rho_f \frac{\partial}{\partial z}(\varepsilon u_y u_z) + \varepsilon \frac{\partial P}{\partial y} \\ + \frac{\partial}{\partial x}(\varepsilon \tau_{yx}) + \frac{\partial}{\partial y}(\varepsilon \tau_{yy}) + \frac{\partial}{\partial z}(\varepsilon \tau_{yz}) - \varepsilon \rho_f g_y - f_y = 0 \end{aligned} \quad (2.1-5)$$

and z -component,

$$\begin{aligned} \rho_f \frac{\partial}{\partial t}(\epsilon u_z) + \rho_f \frac{\partial}{\partial x}(\epsilon u_x u_z) + \rho_f \frac{\partial}{\partial y}(\epsilon u_y u_z) + \rho_f \frac{\partial}{\partial z}(\epsilon u_z u_z) + \epsilon \frac{\partial P}{\partial z} \\ + \frac{\partial}{\partial x}(\epsilon \tau_{xz}) + \frac{\partial}{\partial y}(\epsilon \tau_{yz}) + \frac{\partial}{\partial z}(\epsilon \tau_{zz}) - \epsilon \rho_f g_z - f_z = 0 \end{aligned} \quad (2.1-6)$$

For an incompressible Newtonian fluid, the viscous stress tensor is given by

$$\boldsymbol{\tau} = -\mu_f [(\nabla \mathbf{u}) + (\nabla \mathbf{u})^T] \quad (2.1-7)$$

or, in the form of individual components,

$$\tau_{xx} = -2\mu_f \frac{\partial u_x}{\partial x} \quad (2.1-8)$$

$$\tau_{yy} = -2\mu_f \frac{\partial u_y}{\partial y} \quad (2.1-9)$$

$$\tau_{zz} = -2\mu_f \frac{\partial u_z}{\partial z} \quad (2.1-10)$$

$$\tau_{xy} = \tau_{yx} = -\mu_f \left(\frac{\partial u_x}{\partial y} + \frac{\partial u_y}{\partial x} \right) \quad (2.1-11)$$

$$\tau_{xz} = \tau_{zx} = -\mu_f \left(\frac{\partial u_x}{\partial z} + \frac{\partial u_z}{\partial x} \right) \quad (2.1-12)$$

$$\tau_{yz} = \tau_{zy} = -\mu_f \left(\frac{\partial u_y}{\partial z} + \frac{\partial u_z}{\partial y} \right) \quad (2.1-13)$$

2.2. Governing equations for the discrete phase

Conservation of mass in the particulate phase is implicit in the assumption that the particles neither gain nor lose mass, and that their count remains constant. The behavior of the discrete phase in the bed is dictated by the equations of motion and the forces acting on each particle.

2.2.1 *Equations of motion*

Newtonian physics governs the translational and rotational motion of each individual particle, through conservation of linear (Equation 2.2-1) and angular (Equation 2.2-2) momentum.

$$m_p \frac{d\mathbf{v}_i}{dt} = \sum \mathbf{F}_i \quad (2.2-1)$$

$$I_p \frac{d\bar{\omega}_i}{dt} = \sum \mathbf{T}_i \quad (2.2-2)$$

In addition, the position of the particle is related to its velocity by the kinematic equation

$$\mathbf{v}_i = \frac{d\mathbf{x}_i}{dt} \quad (2.2-3)$$

The subscript i indicates that there is an equation for each particle. For the sake of clarity, this subscript will be dropped in the remaining equations, except where its omission leads to confusion.

2.2.2 *Body forces*

These include the gravitational force \mathbf{F}_g , the buoyancy force \mathbf{F}_b , and the external magnetic force \mathbf{F}_B . In the case of uniform field, the external magnetic force is zero.

$$\mathbf{F}_g = m_p \mathbf{g} \quad (2.2-4)$$

$$\mathbf{F}_b = -\mathcal{V}_p \rho_f \mathbf{g} = -\mathcal{V}_p \nabla P \quad (2.2-5)$$

$$\mathbf{F}_B = \mathbf{m} \cdot \nabla \mathbf{B}_0 \quad (2.2-6)$$

2.2.3. *Drag force*

The most important interaction force exerted between fluid and particles in fluidized beds is the drag force. It is usually expressed in terms of the dimensionless *drag coefficient*, defined as

$$C_D \equiv \frac{|\mathbf{F}_D|}{\frac{1}{2} \rho_f |\mathbf{u} - \mathbf{v}|^2 A} \quad (2.2-7)$$

where A is a characteristic area, usually the particle cross sectional area, normal to the flow [9]. The drag coefficient is a function of Reynolds number and geometry of the particle.

For a spherical particle, the Reynolds number is usually defined in terms of the particle diameter and the relative interstitial velocity between the fluid and the particle

$$\text{Re}_p \equiv \frac{\rho_f d_p |\mathbf{u} - \mathbf{v}|}{\mu_f} \quad (2.2-8)$$

The drag coefficient for a single sphere in a uniform flow field, here denoted by C_{D0} , has been the subject of extensive research. There are a number of correlations that fit the experimental data very well. The most common are listed in Table 2.1.

In the limiting case of very low Reynolds number (*creeping* or *Stokes flow*, $\text{Re}_p \ll 1$), the drag coefficient becomes inversely proportional to the particle Reynolds number

$$\lim_{\text{Re}_p \rightarrow 0} C_{D0} = \frac{24}{\text{Re}_p} \quad (2.2-9)$$

At a critical $Re_p \sim 300,000$, the boundary layer becomes turbulent and there is a sharp decrease in drag coefficient.

Table 2.1 Correlations for drag coefficient of single sphere

Stokes	
$C_{D0} = \frac{24}{Re_p}$	$Re_p < 1$
Onseen (1910)	
$C_{D0} = \frac{24}{Re_p} \left(1 + \frac{3}{16} Re_p \right)$	$Re_p < 5$
Schiller and Naumann (1933)	
$C_{D0} = \frac{24}{Re_p} (1 + 0.15 Re_p^{0.687})$	$Re_p < 800$
Dallavalle (1948) [8]	
$C_{D0} = (0.632 + 4.8 Re_p^{-0.5})^2$	$Re_p < 2 \times 10^5$
Putnam (1961) [22]	
$C_{D0} = \frac{24}{Re_p} \left(1 + \frac{1}{6} Re_p^{2/3} \right)$	$Re_p < 10^3$
$C_{D0} = 0.439$	$10^3 \leq Re_p < 3 \times 10^5$

Table 2.1 (Continued)

Rowe & Henwood (1961) [25]	
$C_{D0} = \frac{24}{Re_p} (1 + 0.15 Re_p^{0.687})$	$Re_p < 1000$
$C_{D0} = 0.44$	$Re_p \geq 1000$
Clift and Gauvin (1970) [3]	
$C_{D0} = \frac{24}{Re_p} \left(1 + 0.15 Re_p^{0.687} + \frac{0.0175 Re_p}{1 + 4.25 \times 10^4 Re_p^{-1.16}} \right)$	$Re_p < 3 \times 10^5$
White (1991) [30]	
$C_{D0} = \frac{24}{Re_p} + \frac{6}{1 + Re_p^{0.5}} + 0.4$	$Re_p \leq 2 \times 10^5$

For the purpose of this research, the drag coefficient was calculated using the correlation by Dallavalle [8], Equation 2.2-10 (see Figure 2.1).

$$C_{D0} = (0.632 + 4.8 Re_p^{-0.5})^2 \quad (2.2-10)$$

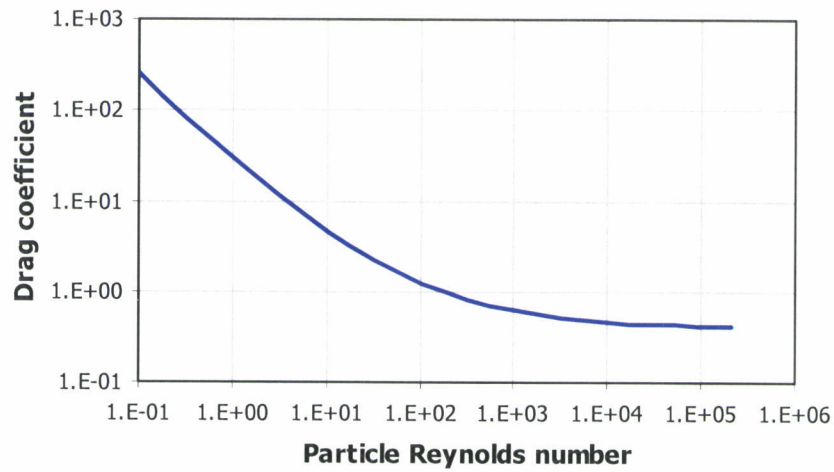


Figure 2.1 Drag coefficient for a single spherical particle.

In a fluidized bed, however, the drag coefficient for spherical particles is different than that of an isolated particle. This is due to the effect of neighboring particles in the flow patterns around any given particle. DiFelice [11] proposed an equation for the drag coefficient applicable to fluidized and packed beds over the full practical range of Re_p . The drag coefficient is expressed as the product of the drag over a single particle C_{D0} , subject to the same fluid interstitial velocity, and a *voidage function* $\varepsilon^{-\beta}$,

$$C_D = C_{D0} \varepsilon^{-\beta} \quad (2.2-11)$$

where the exponent β is given by

$$\beta = 3.7 - 0.65 \exp \left[-\frac{(1.5 - \log_{10} \text{Re}_p)^2}{2} \right] \quad (2.2-12)$$

A plot of Equation 2.2-12 is shown in Figure 2.2.

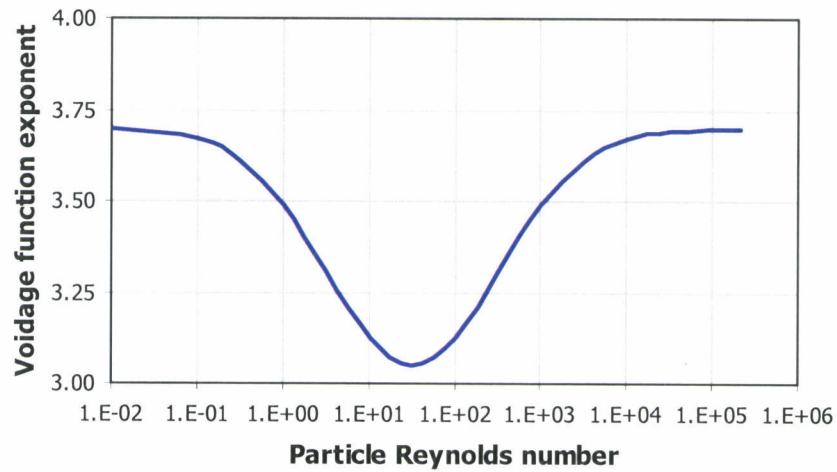


Figure 2.2 The exponent β of the voidage function.

2.2.4 Lift forces

These include the *Saffman force* and the *Magnus force*. The Saffman lift force is due to pressure differences developed around a particle in a velocity gradient. The lower pressure is on the higher velocity side, and the higher

pressure in the lower velocity side, produce this lift force. For low Reynolds number and low shear Reynolds number, the Saffman force is given by

$$\mathbf{F}_{SL} = 1.61 d_p^2 \left(\frac{\mu_f \rho_f}{|\nabla \times \mathbf{u}|} \right)^{\frac{1}{2}} [(\mathbf{u} - \mathbf{v}) \times (\nabla \times \mathbf{u})] \quad (2.2-13)$$

Mei [19] has proposed an empirical correction for the Saffman lift force applicable to a wider range of Reynolds number

$$\frac{\mathbf{F}_{SL}}{\mathbf{F}_{SL,0}} = \begin{cases} (1 - 0.3314\Lambda^{\frac{1}{2}}) \exp(-0.1\text{Re}_\omega) + 0.3314\Lambda^{\frac{1}{2}} & \text{Re}_\omega \leq 40 \\ 0.0524(\Lambda\text{Re}_\omega)^{\frac{1}{2}} & \text{Re}_\omega > 40 \end{cases} \quad (2.2-14)$$

where the parameter Λ is defined as

$$\Lambda = \frac{d_p |\nabla \times \mathbf{u}|}{2|\mathbf{u} - \mathbf{v}|} \quad 0.005 < \Lambda < 0.4 \quad (2.2-15)$$

The relative spin between the fluid and the particle, and the corresponding rotation Reynolds number are defined as

$$\bar{\omega}_r \equiv \bar{\omega} - \frac{1}{2} \nabla \times \mathbf{u} \quad (2.2-16)$$

$$\text{Re}_\omega \equiv \frac{\rho_f d_p^2 |\bar{\omega}_r|}{4\mu_f} \quad (2.2-17)$$

The Magnus force is the lift developed due to rotation of the particle caused by sources other than the velocity gradient. The lift is caused by a pressure differential between both sides of the particle resulting from the

velocity differential due to rotation. The Magnus force is usually expressed in terms of a lift coefficient as

$$\mathbf{F}_{ML} = \frac{1}{2} \rho_f |\mathbf{u} - \mathbf{v}| C_L A \frac{(\mathbf{u} - \mathbf{v}) \times \bar{\omega}_r}{|\bar{\omega}_r|} \quad (2.2-18)$$

For a spherical particle, the characteristic area used is the cross sectional area, $A = \pi r_p^2$. There have been numerous experiments to measure the lift coefficient. Tanaka et al. [27] has suggested a ramp function up to a lift coefficient of 0.5 and a constant value thereafter.

$$C_L = \min \left(0.5, \frac{d_p |\bar{\omega}_r|}{|\mathbf{u} - \mathbf{v}|} \right) \quad (2.2-19)$$

2.2.5 Viscous torque on particle

When the relative spin between the particle and the fluid is non-zero, there is a torque of viscous origin acting on the particle. For a spinning particle in a fluid at rest, this torque will slow down and eventually stop the rotation of the particle. For a non-rotating particle in a fluid velocity gradient, this torque will induce rotation. For a low Reynolds number [16], the torque is given by

$$\mathbf{T} = -\pi \mu_f d_p^3 \bar{\omega}_r \quad (2.2-20)$$

Dennis et al. [10] proposed the following correlation for the viscous torque for rotation Reynolds numbers from 20 to 1000

$$\mathbf{T} = -2.01\mu_f d_p^3 \bar{\omega}_r \left(1 + 0.201|\bar{\omega}_r|^{\frac{1}{2}}\right) \quad (2.2-21)$$

2.2.6 Other fluid-particle interaction forces

The forces listed in this section were not included in the present analysis since they are negligible for the case studied.

The virtual mass force ("added mass") represents the additional momentum necessary to accelerate the fluid in front of and around an accelerating particle. The resulting force is proportional to the volume of the particle and the density of the fluid. It is negligible [4] if the characteristic frequency of the flow field is less than $\frac{36\mu_f}{\rho_f d_p^2}$.

The *Basset force* is an unsteady force produced by lagging boundary layer around accelerating or decelerating particles. Like the virtual mass force, the Basset force can be neglected [4] if the characteristic frequency of the flow field is less than $\frac{36\mu_f}{\rho_f d_p^2}$.

The *Faxen correction* is a contribution to the drag force, the virtual mass, and the Basset force, due to flow curvature effects. It is proportional to $\nabla^2 \mathbf{u}$.

2.2.7 Collision forces

In the collision of particles i and j , the collision force exerted on particle i is decomposed in a normal and a tangential components

$$\mathbf{F}_c = \mathbf{F}_{cn} + \mathbf{F}_{ct} \quad (2.2-22)$$

The tangential force also produces a torque on particle i ,

$$\mathbf{T} = r_p \hat{\mathbf{n}} \times \mathbf{F}_{ct} \quad (2.2-23)$$

By virtue of Newton's Third Law, particle j experiences forces and torque opposite and equal in magnitude to those on particle i .

Collision forces between particles are resolved using the soft-sphere model originally proposed by Cundall and Strack [7]. In this model, the particle deformation at the point of contact is not considered but replaced by an overlap of the particles. The normal and tangential forces are represented as linear spring/dash-pot systems, with an additional frictional slider in the tangential force system (Figure 2.3).

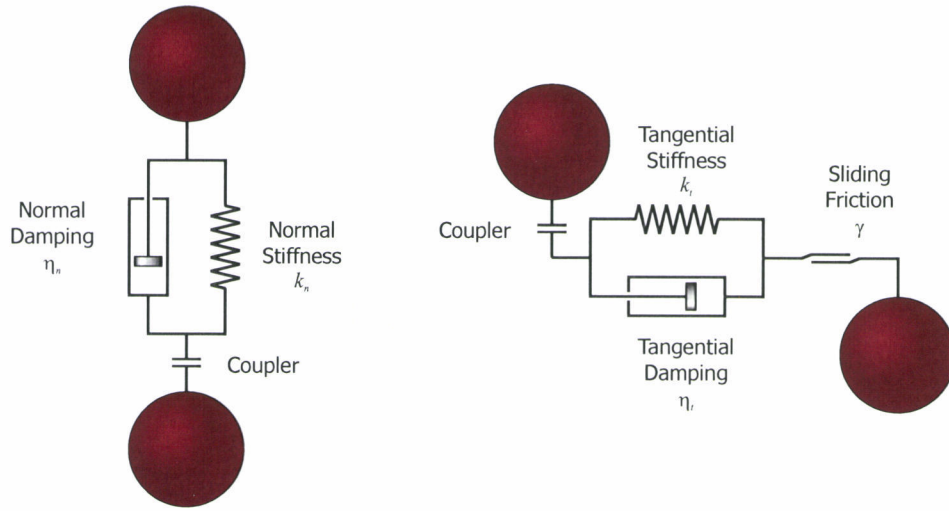


Figure 2.3 Soft sphere model for particle collisions.

The parameters of this model are the normal and tangential stiffness (k_n and k_t), the normal and tangential damping coefficients (η_n and η_t), and the tangential sliding friction coefficient (γ). The damping coefficients are usually estimated in terms of the restitution coefficient (e) as

$$\eta_n = -2\sqrt{m_p k_n} \frac{\ln e}{\sqrt{\pi^2 + (\ln e)^2}} \quad (2.2-24)$$

and likewise for the tangential damping coefficient.

The normal component of the collision force on particle i is given by

$$\mathbf{F}_{cn,ij} = (-k_n \delta_n - \eta_n \mathbf{V} \cdot \hat{\mathbf{n}}) \hat{\mathbf{n}} \quad (2.2-25)$$

where the normal overlap is

$$\delta_n \equiv 2r_p - |\mathbf{x}_j - \mathbf{x}_i| \quad (2.2-26)$$

the relative velocity of particle i with respect to particle j is defined as

$$\mathbf{V} \equiv \mathbf{v}_i - \mathbf{v}_j \quad (2.2-27)$$

and the normal unit vector from particle i towards particle j is

$$\hat{\mathbf{n}} \equiv \frac{\mathbf{x}_j - \mathbf{x}_i}{|\mathbf{x}_j - \mathbf{x}_i|} \quad (2.2-28)$$

The tangential component of the collision force will be different whether the particles are sliding or not. If no sliding occurs,

$$\mathbf{F}_{ct,ij} = -k_t \bar{\delta}_t - \eta_t \mathbf{V}_{ct} \quad (2.2-29)$$

where the tangential slip velocity at the point of contact is given by

$$\mathbf{V}_{ct} = \mathbf{V} - (\mathbf{V} \cdot \hat{\mathbf{n}}) \hat{\mathbf{n}} + r_p (\bar{\omega}_i + \bar{\omega}_j) \times \hat{\mathbf{n}} \quad (2.2-30)$$

If the condition $|\mathbf{F}_{ct,ij}| > \gamma |\mathbf{F}_{cn,ij}|$ is satisfied, the particles slide at the point of contact and the tangential component of the force is given by

$$\mathbf{F}_{ct,ij} = -\gamma |\mathbf{F}_{cn,ij}| \hat{\mathbf{t}} \quad (2.2-31)$$

instead of Equation 2.2-29. The direction of this force is given by the tangential vector defined by the slip velocity

$$\hat{\mathbf{t}} = \frac{\mathbf{V}_{ct}}{|\mathbf{V}_{ct}|} \quad (2.2-32)$$

Note that the tangential displacement $\bar{\delta}_t$ is a vector and not a scalar like its normal counterpart δ_n . It is given by

$$\bar{\delta}_t = \begin{cases} \int_{t_0}^t \mathbf{V}_{ct} dt & \text{if not sliding} \\ \frac{\gamma |\mathbf{F}_{ct,ij}|}{k_t} \hat{\mathbf{t}} & \text{if sliding} \end{cases} \quad (2.2-33)$$

where, if not sliding, the integration is performed from the time of first contact between the particles (t_0) and the current time.

Finally, collisions of particles with the walls are a limiting case of this model, assuming particle j to have infinite radius and mass.

2.2.9 Interparticle magnetic force

Interparticle magnetic forces play a key role in the behavior of magnetofluidized beds. An externally applied magnetic field (\mathbf{B}_0) induces a magnetization on the magnetically susceptible particles. The magnetized particles are usually modeled as ideal magnetic dipoles. The interparticle magnetic force is thus a dipole-dipole interaction. Depending on the orientation of the particles relative to the direction of the field, this force can be attractive or repulsive (Figure 2.4). Due to axial symmetry with respect to the direction of the magnetic field, the interparticle magnetic force is usually expressed in a spherical coordinate system centered in the particle and split into radial and tangential components (Figure 2.5).

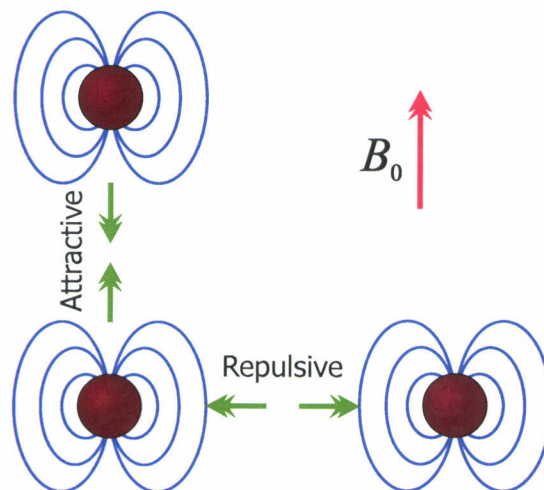


Figure 2.4 Attractive and repulsive limits of the interparticle magnetic force. The particles attract if they are aligned with the field, and repel if they are side by side with respect to the field.

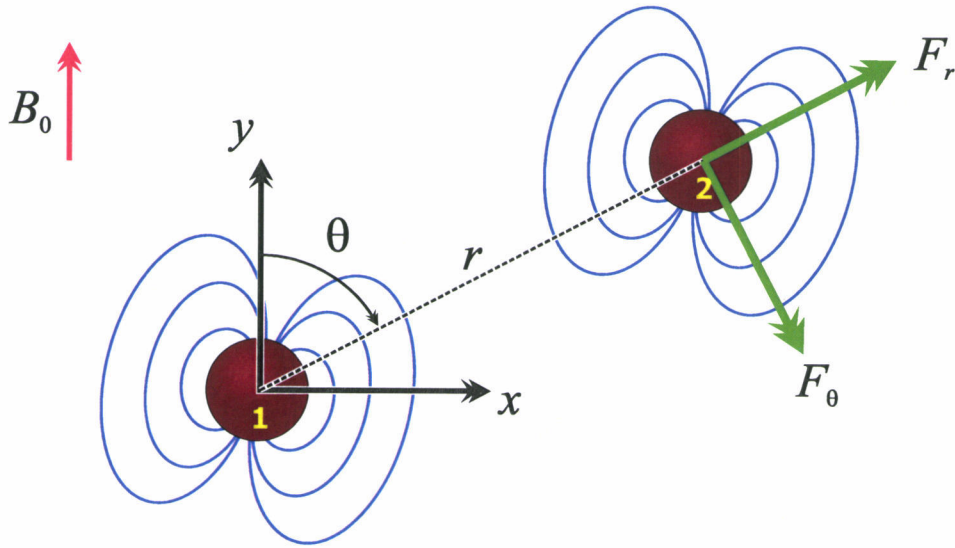


Figure 2.5 Components of the interparticle magnetic force.

The magnetic field of a dipole at the origin is given [15], in coordinate free form, as

$$\mathbf{B}_{dip} = \frac{\mu_0}{4\pi r^3} [3(\mathbf{m} \cdot \hat{\mathbf{r}})\hat{\mathbf{r}} - \mathbf{m}] \quad (2.2-34)$$

In spherical coordinates, the dipole field is symmetric with respect to the polar axis, and has components

$$B_r = \frac{\mu_0 m}{4\pi} \left(\frac{2 \cos \theta}{r^3} \right) \quad (2.2-35)$$

$$B_\theta = \frac{\mu_0 m}{4\pi} \left(\frac{\sin \theta}{r^3} \right) \quad (2.2-36)$$

$$B_\phi = 0 \quad (2.2-37)$$

and the only non-zero components of the field gradient tensor are

$$(\nabla \mathbf{B})_{rr} = -\frac{\mu_0 m}{4\pi} \left(\frac{6 \cos \theta}{r^4} \right) \quad (2.2-38)$$

$$(\nabla \mathbf{B})_{r\theta} = -\frac{\mu_0 m}{4\pi} \left(\frac{2 \sin \theta}{r^4} \right) \quad (2.2-39)$$

$$(\nabla \mathbf{B})_{\theta r} = -\frac{\mu_0 m}{4\pi} \left(\frac{3 \sin \theta}{r^4} \right) \quad (2.2-40)$$

$$(\nabla \mathbf{B})_{\theta\theta} = \frac{\mu_0 m}{4\pi} \left(\frac{\cos \theta}{r^4} \right) \quad (2.2-41)$$

Models of different level of complexity have been proposed to calculate the interparticle magnetic force. In its more general form [18], the potential energy of a magnetic dipole in a magnetic field is given as

$$U = -\mathbf{m} \cdot \mathbf{B}_{loc} \quad (2.2-42)$$

where the local field \mathbf{B}_{loc} is the magnetic field that would exist at the particle location if the particle were not there; this is, the superposition of the externally applied magnetic field (\mathbf{B}_0) and the dipole field of neighboring particles.

$$\mathbf{B}_{loc} = \mathbf{B}_0 + \sum_{j \neq i} \mathbf{B}_{dip,j} \quad (2.2-43)$$

Since the force resulting from gradients in the external field has already been taken into account as the external magnetic force \mathbf{F}_B (Section 2.2.2), its

contribution to the local gradient is not included. The interparticle magnetic force can be obtained thus as the negative gradient of the potential energy,

$$\mathbf{F}_{IM,i} = \nabla \left[\mathbf{m}_i \sum_{j \neq i} \mathbf{B}_{dip,j} \right] \quad (2.2-44)$$

The dipole field and its gradient fall quickly with distance (r^{-3} and r^{-4} , respectively); usually only the neighboring particles within a few particle diameters are included in the summation.

The dipole moment of the particle is the volume integral of the magnetization of the particle,

$$\mathbf{m} = \int_{V_p} \mathbf{M} dV \quad (2.2-45)$$

Since \mathbf{M} is usually considered uniform throughout the particle, the magnetic moment is simply

$$\mathbf{m} = \mathbf{M} V_p \quad (2.2-46)$$

The magnetization is related to the local field by

$$\mathbf{M} = \chi_e \mathbf{H}_{loc} = \chi_e \frac{\mathbf{B}_{loc}}{\mu_0} \quad (2.2-47)$$

where the effective susceptibility is related to the particle susceptibility (a material property) by

$$\chi_e = \frac{\chi_p}{1 + \frac{1}{3}\chi_p} \quad (2.2-48)$$

The factor $\frac{1}{3}$, sometimes referred to as *demagnetization factor*, depends on the shape of the particle and arises from Maxwell's equations at the boundary of the particle.

Substituting Equations 2.2-47 and 2.2-48 into Equation 2.2-46, the magnetic moment of a spherical particle with uniform magnetization produced by a local field can be expressed as

$$\mathbf{m} = \frac{\chi_p \mathcal{V}_p}{(1 + \frac{1}{3}\chi_p)\mu_0} \mathbf{B}_{loc} \quad (2.2-49)$$

In the non-interacting dipoles model, the neighboring contributions to the local field are neglected and the dipole moment of the particles is calculated exclusively from the external field \mathbf{B}_0 . Denoting this dipole moment by \mathbf{m}_0 , the interparticle magnetic force is given by

$$\mathbf{F}_{IM} = \mathbf{m}_0 \cdot \sum_{j \neq i} \nabla \mathbf{B}_{dip,j} \quad (2.2-50)$$

Since the dipole moment of the particle depends now only on the externally applied field, the interparticle magnetic force can be calculated independently for each pair of particles. For two ideal non-interacting dipoles,

$$F_r = \frac{3\mu_0 |\mathbf{m}|^2}{4\pi r^4} (1 - 3\cos^2 \theta) \quad (2.2-51)$$

$$F_\theta = \frac{3\mu_0 |\mathbf{m}|^2}{2\pi r^4} \sin \theta \cos \theta \quad (2.2-52)$$

Pinto-Espinoza [21] has developed an analytical solution for the interparticle magnetic force between two interacting dipoles. This model, however, cannot be readily extended for multiple interacting particles. The calculation of the interparticle magnetic force in such a case would require a numerical approach.

2.3 Explanatory dimensionless numbers

To select a set of suitable explanatory variables, a dimensional analysis is done based on Buckingham's pi theorem. The physical quantities considered are listed in Table 2.2.

Table 2. 2 Physical quantities for dimensional analysis

	Symbol	Units	Dimensions
Particle diameter	d_p	[m]	L
Superficial velocity	u_0	[m/s]	LT^{-1}
Gravity	g	[m/s ²]	LT^{-2}
Density difference	$\Delta\rho$	[kg/m ³]	ML^{-3}
Fluid viscosity	μ_f	[Pa·s]	$ML^{-1}T^{-1}$
Vacuum permeability	μ_0	[T·m/A]	MLQ^{-2}
Particle dipole moment	$ \mathbf{m} $	[A·m ²]	$L^2T^{-1}Q$

In matrix form,

	d_p	u_0	g	$\Delta\rho$	μ_f	μ_0	$ \mathbf{m} $
M	0	0	0	1	1	1	0
L	1	1	1	-3	-1	1	2
T	0	-1	-2	0	-1	0	-1
Q	0	0	0	0	0	-2	1

Since it is possible to form a 4×4 sub matrix with a non-zero determinant, the rank of the matrix is 4. This means that 7-4=3 linearly independent dimensionless groups can be formed from this set of physical

quantities. Choosing d_p , g , $\Delta\rho$, and μ_0 as the primary variables, the following dimensionless groups are formed

$$\pi_1 = d_p^a g^b \Delta\rho^c \mu_0^d u_0 \quad (2.3-1)$$

$$\pi_2 = d_p^a g^b \Delta\rho^c \mu_0^d \mu_f \quad (2.3-2)$$

$$\pi_3 = d_p^a g^b \Delta\rho^c \mu_0^d |\mathbf{m}| \quad (2.3-3)$$

Equation 2.3-1 generates the system of equations

$$\begin{bmatrix} 0 & 0 & 1 & 1 \\ 1 & 1 & -3 & 1 \\ 0 & -2 & 0 & 0 \\ 0 & 0 & 0 & -2 \end{bmatrix} \begin{bmatrix} a \\ b \\ c \\ d \end{bmatrix} = \begin{bmatrix} 0 \\ -1 \\ 1 \\ 0 \end{bmatrix} \quad (2.3-4)$$

with solution

$$\begin{bmatrix} a \\ b \\ c \\ d \end{bmatrix} = \begin{bmatrix} -0.5 \\ -0.5 \\ 0 \\ 0 \end{bmatrix} \quad (2.3-5)$$

Therefore, the first dimensionless parameter is

$$\pi_1 = d_p^{-0.5} g^{-0.5} u_0 = \frac{u_0}{(d_p g)^{0.5}} \quad (2.3-6)$$

This dimensionless group can be identified as a form of *Froude number*,

$$Fr = \frac{u_0^2}{d_p g} \quad (2.3-7)$$

Proceeding similarly for the second group,

$$\pi_2 = d_p^{-1.5} g^{-0.5} \Delta \rho^{-1} \mu_f = \frac{\mu_f}{(d_p^3 g)^{0.5} \Delta \rho} \quad (2.3-8)$$

However, a much more useful dimensionless number can be obtained as

$$\frac{\pi_1}{\pi_2} = \frac{d_p \Delta \rho u_0}{\mu_f} \quad (2.3-9)$$

which is a form of Reynolds number. By using the fluid density and interstitial velocity instead, the *particle Reynolds number* arises

$$Re_p = \frac{\rho_f (u_0 / \varepsilon) d_p}{\mu_f} \quad (2.3-10)$$

Finally, for the third dimensionless group,

$$\pi_3 = d_p^{-3.5} g^{-0.5} \Delta \rho^{-0.5} \mu_0^{0.5} |\mathbf{m}| = \frac{\mu_0^{0.5} |\mathbf{m}|}{(d_p^7 g \Delta \rho)^{0.5}} \quad (2.3-11)$$

Squaring π_3 and regrouping,

$$\pi_3^2 = \frac{\mu_0 |\mathbf{m}|^2}{d_p^4 g \Delta \rho d_p^3} \quad (2.3-12)$$

where the numerator is reminiscent of the interparticle magnetic force between two particles in contact, and the denominator is reminiscent of the buoyant weight of the particle. Thus, the *chain strength parameter* is defined as the dimensionless number

$$\mathcal{B} = \frac{|\mathbf{F}_{IM, \max}|}{(\rho_p - \rho_f) g \mathcal{V}_p} \quad (2.3-13)$$

where the maximum interparticle magnetic force, as given by the non-interacting dipoles model, is

$$|\mathbf{F}_{IM, \max}| = \frac{3\mu_0 |\mathbf{m}|^2}{2\pi d_p^4} \quad (2.3-14)$$

In summary, the three dimensionless numbers chosen as potential explanatory variables for the drag reduction factor are Fr , Re_p , and \mathcal{B} .

CHAPTER 3

EXPERIMENTAL METHODOLOGY

Spock: Interesting.

Scott: I find nothing interesting in the fact that we are about to blow up.

Spock: No, but the method is fascinating.

— Star Trek
“That Which Survives”

The experimental equipment is composed of a fluidized bed with the corresponding flow system, a pressure probe, and a coil for generating the uniform magnetic field.

A schematic representation of the fluidized bed system is shown in Figure 3.1, and a picture of the finished equipment in Figure 3.2. Additional schematics can be found in Appendix A.

3.1 Fluidized bed system

3.1.1 *Bed design*

The fluidized bed (Figure 3.3) is a rectangular column made of polycarbonate. The zone available for fluidization is 0.10m wide, 0.05m thick, and approximately 0.40m high.

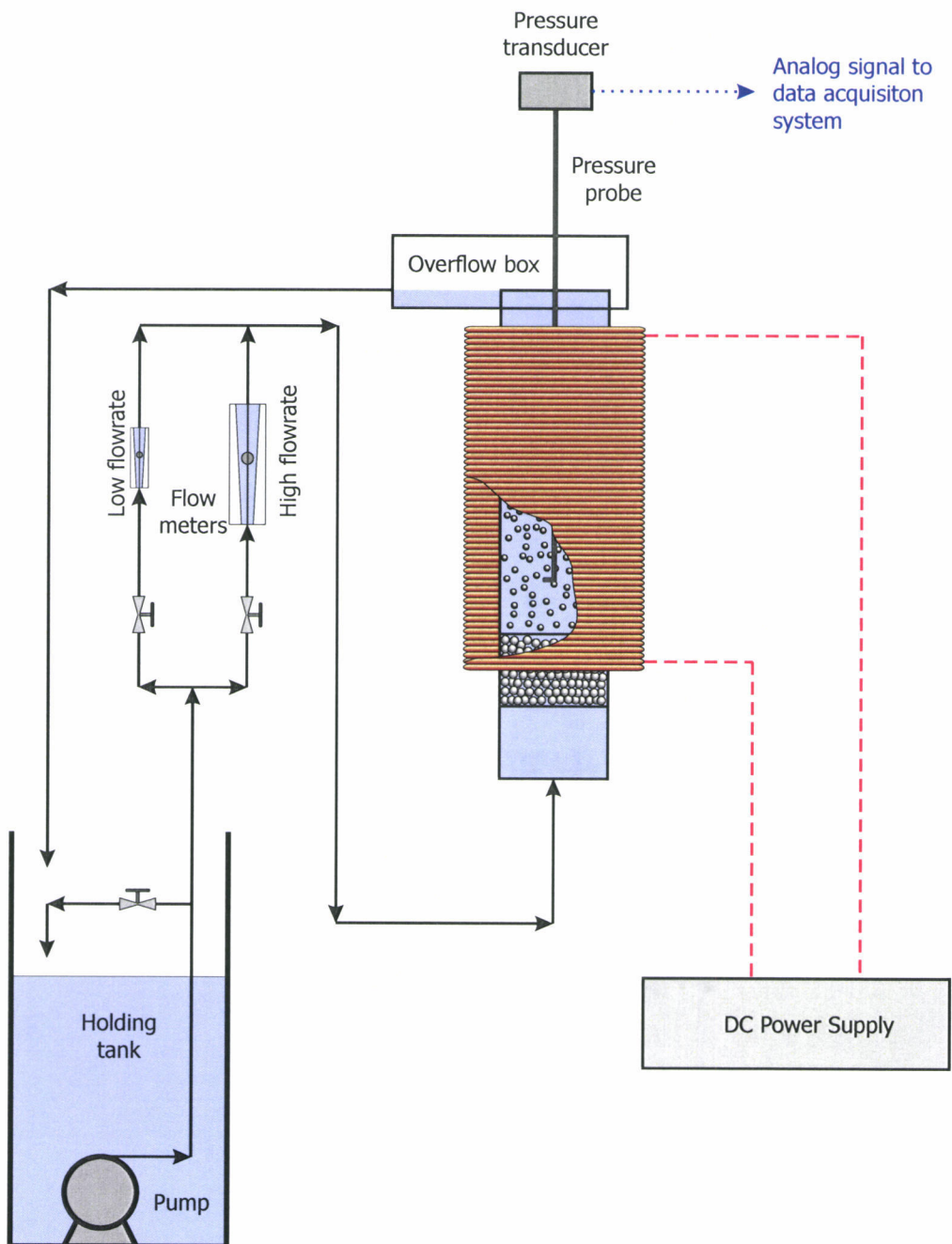


Figure 3.1 Schematic of the experimental apparatus. A section of the coil has been “cut” to show the bed and pressure probe in the interior.

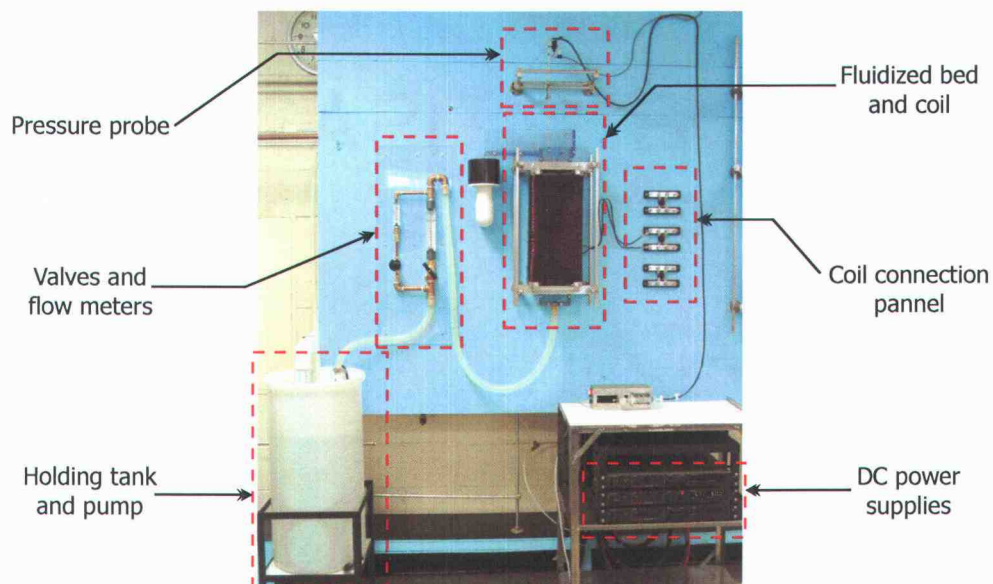


Figure 3.2 Experimental apparatus.

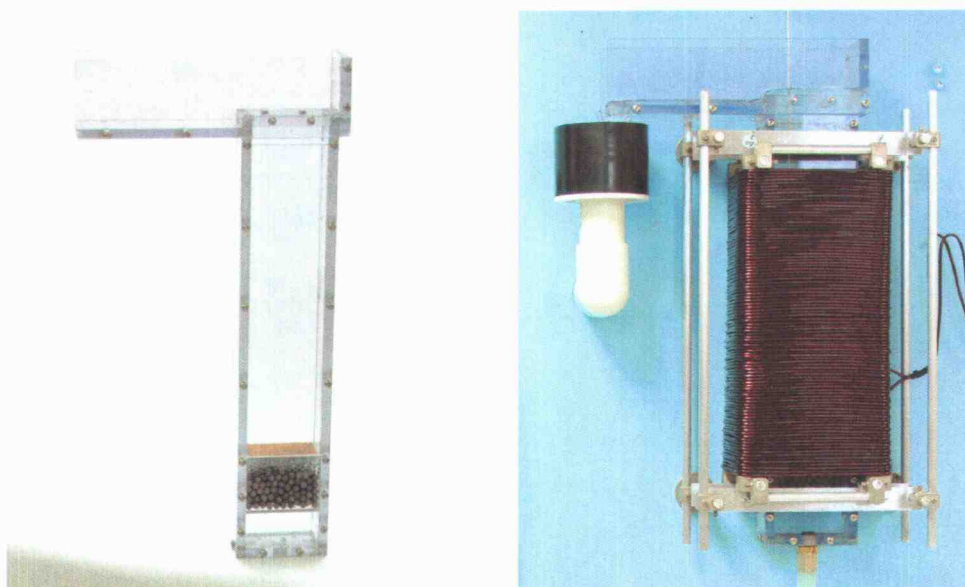


Figure 3.3 Fluidized bed. Alone (right) and mounted fluidized bed (left) with coil in place.

The bed has two calming zones at the bottom to distribute the flow evenly throughout the cross section of the bed (Figure 3.4). The division between the two calming zones is a perforated predistributor plate. The second calming zone contains ceramic and glass beads to distribute the flow uniformly in the cross section of the bed. A copper mesh forms the support (distributor) plate for the fluidized particles.



Figure 3.4 Close up of the calming zones and distributor plate.

The bed is open to the atmosphere at the top. This allows free access for the pressure probe and a free surface at constant atmospheric pressure.

3.1.2 *Flow system*

Water is pumped from the reservoir tank into the bed by a $\frac{1}{4}$ HP submersible centrifugal pump. The outflow of the bed is returned to the reservoir tank by an overflow channel and recirculation pipe, as shown in Figure 3.5.



Figure 3.5 Overflow and recycle.

Regulation of the flow is accomplished by a recirculation loop, two needle valves and two flow meters (4 and 10 liters per minute, for low and high flow rate ranges, respectively). Figure 3.6 shows a close up of the valves and flow meters. The calibration curve for the flow meter used in this study (10 LPM) is shown in Figure 3.7.

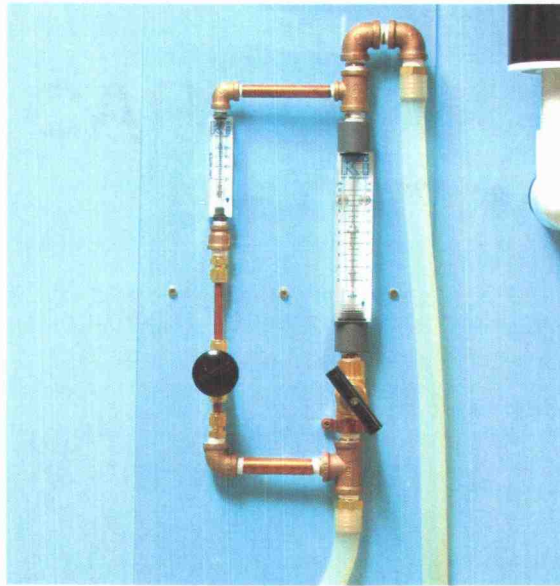


Figure 3.6 Close up of the flow meters.

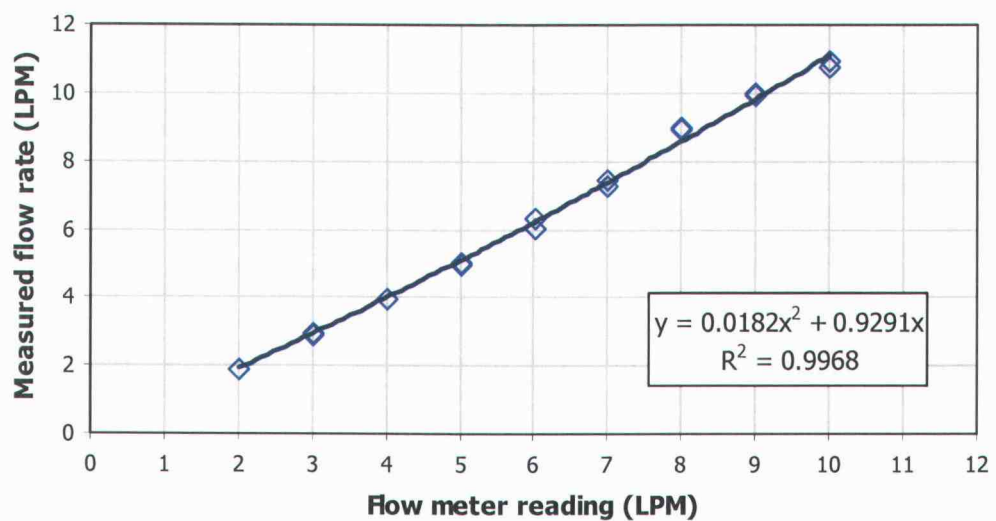


Figure 3.7 Calibration of the 10 LPM flow meter.

The flow rates used in this study, and the corresponding superficial velocities, are listed in Table 3.1. As the experimental data was gathered, it was decided to get an additional set of data at flow rate higher than 10 LPM. This was accomplished by setting the low-range flow meter at 3.5 LPM and the high-range flow meter at 10 LPM. To simplify the notation, the resulting flow rate is designated as 14 LPM.

Table 3.1 Flow rates used in this study

Nominal flow rate	Actual flow rate [m³/s]	Superficial velocity [m/s]
4 LPM	6.68×10^{-5}	0.0134
5 LPM	8.50×10^{-5}	0.0170
6 LPM	1.04×10^{-4}	0.0208
7 LPM	1.23×10^{-4}	0.0247
8 LPM	1.43×10^{-4}	0.0287
9 LPM	1.64×10^{-4}	0.0328
10 LPM	1.85×10^{-4}	0.0370
14 LPM	2.90×10^{-4}	0.0482

3.2 Magnetic field

The uniform magnetic field required for this study is generated by a single coil made of 6 gauge copper wire (polymer coating insulated). The wire was wrapped in a single layer around a frame built with aluminum rods, with a total of 105 turns. The coil dimensions are 0.203 by 0.127 by 0.445 m. The measured total resistance of the coil is 90 m Ω . The coil is connected to a DC electric power supply (8V 125A maximum output).

The magnetic field produced by the coil was measured with a gauss meter. The centerline field per unit electric current in the coil (B/I) is shown in Figure 3.8.

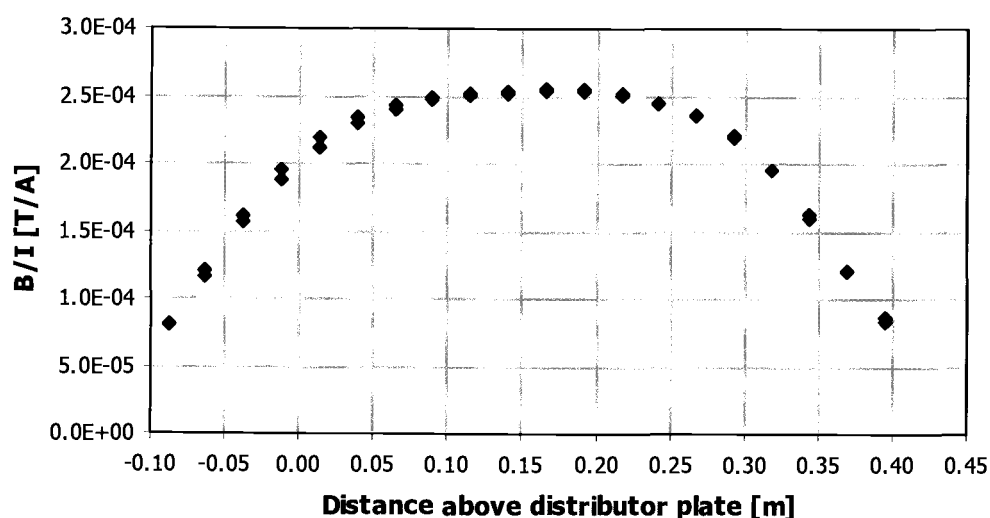


Figure 3.8 Magnetic field along the centerline of the coil. The region of uniform magnetic field is defined between 0.05 and 0.25 m above the distributor plate.

The region between 0.05 and 0.25 m, where the field varies by less than 5%, was chosen as the region of uniform field, where the experimental data will be obtained.

The electric currents used in this study, and the resulting magnetic fields, are listed in Table 3.2.

Table 3.2 Magnetic fields used in this study

Current [A]	Magnetic field [T]
5	0.00128
10	0.00256
20	0.00511
30	0.00767
40	0.0102
60	0.0153

3.3 Pressure measurement

3.3.1 Probe design

The pressure at different locations inside the operating bed is measured using a pressure probe built of 1/8 diameter steel tubing. The upper end of the probe is attached to a polycarbonate plate along with the sensing element (Figure 3.9). The probe is mounted above the bed (Figure 3.10), and can be moved up and down to any location. Grooves marked every centimeter along the tubing are used to determine the probe position.

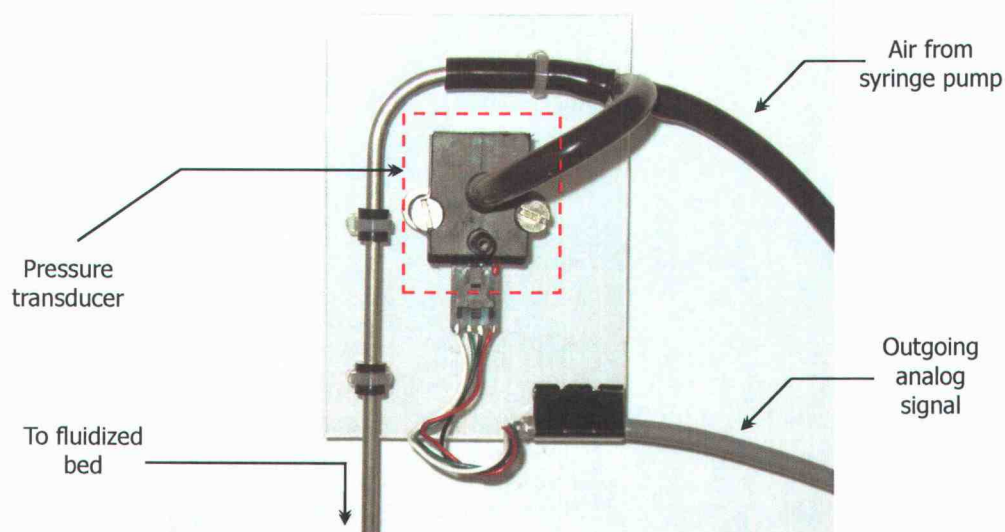


Figure 3.9 Close up of the pressure transducer.

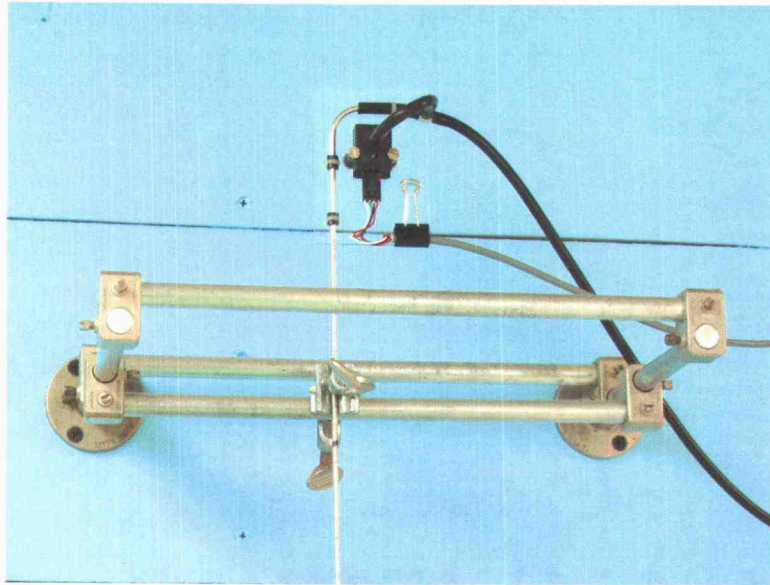


Figure 3.10 Close-up of the mounted pressure probe.

The sensing element is a piezoelectric pressure transducer with a differential range of ± 1.0 PSI (6.9 kPa). The transducer requires an excitation voltage of +5V and produces an analog output of ± 5 V that is sent to the data acquisition system.

A steady flow of air (approximately $0.4 \text{ cm}^3/\text{min}$) is supplied to the probe by a syringe pump. This prevents water from entering the probe as it is moved deeper into regions of higher pressure. The release of bubbles at the tip of the probe is taken into consideration when programming the data acquisition system (see below).

3.3.2 Data acquisition

The analog signal is digitized by a digital-analog data acquisition system, attached to the parallel port of a PC. The data is collected and analyzed using Visual Designer (commercial software). The analysis flow diagram is shown in Figure 3.11. Because of the bubbling at the tip of the probe, the pressure oscillates about its true value. The program records the maximum and minimum values of the pressure, and outputs their average.

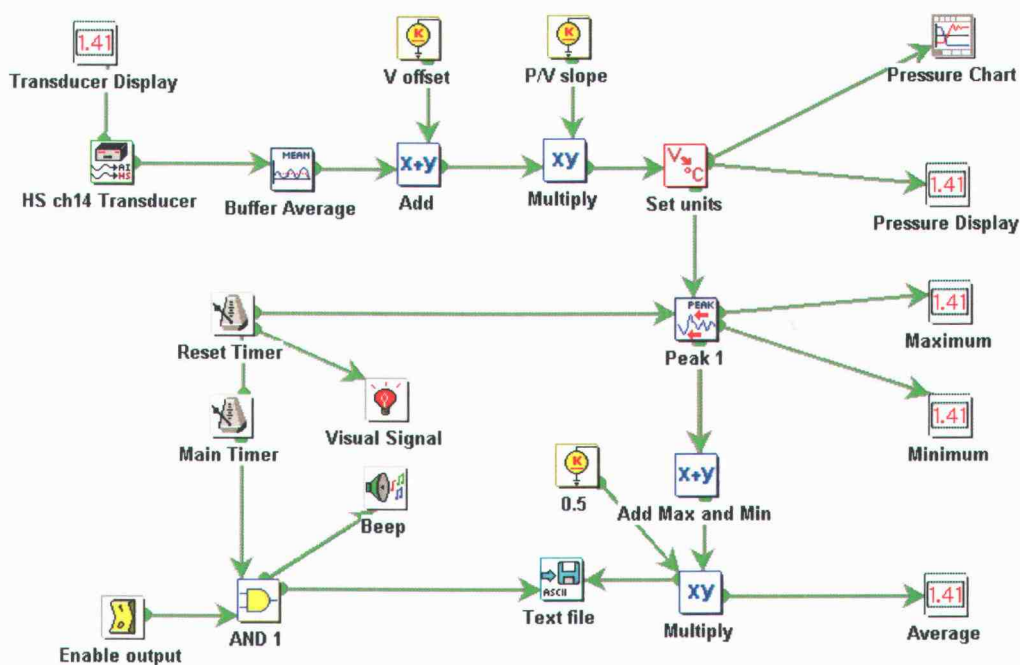


Figure 3.11 Visual Designer diagram for pressure data acquisition.

The use of two timers and audiovisual signals allow for a semi-automated data acquisition. When the program signals the operator, the probe can be moved to the next location. The program will wait a fixed period of time to allow the pressure signal to reach a steady value and then record the data in a text file. The signal is issued again and the process is repeated until all measurements have been done at the given operating conditions.

3.3.3 Probe calibration

The pressure probe is calibrated by submersion in water at different depths. The output voltage from the pressure transducer is then correlated with the known pressure at the probe's depth. The offset voltage and pressure/voltage slope are entered in the Visual Designer diagram as constant parameters. From the calibration data in Figure 3.12, the pressure is obtained from the transducer voltage as

$$P = 3514.9(V - 2.379) \quad (3.3-1)$$

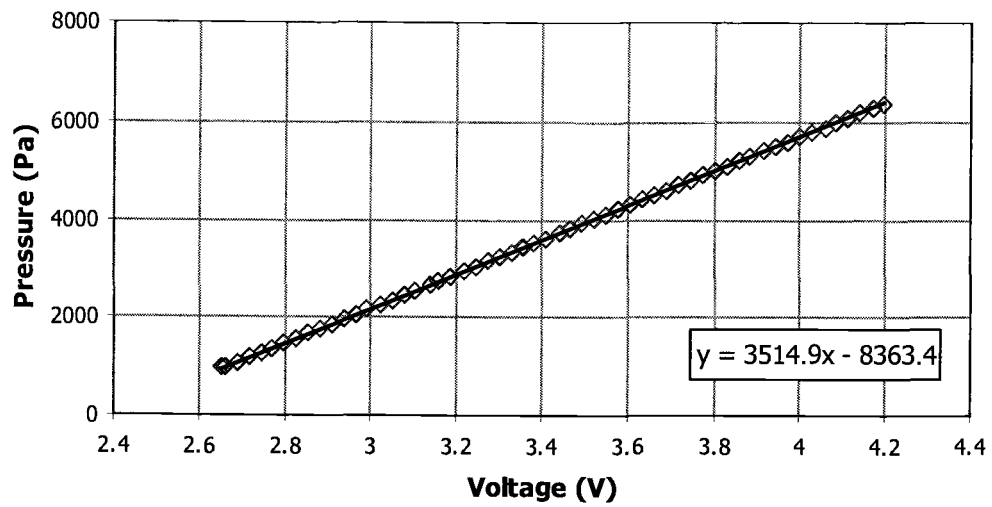


Figure 3.12 Pressure probe calibration data.

3.4 Fluidized media

Alginate-based composite beads are used as fluidized media. The magnetic susceptibility is provided by addition of ferrite powder, a soft ferrimagnetic material ($\rho = 5030 \text{ kg/m}^3$, $\chi = 11.1$; [21]).

3.4.1 *Production*

The composition of the beads is listed in Table 3.3. Three batches of 500 g each are prepared and extruded through a needle into droplets that are crosslinked in a 0.1 M calcium chloride solution. Additional details on the production of alginate beads can be found elsewhere [21, 26].

Table 3.3 Composition of the fluidized media

	Weight %
Sodium alginate	1.2%
Gellan gum	0.3%
Ferrite	10 %
DI Water	88.5 %

3.4.2 *Characterization*

Three properties of the particles are needed: particle size, density, and magnetic susceptibility. The size is measured by digital analysis of a high-resolution digital picture of a representative sample (Figure 3.13).

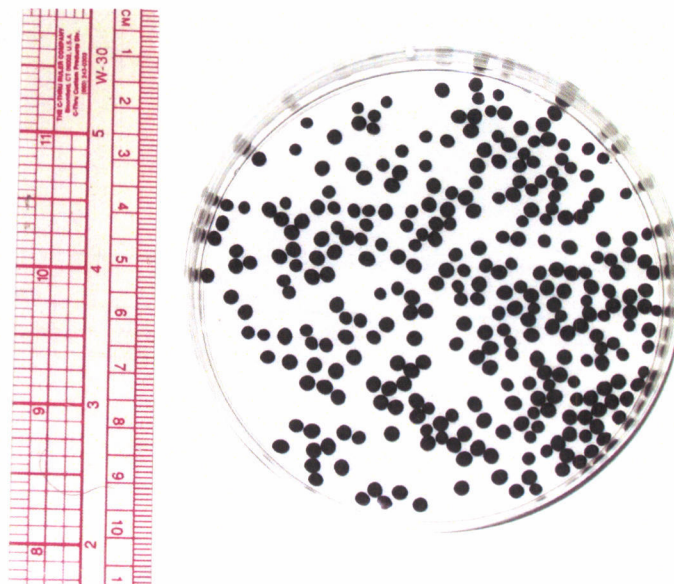


Figure 3.13 Sample of alginate beads used as fluidized media.

The average particle diameter is 2.63 mm (± 0.08 mm, 95% confidence interval, 49 degrees of freedom) with a sample standard deviation of 0.24 mm.

To measure density, a 100 ml volumetric flask is filled with the beads in DI water. By difference in weight with respect to the same flask filled with water, the volume of beads is obtained. Then, the beads are taken out of the flask, placed between two fine screens, and briefly blasted with air to remove the water exterior to the beads without causing significant drying. The beads are then weighted, and their density obtained from this weight and their volume. The density of the beads used in this study is determined as 1181 kg/m^3 ($\pm 21 \text{ kg/m}^3$, 95% confidence interval, 4 degrees of freedom) with a sample standard deviation of 17 kg/m^3 .

To determine the magnetic susceptibility of the particle, recall that the total dipole moment of the particle is related to the magnetization of the bead components as

$$\mathbf{m} = \int_{V_p} \mathbf{M} dV = \int_{V_{ferrite}} \mathbf{M}_{ferrite} dV + \int_{V_{alginate}} \mathbf{M}_{alginate} dV \quad (3.4-1)$$

where the alginate subscript refers to the alginate-gellan-water gel. Assuming that the ferrite is uniformly distributed and that the particle magnetization is uniform, and given that the other components are diamagnetic materials,

$$\mathbf{M}_p V_p = \mathbf{M}_{ferrite} V_{ferrite} \quad (3.4-2)$$

or, in terms of the ferrite volume fraction,

$$\mathbf{M}_p = \mathbf{M}_{ferrite} \Phi_{ferrite} \quad (3.4-3)$$

Since $\mathbf{M} = \chi \mathbf{H}$ and \mathbf{H} is the same for both particle and ferrite,

$$\chi_p = \chi_{ferrite} \Phi_{ferrite} \quad (3.4-4)$$

The volume fraction of ferrite in the beads is related to the weight fraction of ferrite as

$$\phi = \{\% [v/v]\} = \{\% [w/w]\} \frac{\rho_p}{\rho_{ferrite}} \quad (3.4-5)$$

Thus, the volume fraction of ferrite in the beads is 2.35%. The ferrite used has a magnetic susceptibility of 11.12 [21]. Therefore, and the particle magnetic susceptibility of the beads used in this study is 0.261.

CHAPTER 4

NUMERICAL SIMULATION

Denara: You're a computer simulation?
The Doctor: An *incredibly sophisticated* computer simulation.
— Star Trek Voyager,
“Lifesigns”

4.1 Overview

Previous research efforts by Pinto-Espinoza [21] led to the development of a 2D CFD-DPM code for simulation of liquid-solid fluidized beds. However, certain aspects of particulate-fluid systems cannot be properly represented with a two-dimensional model.

This situation prompted the development of a proprietary 3D CFD-DPM code for fluidization simulations (designated “Particle-X”). A general flowchart for Particle-X is presented in Figure 4.1. More information on this simulation code is presented in Appendix B.

After initialization, the program enters the main loop where the first step is the calculation of the voidage as the volume fraction of the cells not occupied by particles. If indicated, the voidage can be calculated in a coarser grid and then linearly interpolated for the fluid grid.

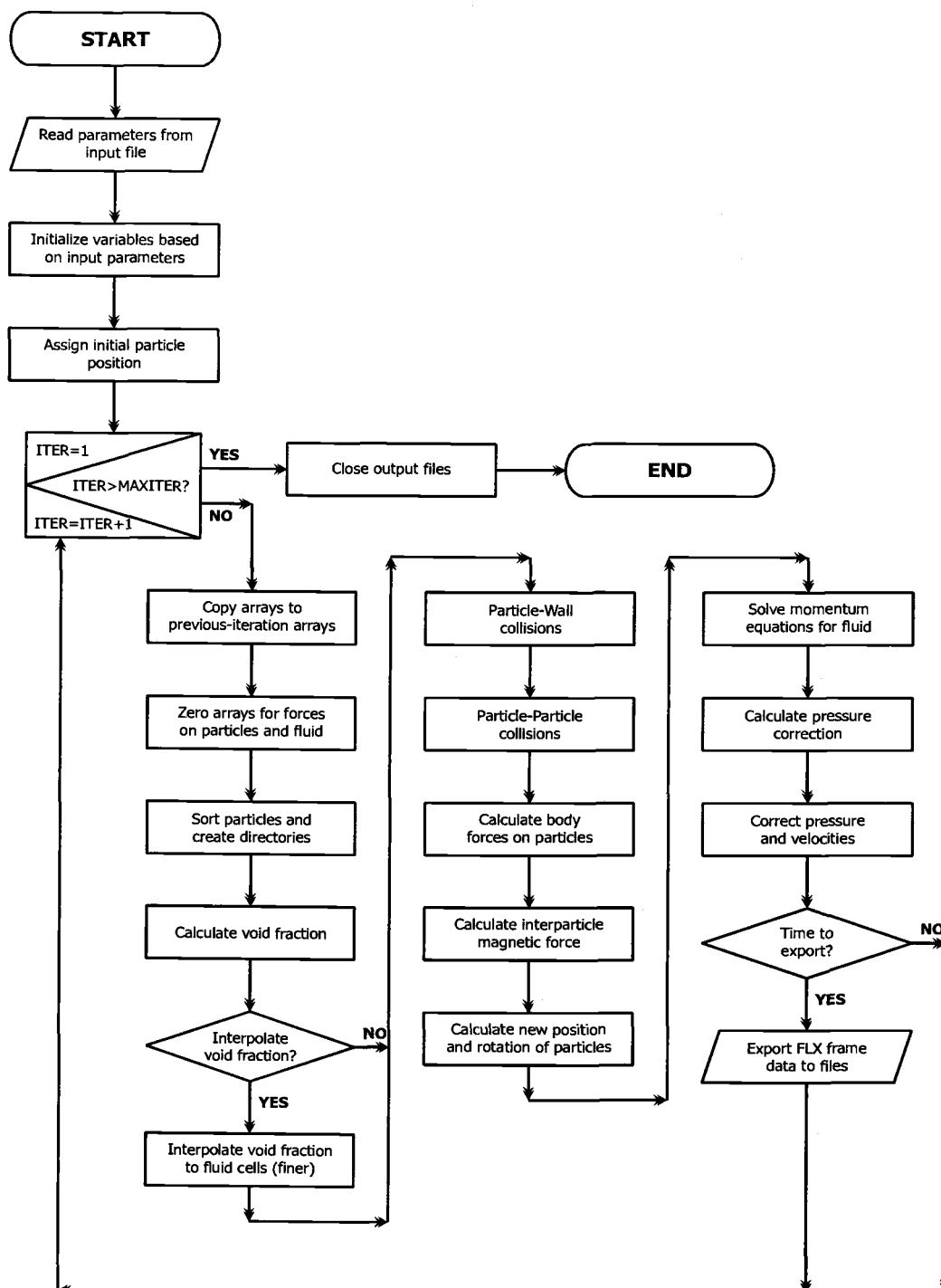


Figure 4.1 Particle-X fluidization simulation code, general flowchart.

Then, all the forces acting on the particles are calculated, including collisions and interparticle magnetic force (if a field is present). The equations of motion (translation and rotation) of the particles are integrated using the Forward Euler method or the second-order Adams-Bashforth method, depending on the user choice.

The fluid velocity and pressure are then calculated using the SIMPLE method (Semi-Implicit Model for Pressure Linked Equations, [20]). The solution domain is discretized in a uniform rectangular grid. A first order upwind scheme is used for the advection terms.

At regular intervals, as specified by user input, the data generated by the simulation code is stored as binary files using the FLU/FLX extensible fluidization data format [5] and visualized using Bolitas 2 [6]. Except for the most recent data, which is temporarily stored in the program cache, the results of the simulation can be visualized as the program runs. See Appendix C for more details on Bolitas 2.

The process is repeated for the next time step until the indicated total simulation time is reached.

4.2 Continuous phase

The transport equations for the fluid phase, presented in Chapter 2, are the continuity equation (Equation 4.2-1) and the momentum conservation equation (Equation 4.2-2),

$$\frac{\partial \varepsilon}{\partial t} + \nabla \cdot (\varepsilon \mathbf{u}) = 0 \quad (4.2-1)$$

$$\rho_f \frac{\partial}{\partial t} (\varepsilon \mathbf{u}) + \rho_f \nabla \cdot (\varepsilon \mathbf{u} \mathbf{u}) + \varepsilon \nabla P + \nabla \cdot (\varepsilon \boldsymbol{\tau}) - \varepsilon \rho_f \mathbf{g} - \mathbf{f} = 0 \quad (4.2-2)$$

subject to the following boundary conditions

- Inlet: $u_x = 0$, $u_y(t)$ given, $u_z = 0$, $\varepsilon = 1$
- Outlet: $u_x = 0$, $\frac{\partial u_y}{\partial y} = 0$, $u_z = 0$, $\varepsilon = 1$, $P = P_0$
- Walls: $u_x = 0$, $u_y = 0$, $u_z = 0$, $\varepsilon = 1$, $\frac{\partial P}{\partial x} = 0$, $\frac{\partial P}{\partial y} = -\rho_f g$, $\frac{\partial P}{\partial z} = 0$

Although physically correct, in practice the boundary condition $\varepsilon = 1$ is usually replaced by $\partial \varepsilon / \partial n = 0$, where n is the direction normal to the wall. This is justified by the finite size of the computational cell being larger than the particle size.

4.2.1 *Computational domain*

The computational domain for fluid flow (Figure 4.2) is divided in LI by LJ by LK cells in the x -, y -, and z -directions, respectively. Additional cells are created around this domain, as placeholder for boundary conditions. Pressure and voidage are calculated at the center of the fluid cells, and the fluid velocity is calculated normal to the faces of the cell. The cells for each of the components of momentum are staggered according to Figure 4.3.

Pressure, voidage, and velocities at other locations can be estimated by interpolation.

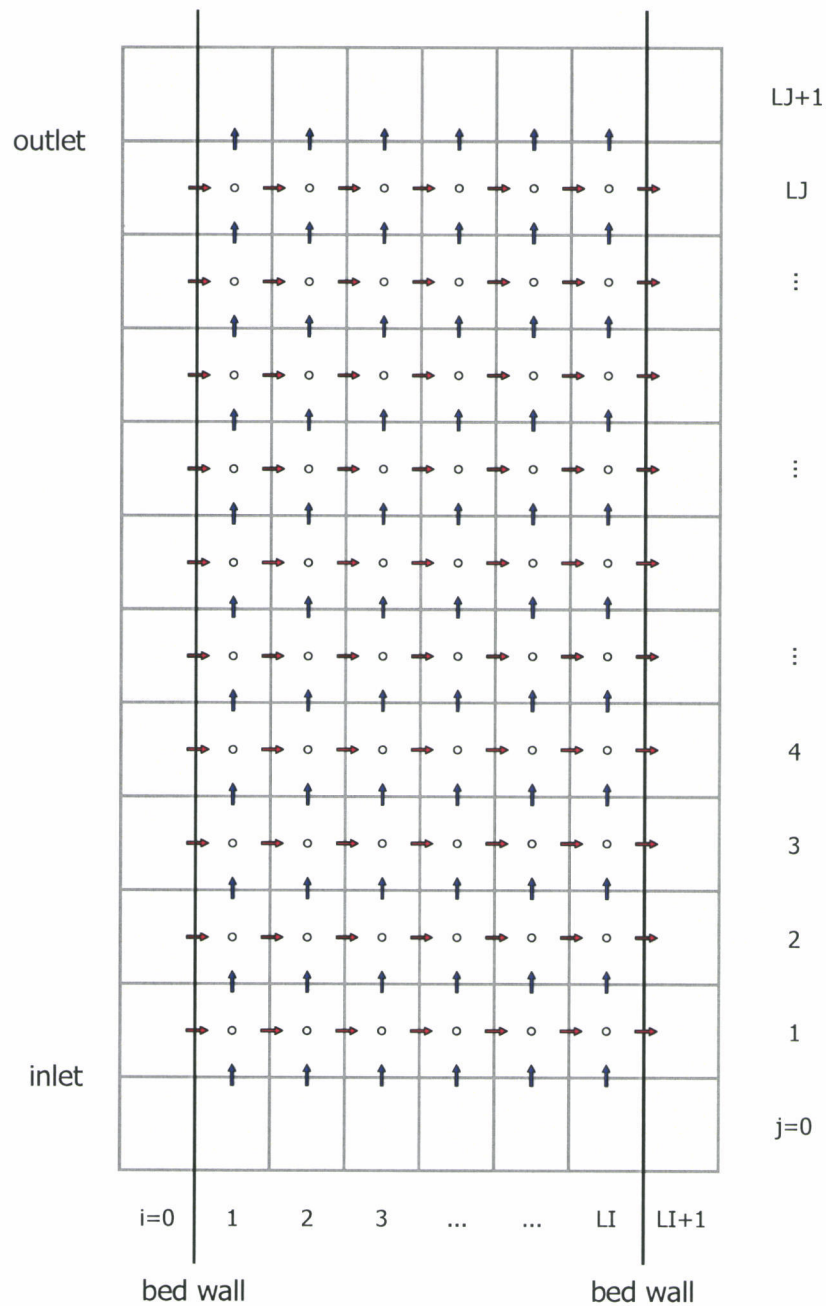


Figure 4.2 Computational domain for momentum transport. Pressure and voidage (circles) are calculated at the center of the cell; velocities (arrows) at the cell interfaces. Only the xy -plane is shown.

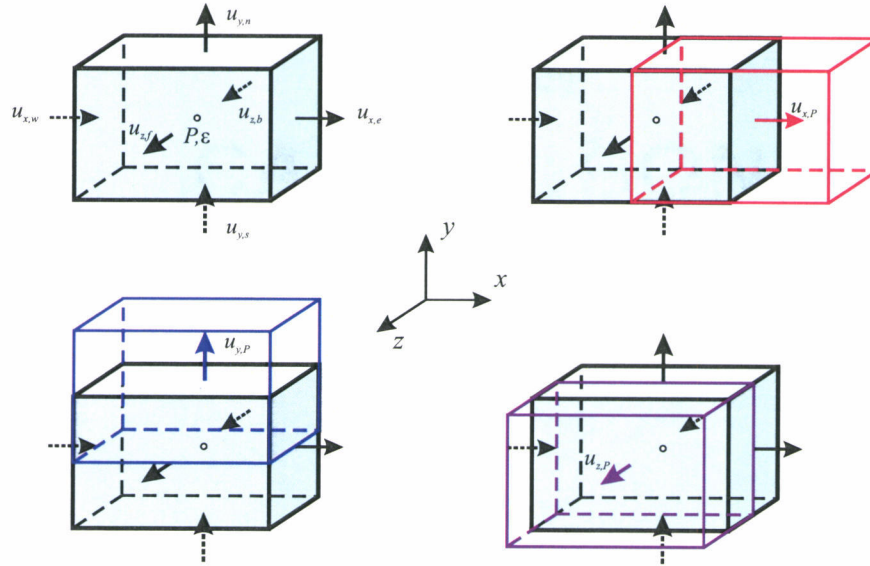


Figure 4.3 Staggered cells for momentum transport and their relation to the pressure correction cell. Top row: Fluid cell (left) and x -momentum cell (right). Bottom row: y -momentum (left) and z -momentum (right) cells.

4.2.2 The SIMPLE algorithm

The SIMPLE algorithm presented by Patankar [20] is used in this simulation for the coupled solution of mass and momentum equations. The key steps in this algorithm are

1. Start with a guessed pressure field P .
2. Solve the momentum conservation equation, to obtain the velocities u_x , u_y , and u_z . These velocities are only approximate, since they depend on the guessed P .

3. Use the mass conservation equation to calculate a pressure correction.
4. Use the pressure correction to correct pressure and velocities.
5. Treat the corrected pressure as the new guessed pressure, and return to step 1 for the next time step.

4.2.3 Discretization of the x -momentum equation

The x -component of Equation 4.2-2 is

$$\begin{aligned} \rho_f \frac{\partial}{\partial t}(\epsilon u_x) + \rho_f \frac{\partial}{\partial x}(\epsilon u_x u_x) + \rho_f \frac{\partial}{\partial y}(\epsilon u_x u_y) + \rho_f \frac{\partial}{\partial z}(\epsilon u_x u_z) + \epsilon \frac{\partial P}{\partial x} \\ + \frac{\partial}{\partial x}(\epsilon \tau_{xx}) + \frac{\partial}{\partial y}(\epsilon \tau_{yx}) + \frac{\partial}{\partial z}(\epsilon \tau_{zx}) - \epsilon \rho_f g_x - f_x = 0 \end{aligned} \quad (4.2-3)$$

This equation is formally integrated in space over the control volume. The resulting terms are replaced by approximations based on the values of the current and neighboring cells, and casted in the linear form

$$a_{x,P} u_{x,P} = a_{x,W} u_{x,W} + a_{x,E} u_{x,E} + a_{x,S} u_{x,S} + a_{x,N} u_{x,N} + a_{x,B} u_{x,B} + a_{x,F} u_{x,F} + b_x \quad (4.2-4)$$

The resulting system of equations (one for each x -momentum cell) are assembled in a matrix and solved by Successive Overrelaxation (SOR) for the new x -velocity profile.

The method is implicit with respect to the fluid velocities. For the advection terms, lagged coefficients are determined using the velocities from the previous time step. Also, the transient term will contain the velocity at the previous time step. Elsewhere, all velocities are those of the current time step.

The velocity inside the control volume is denoted by the subscript P. The neighboring velocities are denoted West/East (x -direction), South/North (y -direction) and Back/Front (z -direction). In general, upper-case subscripts refer to values centered at neighboring cells, and lower-case to cell interfaces.

The bookkeeping of neighboring velocities is essential for a successful discretization of the momentum equation. The control volume used, staggered half cell in the x -direction, is shown in Figure 4.4.

The discretization of the different terms in the x -momentum equation is exemplified in Appendix B. The resulting coefficients are summarized in Table 4.1.

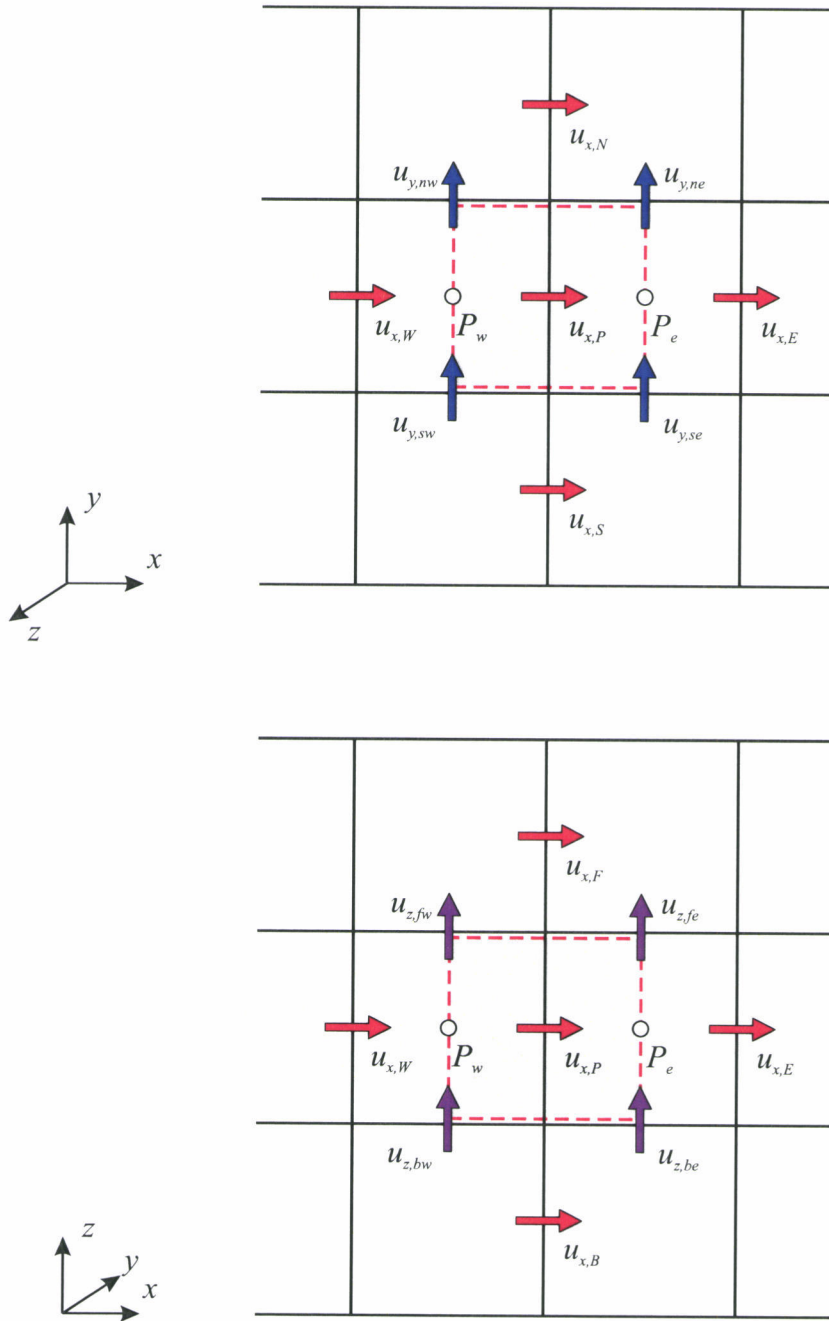


Figure 4.4 Control volume for x -momentum discretization.

Table 4.1 Coefficients of the discretized x -momentum equation

$$a_{x,P}u_{x,P} = a_{x,W}u_{x,W} + a_{x,E}u_{x,E} + a_{x,S}u_{x,S} + a_{x,N}u_{x,N} + a_{x,B}u_{x,B} + a_{x,F}u_{x,F} + b_x$$

Center	$a_{x,P} = a_{x,W} + a_{x,E} + a_{x,S} + a_{x,N} + a_{x,B} + a_{x,F} + \frac{\rho_f \varepsilon_P \Delta \mathcal{V}}{\Delta t}$ $+ \rho_f (\varepsilon_e u_{x,e} - \varepsilon_w u_{x,w}) \Delta y \Delta z + \rho_f (\varepsilon_n u_{y,n} - \varepsilon_s u_{y,s}) \Delta x \Delta z$ $+ \rho_f (\varepsilon_f u_{z,f} - \varepsilon_b u_{z,b}) \Delta x \Delta y$
West	$a_{x,W} = \rho_f \left[0, \varepsilon_w u_{x,w} \right] (\Delta y \Delta z) + \mu_f \left[2\varepsilon_w \frac{\Delta y \Delta z}{\Delta x} \right]$
East	$a_{x,E} = \rho_f \left[0, -\varepsilon_e u_{x,e} \right] (\Delta y \Delta z) + \mu_f \left[2\varepsilon_e \frac{\Delta y \Delta z}{\Delta x} \right]$
South	$a_{x,S} = \rho_f \left[0, \varepsilon_s u_{y,s} \right] (\Delta x \Delta z) + \mu_f \left[\varepsilon_s \frac{\Delta x \Delta z}{\Delta y} \right]$
North	$a_{x,N} = \rho_f \left[0, -\varepsilon_n u_{y,n} \right] (\Delta x \Delta z) + \mu_f \left[\varepsilon_n \frac{\Delta x \Delta z}{\Delta y} \right]$
Back	$a_{x,B} = \rho_f \left[0, \varepsilon_b u_{z,b} \right] (\Delta x \Delta y) + \mu_f \left[\varepsilon_b \frac{\Delta x \Delta y}{\Delta z} \right]$
Front	$a_{x,F} = \rho_f \left[0, -\varepsilon_f u_{z,f} \right] (\Delta x \Delta y) + \mu_f \left[\varepsilon_f \frac{\Delta x \Delta y}{\Delta z} \right]$
Independent	$b_x = \frac{\rho_f (\varepsilon_P u_{x,P}) \Big _{t-\Delta t} \Delta \mathcal{V}}{\Delta t} + \varepsilon_P (P_w - P_e) \Delta y \Delta z$ $+ \mu_f \left[\varepsilon_n (u_{y,ne} - u_{y,nw}) - \varepsilon_s (u_{y,se} - u_{y,sw}) \right] \Delta z$ $+ \mu_f \left[\varepsilon_f (u_{z,ef} - u_{z,wf}) - \varepsilon_b (u_{z,eb} - u_{z,wb}) \right] \Delta y$ $+ \varepsilon_P \rho_f g_x \Delta \mathcal{V} + F_x$

4.2.4 Discretization of the y -momentum equation

The y -component of the momentum equation is

$$\begin{aligned} \rho_f \frac{\partial}{\partial t}(\epsilon u_y) + \rho_f \frac{\partial}{\partial x}(\epsilon u_x u_y) + \rho_f \frac{\partial}{\partial y}(\epsilon u_y u_y) + \rho_f \frac{\partial}{\partial z}(\epsilon u_y u_z) + \epsilon \frac{\partial P}{\partial y} \\ + \frac{\partial}{\partial x}(\epsilon \tau_{yx}) + \frac{\partial}{\partial y}(\epsilon \tau_{yy}) + \frac{\partial}{\partial z}(\epsilon \tau_{yz}) - \epsilon \rho_f g_y - f_y = 0 \end{aligned} \quad (4.2-5)$$

The control volume for y -momentum is shown in Figure 4.5. The discretization of the different terms in Equation 4.2-5 is similar to the one presented in the Appendix B for the x -momentum equation. The coefficients obtained are summarized in Table 4.2.

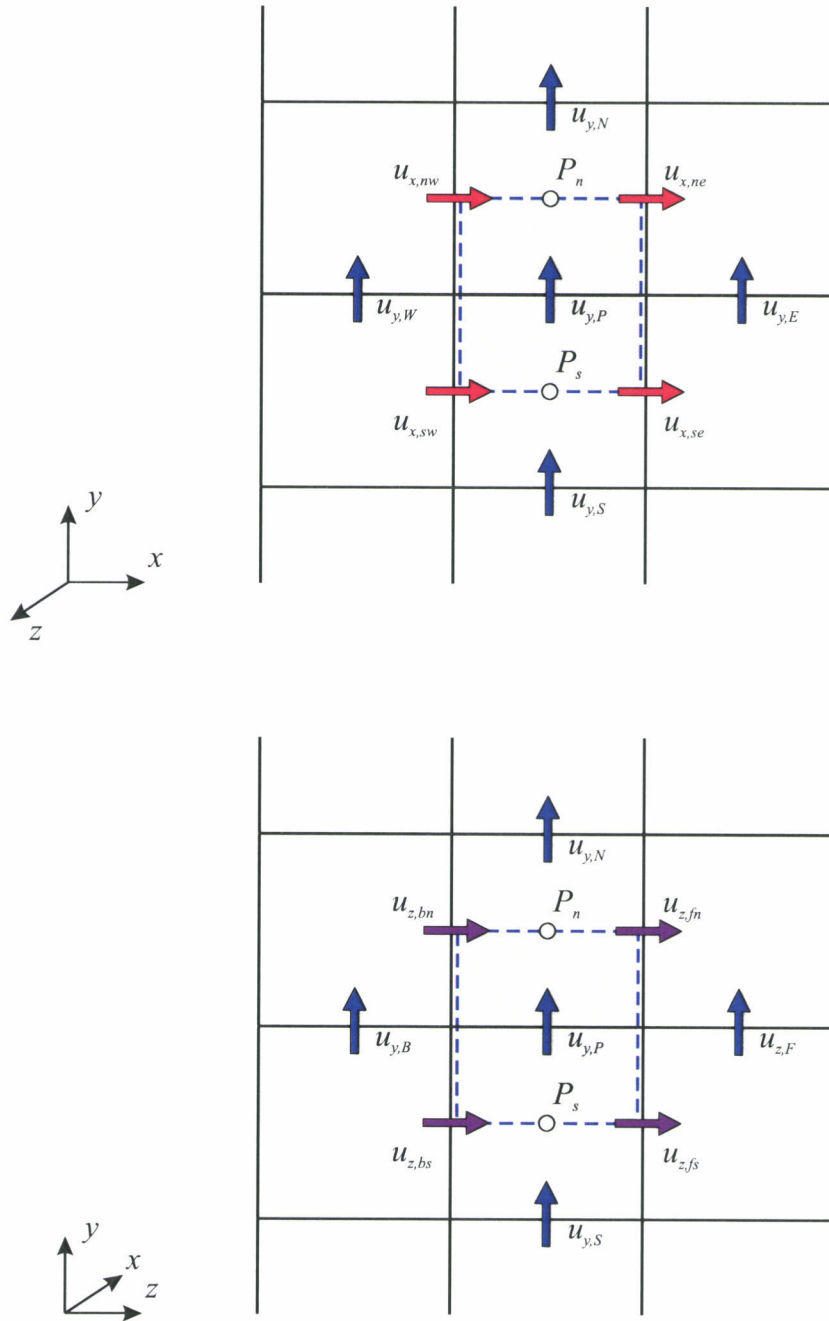


Figure 4.5 Control volume for y -momentum discretization.

Table 4.2 Coefficients of the discretized y -momentum equation

$$a_{y,P}u_{y,P} = a_{y,W}u_{y,W} + a_{y,E}u_{y,E} + a_{y,S}u_{y,S} + a_{y,N}u_{y,N} + a_{y,B}u_{y,B} + a_{y,F}u_{y,F} + b_y$$

Center	$a_{y,P} = a_{y,W} + a_{y,E} + a_{y,S} + a_{y,N} + a_{y,B} + a_{y,F} + \frac{\rho_f \varepsilon_P \Delta \mathcal{V}}{\Delta t}$ $+ \rho_f (\varepsilon_e u_{x,e} - \varepsilon_w u_{x,w}) \Delta y \Delta z + \rho_f (\varepsilon_n u_{y,n} - \varepsilon_s u_{y,s}) \Delta x \Delta z$ $+ \rho_f (\varepsilon_f u_{z,f} - \varepsilon_b u_{z,b}) \Delta x \Delta y$
West	$a_{y,W} = \rho_f \left[0, \varepsilon_w u_{x,w} \right] (\Delta y \Delta z) + \mu_f \left[\varepsilon_w \frac{\Delta y \Delta z}{\Delta x} \right]$
East	$a_{y,E} = \rho_f \left[0, -\varepsilon_e u_{x,e} \right] (\Delta y \Delta z) + \mu_f \left[\varepsilon_e \frac{\Delta y \Delta z}{\Delta x} \right]$
South	$a_{y,S} = \rho_f \left[0, \varepsilon_s u_{y,s} \right] (\Delta x \Delta z) + \mu_f \left[2\varepsilon_s \frac{\Delta x \Delta z}{\Delta y} \right]$
North	$a_{y,N} = \rho_f \left[0, -\varepsilon_n u_{y,n} \right] (\Delta x \Delta z) + \mu_f \left[2\varepsilon_n \frac{\Delta x \Delta z}{\Delta y} \right]$
Back	$a_{y,B} = \rho_f \left[0, \varepsilon_b u_{z,b} \right] (\Delta x \Delta y) + \mu_f \left[\varepsilon_b \frac{\Delta x \Delta y}{\Delta z} \right]$
Front	$a_{y,F} = \rho_f \left[0, -\varepsilon_f u_{z,f} \right] (\Delta x \Delta y) + \mu_f \left[\varepsilon_f \frac{\Delta x \Delta y}{\Delta z} \right]$
Independent	$b_y = \frac{\rho_f (\varepsilon_P u_{y,P}) \Big _{t-\Delta t} \Delta \mathcal{V}}{\Delta t} + \varepsilon_P (P_s - P_n) \Delta x \Delta z$ $+ \mu_f \left[\varepsilon_e (u_{x,ne} - u_{x,se}) - \varepsilon_w (u_{x,nw} - u_{x,sw}) \right] \Delta z$ $+ \mu_f \left[\varepsilon_f (u_{z,ef} - u_{z,wf}) - \varepsilon_b (u_{z,eb} - u_{z,wb}) \right] \Delta x$ $+ \varepsilon_P \rho_f g_y \Delta \mathcal{V} + F_y$

4.2.5 Discretization of the z -momentum equation

The z -component of the momentum equation is

$$\begin{aligned} \rho_f \frac{\partial}{\partial t}(\epsilon u_z) + \rho_f \frac{\partial}{\partial x}(\epsilon u_x u_z) + \rho_f \frac{\partial}{\partial y}(\epsilon u_y u_z) + \rho_f \frac{\partial}{\partial z}(\epsilon u_z u_z) + \epsilon \frac{\partial P}{\partial z} \\ + \frac{\partial}{\partial x}(\epsilon \tau_{xz}) + \frac{\partial}{\partial y}(\epsilon \tau_{yz}) + \frac{\partial}{\partial z}(\epsilon \tau_{zz}) - \epsilon \rho_f g_z - f_z = 0 \end{aligned} \quad (4.2-6)$$

The control volume for z -momentum is shown in Figure 4.6. The discretization of the different terms in Equation 4.2-6 leads to the coefficients summarized in Table 4.3.

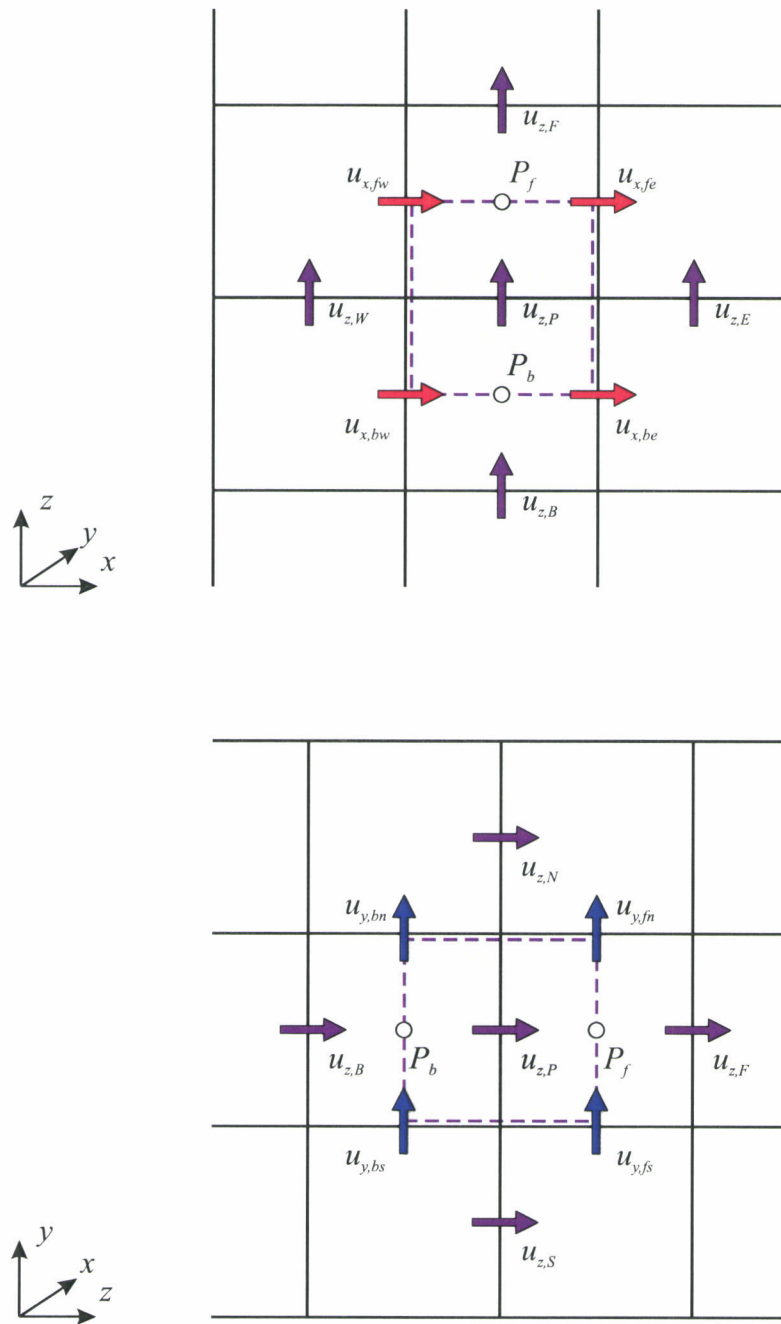


Figure 4.6 Control volume for z -momentum discretization.

Table 4.3 Coefficients of the discretized z -momentum equation

$$a_{z,P}u_{z,P} = a_{z,W}u_{z,W} + a_{z,E}u_{z,E} + a_{z,S}u_{z,S} + a_{z,N}u_{z,N} + a_{z,B}u_{z,B} + a_{z,F}u_{z,F} + b_z$$

Center	$a_{z,P} = a_{z,W} + a_{z,E} + a_{z,S} + a_{z,N} + a_{z,B} + a_{z,F} + \frac{\rho_f \varepsilon_P \Delta \mathcal{V}}{\Delta t}$ $+ \rho_f (\varepsilon_e u_{x,e} - \varepsilon_w u_{x,w}) \Delta y \Delta z + \rho_f (\varepsilon_n u_{y,n} - \varepsilon_s u_{y,s}) \Delta x \Delta z$ $+ \rho_f (\varepsilon_f u_{z,f} - \varepsilon_b u_{z,b}) \Delta x \Delta y$
West	$a_{z,W} = \rho_f \left[0, \varepsilon_w u_{x,w} \right] (\Delta y \Delta z) + \mu_f \left[\varepsilon_w \frac{\Delta y \Delta z}{\Delta x} \right]$
East	$a_{z,E} = \rho_f \left[0, -\varepsilon_e u_{x,e} \right] (\Delta y \Delta z) + \mu_f \left[\varepsilon_e \frac{\Delta y \Delta z}{\Delta x} \right]$
South	$a_{z,S} = \rho_f \left[0, \varepsilon_s u_{y,s} \right] (\Delta x \Delta z) + \mu_f \left[\varepsilon_s \frac{\Delta x \Delta z}{\Delta y} \right]$
North	$a_{z,N} = \rho_f \left[0, -\varepsilon_n u_{y,n} \right] (\Delta x \Delta z) + \mu_f \left[\varepsilon_n \frac{\Delta x \Delta z}{\Delta y} \right]$
Back	$a_{z,B} = \rho_f \left[0, \varepsilon_b u_{z,b} \right] (\Delta x \Delta y) + \mu_f \left[2\varepsilon_b \frac{\Delta x \Delta y}{\Delta z} \right]$
Front	$a_{z,F} = \rho_f \left[0, -\varepsilon_f u_{z,f} \right] (\Delta x \Delta y) + \mu_f \left[2\varepsilon_f \frac{\Delta x \Delta y}{\Delta z} \right]$
Independent	$b_z = \frac{\rho_f (\varepsilon_P u_{z,P}) \Big _{t-\Delta t} \Delta \mathcal{V}}{\Delta t} + \varepsilon_P (P_b - P_f) \Delta x \Delta y$ $+ \mu_f \left[\varepsilon_e (u_{x,fe} - u_{x,be}) - \varepsilon_w (u_{x,fw} - u_{x,bw}) \right] \Delta y$ $+ \mu_f \left[\varepsilon_n (u_{y,fn} - u_{z,bn}) - \varepsilon_s (u_{y,fs} - u_{y,bs}) \right] \Delta x$ $+ \varepsilon_P \rho_f g_z \Delta \mathcal{V} + F_z$

4.2.6 Pressure correction

The velocities calculated from the discretization of the momentum equation do not necessarily satisfy continuity, because the pressure field used may differ from the true pressure field. The pressure correction equation modifies the current pressure field so that the velocities are closer to satisfying the mass conservation equation. The control volume used to derive the pressure correction equation is shown in Figure 4.7.

The difference between the guessed pressure P^* and the real pressure P is called the *pressure correction*

$$P' = P - P^* \quad (4.2-7)$$

The velocities can be corrected in the same fashion, defining

$$u'_x = u_x - u_x^* \quad (4.2-8)$$

$$u'_y = u_y - u_y^*$$

$$u'_z = u_z - u_z^* \quad (4.2-9)$$

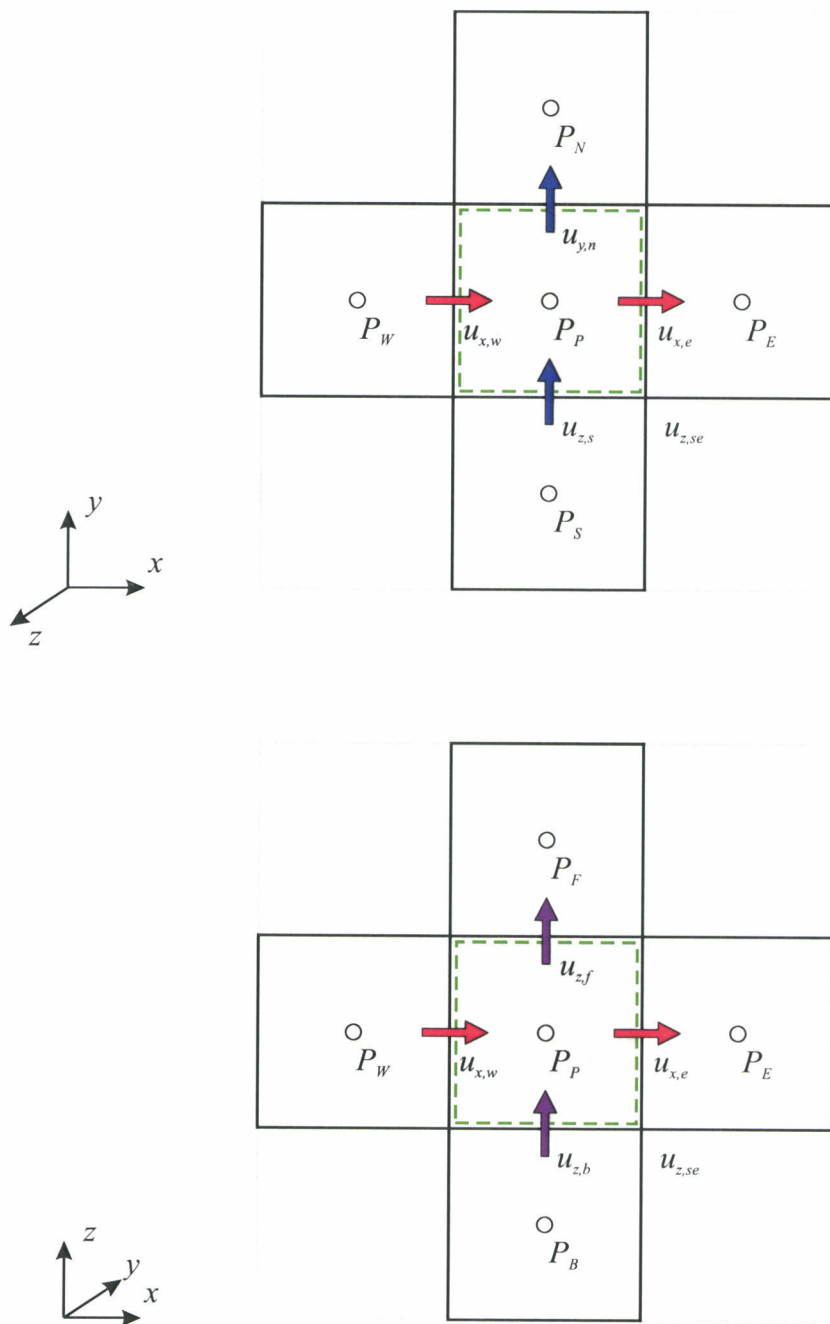


Figure 4.7 Control volume for pressure correction.

Now consider, for instance, the x -momentum balance that was performed for the velocity $u_{x,e}$ as shown in Figure 4.8. It can be written as

$$a_e u_{x,e} = \sum_{\text{adjacent cells}} a u_x + A_e (P_P - P_E) + b \quad (4.2-10)$$

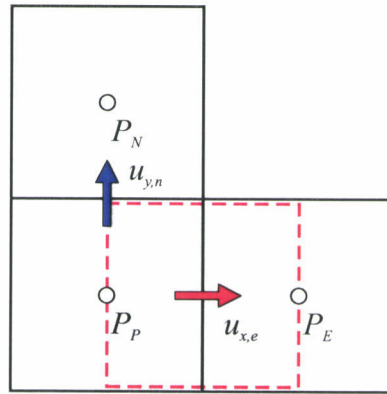


Figure 4.8 Momentum balance for pressure correction.

Note the change in notation, from $u_{x,P}$ to $u_{x,e}$. Equation 4.2-10 will hold true only if the correct pressures are used in the momentum balance. When the guessed pressures are used, the obtained velocities are only approximate

$$a_e u_{x,e}^* = \sum_{\text{adjacent cells}} a u_{x,e}^* + A_e (P_P^* - P_E^*) + b \quad (4.2-11)$$

Subtracting Equation 4.2-11 from Equation 4.2-10,

$$a_e u'_{x,e} = \sum_{\text{adjacent cells}} a u'_x + A_e (P'_P - P'_E) \quad (4.2-12)$$

In the SIMPLE method, [20] the contribution of the adjacent cells is ignored (hence the designation "Semi Implicit"). This omission is acceptable since the pressure correction is just a tool for satisfying continuity. The final converged solution is not affected by the omission. Therefore, Equation 4.2-12 simplifies to

$$u'_{x,e} = \frac{A_e}{a_e} (P'_P - P'_E) \quad (4.2-13)$$

Defining the geometrical factor $\lambda_e \equiv A_e / a_e$, the velocity correction is just $u'_{x,e} = \lambda_e (P'_P - P'_E)$ and the corrected velocity is

$$u_{x,e} = u_{x,e}^* + \lambda_e (P'_P - P'_E) \quad (4.2-14)$$

Proceeding likewise in the other two directions yields

$$u_{y,n} = u_{y,n}^* + \lambda_n (P'_P - P'_N) \quad (4.2-15)$$

$$u_{z,f} = u_{z,f}^* + \lambda_f (P'_P - P'_F) \quad (4.2-16)$$

To find the pressure correction P' , the mass conservation equation is formally integrated over the control volume shown in Figure 4.7.

$$\frac{\partial \varepsilon}{\partial t} + \nabla \cdot (\varepsilon \mathbf{u}) = 0 \quad (4.2-17)$$

$$\int_{\Delta \mathcal{V}} \frac{\partial \varepsilon}{\partial t} d\mathcal{V} + \int_{\Delta \mathcal{V}} \nabla \cdot (\varepsilon \mathbf{u}) d\mathcal{V} = 0 \quad (4.2-18)$$

$$\frac{\partial}{\partial t} \int_{\Delta \mathcal{V}} \varepsilon d\mathcal{V} + \oint_{\Delta \mathcal{S}} (\varepsilon \mathbf{u}) \cdot d\bar{\mathcal{S}} = 0$$

$$\begin{aligned} \frac{\partial}{\partial t} \int_{\Delta \mathcal{V}} \varepsilon d\mathcal{V} + \int_e (\varepsilon u_x) d\mathcal{S} - \int_w (\varepsilon u_x) d\mathcal{S} + \int_n (\varepsilon u_y) d\mathcal{S} \\ - \int_s (\varepsilon u_y) d\mathcal{S} + \int_f (\varepsilon u_z) d\mathcal{S} - \int_b (\varepsilon u_z) d\mathcal{S} = 0 \end{aligned}$$

$$\begin{aligned} \frac{\varepsilon_P - \varepsilon_P|_{t-\Delta t}}{\Delta t} + (\varepsilon_e u_{x,e} - \varepsilon_w u_{x,w}) \Delta y \Delta z + (\varepsilon_n u_{y,n} - \varepsilon_s u_{y,s}) \Delta x \Delta z \\ + (\varepsilon_f u_{z,f} - \varepsilon_b u_{z,b}) \Delta x \Delta y = 0 \end{aligned} \quad (4.2-19)$$

Now, Equations 4.2-14 through 4.2-16 (along with the corresponding to $u_{x,w}$, $u_{y,s}$, and $u_{z,b}$) are substituted into the discretized mass conservation equation, Equation 4.2-19. After collecting terms, it is cast into the form

$$a_P P'_P = a_W P'_W + a_E P'_E + a_S P'_S + a_N P'_N + a_B P'_B + a_F P'_F + b \quad (4.2-20)$$

where the coefficients are given in Table 4.4. The resulting system of linear equations is solved by SOR and the obtained pressure correction is added to the pressure and used to correct radial and axial velocities.

Table 4.4 Coefficients of the discretized pressure correction equation

$$a_P P'_P = a_W P'_W + a_E P'_E + a_S P'_S + a_N P'_N + a_B P'_B + a_F P'_F + b$$

Center	$a = a_W + a_E + a_S + a_N + a_B + a_F$
West	$a_W = \varepsilon_w \lambda_w \Delta y \Delta z$
East	$a_E = \varepsilon_e \lambda_e \Delta y \Delta z$
South	$a_S = \varepsilon_s \lambda_s \Delta x \Delta z$
North	$a_N = \varepsilon_n \lambda_n \Delta x \Delta z$
Back	$a_B = \varepsilon_b \lambda_b \Delta x \Delta y$
Front	$a_F = \varepsilon_f \lambda_f \Delta x \Delta y$
Independent	$b = -\frac{\varepsilon_P - \varepsilon_P _{t-\Delta t}}{\Delta t} - (\varepsilon_e u_{x,e} - \varepsilon_w u_{x,w}) \Delta y \Delta z$ $- (\varepsilon_n u_{y,n} - \varepsilon_s u_{y,s}) \Delta x \Delta z - (\varepsilon_f u_{z,f} - \varepsilon_b u_{z,b}) \Delta x \Delta y$

Note that the independent term is just the negative of the discretized continuity equation. This is the mass residual used to verify convergence of the solution.

The boundary conditions for the pressure correction [20] are

- Velocity at the inlet is known. The coefficient for P'_S is set to zero for the first row of cells at the inlet.
- Velocity at the wall is known. The coefficients of all ghost cells at the walls are set to zero.
- Pressure at outlet is known. For these cells no pressure correction equation is needed, therefore $P'_p = 0$.

4.3 Particle phase

4.3.1 Selection of the time step

In CFD-DPM simulations implementing the soft sphere model, the collisions between particles usually dictate the maximum time step. To accurately capture a collision, it has been recommended [28] using a time step of one tenth of the natural oscillation period of the spring-mass element in the collision model (see Section 2.2.8). Thus, the maximum allowable time step is

$$\Delta t_{\max} = \frac{1}{10} 2\pi \sqrt{\frac{m_p}{k_n}} \quad (4.2-21)$$

If the time step indicated by the user is greater than this maximum, a warning is issued.

4.3.2 *Integration of the equations of motion*

The forces acting on each particle are calculated directly from the equations presented in Chapter 2. The particle acceleration is then calculated as $\mathbf{a} = \mathbf{F} / m_p$. The acceleration is integrated to get the particle velocity. Depending on the user choice, integration is done using the forward Euler method,

$$\mathbf{v}|_{t+\Delta t} = \mathbf{v}|_t + \mathbf{a}|_t \Delta t \quad (4.2-22)$$

or the second-order Adams-Bashforth method (an explicit multistep method)

$$\mathbf{v}|_{t+\Delta t} = \mathbf{v}|_t + (3\mathbf{a}|_t - \mathbf{a}|_{t-\Delta t}) \Delta t \quad (4.2-23)$$

The region of absolute stability of the Adams-Bashforth method is smaller than forward Euler, but still large enough for these simulation cases. Preliminary tests implementing a third-order A-B yielded unstable solutions, however.

After the velocities are calculated, a second integration step gives the particle position. Likewise, the angular acceleration ($\bar{\alpha} = \mathbf{T}/I_p$) is integrated to obtain the particle angular velocity.

The initial conditions for motion of the particles are:

- $\mathbf{x}_i(0)$ given, $\mathbf{v}_i(0) = 0$
- $\bar{\omega}_i(0) = 0$

Forward Euler is used as starting step for the second-order Adam-Bashfort during the first iteration.

CHAPTER 5

RESULTS AND ANALYSIS

Kai Opaka: Prophecy can often be vague, Commander.
That's why we must test it.

— Star Trek: Deep Space Nine,
“Battle Lines”

5.1 Pressure drop measurements

Figures 5.1 and 5.2 are representative samples of the experimental data collected. They correspond to the same flow rate (8 LPM) at the two extremes of the magnetic field applied (corresponding to currents of 0 and 60A, respectively). The bed height, as determined by visual inspection from the top of the bed, is marked by a dashed line. The graphs corresponding to all other experimental runs can be found in Appendix D.

As anticipated, the application of the magnetic field, and the consequent formation of particle chains, cause a decrease in the average drag coefficient. The bed height is reduced.

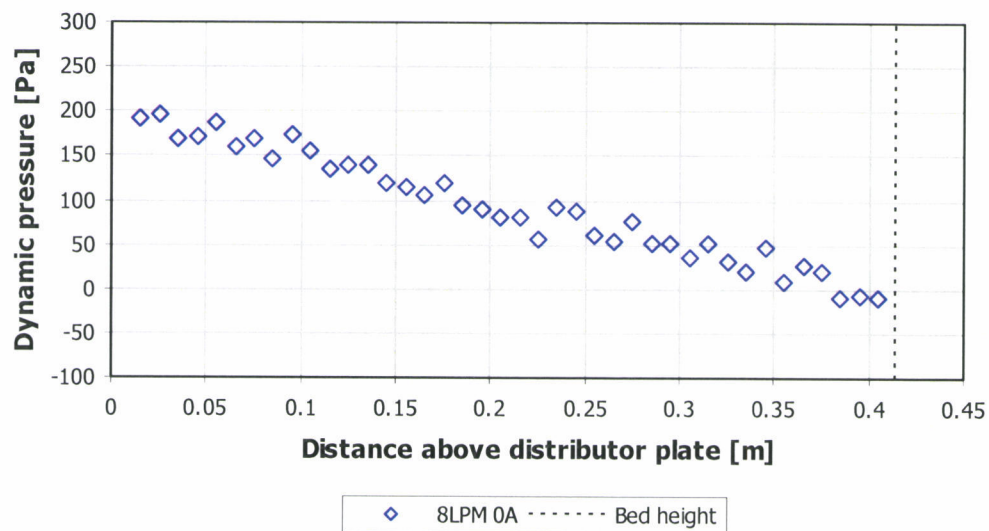


Figure 5.1 Dynamic pressure data for $u_0 = 0.0287$ m/s and $B_0 = 0$.

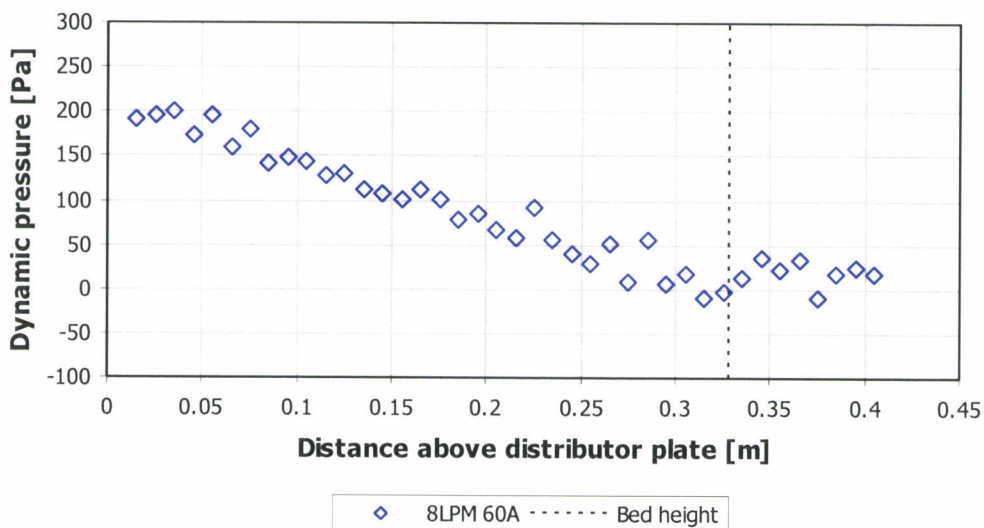


Figure 5.2 Dynamic pressure data for $u_0 = 0.0287$ m/s and $B_0 = 15.3$ mT.

The dynamic (frictional) pressure is defined as the difference between the measured fluid pressure under operating conditions and the static pressure

$$P_d = P - P_h - \rho g(y - h) \quad (5.1-1)$$

where h and P_h are the bed height and the pressure at the top of the bed.

The gradient of the dynamic pressure in the fluidized bed is related to the buoyant weight of the suspended particles [12, 13] as

$$-\frac{dP_d}{dy} = [\rho_p(1-\varepsilon) + \rho_f\varepsilon]g - \rho_f g = (1-\varepsilon)(\rho_p - \rho_f)g \quad (5.1-1)$$

This equation is sometimes referred to as the *manometer formula*. Solving for the voidage,

$$\varepsilon = 1 - \frac{-\frac{dP_d}{dy}}{(\rho_p - \rho_f)g} \quad (5.1-2)$$

The slope of the dynamic pressure gradient is obtained by linear regression of the experimental data between $y = 0.05\text{m}$ and $y = 0.25\text{m}$ (the region of uniform magnetic field) as exemplified in Figures 5.3 and 5.4. This slope is used in Equation 5.1-2 to estimate the voidage.

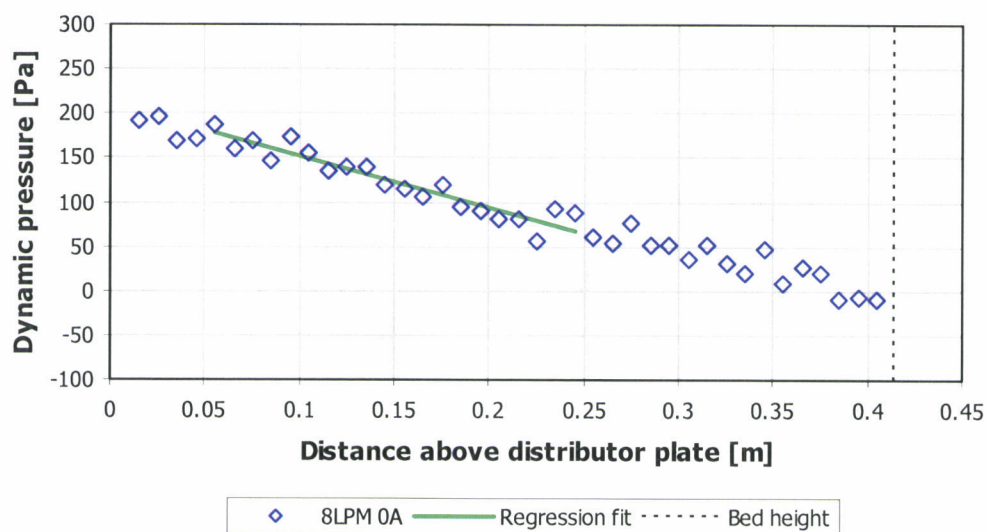


Figure 5.3 Dynamic pressure data for $u_0 = 0.0287$ m/s and $B_0 = 0$. The calculated voidage is $\varepsilon = 0.68$.

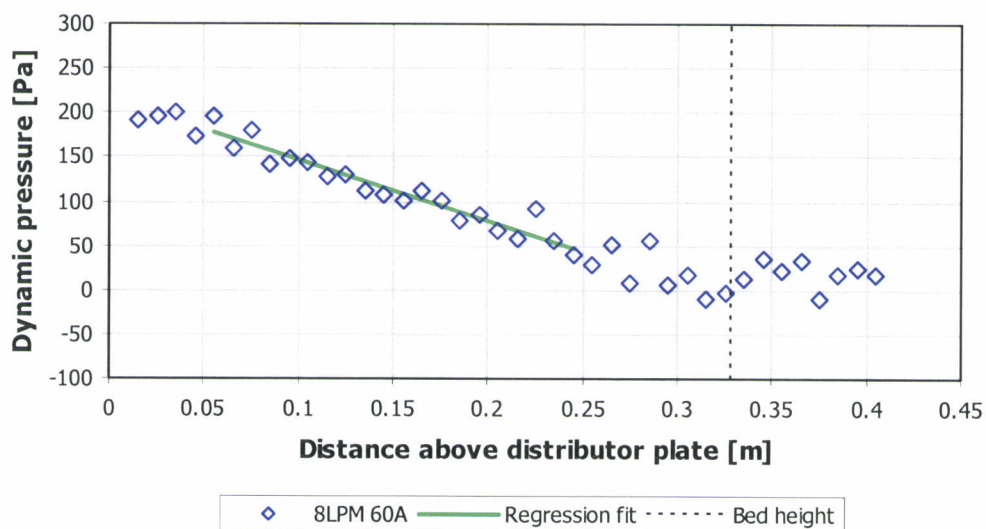


Figure 5.4 Dynamic pressure data for $u_0 = 0.0287$ m/s and $B_0 = 15.3$ mT. The calculated voidage is $\varepsilon = 0.62$.

The estimated voidage, along with the relevant operating conditions for all cases, are listed in Table 5.1. An estimate of the particle Reynolds number is obtained from the superficial velocity and the estimated voidage as

$$\text{Re}_p = \frac{\rho(u_0/\varepsilon)d_p}{\mu} \quad (5.1-3)$$

and the chain strength parameter B is calculated as the ratio of the maximum interparticle attractive force (from the ideal dipole model discussed in Chapter 2) and the buoyant weight of the particle.

$$B = \frac{|F_{IM,\max}|}{(\rho_p - \rho_f)gV_p} \quad (5.1-4)$$

$$|F_{IM,\max}| = \frac{6\mu_0 m^2}{4\pi d_p^4} \quad (5.1-5)$$

The correction factor for the drag coefficient that matches the experimentally determined voidage and particle Reynolds number is also listed in Table 5.1.

Table 5.1 Experimental estimates of voidage and drag reduction factor

Case	u_0 [m/s]	B_0 [T]	ε [-]	Re_p [-]	β [-]	Δ [-]
4LPM 0A	0.0134	0	0.530	74.2	0	1.0000
4LPM 5A	0.0134	0.00128	0.528	74.4	0.0040	0.9674
4LPM 10A	0.0134	0.00256	0.523	75.1	0.0161	0.9257
4LPM 20A	0.0134	0.00511	0.521	75.4	0.0644	0.9092
4LPM 30A	0.0134	0.00767	0.516	76.2	0.1450	0.8690
4LPM 40A	0.0134	0.0102	0.505	77.8	0.2577	0.7853
4LPM 60A	0.0134	0.0153	0.503	78.1	0.5800	0.7707
5LPM 0A	0.0170	0	0.576	86.6	0	1.0000
5LPM 5A	0.0170	0.00128	0.578	86.3	0.0040	1.0000
5LPM 10A	0.0170	0.00256	0.576	86.6	0.0161	0.9958
5LPM 20A	0.0170	0.00511	0.571	87.3	0.0644	0.9550
5LPM 30A	0.0170	0.00767	0.551	90.5	0.1450	0.8072
5LPM 40A	0.0170	0.0102	0.539	92.5	0.2577	0.7263
5LPM 60A	0.0170	0.0153	0.537	92.9	0.5800	0.7136
6LPM 0A	0.0208	0	0.613	99.5	0	0.9644
6LPM 5A	0.0208	0.00128	0.618	98.7	0.0040	1.0000
6LPM 10A	0.0208	0.00256	0.618	98.7	0.0161	1.0000
6LPM 20A	0.0208	0.00511	0.604	101.0	0.0644	0.8984
6LPM 30A	0.0208	0.00767	0.595	102.5	0.1450	0.8369
6LPM 40A	0.0208	0.0102	0.578	105.5	0.2577	0.7279
6LPM 60A	0.0208	0.0153	0.549	111.1	0.5800	0.5692
7LPM 0A	0.0247	0	0.656	110.4	0	1.0000
7LPM 5A	0.0247	0.00128	0.648	111.8	0.0040	0.9484
7LPM 10A	0.0247	0.00256	0.646	112.1	0.0161	0.9345
7LPM 20A	0.0247	0.00511	0.646	112.1	0.0644	0.9345
7LPM 30A	0.0247	0.00767	0.637	113.7	0.1450	0.8744
7LPM 40A	0.0247	0.0102	0.604	119.9	0.2577	0.6766
7LPM 60A	0.0247	0.0153	0.585	123.8	0.5800	0.5804

Table 5.1 (Continued)

Case	u_0 [m/s]	B_0 [T]	ε [-]	Re_p [-]	B [-]	Δ [-]
8LPM 0A	0.0287	0	0.680	123.8	0	1.0000
8LPM 5A	0.0287	0.00128	0.684	123.1	0.0040	0.9608
8LPM 10A	0.0287	0.00256	0.691	121.8	0.0161	1.0000
8LPM 20A	0.0287	0.00511	0.678	124.2	0.0644	0.9205
8LPM 30A	0.0287	0.00767	0.662	127.2	0.1450	0.8207
8LPM 40A	0.0287	0.0102	0.650	129.5	0.2577	0.7513
8LPM 60A	0.0287	0.0153	0.622	135.3	0.5800	0.6073
9LPM 0A	0.0328	0	0.727	132.3	0	1.0000
9LPM 5A	0.0328	0.00128	0.717	134.2	0.0040	0.9663
9LPM 10A	0.0328	0.00256	0.713	134.9	0.0161	0.9412
9LPM 20A	0.0328	0.00511	0.706	136.3	0.0644	0.8969
9LPM 30A	0.0328	0.00767	0.697	138.0	0.1450	0.8435
9LPM 40A	0.0328	0.0102	0.672	143.2	0.2577	0.7061
9LPM 60A	0.0328	0.0153	0.633	152.0	0.5800	0.5280
10LPM 0A	0.0370	0	0.751	144.5	0	1.0000
10LPM 5A	0.0370	0.00128	0.755	143.7	0.0040	1.0000
10LPM 10A	0.0370	0.00256	0.752	144.3	0.0161	0.9965
10LPM 20A	0.0370	0.00511	0.742	146.3	0.0644	0.9346
10LPM 30A	0.0370	0.00767	0.723	150.1	0.1450	0.8242
10LPM 40A	0.0370	0.0102	0.701	154.8	0.2577	0.7085
10LPM 60A	0.0370	0.0153	0.669	162.2	0.5800	0.5646
14LPM 0A	0.0482	0	0.824	171.6	0	1.0000
14LPM 5A	0.0482	0.00128	0.818	172.8	0.0040	0.9660
14LPM 10A	0.0482	0.00256	0.814	173.7	0.0161	0.9432
14LPM 20A	0.0482	0.00511	0.809	174.7	0.0644	0.9153
14LPM 30A	0.0482	0.00767	0.790	179.0	0.1450	0.8151
14LPM 40A	0.0482	0.0102	0.766	184.6	0.2577	0.7005
14LPM 60A	0.0482	0.0153	0.736	192.1	0.5800	0.5761

5.2 Model selection

A preliminary exploratory analysis of the data is used to determine the functional relationship between the possible explanatory variables (as determined in Chapter 2) and the observed drag coefficient reduction. The starting point is the matrix of scatterplots shown in Figure 5.5.

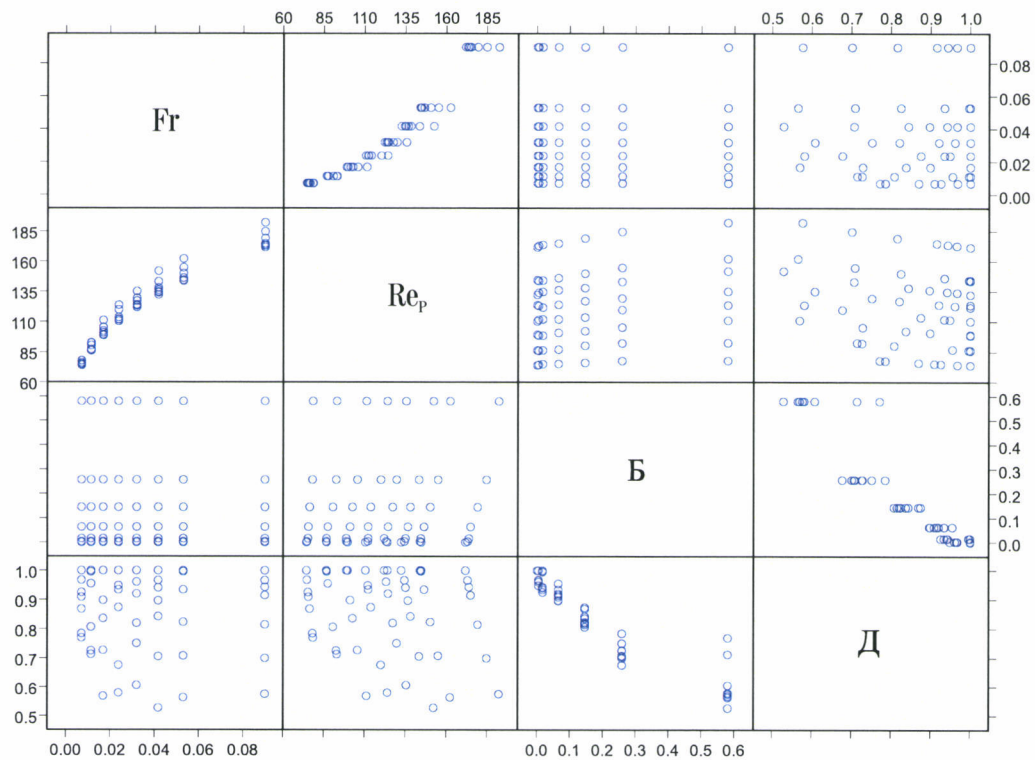


Figure 5.5 Matrix of scatterplots for preliminary exploratory data analysis.

There is clear evidence of a relationship between \mathcal{D} and B . The curvature of the data points and the increased spread as B increases suggests that a logarithmic transformation might be used. There is also a relationship between Fr and Re_p . This is no surprise because the fluid velocity is the main changing variable in both. Also, there is no clear indication of a relationship between \mathcal{D} and Re_p or Fr .

All variables are now transformed using natural logarithms. To help ensuring $\mathcal{D} = 1$ when $B = 0$, the transformation used for \mathcal{D} is $\ln(1 - \mathcal{D})$.

Figure 5.6 shows the resulting matrix of scatterplots.

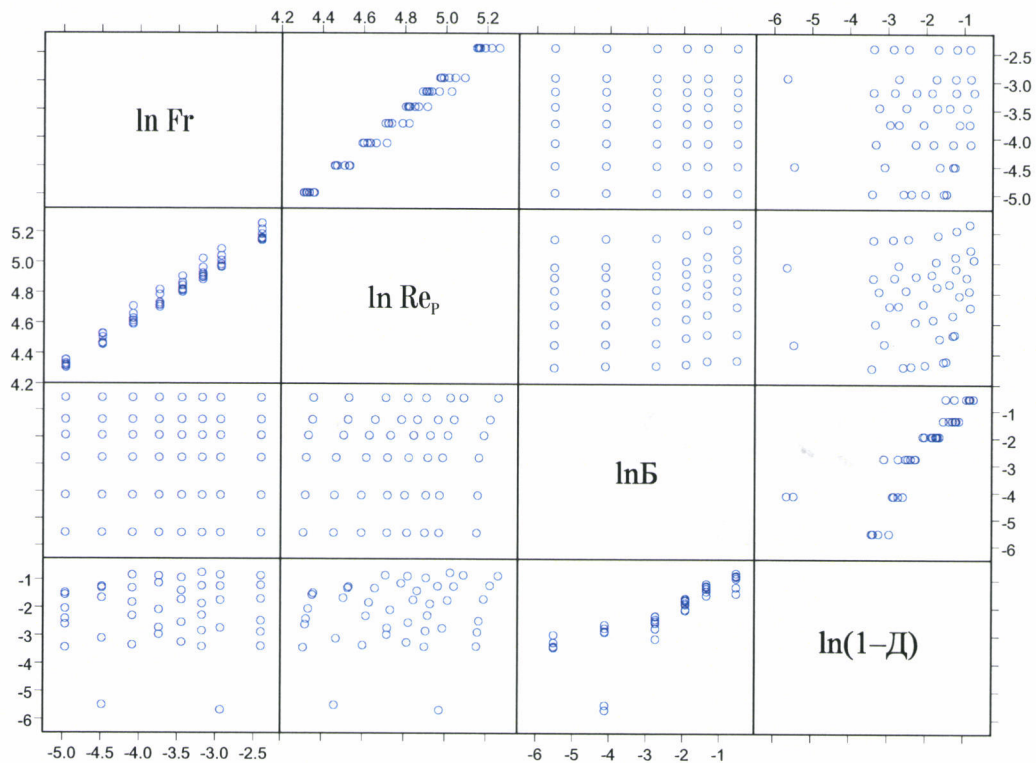


Figure 5.6 Matrix of scatterplots, transformed variables.

Upon transformation of the data, the linear relationship between Δ and B is more evident (with the exception of a couple of outliers). In addition, the variance of the data is more uniform, which is an assumption in multiple linear regression. A linear relationship between $\ln Fr$ and $\ln Re_p$ is very obvious now. Since these two explanatory variables are not linearly independent, they should not be used simultaneously in multiple linear regression. Froude number is dropped at this stage. Hence, the data is analyzed using multiple linear regression with the model

$$\ln(1 - \Delta) = k_1 + k_2 \ln B + k_3 \ln Re_p \quad (5.2-1)$$

The regression coefficients, along with their 95% confidence interval, standard error, t -statistic, and p -value, are shown in Table 5.2.

Table 5.2 Coefficients of multiple linear regression model

$$\ln(1 - \Delta) = k_1 + k_2 \ln B + k_3 \ln Re_p$$

Coefficient	Value	95% CI	SE	t -stat	p -value
k_1	-2.37	± 3.53	1.75	-1.36	0.18
k_2	0.57	± 0.13	0.062	9.1	<0.0001
k_3	0.34	± 0.73	0.36	0.9	0.35

From the p -value corresponding to $\ln R_{ep}$ it is deduced that there is no significant evidence that its coefficient is different than zero. The term containing R_{ep} is therefore removed from the model and the linear regression repeated. The obtained coefficients are listed in Table 5.3.

$$\ln(1 - D) = k_1 + k_2 \ln B \quad (5.2-2)$$

Table 5.3 Coefficients of multiple linear regression model, simplified model

$$\ln(1 - D) = k_1 + k_2 \ln B$$

Coefficient	Value	95% CI	SE	<i>t</i> -stat	<i>p</i> -value
k_1	-0.73	± 0.37	0.18	-4.0	0.0002
k_2	0.57	± 0.126	0.026	9.2	<0.0001

No further simplification of the model is required. Hence, the data was analyzed again, this time by non-linear regression, using the non-linear form of Equation 5.2-2 (notice the change from k_1 to $\ln k_1$). Table 5.4 lists the regression coefficients.

$$D = 1 - k_1 B^{k_2} \quad (5.2-3)$$

Table 5.4 Coefficients of non-linear regression model

$$\mathcal{D} = 1 - k_1 B^{k_2}$$

Coefficient	Value	95% CI	SE	t-stat	p-value
k_1	0.56	± 0.057	0.028	19.6	<0.0001
k_2	0.62	± 0.084	0.042	14.8	<0.0001

Finally, the drag correction factor is given as

$$\mathcal{D} = 1 - 0.56 B^{0.62} \quad (5.2-4)$$

5.3 Comparison between model and experimental data

Figures 5.7 through 5.14 show the experimental values of the drag correction factor and the model fit, plotted against the chain strength parameter, for the different flow rates used.

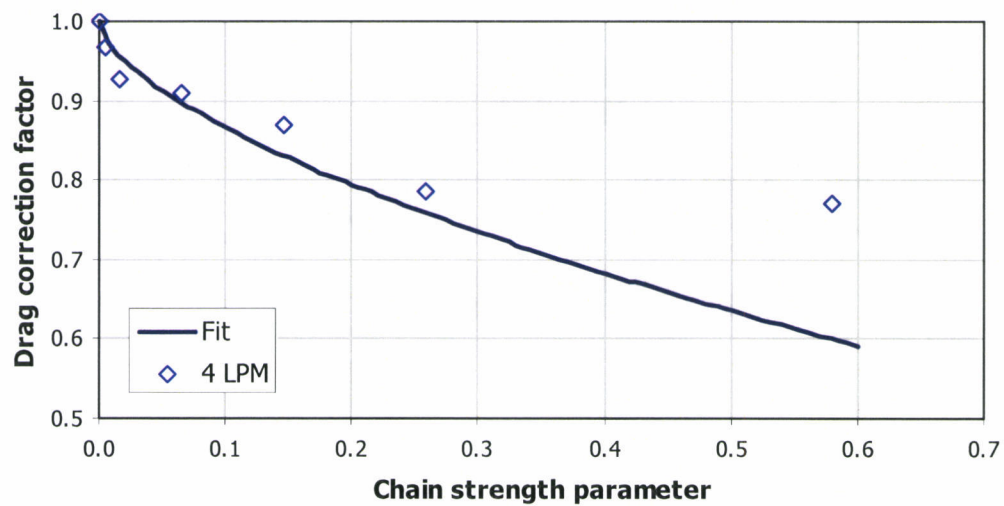


Figure 5.7 Experimentally determined drag correction factor and model fit for 4 LPM runs. Re_p between 74.2 and 78.1.

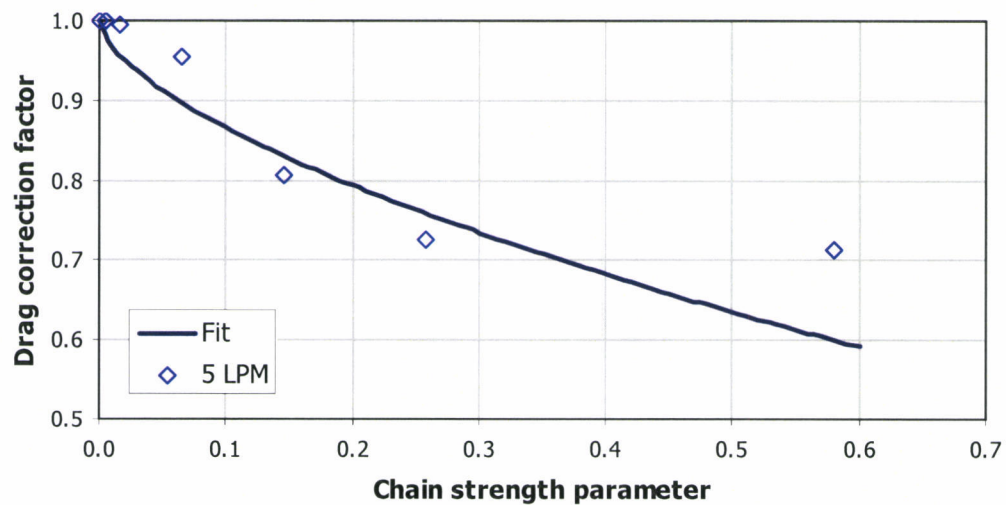


Figure 5.8 Experimentally determined drag correction factor and model fit for 5 LPM runs. Re_p between 86.6 and 92.9.

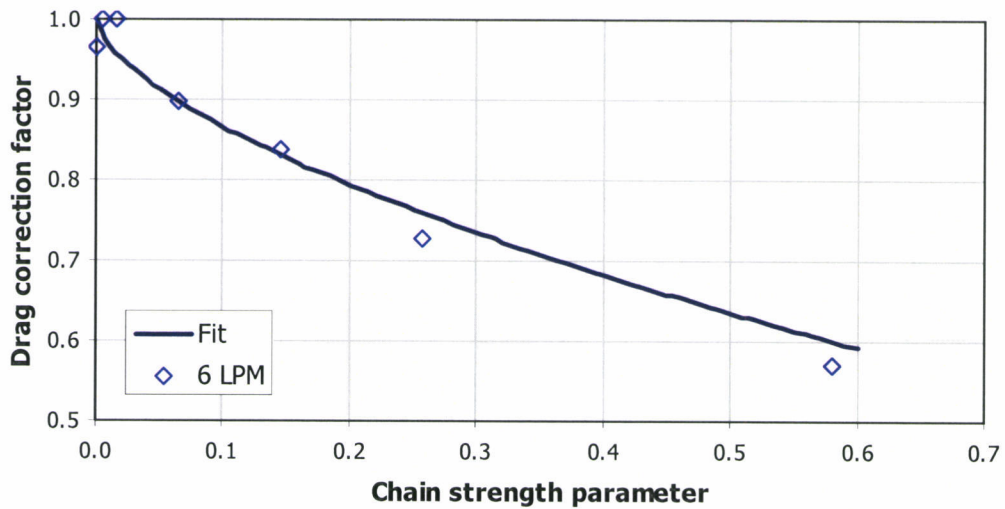


Figure 5.9 Experimentally determined drag correction factor and model fit for 6 LPM runs. Re_p between 99.5 and 111.1.

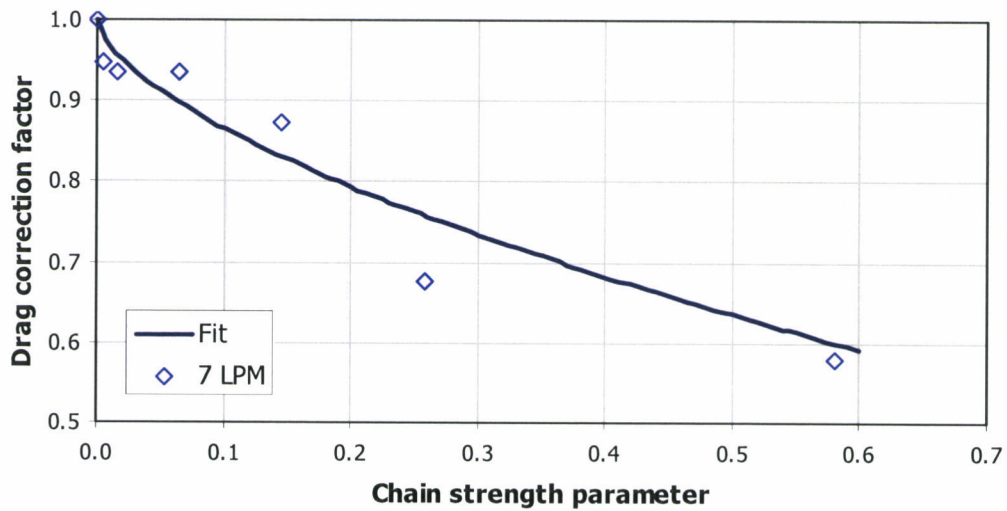


Figure 5.10 Experimentally determined drag correction factor and model fit for 7 LPM runs. Re_p between 110.4 and 123.8.

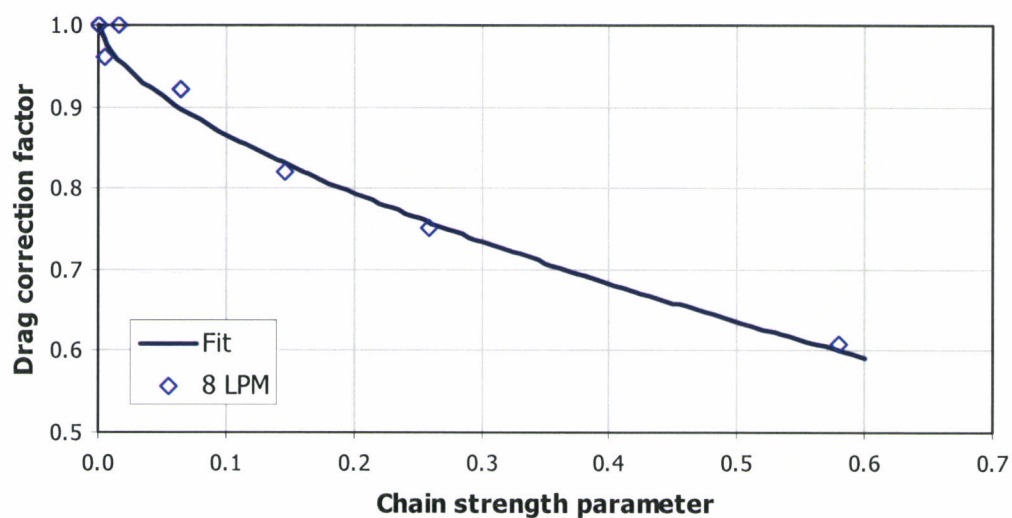


Figure 5.11 Experimentally determined drag correction factor and model fit for 8 LPM runs. Re_p between 123.8 and 135.3.

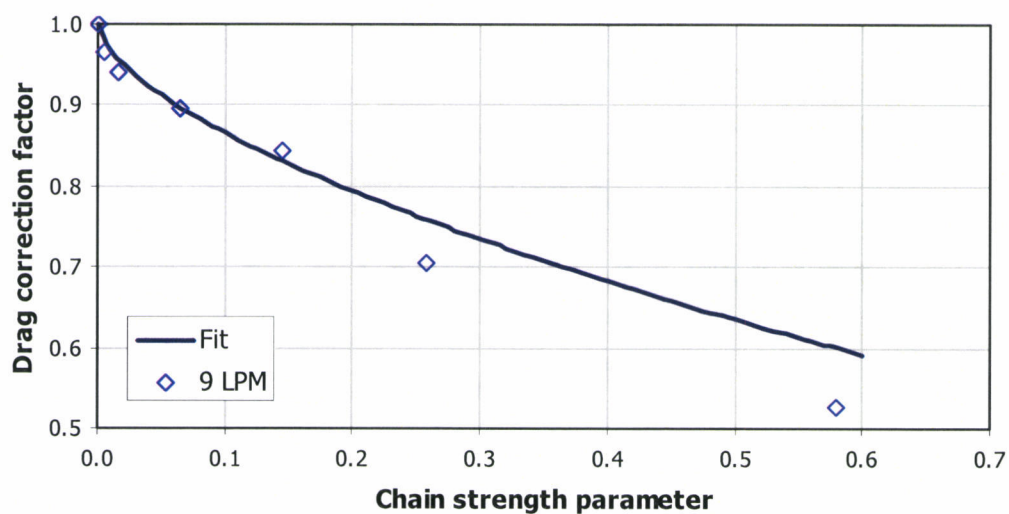


Figure 5.12 Experimentally determined drag correction factor and model fit for 9 LPM runs. Re_p between 132.3 and 152.0.

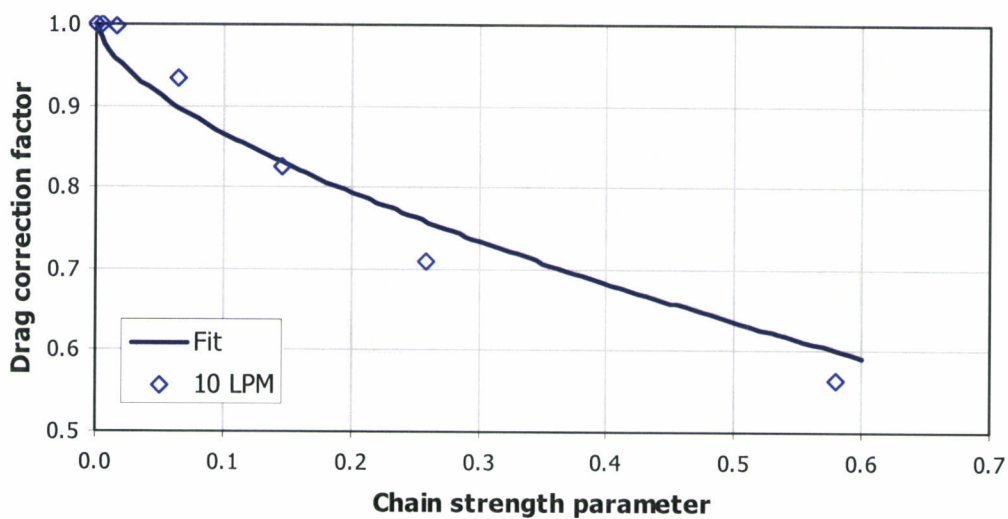


Figure 5.13 Experimentally determined drag correction factor and model fit for 10 LPM runs. Re_p between 144.5 and 162.2.

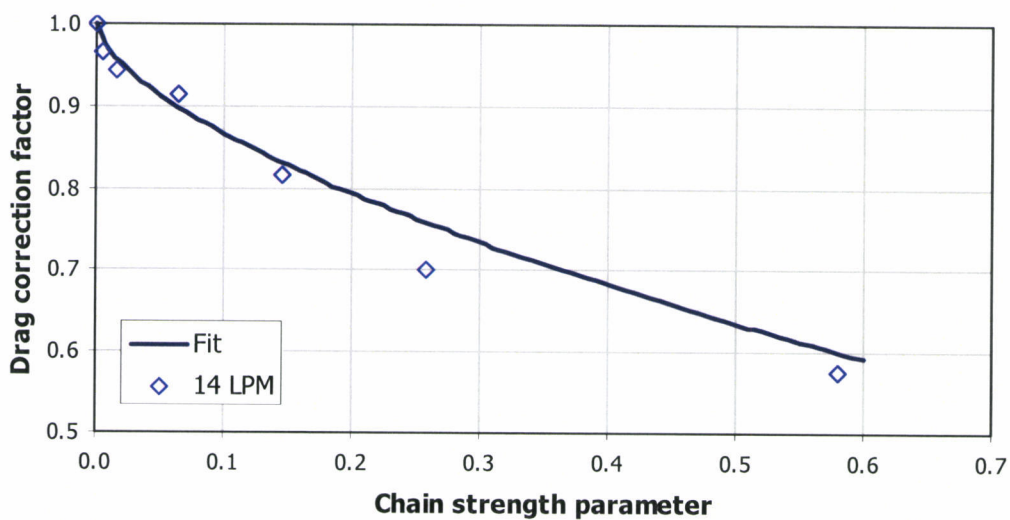


Figure 5.14 Experimentally determined drag correction factor and model fit for 14 LPM runs. Re_p between 171.6 and 192.1.

Figure 5.15 shows the agreement between experimental and predicted values of the drag correction factor. With the exception of a couple of outliers, for which the model underpredicts the correction factor, the model is successful in capturing the trend of the experimental data.

A closer examination of the outliers reveals that they correspond to the cases of highest magnetic field at the two lowest flow rates.

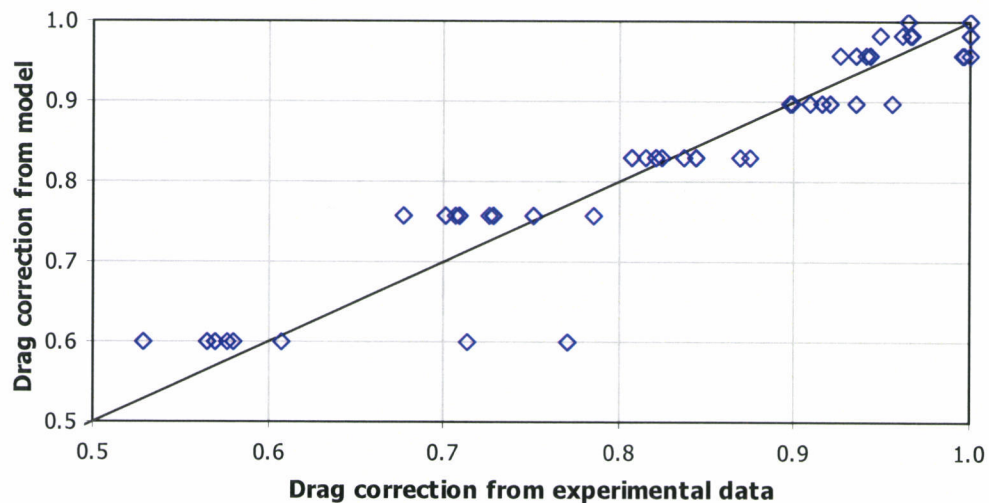


Figure 5.15 Agreement between experimental and predicted values of the drag correction factor.

The simulations were repeated incorporating the equation for Δ (Equation 5.2-4) in the simulation code. The error in bed height, compared to the experimental data is plot in Figure 5.14. Whereas the bed height can be overestimated by up to 70% when no correction is applied, the use of Equation 5.2-4 keeps the error below 10% for practically all the cases.

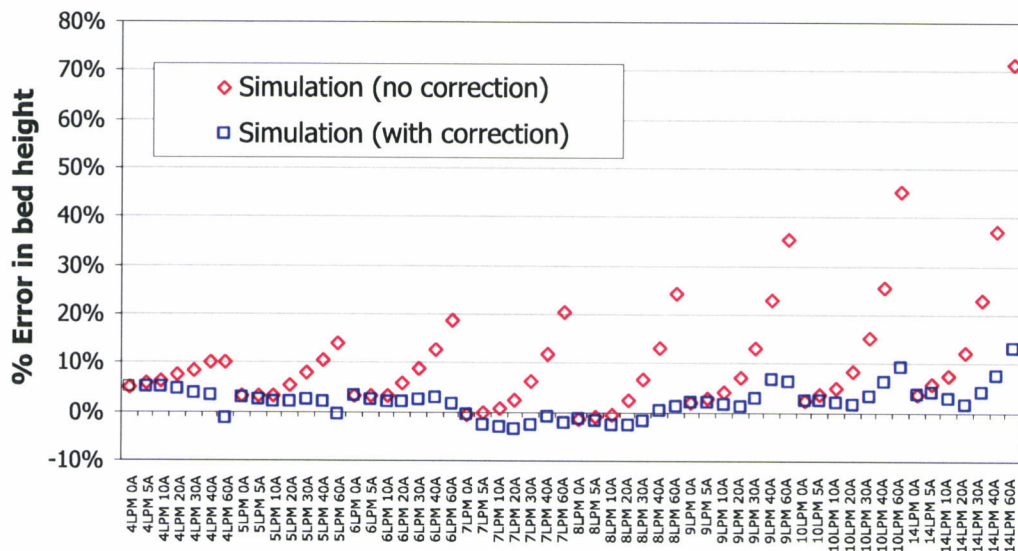


Figure 5.16 Error in bed height as estimated by simulation.

The improvement is also illustrated in Figure 5.17, where the bed height from simulation (with and without correction) is plot against the experimentally determined height. Notice the trend of overestimating the bed height when no correction is used.

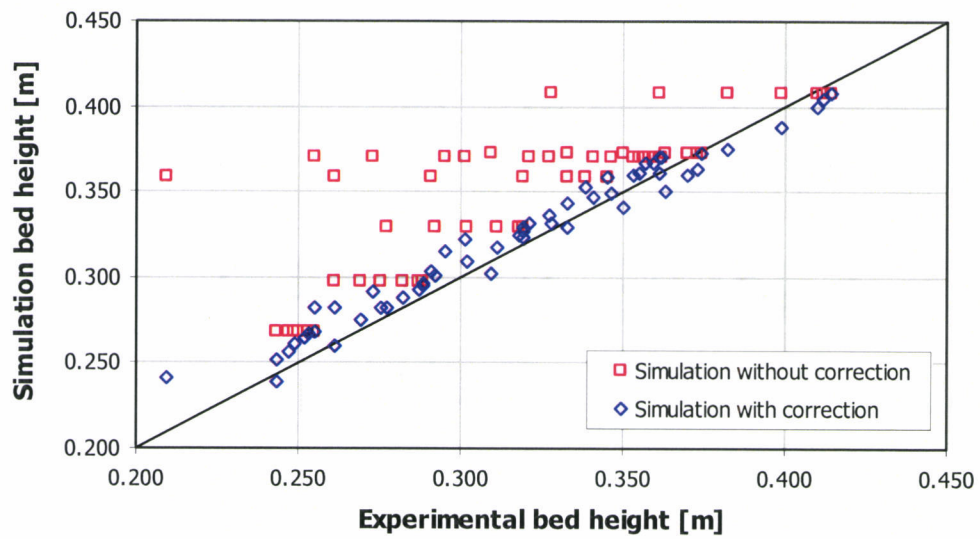


Figure 5.17 Simulation bed height (with and without correction) versus experimental bed height.

CHAPTER 6

CONCLUSIONS AND RECOMMENDATIONS

Q: We wanted to see if you had the ability to expand your mind and your horizons; and, for one brief moment, you did.

Picard: When I realized the paradox.

Q: Exactly. For that one fraction of a second, you were open to options you would never consider. *That* is the exploration that awaits you. Not mapping stars or studying nebulae, but charting the unknown possibilities of existence.

— Star Trek The Next Generation
“All Good Things...”

6.1 Conclusions

The hydrodynamic behavior of a liquid-solid magnetofluidized bed has been studied through measurement of the change in drag coefficient due to particle chaining. The experimental data has been reduced to the three parameter equation

$$\Delta = 1 - 0.56B^{0.62}$$

This equation successfully describes the reduction in drag coefficient within the range of operating conditions studied, $75 < Re_p < 190$ and

$0 < B < 0.58$. Additionally, incorporation of the drag correction in the newly developed CFD-DPM code "Particle-X" reduces the error in bed expansion from an overestimate of up to 70%, to or below 10%. With the aforementioned correction, this simulation code is one step closer to becoming a tool of scientific investigation and design.

6.2 Future work

The experimental data was gathered using only one type of particle. The validity of the correlation for the drag reduction factor should be verified by using particles of different size, density and/or magnetic content. The range of applicability with respect to both parameters (Re_p and B) should be extended in future research. Also, the possibility of extending this type of correlation to mixtures of particles of different properties should be examined.

It is clear that the reduction of drag coefficient comes from the formation of chains and the consequent channeling of fluid. Further studies should establish the relation between the observed drag coefficient and that of the individual structures. This will require identifying a measure of the degree of chaining in the bed.

Since the structures formed by the particles vary in type and abundance, it is necessary to find a suitable way of describing the population of such structures and the degree of anisotropy in the spatial distribution of the particulate phase. Possible tools for this description include a radial distribution analysis (sketched in Appendix E), spatial and/or temporal correlations, and moments of the location of the particles.

REFERENCES

Q: What must I do to convince you people?
 Worf: Die.
 Q: Oh, very clever, Worf. Eat any good books lately?

— Star Trek The Next Generation,
 “Deja Q”

- [1] Anderson, T.B. and R. Jackson (1967). “*A fluid mechanical description of fluidized beds.*” I&EC Fundamentals **6**: 527-539.
- [2] Anderson, T.B. and R. Jackson (1968). “*Fluid mechanical description of fluidized beds: Stability of the state of uniform fluidization.*” Industrial and Engineering Chemistry Fundamentals **7**(1): 12-21.
- [3] Clift, R. and W.H. Gauvin (1970). “*The motion of particles in turbulent gas streams.*” Proc Chemeca '70 **1**: 14.
- [4] Crowe, C., M. Sommerfeld, and Y. Tsuji (1997). Multiphase flow with droplets and particles. CRC Press, 471 pp.
- [5] Cruz-Fierro, C.F. (2004). *FLU/FLX extensible data format for fluidization simulation data*. <http://cruzfierro.com/academic/bolitas/fluformat.pdf>.
- [6] Cruz-Fierro, C.F., B.P. Reed, and J. Pinto-Espinoza (2004). *Bolitas 2*. <http://cruzfierro.com/academic/bolitas.htm>.
- [7] Cundall, P.A. and O.D.L. Strack (1979). “*A discrete numerical model for granular assemblies.*” Géotechnique **29**(1): 47-65.
- [8] Dallavalle, J.M. (1948). Micromeritics. Pitman.
- [9] Darby, R. (1996). Chemical Engineering Fluid Mechanics. Marcel Dekker, Inc., 488 pp.

- [10] Dennis, S.C.R., S.N. Singh, and D.B. Ingham (1980). "*The steady flow due to a rotating sphere at low and moderate Reynolds numbers.*" Journal of Fluid Mechanics **101**(2): 257.
- [11] Di Felice, R. (1994). "*The voidage function for fluid-particle interaction systems.*" International Journal of Multiphase Flow **20**(1): 153-159.
- [12] Epstein, N. (2003). Liquid-Solids Fluidization. Handbook of Fluidization and Fluid-Particle Systems. W.-C. Yang., Marcel Dekker, Inc.: 705-764.
- [13] Gidaspow, D. Multiphase Flow and Fluidization. Academic Press.
- [14] Graham, L. (1998). Dechlorination of p-chlorophenol on bimetallic Pd/Fe catalyst in a magnetically stabilized fluidized bed: experiment and theory. PhD Thesis, Oregon State University, 168 pp.
- [15] Griffiths, D.J. (1999). Introduction to electrodynamics. Prentice Hall, 576 pp.
- [16] Happel, J. and H. Brenner (1973). Low Reynolds Number Hydrodynamics. Hoordhoff Intl. Pub.
- [17] Honorez, L. (1994). Fluid dynamic characteristics of a magnetically stabilized liquid-solid fluidized bed. MS Thesis, Oregon State University, 81 pp.
- [18] Jackson, J.D. (1999). Classical electrodynamics. John Wiley & Sons, 808 pp.
- [19] Mei, R. (1992). "*An approximate expression for the shear lift on a spherical particle at finite Reynolds number.*" International Journal of Multiphase Flow **18**: 145.
- [20] Patankar, S.V. (1977). Numerical heat transfer and fluid flow. McGraw-Hill, 197 p.
- [21] Pinto-Espinoza, J. (2003). Dynamic behavior of ferromagnetic particles in a liquid-solid magnetically assisted fluidized bed (MAFB): Theory, experiment, and CFD-DPM simulation. PhD Thesis, Oregon State University, 271 pp.

- [22] Putnam, A. (1961). "*Integrable form of droplet drag coefficient.*" ARS Journal **31**: 1467.
- [23] Rosensweig, R.E. (1979). "*Fluidization: Hydrodynamic Stabilization with a Magnetic Field.*" Science **204**(4388): 57-60.
- [24] Rosensweig, R.E. (1979). "*Magnetic Stabilization of the State of Uniform Fluidization.*" Industrial and Engineering Chemistry Fundamentals **18**(3): 260-269.
- [25] Rowe, P.N. and G.A. Henwood (1961). "*Drag forces in a hydraulic model of a fluidized bed, part I.*" Transactions of the Institute of Chemical Engineers **39**: 43-54.
- [26] Sornchamni, T. (2004). Magnetically assisted liquid-solid fluidization in a gradient magnetic field: Theory and application. PhD Thesis, Oregon State University, 121 pp.
- [27] Tanaka, T., K. Yamagata, and Y. Tsuji (1990). "*Experiment on fluid forces on a rotating sphere and spheroid.*" Proc. Second KSME-JSME Fluids Engr. Conf. **1**: 366.
- [28] Tsuji, Y., T. Kawaguchi, and T. Tanaka (1993). "*Discrete particle simulation of two-dimensional fluidized bed.*" Powder Technology **77**: 79-87.
- [29] Villers, F. (1995). Bed porosity in a magnetically stabilized liquid-solid fluidized bed. MS Thesis, Oregon State University, 79 pp.
- [30] White, F.M. (1991). Viscous fluid flow. McGraw-Hill, Inc., 614 pp.

APPENDICES

APPENDIX A

ADDITIONAL EQUIPMENT SPECIFICATIONS

Cochrane: On this site, a powerful engine will be built. An engine that will someday help us to travel a hundred times faster than we can today. Imagine it: thousands of inhabited planets at our fingertips. And we'll be able to explore those strange, new worlds, and seek out new life and new civilizations. This engine will let us go boldly, where no man has gone before.

— Star Trek Enterprise,
“Broken Bow”

Figures A.1 through A.7 show the main pieces required to assemble the fluidized bed used in this research.

Note that the bed is designed to have interchangeable side, bottom, and top pieces. This modular design allows for easy assembly of beds of different thicknesses, using the same front and back pieces. The overflow box is also designed under this idea. For experiments requiring a closed system, the overflow can be replaced by another piece similar to the bottom piece of Figure A.3.

Figure A.8 is the template of the mounting plate for the pressure transducer.

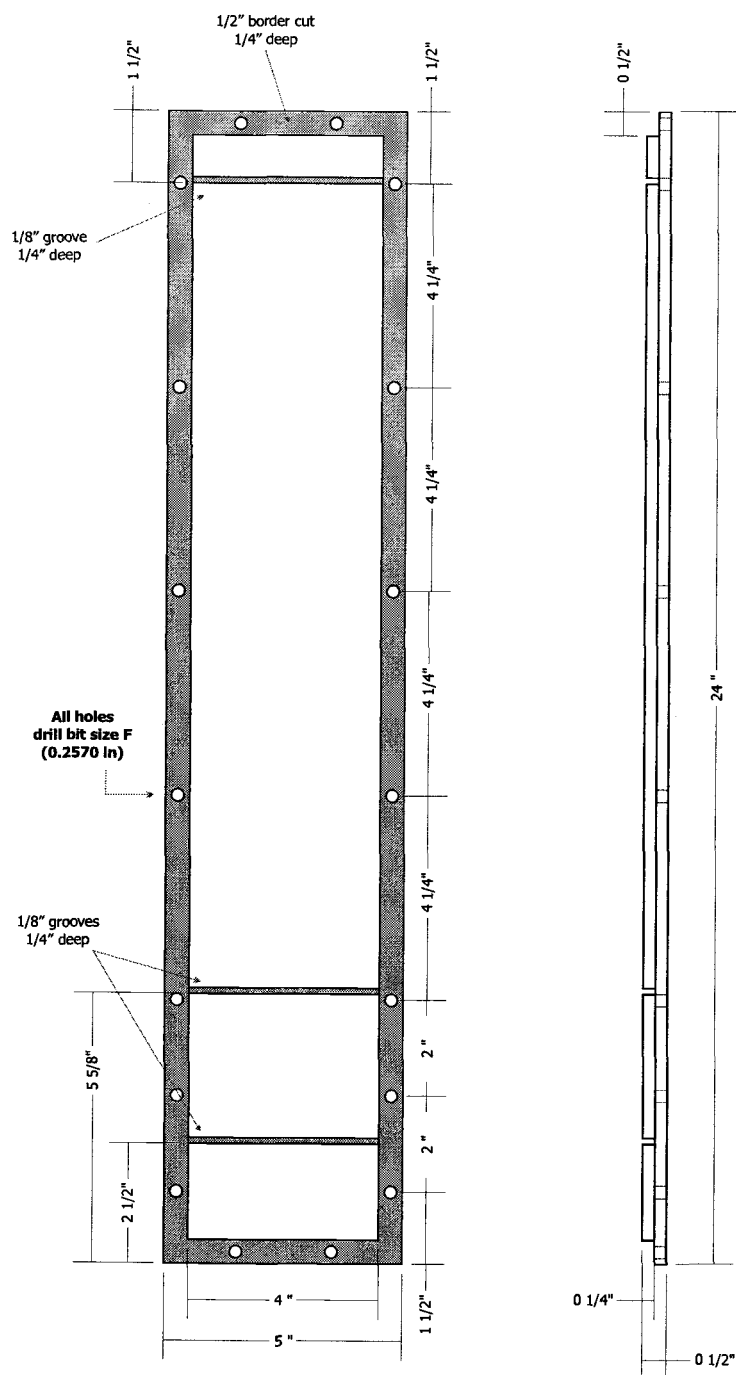


Figure A.1 Front/back piece of fluidized bed. Scale 1:4, measures in inches. Two of this piece are required.

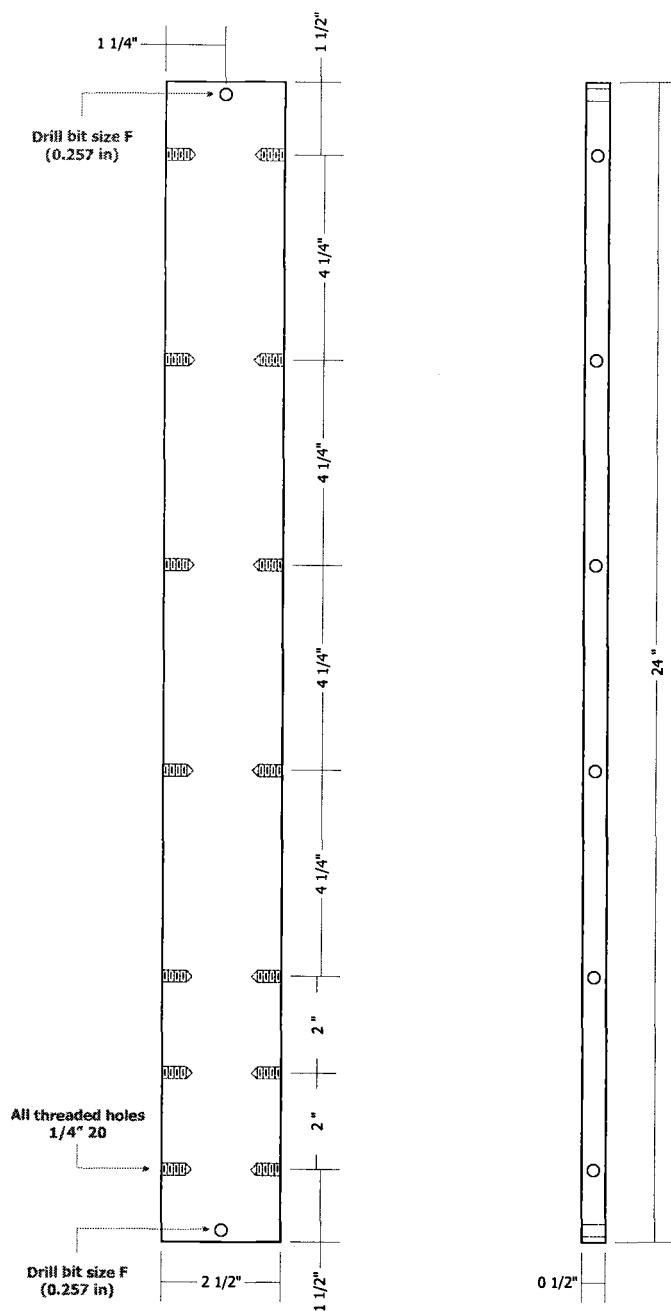


Figure 2.2 Side piece of fluidized bed. Scale 1:4, measures in inches. Two of this piece are required.

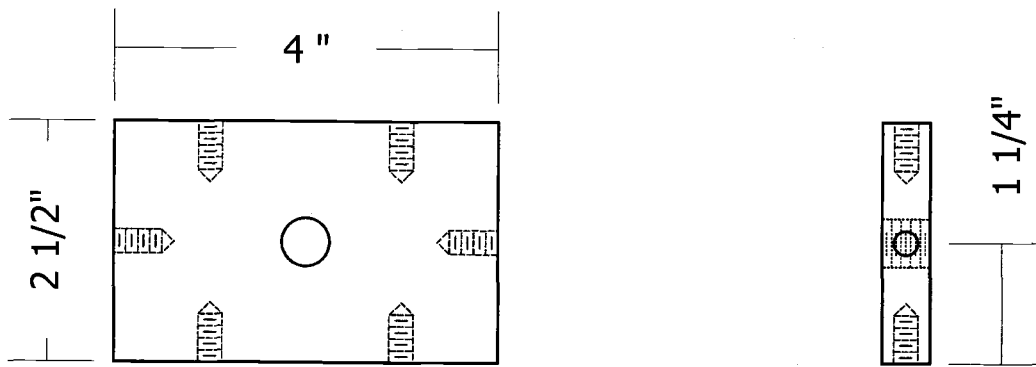


Figure A.3 Bottom piece of fluidized bed. Scale 1:1, measures in inches.

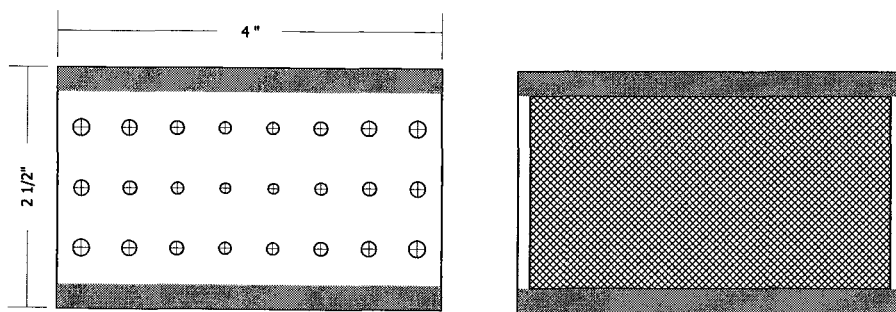


Figure A.4 Pre-distributor plate (left) and distributor plate (right). Scale 1:2, measures in inches. Gray shading indicates unavailable area inserted in grooves. The distributor plate is a frame supporting copper mesh.

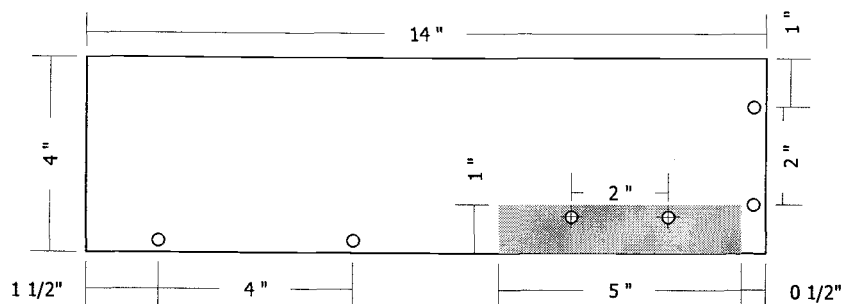


Figure A.5 Front/back piece for overflow box. Scale 1:4, measures in inches. Gray shading indicates where the bed will fit. Two of this piece are required

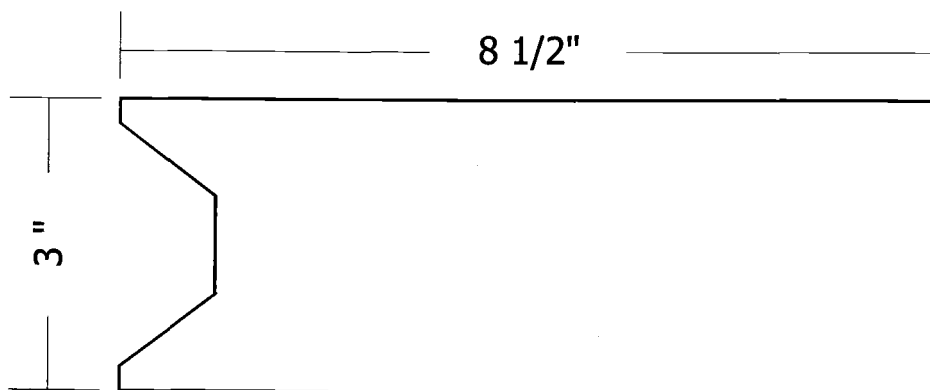


Figure A.6 Bottom piece for overflow box. Scale 1:2, measures in inches.

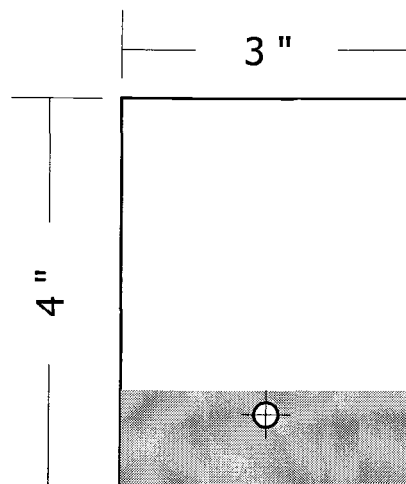


Figure A.7 Side piece for overflow box. Scale 1:2, measures in inches. Gray shading indicates where the bed will fit.

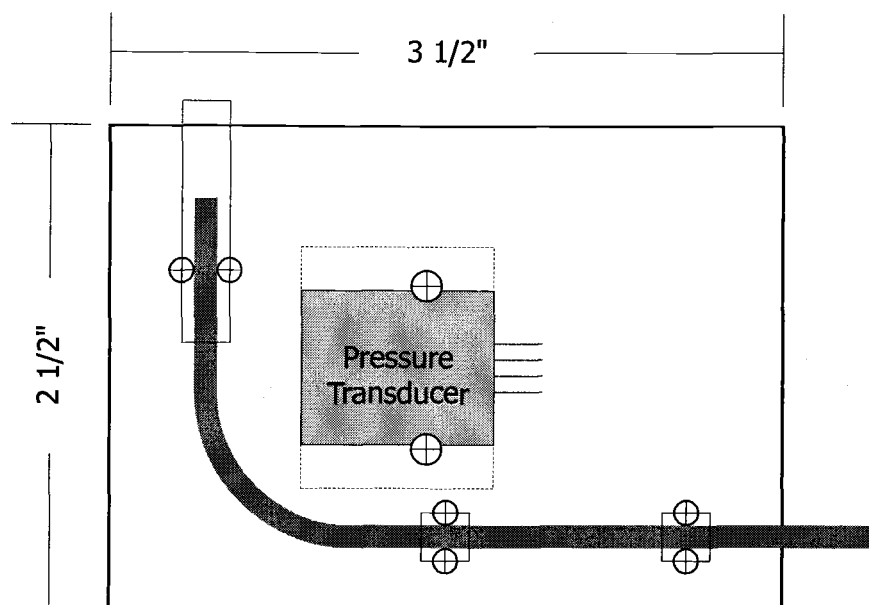


Figure A.8 Mounting plate for pressure transducer. Scale 1:1, measures in inches. Thick gray line indicates where the top of the probe will fit.

APPENDIX B

NOTES ON PARTICLE-X CODE

Borg Queen: You think in such three-dimensional terms.
How small have you become.
— Star Trek First Contact

This appendix includes some additional information about the 3D CFD-DPM simulation code.

B.1 Discretization of the momentum equations

This is the step-by-step procedure for obtaining the discretized form of the x -momentum equation. When collected and grouped by u_x velocity, these discretized terms give rise to the coefficients in Table 4.1. The process is essentially the same for the other three components of the momentum equation.

Transient term

$$\rho_f \frac{\partial}{\partial t} (\epsilon u_x)$$

$$\rho_f \int_{\Delta V} \frac{\partial}{\partial t} (\epsilon u_x) dV$$

$$= \rho_f \frac{\partial}{\partial t} \int_{\Delta V} (\epsilon u_x) dV$$

$$\begin{aligned}
&\cong \rho_f \frac{\partial}{\partial t} (\varepsilon_p u_{x,p}) \Delta \mathcal{V} \\
&\cong \rho_f \frac{(\varepsilon_p u_{x,p}) - (\varepsilon_p u_{x,p})|_{t-\Delta t}}{\Delta t} \Delta \mathcal{V} \\
&\cong \left[\frac{\rho_f \varepsilon_p \Delta \mathcal{V}}{\Delta t} \right] u_{x,p} - \left[\frac{\rho_f (\varepsilon_p u_{x,p})|_{t-\Delta t} \Delta \mathcal{V}}{\Delta t} \right]
\end{aligned}$$

Advective terms

$$\begin{aligned}
&\rho_f \frac{\partial}{\partial x} (\varepsilon u_x u_x) + \rho_f \frac{\partial}{\partial y} (\varepsilon u_x u_y) + \rho_f \frac{\partial}{\partial z} (\varepsilon u_x u_z) \\
&\rho_f \int_{\Delta \mathcal{V}} \left[\frac{\partial}{\partial x} (\varepsilon u_x u_x) + \frac{\partial}{\partial y} (\varepsilon u_x u_y) + \frac{\partial}{\partial z} (\varepsilon u_x u_z) \right] d\mathcal{V} = \rho_f \int_{\Delta \mathcal{V}} \nabla \cdot (\varepsilon u_x \mathbf{u}) d\mathcal{V} \\
&= \rho_f \oint_{\Delta \mathcal{S}} (\varepsilon u_x \mathbf{u}) \cdot d\bar{\mathcal{S}} \\
&= \rho_f \int_e (\varepsilon u_x u_x) d\mathcal{S} - \rho_f \int_w (\varepsilon u_x u_x) d\mathcal{S} + \rho_f \int_n (\varepsilon u_x u_y) d\mathcal{S} \\
&\quad - \rho_f \int_s (\varepsilon u_x u_y) d\mathcal{S} + \rho_f \int_f (\varepsilon u_x u_z) d\mathcal{S} - \rho_f \int_b (\varepsilon u_x u_z) d\mathcal{S} \\
&\cong \rho_f (\varepsilon u_x u_x)_e \Delta y \Delta z - \rho_f (\varepsilon u_x u_x)_w \Delta y \Delta z + \rho_f (\varepsilon u_x u_y)_n \Delta x \Delta z \\
&\quad - \rho_f (\varepsilon u_x u_y)_s \Delta x \Delta z + \rho_f (\varepsilon u_x u_z)_f \Delta x \Delta y - \rho_f (\varepsilon u_x u_z)_b \Delta x \Delta y
\end{aligned}$$

The upwind scheme is used to approximate the fluxes at the interfaces, hence

$$\begin{aligned}
&\equiv \rho_f \left(u_{x,P} \left[0, \varepsilon_e u_{x,e} \right] - u_{x,E} \left[0, -\varepsilon_e u_{x,e} \right] \right) \Delta y \Delta z \\
&- \rho_f \left(u_{x,W} \left[0, \varepsilon_w u_{x,w} \right] - u_{x,P} \left[0, -\varepsilon_w u_{x,w} \right] \right) \Delta y \Delta z \\
&+ \rho_f \left(u_{x,N} \left[0, \varepsilon_n u_{y,n} \right] - u_{x,N} \left[0, -\varepsilon_n u_{y,n} \right] \right) \Delta x \Delta z \\
&- \rho_f \left(u_{x,S} \left[0, \varepsilon_s u_{y,s} \right] - u_{x,P} \left[0, -\varepsilon_s u_{y,s} \right] \right) \Delta x \Delta z \\
&+ \rho_f \left(u_{x,P} \left[0, \varepsilon_f u_{z,f} \right] - u_{x,F} \left[0, -\varepsilon_f u_{z,f} \right] \right) \Delta x \Delta y \\
&+ \rho_f \left(u_{x,B} \left[0, \varepsilon_b u_{z,b} \right] - u_{x,P} \left[0, -\varepsilon_b u_{z,b} \right] \right) \Delta x \Delta y
\end{aligned}$$

collecting terms by u_x at the different cells,

$$\begin{aligned}
&\equiv \rho_f \left(\left[0, \varepsilon_e u_{x,e} \right] \Delta y \Delta z - \left[0, -\varepsilon_w u_{x,w} \right] \Delta y \Delta z + \left[0, \varepsilon_n u_{y,n} \right] \Delta x \Delta z \right. \\
&- \left[0, -\varepsilon_s u_{y,s} \right] \Delta x \Delta z + \left[0, \varepsilon_f u_{z,f} \right] \Delta x \Delta z - \left[0, -\varepsilon_b u_{z,b} \right] \Delta x \Delta z \left. \right) u_{x,P} \\
&- \rho_f \left[0, -\varepsilon_e u_{x,e} \right] (\Delta y \Delta z) u_{x,E} - \rho_f \left[0, \varepsilon_w u_{x,w} \right] (\Delta y \Delta z) u_{x,W} \\
&- \rho_f \left[0, -\varepsilon_n u_{y,n} \right] (\Delta x \Delta z) u_{x,N} - \rho_f \left[0, \varepsilon_s u_{y,s} \right] (\Delta x \Delta z) u_{x,S} \\
&- \rho_f \left[0, -\varepsilon_f u_{z,f} \right] (\Delta x \Delta y) u_{x,F} - \rho_f \left[0, \varepsilon_b u_{z,b} \right] (\Delta x \Delta y) u_{x,B}
\end{aligned}$$

It can be shown that the coefficient of $u_{x,P}$ is equal to the sum of the coefficients of the other neighboring cells, plus the net flux contribution given by $\rho_f (\varepsilon_e u_{x,e} - \varepsilon_w u_{x,w}) \Delta y \Delta z + \rho_f (\varepsilon_n u_{y,n} - \varepsilon_s u_{y,s}) \Delta x \Delta z + \rho_f (\varepsilon_f u_{z,f} - \varepsilon_b u_{z,b}) \Delta x \Delta y$

Pressure term

$$\varepsilon \frac{\partial P}{\partial x}$$

$$\int_{\Delta \mathcal{V}} \varepsilon \frac{\partial P}{\partial x} d\mathcal{V} = \int_{\Delta \mathcal{V}} \hat{\mathbf{x}} \cdot \nabla \cdot (P \mathbf{I}) d\mathcal{V}$$

$$\begin{aligned}
&\cong \varepsilon_p \hat{\mathbf{x}} \cdot \int_{\Delta \mathcal{V}} \nabla \cdot (P \mathbf{I}) d\mathcal{V} \\
&\cong \varepsilon_p \hat{\mathbf{x}} \cdot \oint_{\Delta \mathcal{S}} \nabla \cdot (P \mathbf{I}) \cdot d\bar{\mathcal{S}} \\
&\cong \varepsilon_p \int_e P d\mathcal{S} - \varepsilon_p \int_w P d\mathcal{S} \\
&\cong \varepsilon_p (P_e - P_w) \Delta y \Delta z
\end{aligned}$$

Viscous terms

$$\frac{\partial}{\partial x}(\varepsilon \tau_{xx}) + \frac{\partial}{\partial y}(\varepsilon \tau_{yx}) + \frac{\partial}{\partial z}(\varepsilon \tau_{zx})$$

$$\begin{aligned}
&\int_{\Delta \mathcal{V}} \left[\frac{\partial}{\partial x}(\varepsilon \tau_{xx}) + \frac{\partial}{\partial y}(\varepsilon \tau_{yx}) + \frac{\partial}{\partial z}(\varepsilon \tau_{zx}) \right] d\mathcal{V} = \int_{\Delta \mathcal{V}} \hat{\mathbf{x}} \cdot \nabla \cdot (\varepsilon \boldsymbol{\tau}) d\mathcal{V} \\
&= \hat{\mathbf{x}} \cdot \oint_{\Delta \mathcal{S}} \nabla \cdot (\varepsilon \boldsymbol{\tau}) \cdot d\bar{\mathcal{S}} \\
&= \int_e (\varepsilon \tau_{xx}) d\mathcal{S} - \int_w (\varepsilon \tau_{xx}) d\mathcal{S} + \int_n (\varepsilon \tau_{yx}) d\mathcal{S} \\
&\quad - \int_s (\varepsilon \tau_{yx}) d\mathcal{S} + \int_f (\varepsilon \tau_{zx}) d\mathcal{S} - \int_b (\varepsilon \tau_{zx}) d\mathcal{S} \\
&\cong (\varepsilon_e \tau_{xx,e} - \varepsilon_w \tau_{xx,w}) \Delta y \Delta z + (\varepsilon_n \tau_{yx,n} - \varepsilon_s \tau_{yx,s}) \Delta x \Delta z \\
&\quad + (\varepsilon_f \tau_{zx,f} - \varepsilon_b \tau_{zx,b}) \Delta x \Delta y
\end{aligned}$$

The corresponding viscous stresses are approximated, for a Newtonian fluid, as

$$\tau_{xx,e} \cong -\frac{2\mu_f}{\Delta x} (u_{x,E} - u_{x,P})$$

$$\tau_{xx,w} \cong -\frac{2\mu_f}{\Delta x} (u_{x,P} - u_{x,E})$$

$$\tau_{yx,n} \cong -\mu_f \left(\frac{u_{x,N} - u_{x,P}}{\Delta y} + \frac{u_{y,ne} - u_{y,nw}}{\Delta x} \right)$$

$$\tau_{yx,s} \cong -\mu_f \left(\frac{u_{x,P} - u_{x,S}}{\Delta y} + \frac{u_{y,se} - u_{y,sw}}{\Delta x} \right)$$

$$\tau_{zx,f} \cong -\mu_f \left(\frac{u_{x,F} - u_{x,P}}{\Delta z} + \frac{u_{z,ef} - u_{z,wf}}{\Delta x} \right)$$

$$\tau_{zx,b} \cong -\mu_f \left(\frac{u_{x,P} - u_{x,B}}{\Delta z} + \frac{u_{z,eb} - u_{z,wb}}{\Delta x} \right)$$

Upon substitution of the viscous stresses and collecting terms by u_x at the different cells, this is the final discretized form of the viscous terms

$$\begin{aligned} &\cong \mu_f \left[2(\varepsilon_e + \varepsilon_w) \frac{\Delta y \Delta z}{\Delta x} + (\varepsilon_n + \varepsilon_s) \frac{\Delta x \Delta z}{\Delta y} + (\varepsilon_f + \varepsilon_b) \frac{\Delta x \Delta y}{\Delta z} \right] u_{x,P} \\ &- \mu_f \left[2\varepsilon_e \frac{\Delta y \Delta z}{\Delta x} \right] u_{x,E} - \mu_f \left[2\varepsilon_w \frac{\Delta y \Delta z}{\Delta x} \right] u_{x,W} - \mu_f \left[\varepsilon_n \frac{\Delta x \Delta z}{\Delta y} \right] u_{x,N} \\ &- \mu_f \left[\varepsilon_s \frac{\Delta x \Delta z}{\Delta y} \right] u_{x,S} - \mu_f \left[\varepsilon_n \frac{\Delta x \Delta y}{\Delta z} \right] u_{x,F} - \mu_f \left[\varepsilon_b \frac{\Delta x \Delta y}{\Delta z} \right] u_{x,B} \\ &- \mu_f \left[\varepsilon_n (u_{y,ne} - u_{y,nw}) - \varepsilon_s (u_{y,se} - u_{y,sw}) \right] \Delta z \\ &- \mu_f \left[\varepsilon_f (u_{z,ef} - u_{z,wf}) - \varepsilon_b (u_{z,eb} - u_{z,wb}) \right] \Delta y \end{aligned}$$

Note that the coefficient of $u_{x,P}$ is equal to the (negative) sum of the coefficients of the neighboring velocities.

Gravity and external force terms

$$-\varepsilon\rho_f\mathbf{g}-\mathbf{f}$$

$$\begin{aligned} -\int_{\Delta\mathcal{V}}(\varepsilon\rho_f\mathbf{g}_x+f_x)d\mathcal{V} &\cong -\varepsilon_p\rho_f\mathbf{g}_x\Delta\mathcal{V}-f_x\Delta\mathcal{V} \\ &\cong -\varepsilon_p\rho_f\mathbf{g}_x\Delta\mathcal{V}-F_x \end{aligned}$$

where F_x is the total external force over the fluid in the cell, including fluid-particle interactions.

B.2 Particle-X main program

Since the complete code is approximately 250 pages long, only the main program and the declaration of global variables are listed. The interested reader should consult the included CD.

```
PROGRAM PARTICLEX
```

```
USE GLOBVARS           ! GLOBAL VARIABLES

USE BOLITAS            ! OUTPUT ROUTINES FOR VISUALIZATION
USE COLLISIONSWALLS    ! PARTICLE-WALL COLLISIONS
USE COLLISIONSPARTICLES ! PARTICLE-PARTICLE COLLISIONS
USE COLORFUL           ! COLOR SUBROUTINES
USE DIRECTORY          ! PARTICLE DIRECTORY
USE F2PINTERP          ! FLUID PROPERTIES INTERP AT PARTICLE LOCATIONS
USE FLUIDVELGRAD       ! FLUID VELOCITY GRADIENTS
USE FPBUOYANCY         ! BUOYANCY FORCE OVER PARTICLES
USE FPDRAW             ! DRAG FORCE OVER PARTICLES
USE FPGRAVITY          ! LOAD PARTICLE-GRAVITY INTERACTION ROUTINES
USE FPROTATION         ! ROTATION-DEPENDENT FORCES
USE INIT               ! INITIALIZATION SUBROUTINE
USE INPUT              ! INPUT SUBROUTINE
USE MAGNETICEXTERNAL   ! EXTERNAL MAGNETIC FORCE CALCULATION
USE MAGNETICIMF        ! INTERPARTICLE MAGNETIC FORCE CALCULATION
USE OUTPUT             ! OUTPUT TO TEXT FILES
USE PARTICLEINDEX      ! INDEXING AND SEARCH OF PARTICLES BY LOCATION
```

```

USE PAIRDETECTION      ! PARTICLE PAIR DETECTION ROUTINES
USE PAIRMEMORY         ! ELASTIC-TANGENTIAL MEMORY FOR P-P COLLISIONS
USE PAIRTABLE          ! PARTICLE PAIR TABLE
USE PARTICLE_ICS       ! PARTICLE INITIAL CONDITION ROUTINES
USE PARTICLE_MOTION    ! PARTICLE MOTION CALCULATION ROUTINES
USE PRESSCORRECT       ! PRESSURE CORRECTION SUBROUTINE
USE PROGRESS           ! PROGRESS REPORT ON SCREEN
USE TIMELINE           ! TIMELINE EVENT HANDLING
USE VALIDATION         ! INPUT AND RUNTIME CHECKS
USE VOIDAGECALC        ! LOADS VOIDAGE CALCULATION ROUTINES
USE VOIDAGEINTERP      ! VOID FRACTION INTERPOLATION SUBROUTINES
USE WISDOM             ! JOHN DOE'S WISDOM
USE XMOMENTUM          ! X-MOMENTUM SUBROUTINE
USE YMOMENTUM          ! Y-MOMENTUM SUBROUTINE
USE ZMOMENTUM          ! Y-MOMENTUM SUBROUTINE

```

```

IMPLICIT NONE

```

```

INTEGER:: I,K
LOGICAL:: FILEEXIST
INTEGER:: ITERPART

```

```

! *****
!           MAIN SUBROUTINE BEGINS HERE
! *****

```

```

! SHOW WELCOME SCREEN
CALL WELCOME

```

```

! ITERATION COUNTER SET TO ZERO
ITER = 0

```

```

! USER INPUT IS PROCESSED
CALL GETINPUT
CALL TIMELINEREAD

```

```

! *** VARIABLES ARE INITIALIZED BASED ON USER INPUT ***
CALL INITIALIZE

```

```

! *** ADDITIONAL INITIALIZATIONS FOR SPECIALIZED SUBROUTINES
CALL INITXMOM
CALL INITYMOM
CALL INITZMOM
CALL INITPRESSURECORRECTOR
CALL VOIDINIT

```

```

IF (NP.GT.0) THEN
! PREPARES THE TABLE OF PARTICLE PAIRS
CALL PAIRTABLERESET(2*NP)
! PREPARES MEMORY OF TANGENTIAL DISPLACEMENT IN PP COLLISIONS
CALL PAIRMEMORY_INIT
END IF

```

```

! *** INITIALIZE BOUNDARY CONDITIONS ***
CALL BOUNDARYCOND

```

```

! INITIALIZE RANDOM NUMBER GENERATOR
CALL INITRANDOM

```

```

IF (NP.GT.0) THEN

    ! VALIDATION OF TIME STEP FOR COLLISIONS
    CALL CHECK_DT

    ! VALIDATION OF CELL SIZE VERSUS PARTICLE SIZE
    CALL CHECK_CELLSIZE

END IF

! *** PARTICLE INITIAL CONDITIONS SET BASED ON USER CHOICE ***

IF (NP.GT.0) THEN

    SELECT CASE (CHOICEPARTICLEPOSITION)
    CASE (1)
        ! PLACES PARTICLES MUCH NEARER TO A SETTLED STATE (LESS FALL TIME)
        CALL ACLOSEPACK
    CASE (2)
        ! USING FULL BED VOLUME
        CALL ATOTVOLMTHD
    CASE (3)
        INQUIRE (FILE='INPUTPARTLOC.TXT', EXIST=FILEEXIST)
        IF (FILEEXIST) THEN
            ! READ FROM FILE
            CALL READPARTLOC
        ELSE
            ! USE DEFAULT METHOD INSTEAD
            CALL ACLOSEPACK
        END IF
    CASE DEFAULT
        CALL ACLOSEPACK
    END SELECT

    ! AFTER LOCATING THE PARTICLES, SORT THE INDEXES BY INSERTION SORT
    WRITE(*,*) ' '
    WRITE(*,*) 'INITIAL SORTING OF PARTICLE INDEXES...'
    CALL INSERTIONSORT
    WRITE(*,*) 'FINISHED SORTING INDEXES'
    WRITE(*,*) ' '

    ! CHECK THAT ALL PARTICLES ARE INITIALLY WITHIN THE BED
    CALL CHECK_CONTAINMENT

    IF (CHOICEPAIRDETECTION.EQ.3) THEN
        ! INITIALIZATION OF GRID-BASED PAIR DETECTION
        CALL PAIRDETECTGRIDINIT(MAXSEARCHDIST)
    END IF

END IF

! *** CALCULATE AND INTERPOLATE VOIDAGE ***
CALL EQVOLVOID2
CALL VOIDINTERPOLATE
EPO=EP

! *** BOLITAS INITIALIZATION AND WRITING OF FRAME ZERO ***
CALL BOLITASINIT
CALL FLUWRITE
CALL FLSCREATE

```

```

CALL FLXCREATE
CALL FLXWRITE

! OTHER TEXT FILE OUTPUT
IF (NP.GT.0) CALL WRITEPARTLOC

! ITERATION COUNTER SET TO ZERO
ITER = 0

! GET CPU START TIME FOR PROGRESS REPORTS
CALL CPU_TIME(CPUTIMESTART)

! LEAVE BLANK LINE IN SCREEN
WRITE (*,*) ' '

! *****
! *                MAIN PROGRAM LOOP                *
! *****

DO WHILE (ITER .LT. ENDITER)

! CURRENT ITERATION NUMBER AND TIME
ITER=ITER+1
CURRTIME=ITER*ENDTIME/ENDITER

! APPLY TIMELINE EVENTS
CALL TIMELINEAPPLY

! APPLY INLET FACTOR TO DISTRIBUTOR PLATE
DO K=1,LK
  DO I=1,LI
    UY(I,0,K)=INLETFACOR*UYDIST(I,K)
  END DO
END DO

! *** ZERO FORCES ON FLUID CELLS ***
FFX=0.0
FFY=0.0
FFZ=0.0

! *** COPY NEW VALUES TO PREVIOUS ITERATION PLACE HOLDER ***
! INTERPOLATED FLUID VELOCITIES AT PARTICLE LOCATIONS
F2PUX00=F2PUX; F2PUY00=F2PUY; F2PUZ00=F2PUZ

UX0=UX; UY0=UY; UZ0=UZ

! FLUID PROPERTY ARRAYS COPIED
EP0=EP

! *****
! *****

! CALCULATIONS FOR PARTICLES BEGIN HERE

IF (NP.GT.0) THEN

! RESET ITERATION NUMBER BECAUSE IT WILL BE

```

```

! INCREMENTED AGAIN INSIDE THE INNER LOOP
ITER=ITER-1

! NOTE THAT FORCES ON FLUID (FFX,FFY,FFZ) ARE NOT RESET TO ZERO
! THEY WILL ACCUMULATE THE FORCES FROM EACH INNER ITERATION
! AND THE FINAL RESULT NEEDS TO BE DIVIDED BY DTRATIO

DO ITERPART=1,DTRATIO

  ! INNTER ITERATIONS FOR PARTICLES

  ITER=ITER+1
  CURRTIME=ITER*ENDTIME/ENDITER

  ! PREVIOUS PARTICLE VELOCITY ARRAYS COPIED
  VX00=VX0; VY00=VY0; VZ00=VZ0
  VX0=VX; VY0=VY; VZ0=VZ

  ! *** CALL DIRECTORY ROUTINES TO LOCATE AND SORT PARTICLES ***
  ! FLUID CELL OCCUPIED BY PARTICLE CENTER
  CALL FLUIDLOCATE
  CALL PARTICLECUT

  ! *** INTERPOLATE FLUID PROPERTIES AT PARTICLE LOCATIONS
  CALL TRILINEARFACTORS
  CALL F2PVELOCITY

  ! *** CALCULATE AND INTERPOLATE VOID FRACTION ***
  CALL EQVOLVOID2
  CALL VOIDINTERPOLATE
  CALL F2PVOIDAGE

  ! FIRST FORCES AND TORQUES ARE ZEROED
  FPX=0.0; FPY=0.0; FPZ=0.0
  TAUPX=0.0; TAUPY=0.0; TAUPZ=0.0

  ! *** PARTICLE COLLISIONS ***
  ! CLEAR COLLISION COUNTERS
  PWCOUNT=0
  CONTACTS=0
  PPCOUNT=0

  ! PARTICLE-WALL COLLISIONS
  CALL WALLCOLL

  ! PARTICLE-PARTICLE COLLISIONS (PAIR TABLE BASED METHOD)
  CALL PAIRTABLECLEAR

  ! DETERMINE SEARCH DISTANCE AND DETECT PARTICLE PAIRS
  ! FOR IMF TENTATIVELY DISTANCE=3*DP
  IF (IMFSWITCH) THEN
    CALL PAIRDETECT(6.0*RPMAX)
  ELSE
    CALL PAIRDETECT(2.0*RPMAX)
  END IF

  IF (IMFSWITCH) THEN
    ! CALCULATE INTERPARTICLE MAGNETIC FORCE

```

```

      CALL FPIMF

      ! DEFLATE TABLE TO ELIMINATE ALL ENTRIES WITH
      ! DISTANCE GREATER THAN 2*RPMAX
      CALL PAIRTABLEDEFLATE(2.0*RPMAX)

      END IF

      ! NOW PROCEED WITH COLLISION CALCULATIONS
      CALL PARTCOLL

      ! *** FORCES ON INDIVIDUAL PARTICLES

      ! GRAVITATIONAL AND BUOYANCY FORCE
      CALL FPGRV
      CALL FPBUOY

      ! DRAG FORCE
      CALL DRAGFORCE

      ! ROTATION-DEPENDENT FORCES
      CALL ROTATIONFORCES

      ! *** CALCULATE PARTICLE MOTION AND ROTATION ***
      CALL PARTICLEMOTION2
      CALL PARTICLEROTATION

      ! AFTER MOVING THE PARTICLES, RE-SORT THE INDEXES BY INSERTION SORT
      CALL INSERTIONSORT

      ! VERIFY THAT NO PARTICLE HAS LEFT THE BED
      CALL CHECK_CONTAINMENT

      ! *** BOLITAS FLX FRAME OUTPUT ***
      IF (CURRTIME.GE.BOLTIMER) THEN
        CALL FLXWRITE
        CALL FLSUPDATE
        BOLTIMER=BOLTIMER+1.0/BOLFPS

        ! OTHER TEXT FILE OUTPUT
        CALL WRITEPARTLOC
      END IF

      END DO

      IF (DTRATIO.GT.1) THEN
        ! OBTAIN AVERAGED FORCE OVER FLUID
        FFX=FFX/REAL(DTRATIO)
        FFY=FFY/REAL(DTRATIO)
        FFZ=FFZ/REAL(DTRATIO)
      END IF

      END IF

      ! *****
      ! *****

      ! CALCULATONS FOR PARTICLES ENO HERE

```

```

! *** CALCULATE FLUID EQUATIONS ***
CALL XMOM
CALL YMOM
CALL ZMOM
CALL PRESSURECORRECTOR

! *** CALCULATE VELOCITY GRADIENTS ***
CALL VELGRADIENTS

! *** BOLITAS FLX FRAME OUTPUT ***
IF (CURRTIME.GE.BOLTIMER .AND. NP.EQ.0) THEN
  ! OUTPUT HERE ONLY IF NO PARTICLES
  CALL FLXWRITE
  CALL FLSUPDATE
  BOLTIMER=BOLTIMER+1.0/BOLFPS
END IF

! *** UPDATE SIMULATION PROGRESS TO SCREEN ***
IF (ITER.GE.UPDATEITER) THEN
  ! MUST UPDATE SCREEN IN THIS ITERATION
  CALL PROGRESSREPORT
  ! SHARE JOHNDOE'S WISDOM
  CALL SHAREWISDOM
  ! UPDATE BOLITAS STATUS FILE
  CALL FLSUPDATE
END IF

END DO

! *****
! *                END MAIN PROGRAM LOOP                *
! *****

! BOLITAS CLOSE FLX FILES AND SIGNAL END OF SIMULATION STATUS
CALL FLXCLOSE
CALL FLSEND

! CPU TIME FOR SIMULATION IS CALCULATED AND OUTPUT TO SCREEN
CALL CPU_TIME(CPUTIMENOW)
CPUTIMEELAPSED=CPUTIMENOW-CPUTIMESTART

WRITE(*,*) ' '
WRITE(*,*) 'CPU TIME USED IN MIN= ',CPUTIMEELAPSED/60
WRITE(*,*) 'PRESS ENTER TO EXIT PROGRAM'
PAUSE

! OTHER TEXT FILE OUTPUT
IF (NP.GT.0) CALL WRITEPARTLOC

END PROGRAM PARTICLEX

```

B.3 Particle-X global variables

MODULE GLOBVARS

! GLOBAL CONSTANTS

REAL,PARAMETER::	PI = 3.14159265359	! GEOMETRICAL CONSTANT PI
REAL,PARAMETER::	MUZERO = 1.256637E-6	! PERMEABILITY OF FREE SPACE [N/A ²],[Tm/A]
REAL,PARAMETER::	G = 9.80665	! EARTH'S GRAVITATIONAL CONSTANT [m/s ²]

! OFFICIAL PROGRAM NAME AND VERSION

CHARACTER(*),PARAMETER::	MYNAME='Particle-X'	! PROGRAM NAME
INTEGER,PARAMETER::	VERSIONMAJOR=1	! MAJOR VERSION NUMBER
INTEGER,PARAMETER::	VERSIONMINOR=0	! MINOR VERSION NUMBER
INTEGER,PARAMETER::	VERSIONREV=12	! REVISION NUMBER

! DIMENSIONALITY OF THE PROGRAM - 3D BY DEFAULT

INTEGER,PARAMETER::	DIMENSIONS=3	! NUMBER OF DIMENSIONS (2 OR 3)
---------------------	--------------	---------------------------------

! GRAVITY

REAL::	GX	! X-COMPONENT OF GRAVITY [m/s ²]
REAL::	GY	! Y-COMPONENT OF GRAVITY [m/s ²]
REAL::	GZ	! Z-COMPONENT OF GRAVITY [m/s ²]

! SIMULATION PARAMETERS

REAL::	DT	! TIME STEP FOR SIMULATION [s]
REAL::	ENDTIME	! TOTAL TIME FOR SIMULATION [s]
INTEGER::	ENDITER	! TOTAL NUMBER OF MAIN LOOP ITERATIONS
INTEGER::	ITER	! CURRENT MAIN LOOP ITERATION
REAL::	CURRTIME	! CURRENT SIMULATION TIME
INTEGER::	DTRATIO	! NUMBER OF PARTICLE TIME STEPS PER FLUID TIME STEP
REAL::	DTFLUID	! TIME STEP FOR FLUID FLOW CALCULATIONS
INTEGER::	ITPERSECOND	! NUMBER OF ITERATIONS PER SECOND OF SIMULATION TIME

! COLUMN GEOMETRY

REAL::	COLUMNX	! COLUMN WIDTH (X)	[m]
REAL::	COLUMNY	! COLUMN HIGHT (Y)	[m]
REAL::	COLUMNZ	! COLUMN DEPTH (Z)	[m]
REAL::	DV	! FLUID CELL VOLUME [m ³]	
REAL::	DX	! FLUID CELL LENGTH IN X	
REAL::	DXDY	! DX*DY	
REAL::	DXDZ	! DX*DZ	
REAL::	DY	! FLUID CELL LENGTH IN Y	
REAL::	DYDZ	! DY*DZ	
REAL::	DZ	! FLUID CELL LENGTH IN Z	
INTEGER::	LI	! NUMBER OF FLUID CELLS FOR COLUMN IN X DIRECTION	
INTEGER::	LIJK	! TOTAL NUMBER OF FLUID CELLS	
INTEGER::	LJ	! NUMBER OF FLUID CELLS FOR COLUMN IN Y DIRECTION	
INTEGER::	LK	! NUMBER OF FLUID CELLS FOR COLUMN IN Z DIRECTION	

! INLET

REAL::	UINLET	! INLET VELOCITY (IF INPUTDISTPLATE=.FALSE.)
REAL,ALLOCATABLE::	UYDIST(:,,:)	! DISTRIBUTOR PLATE VELOCITY PROFILE (X,Z) @ Y=0


```

REAL::          INLETOPENFRACTION=1.0      ! OPEN FRACTION AT DISTRIBUTOR PLATE [-]
REAL::          INLETFACOR=1.0      ! DISTRIBUTOR PLATE VELOCITY FACTOR

! FLUID PROPERTIES
REAL::          ROF          ! DENISTY OF FLUID (CONSTANT)
REAL::          MUF          ! VISCOSITY OF FLUID (CONSTANT)

! FLUID PRESSURE
REAL,ALLOCATABLE:: P(:, :, :) ! PRESSURE AT CENTER OF CELL (X,Y,Z)
REAL,ALLOCATABLE:: PDYN(:, :, :) ! DYNAMIC PRESSURE AT CENTER OF CELL
REAL,ALLOCATABLE:: PSTAT(:, :, :) ! HYDROSTATIC PRESSURE AT CENTER OF CELL

! PRESSURE CORRECTION VARIABLES
REAL,ALLOCATABLE:: PCORRO(:, :, :) ! INITIAL GUESS TO PRESSUE CORRECTION
REAL,ALLOCATABLE:: PCORR(:, :, :) ! PRESSURE CORRECTION ARRAY
REAL,ALLOCATABLE:: DPX(:, :, :) ! X-CONTRIBUTION OF PRESSURE CORRECTION
REAL,ALLOCATABLE:: DPY(:, :, :) ! Y-CONTRIBUTION OF PRESSURE CORRECTION
REAL,ALLOCATABLE:: DPZ(:, :, :) ! Z-CONTRIBUTION OF PRESSURE CORRECTION

! FLUID VELOCITY
REAL,ALLOCATABLE:: UMAG(:, :, :) ! VELOCITY MAGNITUDE AT CELL
REAL,ALLOCATABLE:: UX(:, :, :) ! X-VELOCITY AT FACE OF CELL
REAL,ALLOCATABLE:: UX0(:, :, :) ! X-VELOCITY AT FACE OF CELL PREVIOUS ITERATION
REAL,ALLOCATABLE:: UY(:, :, :) ! Y-VELOCITY AT FACE OF CELL
REAL,ALLOCATABLE:: UY0(:, :, :) ! Y-VELOCITY AT FACE OF CELL PREVIOUS ITERATION
REAL,ALLOCATABLE:: UZ(:, :, :) ! Z-VELOCITY AT FACE OF CELL
REAL,ALLOCATABLE:: UZ0(:, :, :) ! Z-VELOCITY AT FACE OF CELL PREVIOUS ITERATION
REAL,ALLOCATABLE:: UYDEV(:, :, :) ! Y-VELOCITY DEVIATION FROM INLET

! FLUID VELOCITY GRADIENTS
REAL, ALLOCATABLE:: UXGRADX(:, :, :) ! FLUID X-VEL, GRADIENT IN X
REAL, ALLOCATABLE:: UXGRADY(:, :, :) ! FLUID X-VEL, GRADIENT IN Y
REAL, ALLOCATABLE:: UXGRADZ(:, :, :) ! FLUID X-VEL, GRADIENT IN Z
REAL, ALLOCATABLE:: UYGRADX(:, :, :) ! FLUID Y-VEL, GRADIENT IN X
REAL, ALLOCATABLE:: UYGRADY(:, :, :) ! FLUID Y-VEL, GRADIENT IN Y
REAL, ALLOCATABLE:: UYGRADZ(:, :, :) ! FLUID Y-VEL, GRADIENT IN Z
REAL, ALLOCATABLE:: UZGRADX(:, :, :) ! FLUID Z-VEL, GRADIENT IN X
REAL, ALLOCATABLE:: UZGRADY(:, :, :) ! FLUID Z-VEL, GRADIENT IN Y
REAL, ALLOCATABLE:: UZGRADZ(:, :, :) ! FLUID Z-VEL, GRADIENT IN Z

! FORCE ON FLUID
REAL,ALLOCATABLE:: FFX(:, :, :) ! X-COMP EXTERNAL FORCE ON FLUID (DRAG & OTHERS) [N]
REAL,ALLOCATABLE:: FFY(:, :, :) ! Y-COMP EXTERNAL FORCE ON FLUID (DRAG & OTHERS) [N]
REAL,ALLOCATABLE:: FFZ(:, :, :) ! Z-COMP EXTERNAL FORCE ON FLUID (DRAG & OTHERS) [N]

! SUCCESIVE OVERRELAXATION PARAMETERS
REAL::          MAXTOL          ! FLUID VELOCITY CONVERG. TOLERANCE
REAL::          AVETOL          ! FLUID VELOCITY AVERAGE TOLERANCE
REAL::          PMAXTOL          ! PRESSUE CORR. CONVERG. TOLERANCE
REAL::          PAVETOL          ! PRESSUE CORR. AVERAGE TOLERANCE
REAL::          RELAXX          ! RELAXATION COEFF FOR X-MOMENTUM
INTEGER::       MAXITERX ! MAXIMUM ITERATION FOR X-MOMENTUM
REAL::          RELAXY          ! RELAXATION COEFF FOR Y-MOMENTUM
INTEGER::       MAXITERY ! MAXIMUM ITERATION FOR Y-MOMENTUM
REAL::          RELAXZ          ! RELAXATION COEFF FOR Z-MOMENTUM

```

```

INTEGER::          MAXITERZ ! MAXIMUM ITERATION FOR Z-MOMENTUM
INTEGER::          MAXITERPC ! MAXIMUM PRESSURE CORRECTION ITERATION
REAL::            RELAXPC    ! PRESSURE CORRECTION SOLVER RELAXATION
REAL::            RELAXP     ! PRESSURE RELAXATION COEFFICIENT

! INNER ITERATION COUNTERS
INTEGER:: ITERPC          ! ITERATION COUNTER FOR PRESSURE CORRECTION SOLVER
INTEGER:: ITERUX          ! ITERATION COUNTER FOR X-MOMENTUM SOLVER
INTEGER:: ITERUY          ! ITERATION COUNTER FOR Y-MOMENTUM SOLVER
INTEGER:: ITERUZ          ! ITERATION COUNTER FOR Z-MOMENTUM SOLVER

! RESIDUALS
REAL:: NORMRESUX          ! NORMALIZED RESIDUAL AND TOLERANCE FOR X-MOM
REAL:: TOLRESUX,TOLNORMRESUX ! TOLERANCE FOR ABSOLUTE AND NORMALIZED RESIDUAL X-MOM
REAL:: NORMRESUY          ! NORMALIZED RESIDUAL AND TOLERANCE FOR Y-MOM
REAL:: TOLRESUY,TOLNORMRESUY ! TOLERANCE FOR ABSOLUTE AND NORMALIZED RESIDUAL Y-MOM
REAL:: NORMRESUZ          ! NORMALIZED RESIDUAL AND TOLERANCE FOR Z-MOM
REAL:: TOLRESUZ,TOLNORMRESUZ ! TOLERANCE FOR ABSOLUTE AND NORMALIZED RESIDUAL Z-MOM
REAL:: NORMRESMASS        ! NORMALIZED RESIDUAL AND TOLERANCE FOR PRESS CORR
REAL:: TOLRESMASS,TOLNORMRESMASS ! TOLERANCE FOR ABS AND NORMALIZED RESIDUAL PRESS CORR
REAL, ALLOCATABLE:: CELLRESMASS(:,:,:) ! CELL RESIDUAL MASS [kg/s]
REAL, ALLOCATABLE:: CELLRESUX(:,:,:) ! CELL RESIDUAL X-MOMENTUM [kg.m/s^2]
REAL, ALLOCATABLE:: CELLRESUY(:,:,:) ! CELL RESIDUAL Y-MOMENTUM [kg.m/s^2]
REAL, ALLOCATABLE:: CELLRESUZ(:,:,:) ! CELL RESIDUAL Z-MOMENTUM [kg.m/s^2]

! VOIDAGE CELL PROPERTIES
REAL,ALLOCATABLE:: EPC(:,:,:) ! VOID CELL VOID FRACTION (COARSE GRID)
INTEGER::          CELLRATIO ! RATIO OF FLUID CELL TO VOID CELL LENGTH
REAL,ALLOCATABLE:: EP(:,:,:) ! INTERPOLATED FLUID CELL VOID FRACTION (FINE GRID)
REAL,ALLOCATABLE:: EPO(:,:,:) ! INTERPOLATED FLUID CELL VOID FRACTION (FINE GRID)
INTEGER::          LVI       ! NUMBER OF VOID CELLS FOR COLUMN IN X DIRECTION
INTEGER::          LVJ       ! NUMBER OF VOID CELLS FOR COLUMN IN Y DIRECTION
INTEGER::          LVK       ! NUMBER OF VOID CELLS FOR COLUMN IN Z DIRECTION
REAL::            DXC        ! VOID FRACTION CELL LENGTH IN X
REAL::            DYC        ! VOID FRACTION CELL LENGTH IN Y
REAL::            DZC        ! VOID FRACTION CELL LENGTH IN Z

! BED PROPERTIES
REAL::            ABEDH       ! AVERAGE HEIGHT OF THE BED [m]
INTEGER::          ABEDHYCELL ! FLUID CELL (IN Y) WHICH IS AT AVE HEIGHT
REAL::            APRESSDROP ! AVERAGE BED PRESSURE DROP [Pa]
REAL,ALLOCATABLE:: MPHEIGHT(:,:) ! BED HEIGHT FOR EACH VERTICAL FLUID COLUMN
INTEGER,ALLOCATABLE:: TOPCELL(:,:) ! HIGHEST FLUID CELL WITH PARTICLES FOR EACH X,Z
! IN WHICH 95% OF PARTICLES ARE IN OR BELOW
INTEGER,ALLOCATABLE:: BOTCELL(:,:) ! HIGHEST FLUID CELL WITH PARTICLES FOR EACH X,Z
! IN WHICH 95% OF PARTICLES ARE IN OR ABOVE
REAL::            AVOIDAGE ! AVERAGE VOIDAGE BASED ON AVERAGE BED HEIGHT

! PARTICLE PROPERTIES
INTEGER::          NP         ! NUMBER OF PARTICLES IN SIMULATION
REAL::            MP         ! MASS OF THE PARTICLE (CONSTANT)
REAL::            MPMIN      ! SMALLEST MASS OF PARTICLE
REAL::            MPMAX      ! LARGEST MASS OF PARTICLE
REAL::            IMP        ! MOMENT OF INERTIA OF PARTICLE (CONSTANT)
REAL::            RP         ! PARTICLE RADIUS (CONSTANT)
REAL::            DP         ! PARTICLE DIAMETER
REAL::            RPMAX      ! LARGEST PARTICLE RADIUS

```

```

REAL::      RPMIN      ! SMALLEST PARTICLE RADIUS
REAL::      SP         ! PARTICLE SURFACE AREA (CONSTANT)
REAL::      VP         ! VOLUME OF PARTICLE
REAL::      CSP        ! PARTICLE CROSS SECTION AREA
REAL::      ROP        ! PARTICLE DENSITY (CONSTANT)
REAL::      XHIP       ! PARTICLE SUSCEPTIBILITY (CONSTANT)
REAL::      XHIE       ! PARTICLE EFFECTIVE SUSCEPTIBILITY (CONSTANT)
REAL::      EFFXHIP    ! COEFFICIENT OF PARTICLE MAGNETIC FORCE [ $\mu \cdot X_e \cdot V_p$ ]
REAL::      FBPC       ! COEFFICIENT = EFFXHIP*MODIFYING PARAMETERS
REAL::      MO         ! DIPOLE MOMENT FOR CONSTANT PROP CASE, UNIFORM FIELD
INTEGER,ALLOCATABLE:: PCOLOR(:) ! COLOR OF THE PARTICLE

```

! POSITION OF PARTICLES

```

REAL, ALLOCATABLE:: X(:)      ! X-LOCATION OF PARTICLES
REAL, ALLOCATABLE:: Y(:)      ! Y-LOCATION OF PARTICLES
REAL, ALLOCATABLE:: Z(:)      ! Z-LOCATION OF PARTICLES

```

! PARTICLE DIRECTORY VARIABLES

```

INTEGER, ALLOCATABLE:: FDIRI(:) ! STORES THE FLUID CELL (I) LOCATION OF THE PARTICLE
INTEGER, ALLOCATABLE:: FDIRJ(:) ! STORES THE FLUID CELL (J) LOCATION OF THE PARTICLE
INTEGER, ALLOCATABLE:: FDIRK(:) ! STORES THE FLUID CELL (K) LOCATION OF THE PARTICLE
INTEGER, ALLOCATABLE:: FDIRSI(:) ! LOCATION OF THE PARTICLE IN THE STAGGERED X-GRID
INTEGER, ALLOCATABLE:: FDIRSJ(:) ! LOCATION OF THE PARTICLE IN THE STAGGERED X-GRID
INTEGER, ALLOCATABLE:: FDIRSK(:) ! LOCATION OF THE PARTICLE IN THE STAGGERED X-GRID
INTEGER, ALLOCATABLE:: FCUTI(:) ! CASE # FOR PARTICLES CUT BY FLUID CELLS
INTEGER, ALLOCATABLE:: VCUTI(:) ! CASE # FOR PARTICLES CUT BY VOIDAGE CELLS

```

! PARTICLE LOCATION INDEXING

```

INTEGER, ALLOCATABLE:: PINDEXX(:) ! INDEX OF PARTICLES SORTED BY X-POSITION
INTEGER, ALLOCATABLE:: PINDEXY(:) ! INDEX OF PARTICLES SORTED BY Y-POSITION
INTEGER, ALLOCATABLE:: PINDEZX(:) ! INDEX OF PARTICLES SORTED BY Z-POSITION
REAL::      MAXSEARCHDIST ! THE SEARCH DISTANCE FOR PARTICLE PAIRS

```

! PARTICLE VELOCITY

```

REAL, ALLOCATABLE:: VX(:)      ! X-VELOCITY OF PARTICLES
REAL, ALLOCATABLE:: VY(:)      ! Y-VELOCITY OF PARTICLES
REAL, ALLOCATABLE:: VZ(:)      ! Z-VELOCITY OF PARTICLES
REAL, ALLOCATABLE:: KINETIC(:) ! PARTICLE KINETIC ENERGY

```

! PARTICLE ANGULAR VELOCITY

```

REAL, ALLOCATABLE:: WX(:)      ! X-ANGULAR VELOCITY OF PARTICLE
REAL, ALLOCATABLE:: WY(:)      ! Y-ANGULAR VELOCITY OF PARTICLE
REAL, ALLOCATABLE:: WZ(:)      ! Z-ANGULAR VELOCITY OF PARTICLE

```

! FORCE ON PARTICLES

```

REAL,ALLOCATABLE:: FPX(:)      ! ARRAY OF TOTAL FORCE ON PARTICLE (X)
REAL,ALLOCATABLE:: FPY(:)      ! ARRAY OF TOTAL FORCE ON PARTICLE (Y)
REAL,ALLOCATABLE:: FPZ(:)      ! ARRAY OF TOTAL FORCE ON PARTICLE (Z)

```

! TORQUE ON PARTICLES

```

REAL,ALLOCATABLE:: TAUPX(:) ! PARTICLE TORQUE IN (X)
REAL,ALLOCATABLE:: TAUPY(:) ! PARTICLE TORQUE IN (Y)
REAL,ALLOCATABLE:: TAUPZ(:) ! PARTICLE TORQUE IN (Z)
REAL,ALLOCATABLE:: REYNOLDSP(:) ! PARTICLE REYNOLDS NUMBER
REAL,ALLOCATABLE:: REYNOLDSROT(:) ! PARTICLE ROTATIONAL REYNOLDS NUMBER

```

```

! VARIABLES FOR HIGHER-ORDER INTEGRATION METHODS
REAL, ALLOCATABLE:: HISTORYAX(:, :) ! HISTORY OF PARTICLE ACCELERATION, X-COMPONENT
REAL, ALLOCATABLE:: HISTORYAY(:, :) ! HISTORY OF PARTICLE ACCELERATION, Y-COMPONENT
REAL, ALLOCATABLE:: HISTORYAZ(:, :) ! HISTORY OF PARTICLE ACCELERATION, Z-COMPONENT
REAL, ALLOCATABLE:: HISTORYVX(:, :) ! HISTORY OF PARTICLE VELOCITY, X-COMPONENT
REAL, ALLOCATABLE:: HISTORYVY(:, :) ! HISTORY OF PARTICLE VELOCITY, Y-COMPONENT
REAL, ALLOCATABLE:: HISTORYVZ(:, :) ! HISTORY OF PARTICLE VELOCITY, Z-COMPONENT
INTEGER:: ABK=1 ! ADAM-BASHFORTH METHOD ORDER
INTEGER:: ABLOC1=0, ABLOC2=0, ABLOC3=0 ! INDEX OF THE NEWEST VALUES IN THE HISTORY ARRAYS
INTEGER:: CHOICEPMINTEGRATION=1 ! CHOICE OF INTEGRATION METHOD FOR PARTICLE MOTION

! COLLISION COUNTERS
INTEGER, ALLOCATABLE:: CONTACTS(:) ! NUMBER OF CONTACTS WITH OTHER PARTICLES
INTEGER:: PPCOUNT ! TOTAL COUNT OF P-P COLLISIONS
INTEGER:: PWCOUNT ! TOTAL COUNT OF P-W COLLISIONS

! VARIABLES FOR GRID CELL BASED COLLISION CALCULATIONS
INTEGER:: NGX, NGY, NGZ ! THE NUMBER OF GRID UNITS IN X, Y, Z (NOT INCLUDING GHOSTS)
REAL:: LX, LY, LZ ! THE LENGTHS OF THE GRID UNITS IN X, Y, Z
INTEGER:: NGRIDTOTAL ! TOTAL NUMBER OF GRID UNITS
INTEGER:: MPPGRID ! MAXIMUM PARTICLES PER GRID UNIT
INTEGER, ALLOCATABLE:: GRID(:, :)
INTEGER, ALLOCATABLE:: NPGRID(:)
INTEGER:: GRIDOFS(13) ! ARRAY OF GRID OFFSET VALUES (BASE VALUE)
INTEGER:: CUROFS(13) ! ARRAY OF CURRENT GRID OFFSET VALUES
INTEGER:: OFFSETMAP(28) ! ARRAY OF OFFSET MAPS FOR COLLISION OPTIM

! COLLISION PARAMETERS - PARTICLE-WALL
REAL:: RESTITUTIONPW ! P-W RESTITUTION COEFFICIENT [-]
REAL:: FRICTIONPW ! P-W FRICTION COEFFICIENT [-]
REAL:: STIFFNESSPW ! P-W NORMAL STIFFNESS (SPRING CONSTANT) [N/m]
REAL:: STIFFNESSPWT ! P-W TANGENTIAL STIFFNESS (SPRING CONSTANT) [N/m]
REAL:: DAMPINGPW ! P-W NORMAL DAMPING COEFFICIENT [-]
REAL:: DAMPINGPWT ! P-W TANGENTIAL DAMPING COEFFICIENT [-]

! TANGENTIAL DISPLACEMENT FOR CONTACT WITH WALLS
! NOTE THAT EACH PARTICLE COLLIDING WITH A WALL CAN HAS 3 COMPONENTS OF
! TANGENTIAL DISPLACEMENT, EVEN THOUGH ONE IS ALWAYS ZERO BECAUSE WALLS
! ARE NORMAL TO COORDINATE AXES
REAL, ALLOCATABLE:: WEWALLDTX(:) ! WEST/EAST WALL TANGENTIAL DISPLACEMENT IN X
REAL, ALLOCATABLE:: WEWALLDTY(:) ! WEST/EAST WALL TANGENTIAL DISPLACEMENT IN Y
REAL, ALLOCATABLE:: WEWALLDTZ(:) ! WEST/EAST WALL TANGENTIAL DISPLACEMENT IN Z
REAL, ALLOCATABLE:: SNWALLDTX(:) ! SOUTH/NORTH WALL TANGENTIAL DISPLACEMENT IN X
REAL, ALLOCATABLE:: SNWALLDTY(:) ! SOUTH/NORTH WALL TANGENTIAL DISPLACEMENT IN Y
REAL, ALLOCATABLE:: SNWALLDTZ(:) ! SOUTH/NORTH WALL TANGENTIAL DISPLACEMENT IN Z
REAL, ALLOCATABLE:: BWALLDTX(:) ! FRONT/BACK WALL TANGENTIAL DISPLACEMENT IN X
REAL, ALLOCATABLE:: BWALLDTY(:) ! FRONT/BACK WALL TANGENTIAL DISPLACEMENT IN Y
REAL, ALLOCATABLE:: BWALLDTZ(:) ! FRONT/BACK WALL TANGENTIAL DISPLACEMENT IN Z
INTEGER, ALLOCATABLE:: WEWALLLASTIT(:) ! LAST ITER THAT PARTICLES WERE COLLIDING W/E WALL
INTEGER, ALLOCATABLE:: SNWALLLASTIT(:) ! LAST ITER THAT PARTICLES WERE COLLIDING S/N WALL
INTEGER, ALLOCATABLE:: BWALLLASTIT(:) ! LAST ITER THAT PARTICLES WERE COLLIDING B/F WALL

! COLLISION PARAMETERS - PARTICLE-PARTICLE
REAL:: RESTITUTIONPP ! P-P RESTITUTION COEFFICIENT [-]
REAL:: FRICTIONPP ! P-P FRICTION COEFFICIENT [-]

```

```

REAL::          STIFFNESSPPN      ! P-P NORMAL STIFFNESS (SPRING CONSTANT) [N/m]
REAL::          STIFFNESSPPT      ! P-P TANGENTIAL STIFFNESS (SPRING CONSTANT) [N/m]
REAL::          DAMPINGPPN        ! P-P NORMAL DAMPING COEFFICIENT [-]
REAL::          DAMPINGPPT        ! P-P TANGENTIAL DAMPING COEFFICIENT [-]

! MAGNETIC FIELD PARAMETERS
INTEGER::       EXTMAGFLD         ! CHOICE OF MAGNETIC FIELD CONFIGURATION (0,1,2,3,4)
LOGICAL::       IMFSWITCH         ! SWITCH FOR INTERPARTICLE MAGNETIC FORCES
REAL::         BO                 ! MAGNITUDE OF THE FIELD FOR CONSTANT FIELD CASE [T]
REAL::         BXO               ! EXTERNAL MAGNETIC FIELD X-COMPONENT [T] AT x=0
REAL::         BYO               ! EXTERNAL MAGNETIC FIELD Y-COMPONENT [T] AT y=0
REAL::         BZO               ! EXTERNAL MAGNETIC FIELD Z-COMPONENT [T] AT z=0
REAL::         IMFMAX            ! MAXIMUM ATTRACTIVE IMF [N]
REAL::         BE                ! CHAIN STRENGTH PARAMETER [-]
LOGICAL::       SWITCHDRAGCORR=.FALSE. ! SWITCH FOR APPLYING DRAG CORRECTION FACTOR

! USER CHOICE OF METHODS (READ FROM INPUT FILE)
INTEGER::       CHOICEPPCOL       ! CHOICE FOR PARTICLE-PARTICLE COLLISION DETECTION
INTEGER::       CHOICEWALLCOLL    ! CHOICE FOR PARTICLE-WALL COLLISION DETECTION
INTEGER::       CHOICEDRAGMODEL  ! CHOICE FOR DRAG FORCE CALCULATION MODEL
LOGICAL::       CHOICEHEATTRANSFER ! CHOICE FOR HEAT TRANSFER CONSIDERATION
INTEGER::       CHOICEWALLHEATTRANS ! MODEL FOR WALL-FLUID HEAT TRANS (0,1,2)
LOGICAL::       CHOICEMASSTRANSFER ! CHOICE FOR MASS TRANSFER CONSIDERATION
LOGICAL::       INPUTDISTPLATE   ! FLAG FOR READING DISTRIBUTOR PLATE FROM A FILE
INTEGER::       CHOICEPARTICLEPOSITION ! CHOICE FOR INITIAL PARTICLE POSITIONING
INTEGER::       CHOICEPAIRDETECTION ! CHOICE FOR PARTICLE PAIR DETECTION METHOD

! VARIABLES FOR TRILINEAR INTERPOLATION
REAL, ALLOCATABLE:: F2PX(:)      ! FLUID CELL TO PARTICLE INTERPOLATION FACTOR X
REAL, ALLOCATABLE:: F2PY(:)      ! FLUID CELL TO PARTICLE INTERPOLATION FACTOR Y
REAL, ALLOCATABLE:: F2PZ(:)      ! FLUID CELL TO PARTICLE INTERPOLATION FACTOR Z
REAL, ALLOCATABLE:: F2PSX(:)     ! FLUID TO PARTICLE INTERPOLATION FACTOR X STAGGERED
REAL, ALLOCATABLE:: F2PSY(:)     ! FLUID TO PARTICLE INTERPOLATION FACTOR X STAGGERED
REAL, ALLOCATABLE:: F2PSZ(:)     ! FLUID TO PARTICLE INTERPOLATION FACTOR X STAGGERED
REAL, ALLOCATABLE:: F2P000(:)    ! FLUID TO PARTICLE INTERPOLATION FACTOR 000
REAL, ALLOCATABLE:: F2P100(:)    ! FLUID TO PARTICLE INTERPOLATION FACTOR 100
REAL, ALLOCATABLE:: F2P010(:)    ! FLUID TO PARTICLE INTERPOLATION FACTOR 010
REAL, ALLOCATABLE:: F2P110(:)    ! FLUID TO PARTICLE INTERPOLATION FACTOR 110
REAL, ALLOCATABLE:: F2P001(:)    ! FLUID TO PARTICLE INTERPOLATION FACTOR 001
REAL, ALLOCATABLE:: F2P101(:)    ! FLUID TO PARTICLE INTERPOLATION FACTOR 101
REAL, ALLOCATABLE:: F2P011(:)    ! FLUID TO PARTICLE INTERPOLATION FACTOR 011
REAL, ALLOCATABLE:: F2P111(:)    ! FLUID TO PARTICLE INTERPOLATION FACTOR 111

! INTERPOLATED FLUID PROPERTIES AT PARTICLE LOCATIONS
REAL, ALLOCATABLE:: F2PUX(:)     ! INTERPOLATED FLUID VELOCITY X
REAL, ALLOCATABLE:: F2PUY(:)     ! INTERPOLATED FLUID VELOCITY Y
REAL, ALLOCATABLE:: F2PUZ(:)     ! INTERPOLATED FLUID VELOCITY Z
REAL, ALLOCATABLE:: F2PUX00(:)   ! INTERPOLATED FLUID VELOCITY X AT ITER I-2
REAL, ALLOCATABLE:: F2PUY00(:)   ! INTERPOLATED FLUID VELOCITY Y AT ITER I-2
REAL, ALLOCATABLE:: F2PUZ00(:)   ! INTERPOLATED FLUID VELOCITY Z AT ITER I-3
REAL, ALLOCATABLE:: F2PEP(:)     ! INTERPOLATED VOIDAGE AT PARTICLE LOCATIONS

! PROGRESS REPORTING
REAL:: CPUTIMESTART              ! CPU TIME AT BEGINNING OF SIMULATION
REAL:: CPUTIMENOW                ! CURRENT CPU TIME USED
REAL:: CPUTIMEELAPSED            ! ELAPSED CPU TIME: CPUTIMENOW-CPUTIMESTART
REAL:: PROGRESSTIMER             ! INTERVAL IN SECONDS FOR SCREEN PROGRESS UPDATE

```

```

INTEGER:: UPDATEITER=1                ! ITERATION FOR NEXT UPDATE

! BOLITAS
INTEGER*4::      FINGERPRINT      ! SIMULATION IDENTIFIER
INTEGER::        BOLFPS=0 ! FRAMERATE FOR BOLITAS VISUALIZATION
REAL::          BOLTIMER ! TIME OF NEXT BOLITAS OUTPUT

! MISCELLANEOUS VARIABLES
REAL::          WISDOMLEVEL      ! WISDOM LEVEL, BETWEEN 0.0 AND 1.0
LOGICAL::        RANDOMIZE      ! SET SEED FOR RANDOM NUMBERS BASED ON CURRENT TIME

END MODULE GLOBVARS

```

B.4 Sample input file

The format of the input file is similar to the Windows INI files.

Comments and blank lines are allowed, and so is indentation of the lines.

```
! Particle-X Main Input File
```

```

[Method Choices]
CHOICEWALLCOLL = 2
CHOICEPAIRDETECTION = 3
CHOICEDRAGMODEL = 4
CHOICEPARTICLEPOSITION = 3
RANDOMIZE = .FALSE.
INPUTDISTPLATE = .FALSE.

```

```

[Column]
COLUMNX = 0.100
COLUMNY = 0.450
COLUMNZ = 0.050
LVI = 20
LVJ = 90
LVK = 10
CELLRATIO = 1
UINLET = 0.0328

```

```

[Control Parameters]
DT = 2.0E-4
DTRATIO = 50
ENDTIME = 10.0

```

MAXITERX = 20
 MAXITERY = 20
 MAXITERZ = 20
 MAXITERENERGY = 20
 MAXITERPC = 1000

[Absolute Residual Tolerances]

TOLRESUX = 1E-7
 TOLRESUY = 1E-7
 TOLRESUZ = 1E-7
 TOLRESENERGY=1E-3
 TOLRESMASS = 1E-7

[Normalized Residual Tolerances]

TOLNORMRESUX = 0.01
 TOLNORMRESUY = 0.01
 TOLNORMRESUZ = 0.01
 TOLNORMRESENERGY = 0.01
 TOLNORMRESMASS = 0.05

[Relaxation Parameters]

RELAXX = 0.9
 RELAXY = 0.9
 RELAXZ = 0.9
 RELAXP = 0.7
 RELAXPC = 1.8

[Boltas]

BOLFPS = 60
 FINGERPRINT = -821469018

[Gravity]

GX = 0
 GY = -9.81
 GZ = 0

[Particles]

NP = 48750
 RP = 0.001315
 ROP = 1181.0
 XHIP = 0.264

[Fluid]

MUF = 0.000894
 ROF = 997.0

[Magnetic Field]

EXTMAGFLD = 1
 BXO = 0.0
 BYO = 0.0153
 BZO = 0.0
 BXGRAD = 0.0
 BYGRAD = 0.0
 BZGRAD = 0.0
 BXCONSTF = 0.0
 BYCONSTF = 0.0
 BZCONSTF = 0.0
 IMFSWITCH = .TRUE.

[P-W collision parameters]

RESTITUTIONPW = 0.9
 FRICTIONPW = 0.3

```

STIFFNESSPWN = 80.0
STIFFNESSPWT = 8.0

[P-P collision parameters]
RESTITUTIONPP = 0.9
FRICTIONPP = 0.3
STIFFNESSPPN = 80.0
STIFFNESSPPT = 8.0

[Miscellaneous]
WISDOMLEVEL = 0.07
PROGRESSTIMER = 7.0

```

B.5 Sample timeline file

The format of the timeline file is described in the comments at the beginning of the file (see below).

```

! PARTICLE-X TIMELINE SCRIPT
! =====
!
! The format for a timeline event is as follows
!
! BEGIN EVENT
!   VARID =
!   START =
!   END =
!   TYPE =
!   ACTIVE =
!   PARAMETERS =
! END EVENT
!
! Capitalization is irrelevant.
! BEGIN EVENT and END EVENT must spell exactly like this
! The order of different lines within BEGIN EVENT and END EVENT is irrelevant.
!
! VARID is a string identifying the variable to change
! START is a real value indicating the start time for this event
! END is a real value indicating the end time for this event
!
! TYPE can be one of the following
!
!   CONSTANT
!   LINEAR
!   LINEARTWOPOINT
!   QUADRATIC

```



```

!      CUBIC
!      EXPONENTIAL
!      POWER
!      SINE
!
! LINEARTWOPOINT is a special case of LINEAR where the two parameters
!   are the initial and final value for the variable
!
! ACTIVE can be .TRUE. or .FALSE (actually, .t or .f suffices)
!   If .FALSE. the event is just ignored
!
! PARAMETERS are real values (separated by commas or spaces) that the
!   equation defined by TYPE will use as parameters
!
! EXAMPLE:
!
! BEGIN EVENT
!   VARID = INLETFACOR
!   START = 0.1
!   END = 1.0
!   TYPE = SINE
!   ACTIVE = .FALSE.
!   PARAMETERS = 0.8,0.2,0.0,62.8318
! END EVENT
!

BEGIN EVENT
  VARID = INLETFACOR
  START = 0.0
  END = 0.1
  TYPE = CUBIC
  ACTIVE = .TRUE.
  PARAMETERS = 0.0 0.0 300.0 -2000.0
END EVENT

BEGIN EVENT
  VARID = INLETFACOR
  START = 0.1
  END = 60.0
  TYPE = CONSTANT
  ACTIVE = .TRUE.
  PARAMETERS = 1.0
END EVENT

```

B.6 Dynamic behavior of the program

This code was used to gather data at stable operating conditions, for which it yields results in agreement with experimental evidence. Yet, it is important to include at least a note on the validity of its dynamic behavior.

Figures B.1 through B.11 show the start-up of fluidization, as the flow rate is suddenly increased from zero to ten LPM. The simulation, with the same physical characteristics, matches bed height, overall behavior, and time to reach a steady bed expansion very well.

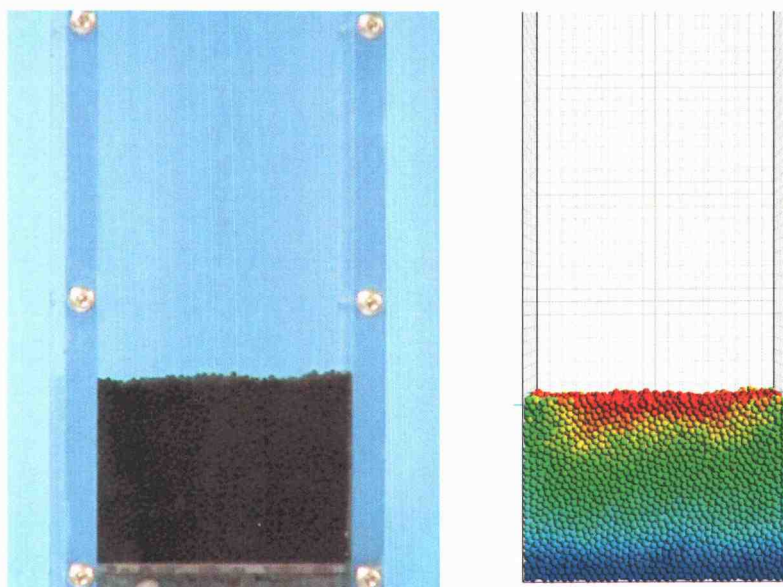


Figure B.1 Dynamic comparison between experiment (left) and simulation (right), $t = 0$ s.

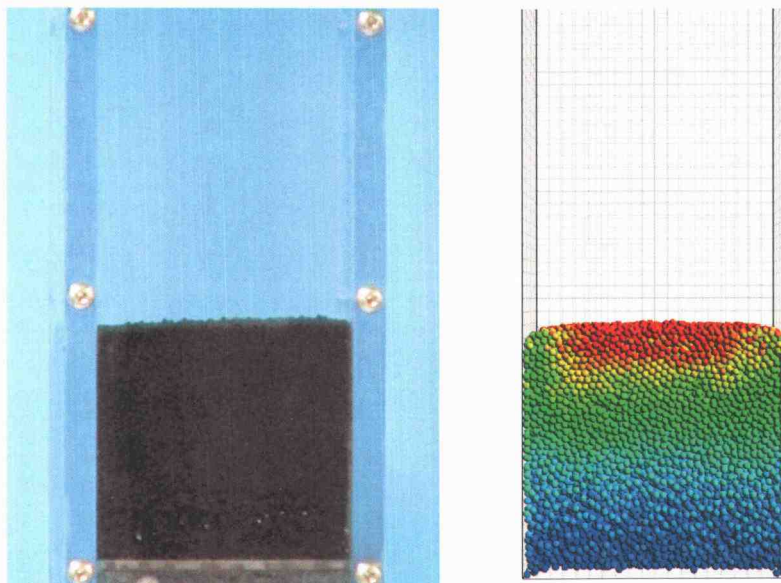


Figure B.2 Dynamic comparison between experiment (left) and simulation (right), $t = 1$ s.

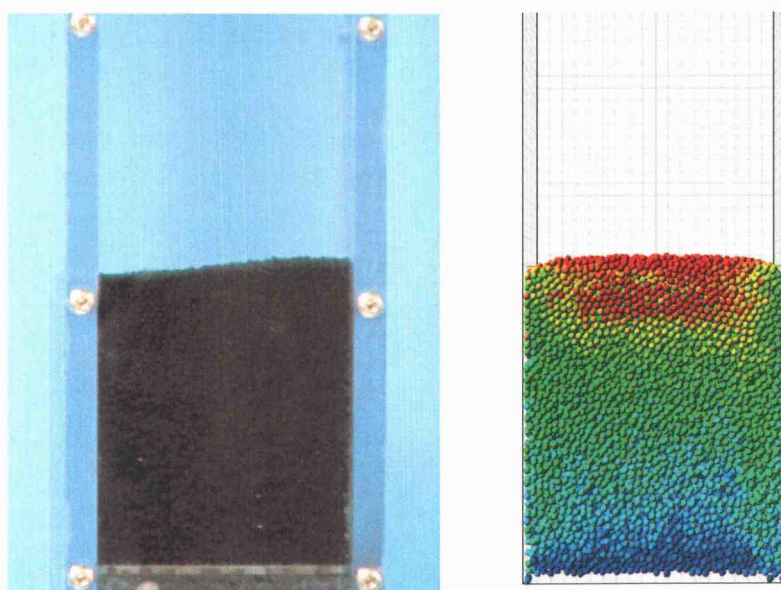


Figure B.3 Dynamic comparison between experiment (left) and simulation (right), $t = 2$ s.

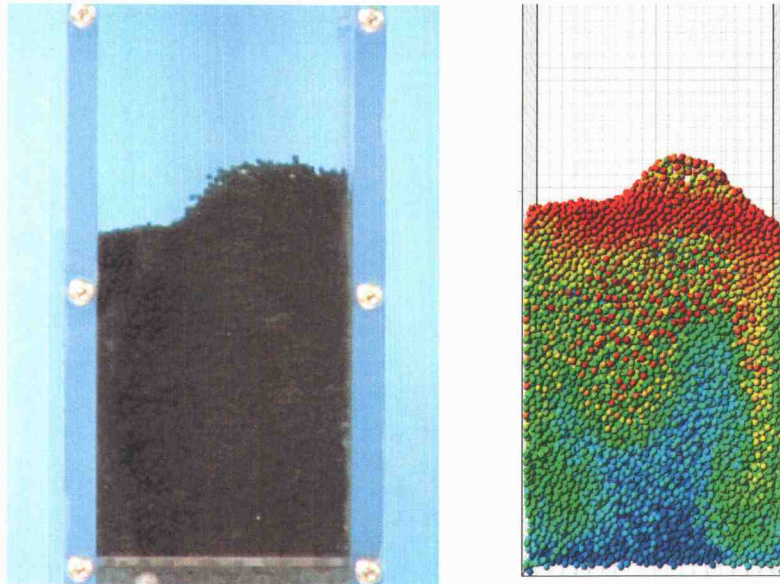


Figure B.4 Dynamic comparison between experiment (left) and simulation (right), $t = 3$ s.

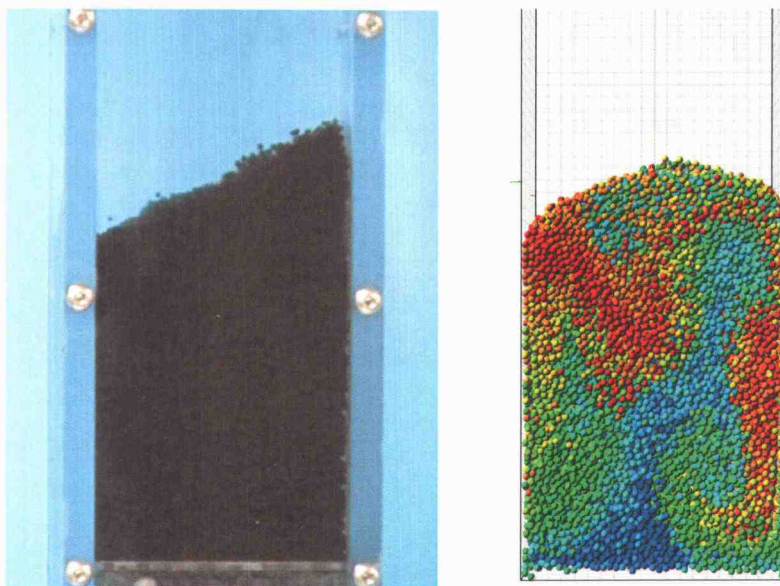


Figure B.5 Dynamic comparison between experiment (left) and simulation (right), $t = 4$ s.

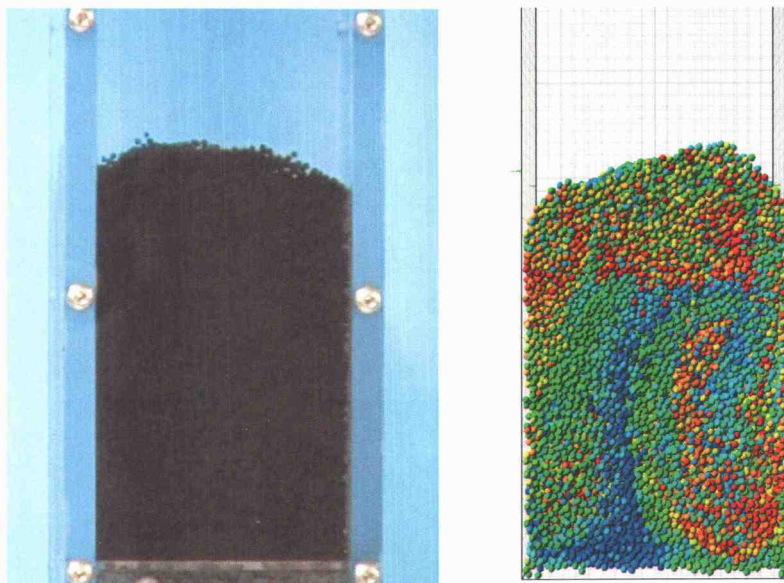


Figure B.6 Dynamic comparison between experiment (left) and simulation (right), $t = 5$ s.

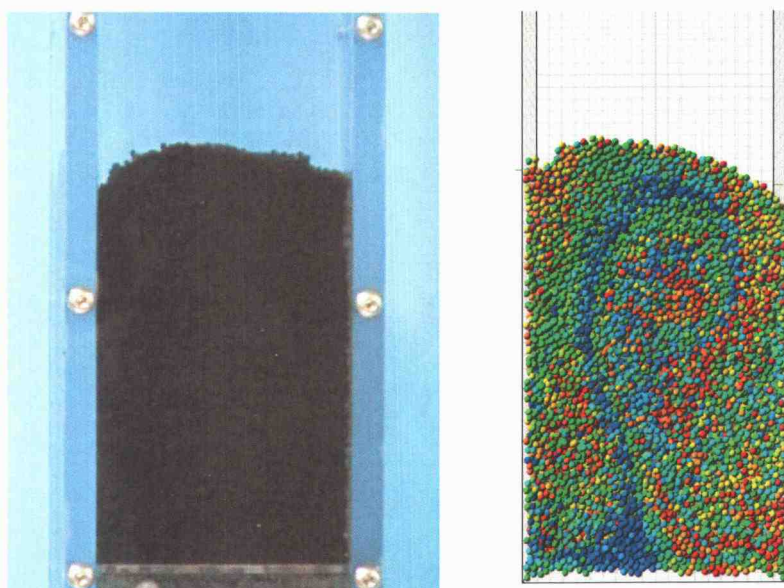


Figure B.7 Dynamic comparison between experiment (left) and simulation (right), $t = 6$ s.

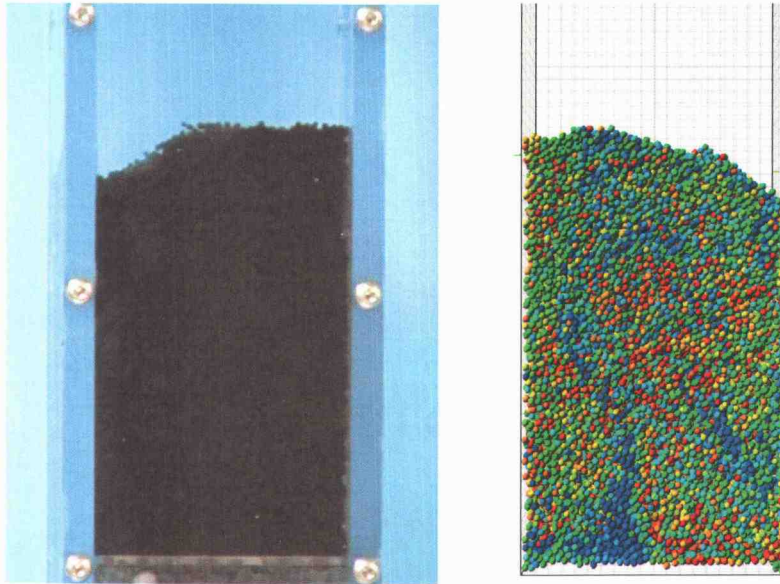


Figure B.8 Dynamic comparison between experiment (left) and simulation (right), $t = 7$ s.

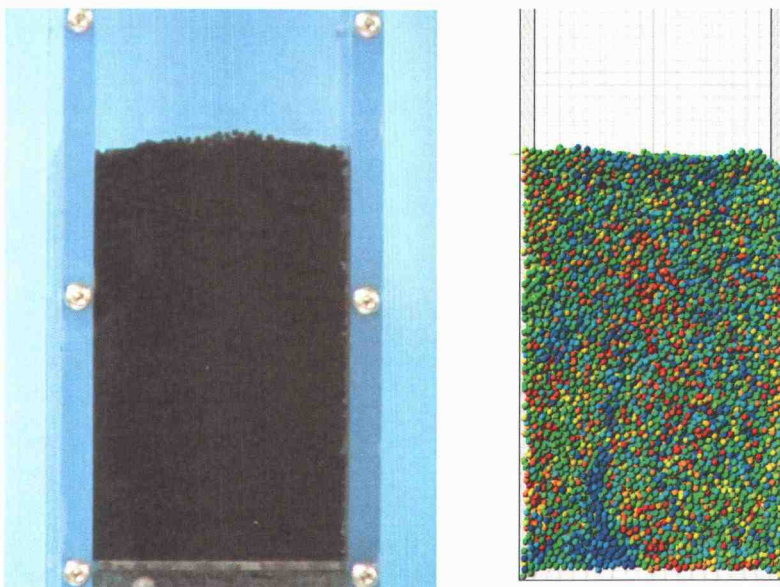


Figure B.9 Dynamic comparison between experiment (left) and simulation (right), $t = 8$ s.

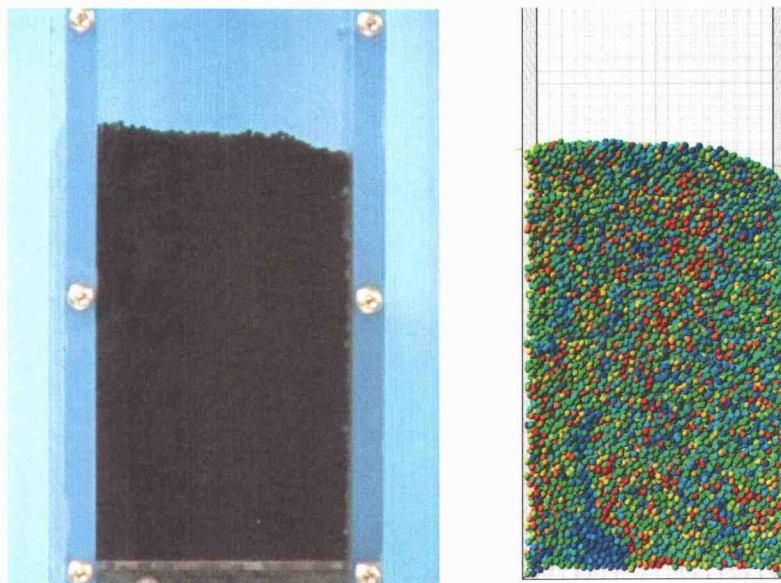


Figure B.10 Dynamic comparison between experiment (left) and simulation (right), $t = 9$ s.

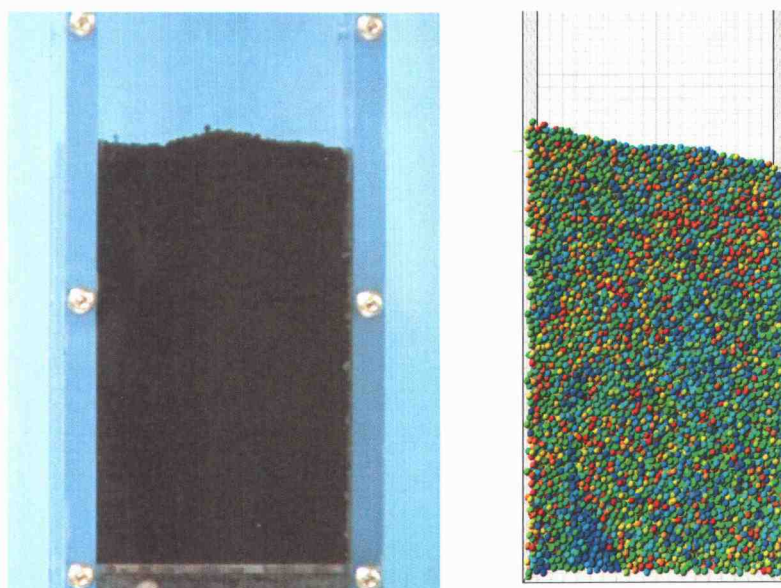


Figure B.11 Dynamic comparison between experiment (left) and simulation (right), $t = 10$ s.

APPENDIX C

NOTES ON BOLITAS 2 VISUALIZATION SOFTWARE

The Doctor: I too come from a distinguished line.

Kim: His cousin is an electric shaver.

The Doctor: Hardly. My program was compiled from the most advanced holomatrices in the Federation... My cousin was a prize-winning chess program.

— Star Trek Voyager
“11:59”

C.1 Overview

Bolitas began a few years ago as a favor for a friend who was working in a 2D CFD-DPM code. It started as a small project in Visual Basic, just to draw circles representing the particles, based on one of the output files generated by the code. It proved to be an incredible time-saver in the debugging stage of the code. Instead of browsing through endless listings of numbers, it was possible just to «have a look» and easily spot any misbehaving particle. Also, it was easy to identify overall trends that were very difficult to track with only text output.

Some features were added, and Bolitas became a tool for debugging and generating pictures and videos for presentations. That was version 1.

At the beginning of this research, it was clear that Bolitas needed some fundamental upgrade to meet the requirements of the new simulation code,

Particle-X. A new drawing engine was written, based in the popular graphics language OpenGL. Most of the user interface was renewed. The file format used for the exchange of information was created from scratch, keeping in mind the need for flexibility. All things considered, Bolitas got THE facelift. And a suntan that gave it a characteristic blue skin color.

Keeping up with its tradition, Bolitas has proven to be a very valuable tool that has made the development and debugging of Particle-X more expedite. Or less arduous, at least.

Bolitas is available free of charge for personal and academic use. My best reward is knowing that it is a tool useful for someone. Bear in mind that it is also offered without any explicit or implicit warranty. I am not a professional programmer, and I created most of Bolitas in my spare time. The user interface is not complete yet as of the time of this writing, and I know it is not devoid of errors that can even cause it to crash. But what program does not, may I ask? I do not recommend using Bolitas in the design of any faster-than-light travel engine.

The latest version of Bolitas, can be found at

<http://cruzfierro.com/academic/bolitas.htm>

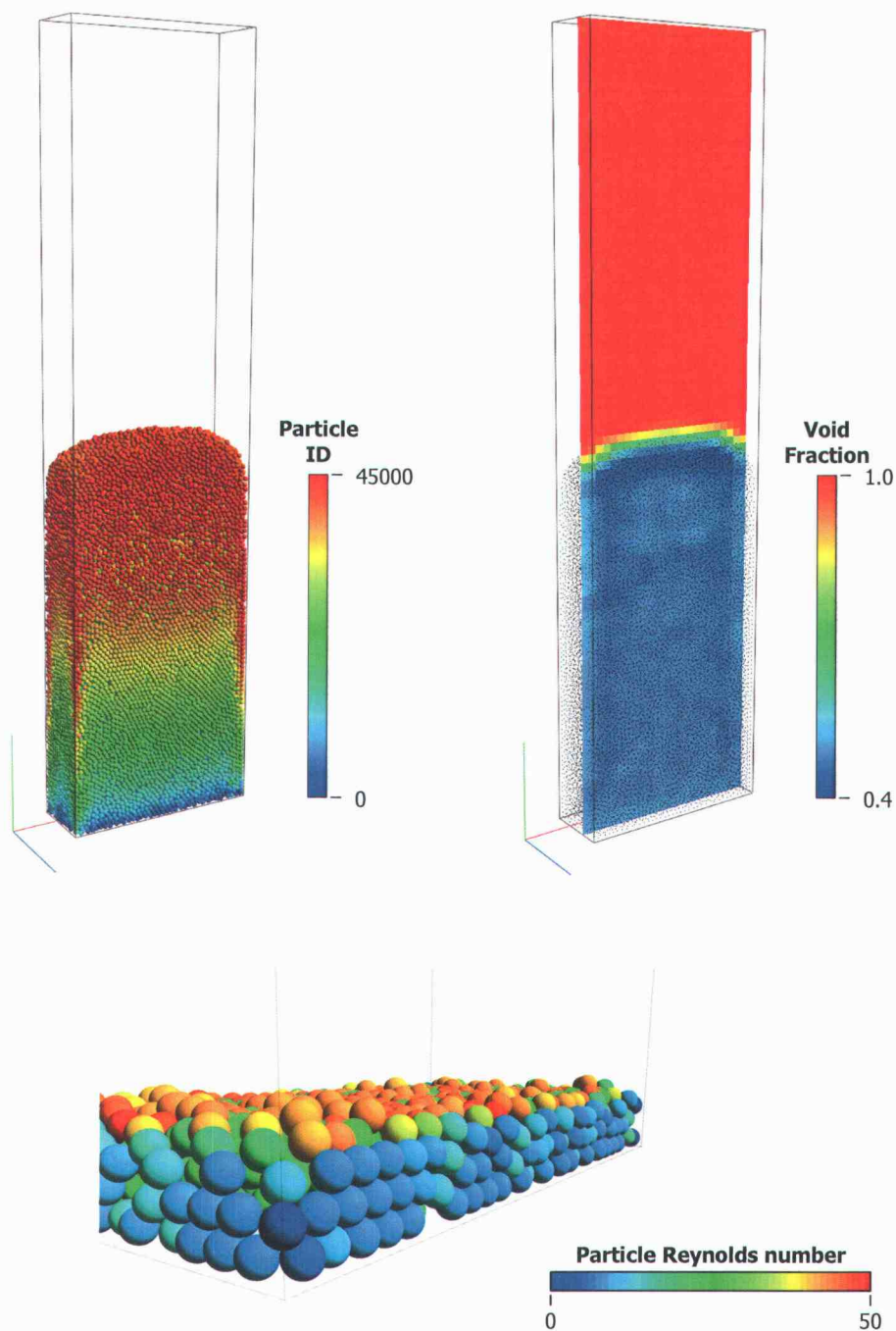


Figure C.1 Representative samples of Bolitas output. Top left: 45,000, colored by their ID number. Top right: Same case and time, showing void fraction in scalar plane, particles shown as dots. Bottom: Close up of another simulation, particles colored by their Reynolds number.

C.2 List of defined variable identifiers

BOLITAS 2

File number assignments

Bolitas FLX range: 1000-1999

1000-1099: Reserved

1000: PARTICLE.ALIVE
1011: PARTICLE.INDEX.X
1012: PARTICLE.INDEX.Y
1013: PARTICLE.INDEX.Z

1100-1299: General use

1101: BFIELD.X
1102: BFIELD.Y
1103: BFIELD.Z
1111: BFIELD.X.GRAD.X
1112: BFIELD.X.GRAD.Y
1113: BFIELD.X.GRAD.Z
1114: BFIELD.Y.GRAD.X
1115: BFIELD.Y.GRAD.Y
1116: BFIELD.Y.GRAD.Z
1117: BFIELD.Z.GRAD.X
1118: BFIELD.Z.GRAD.Y
1119: BFIELD.Z.GRAD.Z

1300-1499: Particle properties

1300: PARTICLE.COLOR
1310: PARTICLE.RADIUS
1311: PARTICLE.DENSITY
1312: PARTICLE.KINETIC.ENERGY
1313: PARTICLE.INTERNAL.ENERGY
1319: PARTICLE.CONTACTS
1321: PARTICLE.X
1322: PARTICLE.Y
1323: PARTICLE.Z
1331: PARTICLE.VELOCITY.X
1332: PARTICLE.VELOCITY.Y
1333: PARTICLE.VELOCITY.Z
1341: PARTICLE.ACCELERATION.X
1342: PARTICLE.ACCELERATION.Y
1343: PARTICLE.ACCELERATION.Z
1361: PARTICLE.ANG.VEL.X
1362: PARTICLE.ANG.VEL.Y
1363: PARTICLE.ANG.VEL.Z
1371: PARTICLE.ANG.ACCEL.X
1372: PARTICLE.ANG.ACCEL.Y

1373: PARTICLE.ANG.ACCEL.Z
1381: PARTICLE.FORCE.X
1382: PARTICLE.FORCE.Y
1383: PARTICLE.FORCE.Z
1391: PARTICLE.TORQUE.X
1392: PARTICLE.TORQUE.Y
1393: PARTICLE.TORQUE.Z
1400: PARTICLE.TEMPERATURE
1401: PARTICLE.GRANULAR.TEMP
1450: PARTICLE.DIPOLE
1451: PARTICLE.DIPOLE.X
1452: PARTICLE.DIPOLE.Y
1453: PARTICLE.DIPOLE.Z
1497: PARTICLE.NUSSELT
1498: PARTICLE.REYNOLDS.ROTATION
1499: PARTICLE.REYNOLDS

1500-1699: Fluid properties

1501: FLUID.DENSITY
1502: FLUID.VISCOSITY
1503: FLUID.KINEMATIC.VISCOSITY
1504: FLUID.HEAT.CAPACITY
1510: FLUID.VOIDAGE.COARSE
1511: FLUID.VOIDAGE; FLUID.VOIDAGE.FINE
1520: FLUID.U
1521: FLUID.UX
1522: FLUID.UY
1523: FLUID.UZ
1530: FLUID.PRESSURE
1531: FLUID.PRESSURE.STATIC
1532: FLUID.PRESSURE.DYNAMIC
1539: FLUID.PRESSURE.CORRECTION
1541: FLUID.UX.GRAD.X
1542: FLUID.UX.GRAD.Y
1543: FLUID.UX.GRAD.Z
1544: FLUID.UY.GRAD.X
1545: FLUID.UY.GRAD.Y
1546: FLUID.UY.GRAD.Z
1547: FLUID.UZ.GRAD.X
1548: FLUID.UZ.GRAD.Y
1549: FLUID.UZ.GRAD.Z
1551: FLUID.FORCE.X
1552: FLUID.FORCE.Y
1553: FLUID.FORCE.Z
1560: FLUID.TEMPERATURE
1670: FLUID.RESIDUAL.MASS
1671: FLUID.RESIDUAL.UX
1672: FLUID.RESIDUAL.UY
1673: FLUID.RESIDUAL.UZ
1674: FLUID.RESIDUAL.ENERGY
1680: FLUID.NORM.RESIDUAL.MASS

1681: FLUID.NORM.RESIDUAL.UX
1682: FLUID.NORM.RESIDUAL.UY
1683: FLUID.NORM.RESIDUAL.UZ
1684: FLUID.NORM.RESIDUAL.ENERGY

1700-1899: Interpolated fluid to particle

1701: FLUID.2.PARTICLE.VOIDAGE
1711: FLUID.2.PARTICLE.UX
1712: FLUID.2.PARTICLE.UY
1713: FLUID.2.PARTICLE.UZ

1900-1999: Overall bed properties

1901: BED.HEIGHT.MAP
1902: BED.HEIGHT.AVERAGE
1911: BED.PRESSURE.DROP.AVERAGE
1921: COLLISION.COUNT.PP
1922: COLLISION.COUNT.PW
1930: BED.VOIDAGE.AVERAGE

APPENDIX D

ADDITIONAL EXPERIMENTAL DATA

Data: Captain, in another 41 minutes we will see the information of the Tsiolkovsky downloaded to us.

Picard: Why so slow?

Data: Slow, sir? The Tsiolkovsky has been eight months accumulating it.

— Star Trek The Next Generation,
“The Naked Now”

Figures D.1 through D.56 present the dynamic pressure drop measured in the fluidized bed, at the different operating conditions. The linear regression fit corresponds to the data points within the region of uniform field ($0.05 < y < 0.25$ m). Recall that the voidage is obtained from the slope of this line, as given by Equation 5.1-2.

Runs at 9, 10, and 14 LPM had fewer particles because of the increased bed expansion.

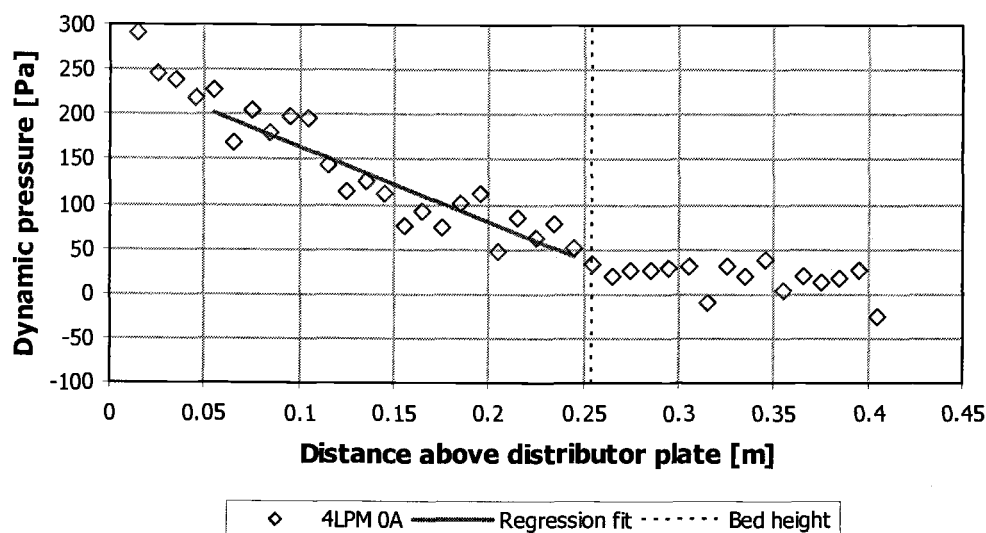


Figure D.1 Dynamic pressure data for $u_0 = 0.0134$ m/s and $B_0 = 0$. The calculated voidage is $\varepsilon = 0.530$.

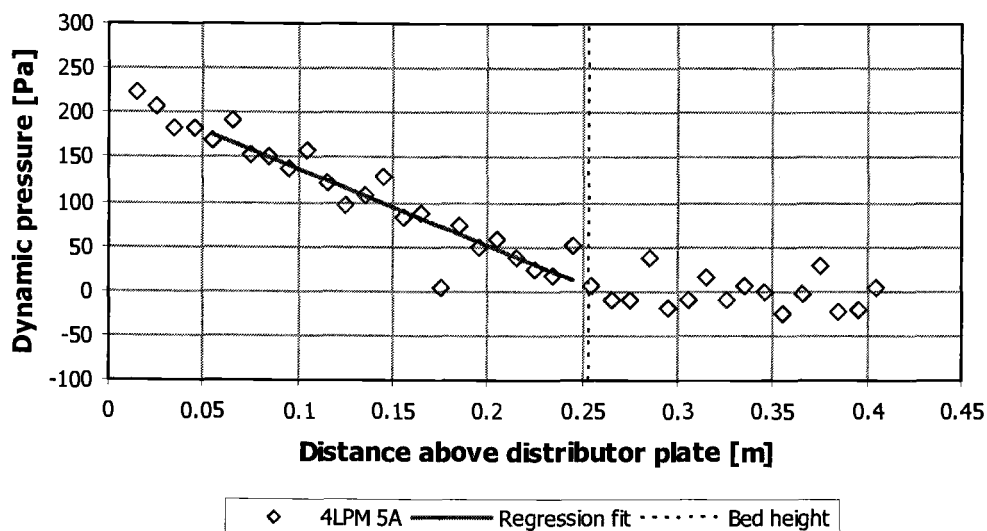


Figure D.2 Dynamic pressure data for $u_0 = 0.0134$ m/s and $B_0 = 1.28$ mT. The calculated voidage is $\varepsilon = 0.528$.

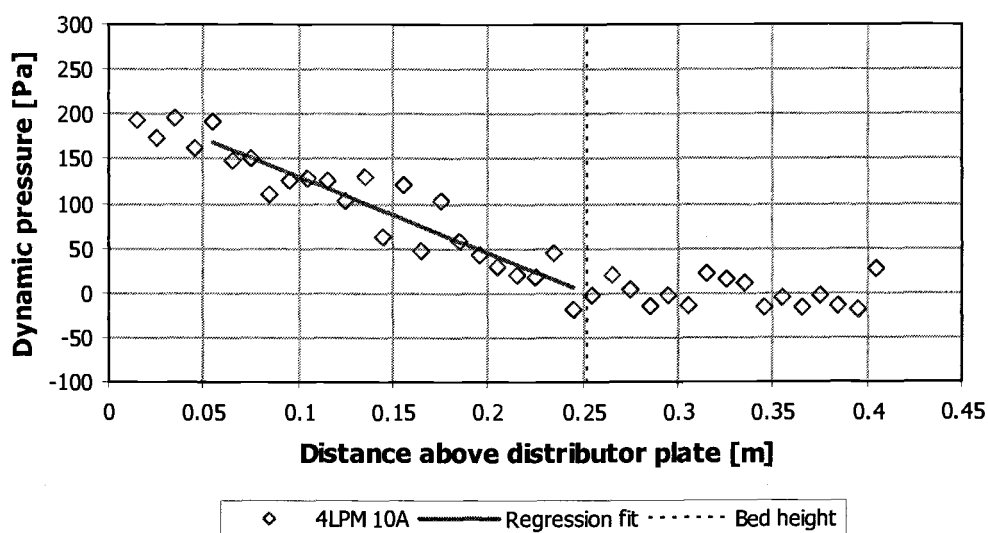


Figure D.3 Dynamic pressure data for $u_0 = 0.0134$ m/s and $B_0 = 2.56$ mT. The calculated voidage is $\varepsilon = 0.523$.

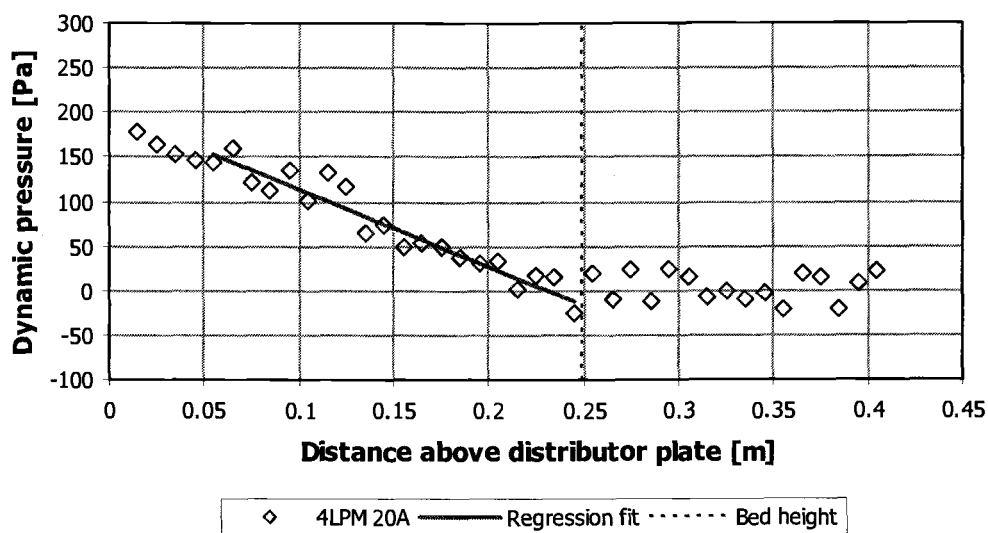


Figure D.4 Dynamic pressure data for $u_0 = 0.0134$ m/s and $B_0 = 5.11$ mT. The calculated voidage is $\varepsilon = 0.521$.

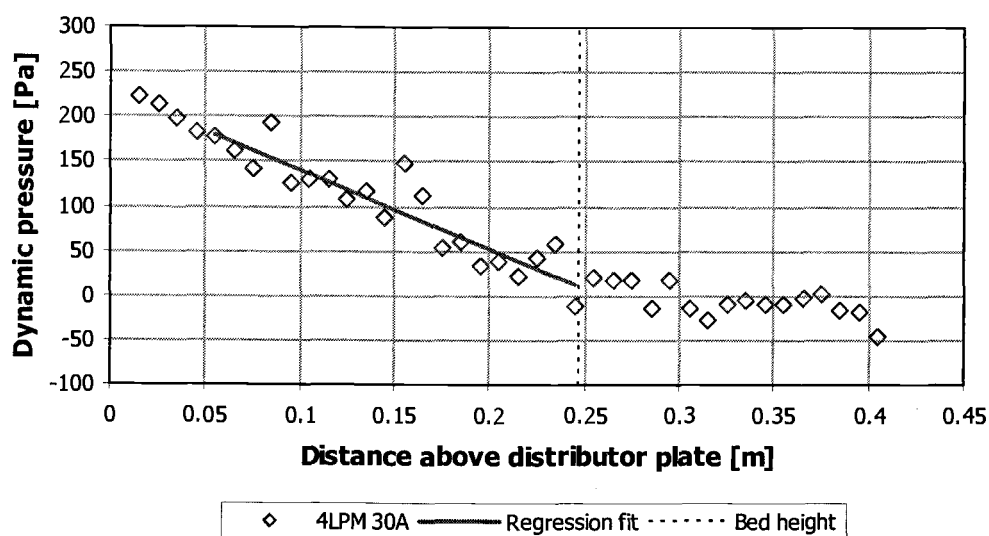


Figure D.5 Dynamic pressure data for $u_0 = 0.0134$ m/s and $B_0 = 7.67$ mT. The calculated voidage is $\varepsilon = 0.516$.

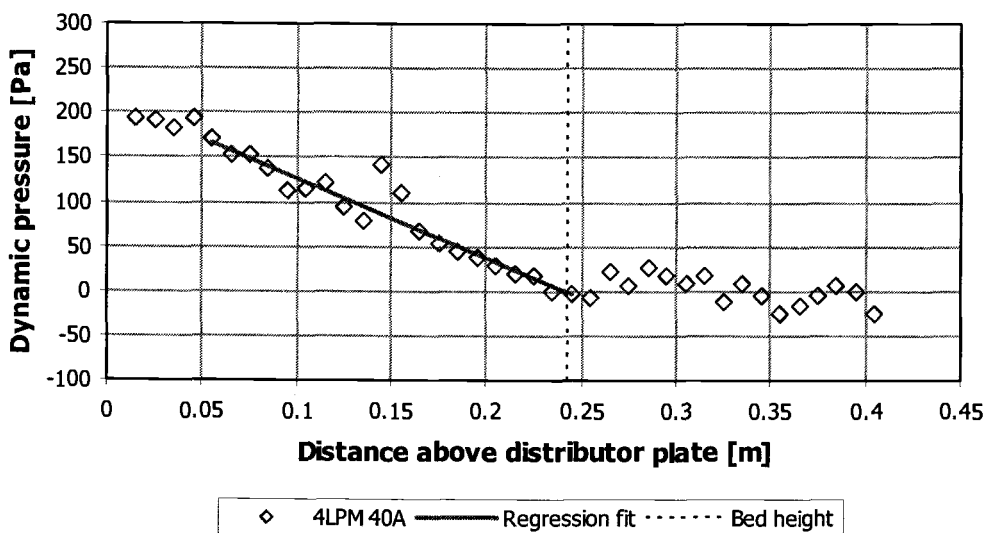


Figure D.6 Dynamic pressure data for $u_0 = 0.0134$ m/s and $B_0 = 10.2$ mT. The calculated voidage is $\varepsilon = 0.505$.

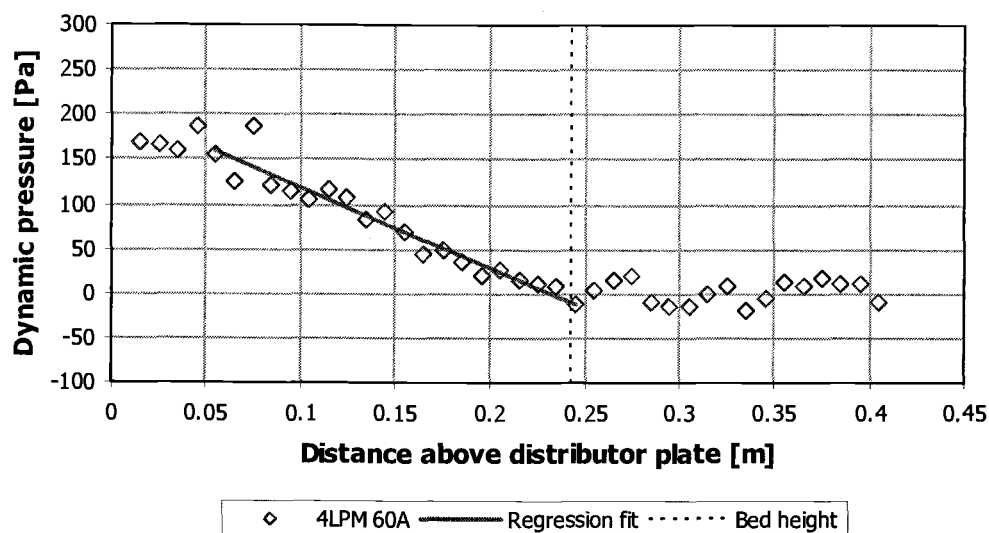


Figure D.7 Dynamic pressure data for $u_0 = 0.0134$ m/s and $B_0 = 15.3$ mT. The calculated voidage is $\varepsilon = 0.503$.

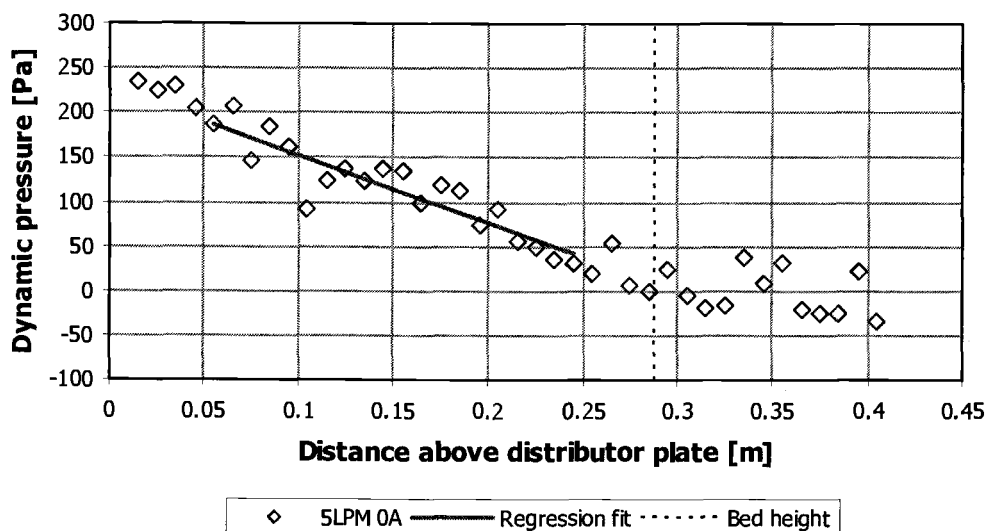


Figure D.8 Dynamic pressure data for $u_0 = 0.0170$ m/s and $B_0 = 0$. The calculated voidage is $\varepsilon = 0.576$.

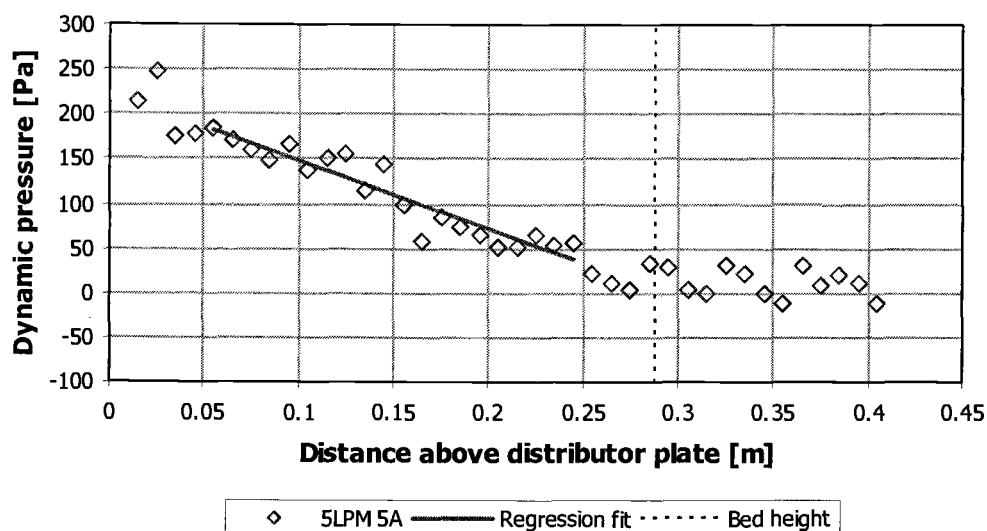


Figure D.9 Dynamic pressure data for $u_0 = 0.0170$ m/s and $B_0 = 1.28$ mT. The calculated voidage is $\varepsilon = 0.578$.

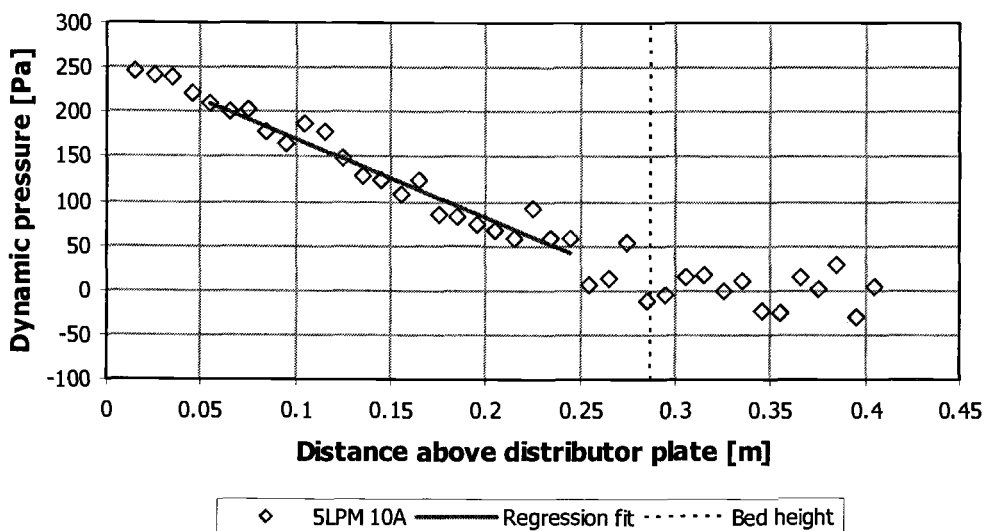


Figure D.10 Dynamic pressure data for $u_0 = 0.0170$ m/s and $B_0 = 2.56$ mT. The calculated voidage is $\varepsilon = 0.576$.

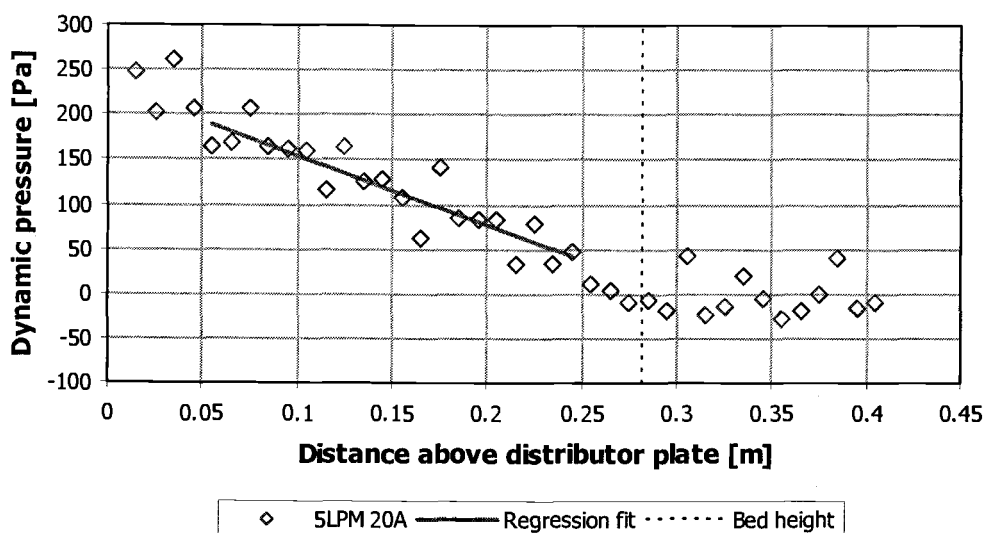


Figure D.11 Dynamic pressure data for $u_0 = 0.0170$ m/s and $B_0 = 5.11$ mT. The calculated voidage is $\varepsilon = 0.571$.

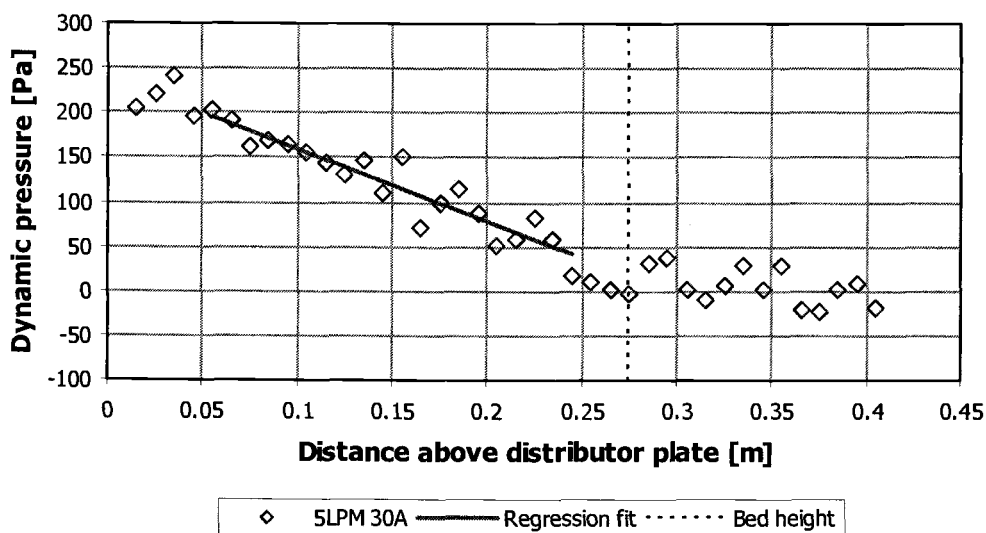


Figure D.12 Dynamic pressure data for $u_0 = 0.0170$ m/s and $B_0 = 7.67$ mT. The calculated voidage is $\varepsilon = 0.551$.

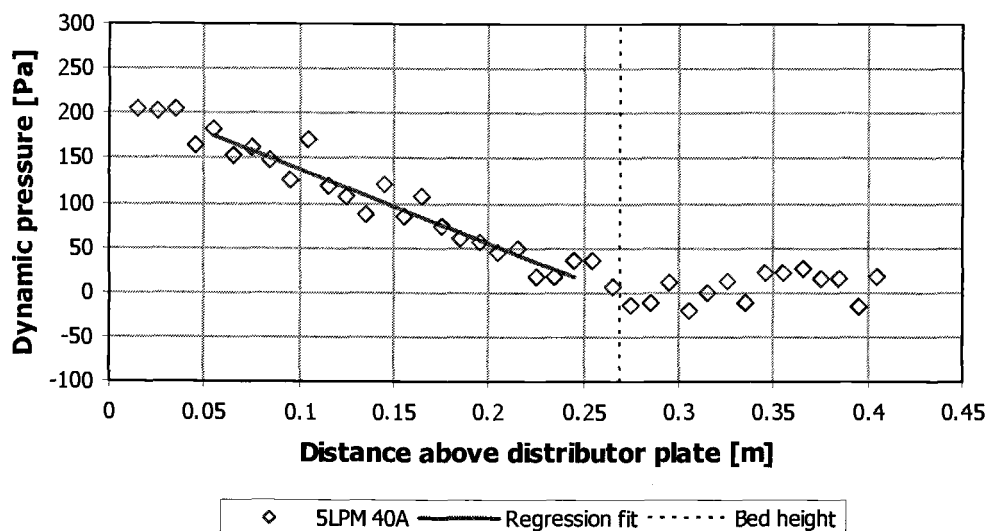


Figure D.13 Dynamic pressure data for $u_0 = 0.0170$ m/s and $B_0 = 10.2$ mT. The calculated voidage is $\varepsilon = 0.539$.

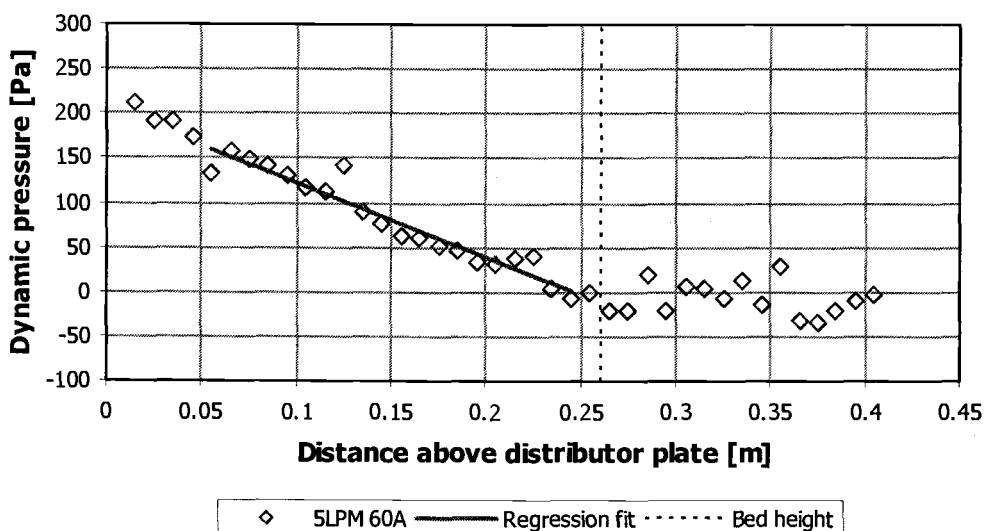


Figure D.14 Dynamic pressure data for $u_0 = 0.0170$ m/s and $B_0 = 15.3$ mT. The calculated voidage is $\varepsilon = 0.537$.

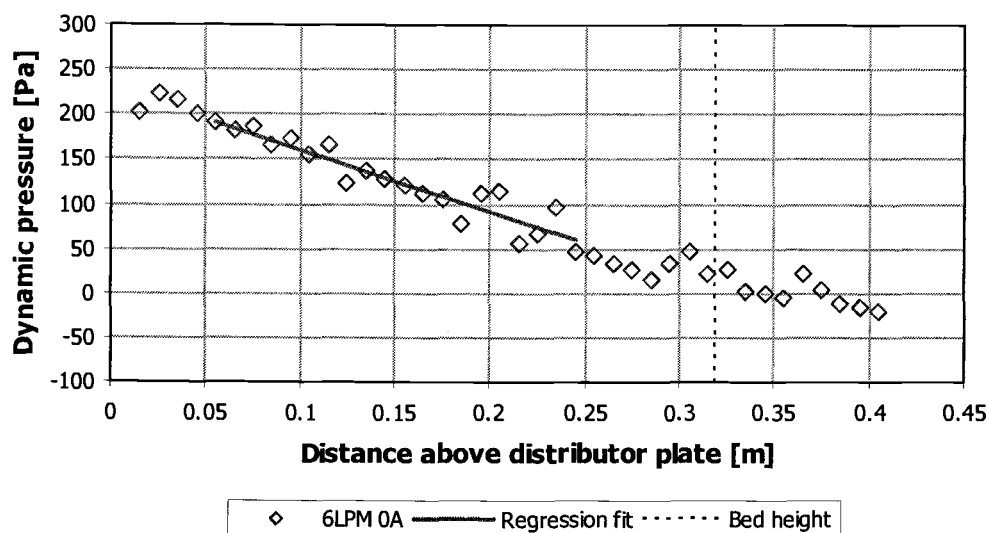


Figure D.15 Dynamic pressure data for $u_0 = 0.0208$ m/s and $B_0 = 0$. The calculated voidage is $\varepsilon = 0.613$.

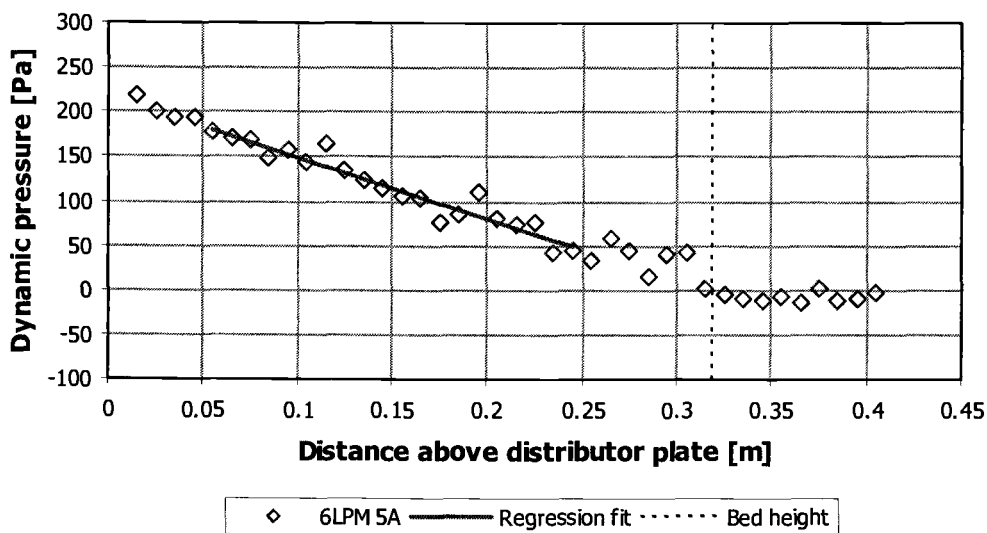


Figure D.16 Dynamic pressure data for $u_0 = 0.0208$ m/s and $B_0 = 1.28$ mT. The calculated voidage is $\varepsilon = 0.618$.

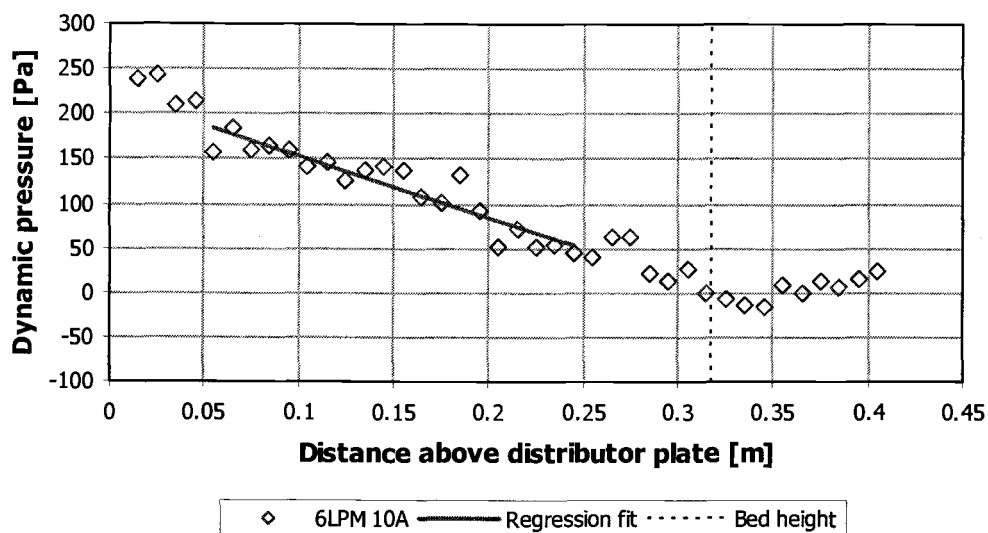


Figure D.17 Dynamic pressure data for $u_0 = 0.0208$ m/s and $B_0 = 2.56$ mT. The calculated voidage is $\varepsilon = 0.618$.

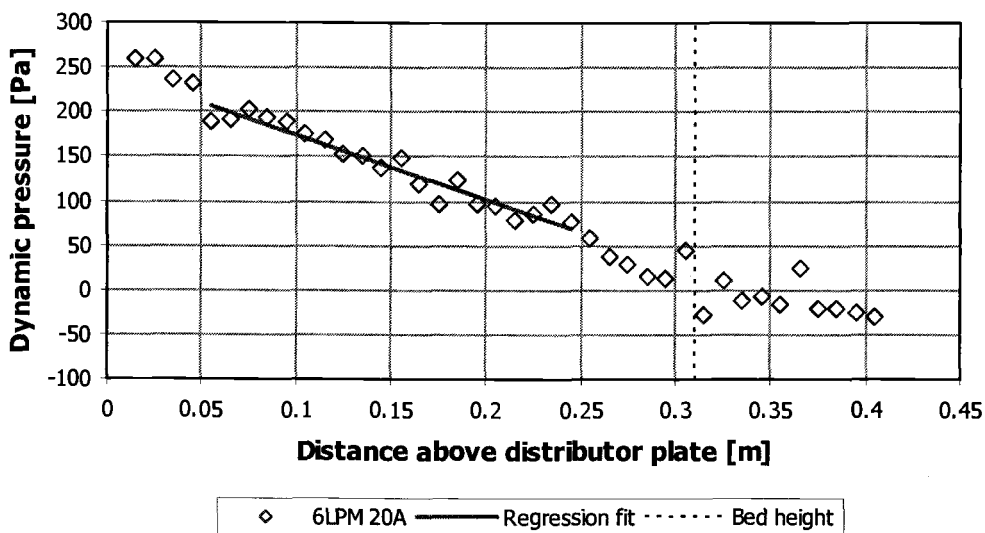


Figure D.18 Dynamic pressure data for $u_0 = 0.0208$ m/s and $B_0 = 5.11$ mT. The calculated voidage is $\varepsilon = 0.604$.

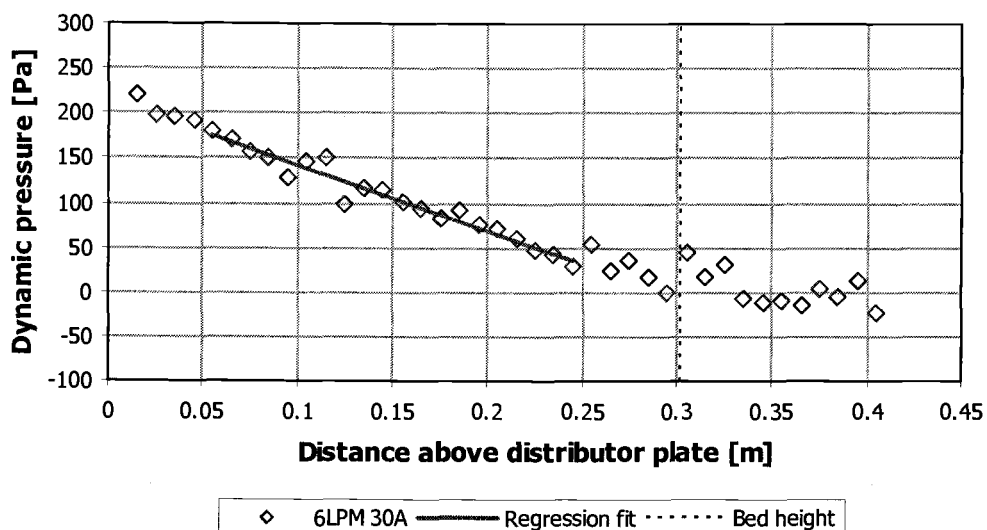


Figure D.19 Dynamic pressure data for $u_0 = 0.0208$ m/s and $B_0 = 7.67$ mT. The calculated voidage is $\varepsilon = 0.595$.

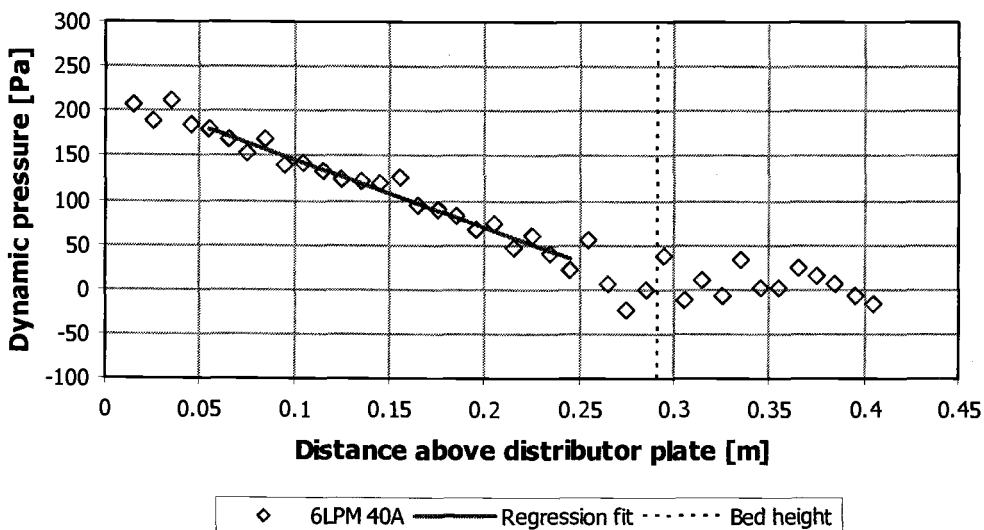


Figure D.20 Dynamic pressure data for $u_0 = 0.0208$ m/s and $B_0 = 10.2$ mT. The calculated voidage is $\varepsilon = 0.578$.

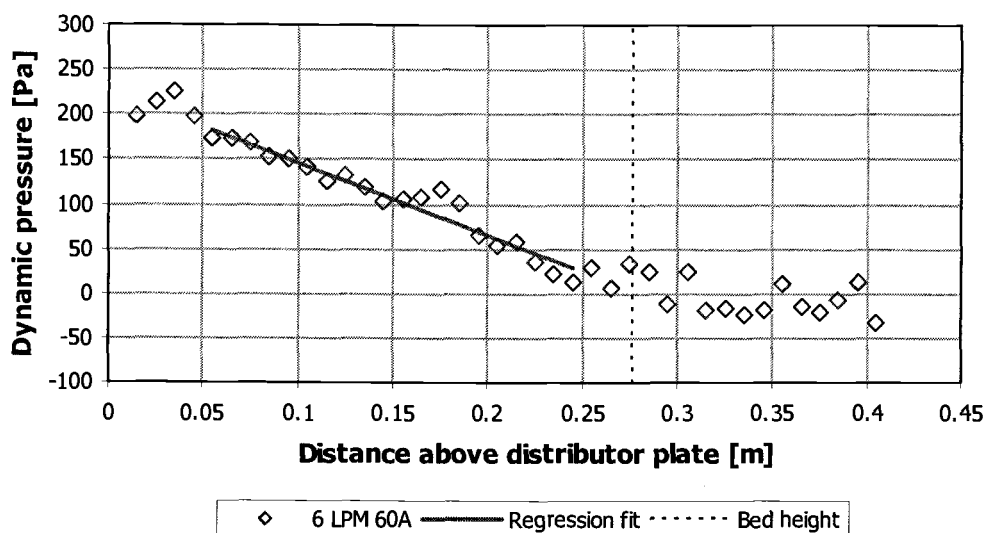


Figure D.21 Dynamic pressure data for $u_0 = 0.0208$ m/s and $B_0 = 15.3$ mT. The calculated voidage is $\varepsilon = 0.549$.

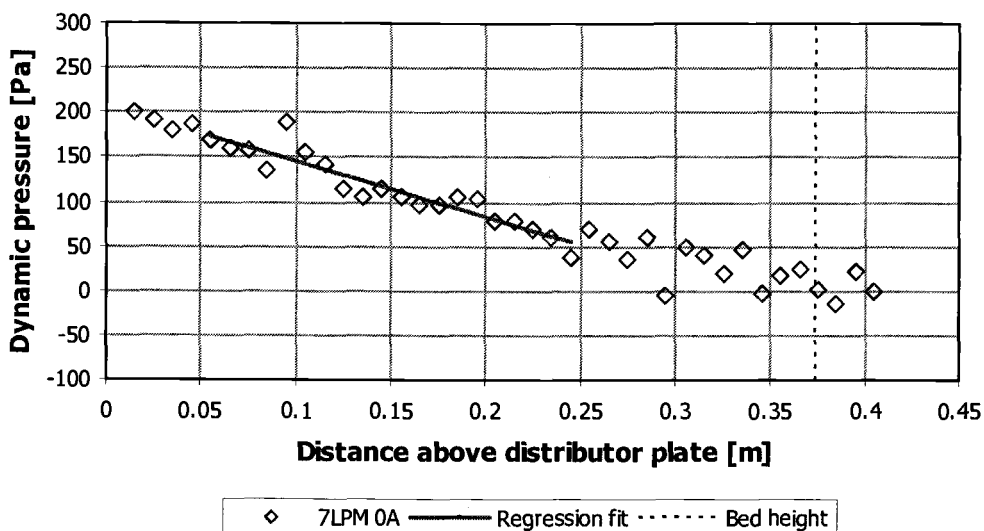


Figure D.22 Dynamic pressure data for $u_0 = 0.0247$ m/s and $B_0 = 0$. The calculated voidage is $\varepsilon = 0.656$.

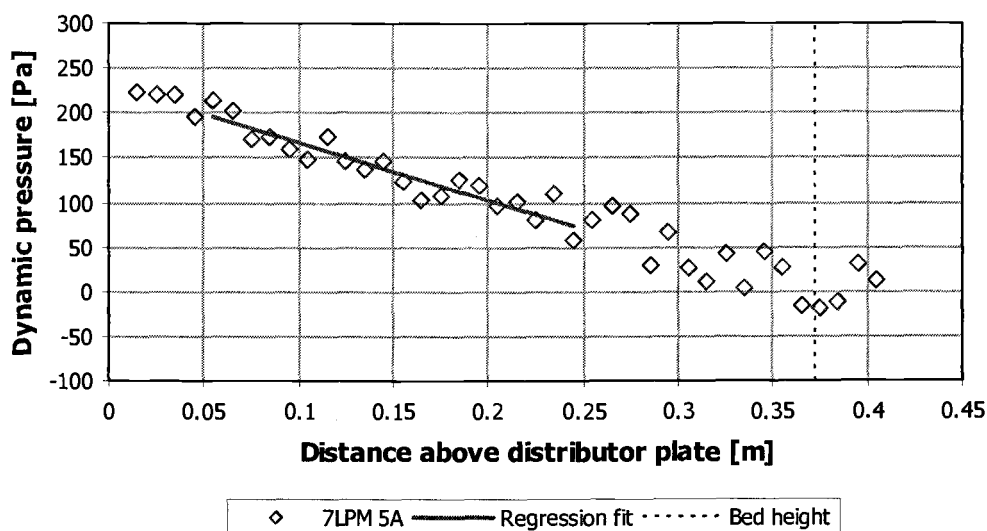


Figure D.23 Dynamic pressure data for $u_0 = 0.0247$ m/s and $B_0 = 1.28$ mT. The calculated voidage is $\varepsilon = 0.648$.

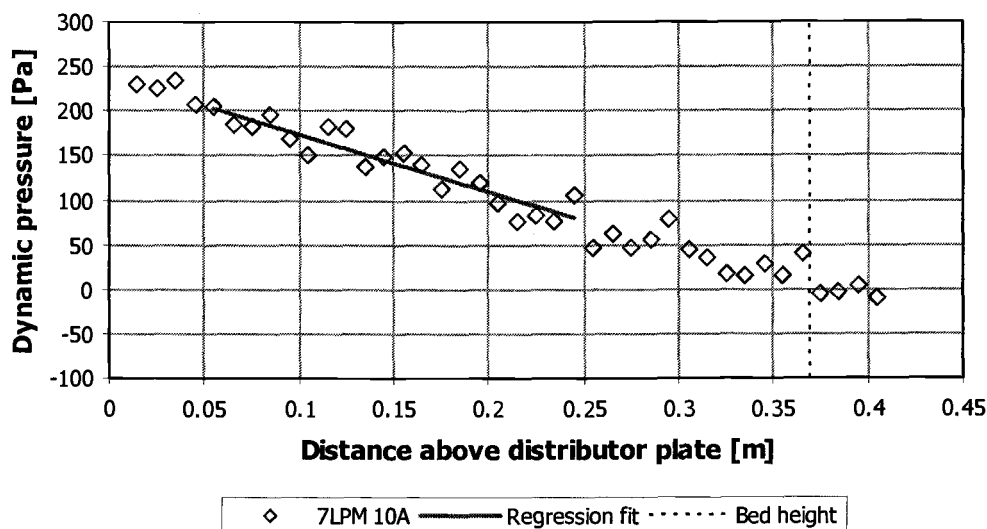


Figure D.24 Dynamic pressure data for $u_0 = 0.0247$ m/s and $B_0 = 2.56$ mT. The calculated voidage is $\varepsilon = 0.646$.

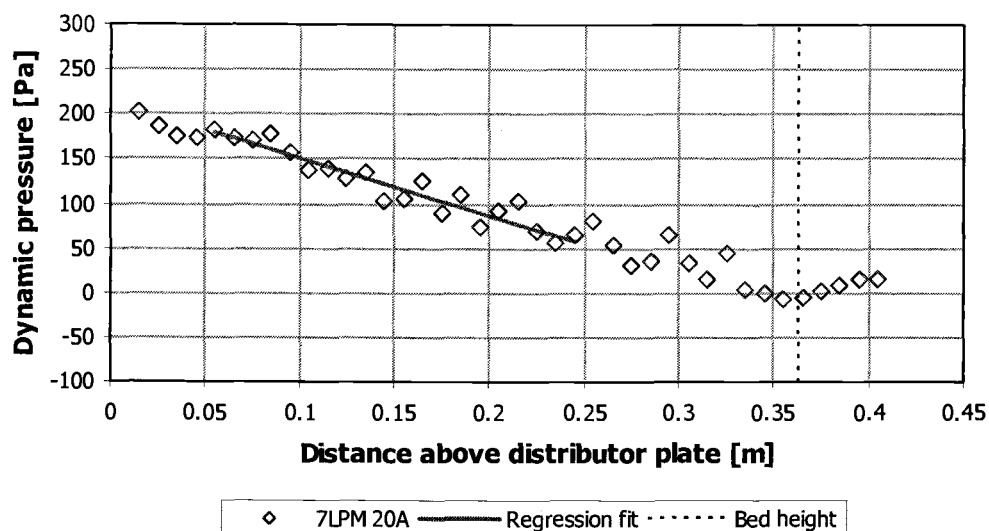


Figure D.25 Dynamic pressure data for $u_0 = 0.0247$ m/s and $B_0 = 5.11$ mT. The calculated voidage is $\varepsilon = 0.646$.

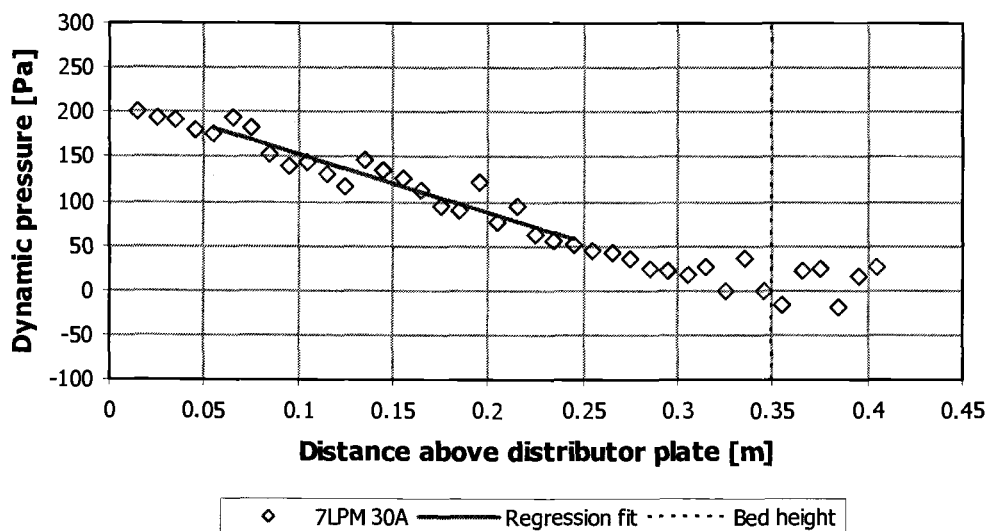


Figure D.26 Dynamic pressure data for $u_0 = 0.0247$ m/s and $B_0 = 7.67$ mT. The calculated voidage is $\varepsilon = 0.637$.

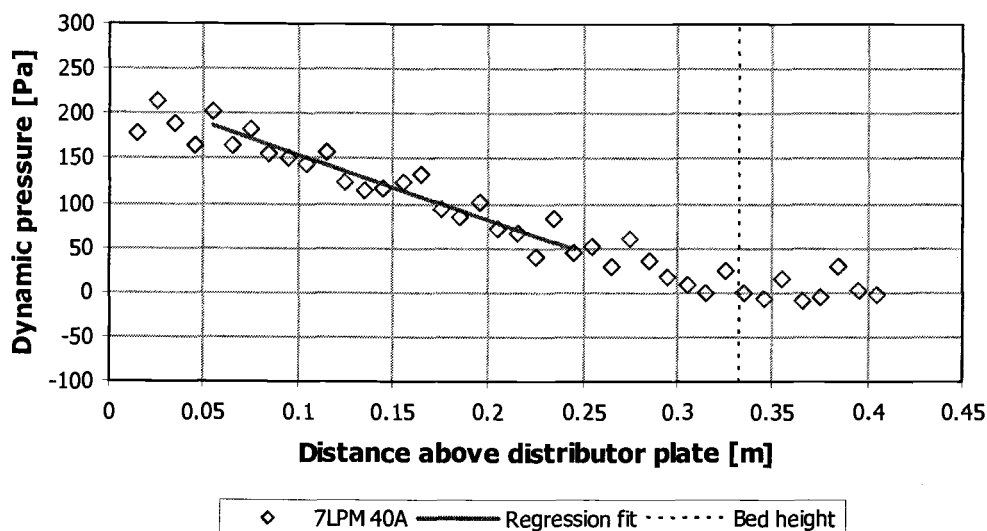


Figure D.27 Dynamic pressure data for $u_0 = 0.0247$ m/s and $B_0 = 10.2$ mT. The calculated voidage is $\varepsilon = 0.604$.

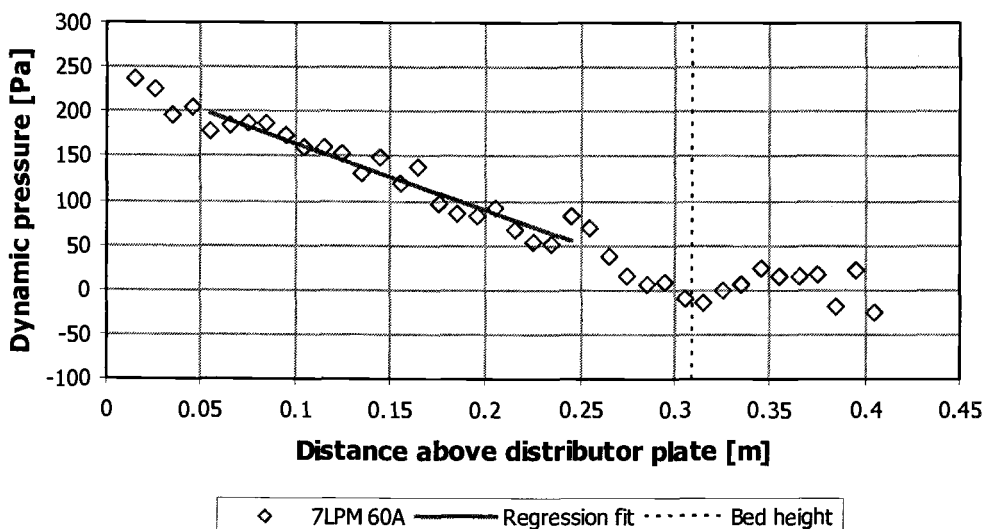


Figure D.28 Dynamic pressure data for $u_0 = 0.0247$ m/s and $B_0 = 15.3$ mT. The calculated voidage is $\varepsilon = 0.585$.

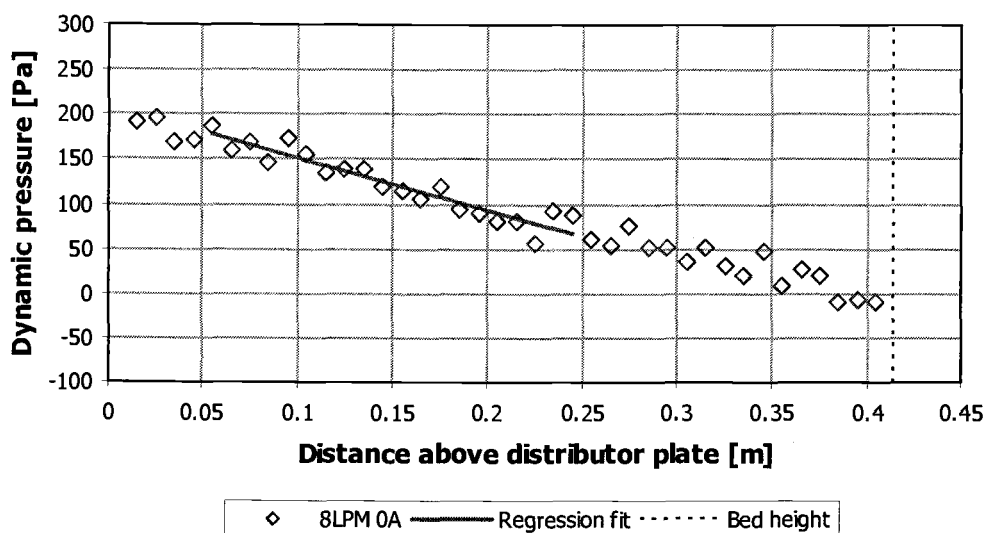


Figure D.29 Dynamic pressure data for $u_0 = 0.0287$ m/s and $B_0 = 0$. The calculated voidage is $\varepsilon = 0.680$.

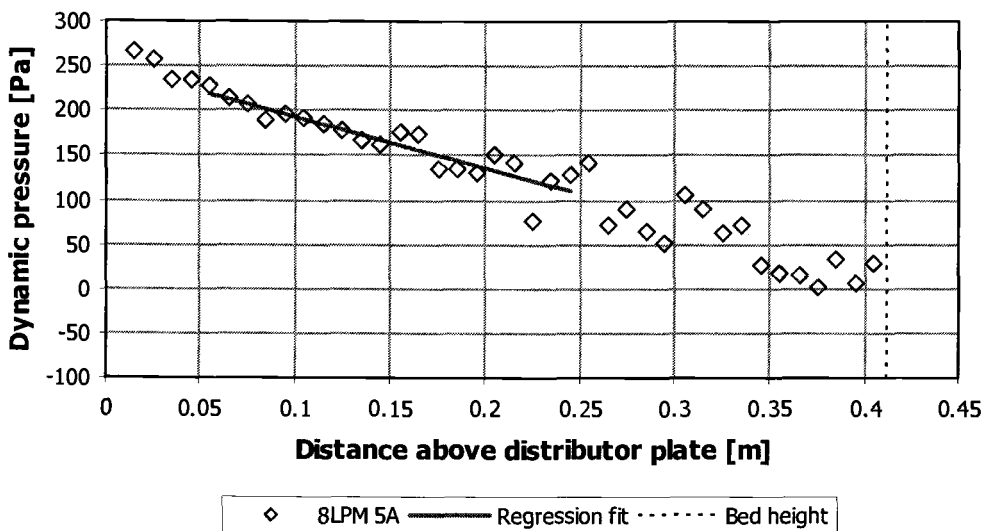


Figure D.30 Dynamic pressure data for $u_0 = 0.0287$ m/s and $B_0 = 1.28$ mT. The calculated voidage is $\varepsilon = 0.684$.

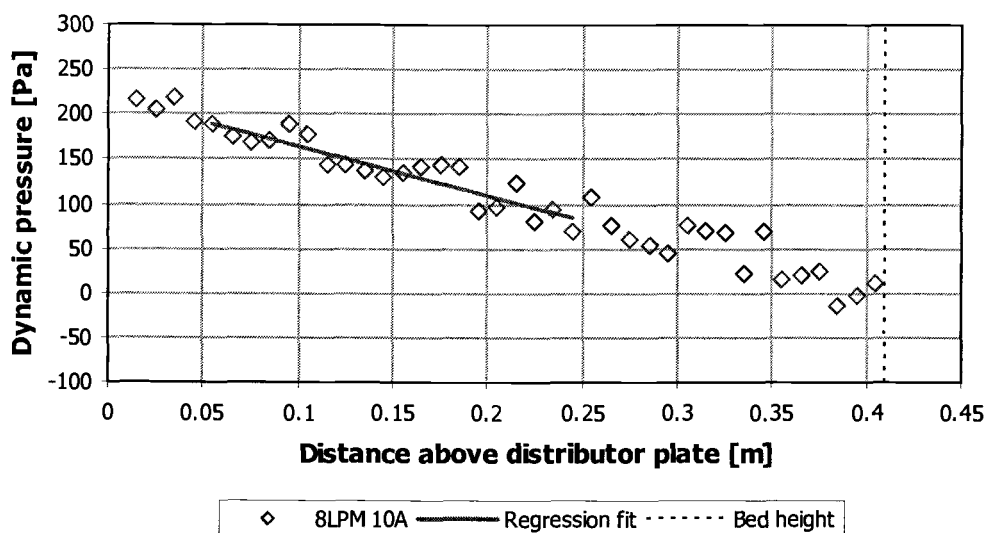


Figure D.31 Dynamic pressure data for $u_0 = 0.0287$ m/s and $B_0 = 2.56$ mT. The calculated voidage is $\varepsilon = 0.691$.

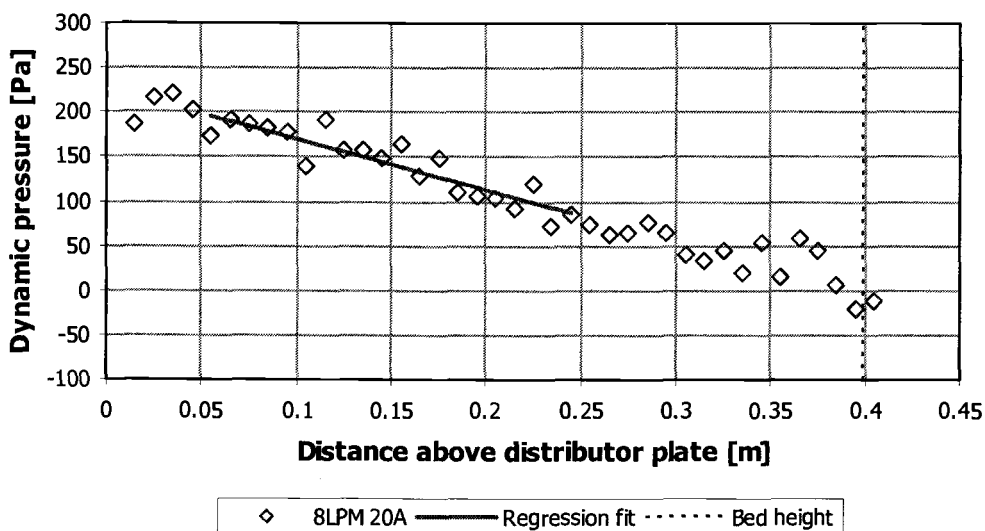


Figure D.32 Dynamic pressure data for $u_0 = 0.0287$ m/s and $B_0 = 5.11$ mT. The calculated voidage is $\varepsilon = 0.678$.

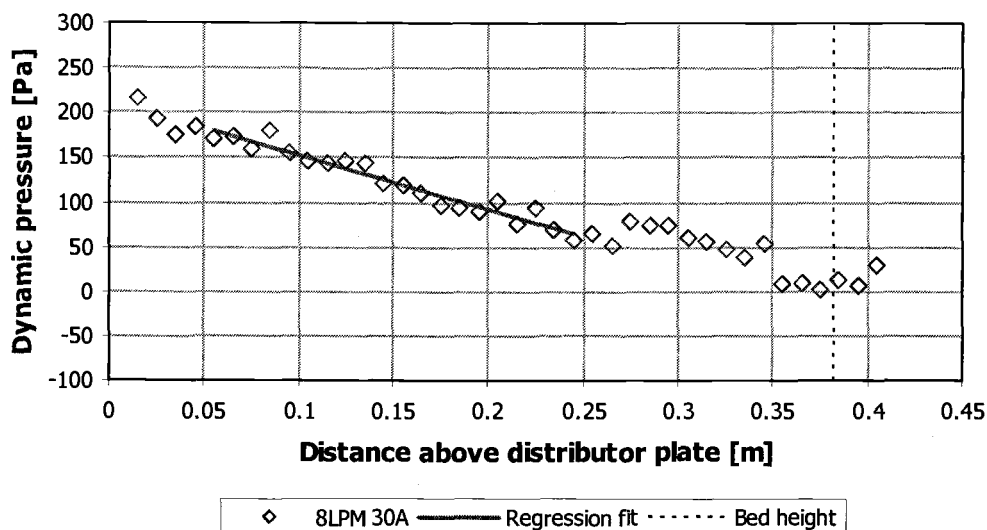


Figure D.33 Dynamic pressure data for $u_0 = 0.0287$ m/s and $B_0 = 7.67$ mT. The calculated voidage is $\varepsilon = 0.662$.

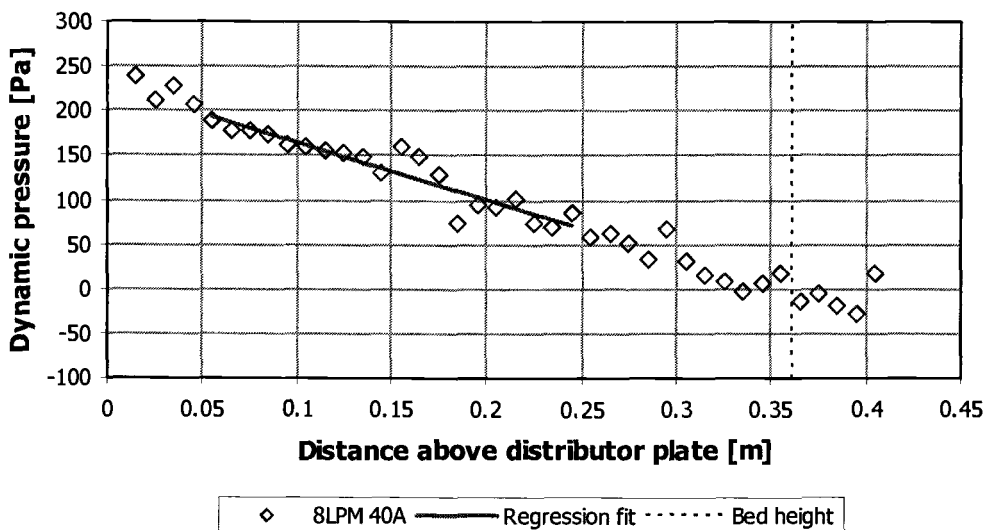


Figure D.34 Dynamic pressure data for $u_0 = 0.0287$ m/s and $B_0 = 10.2$ mT. The calculated voidage is $\varepsilon = 0.650$.

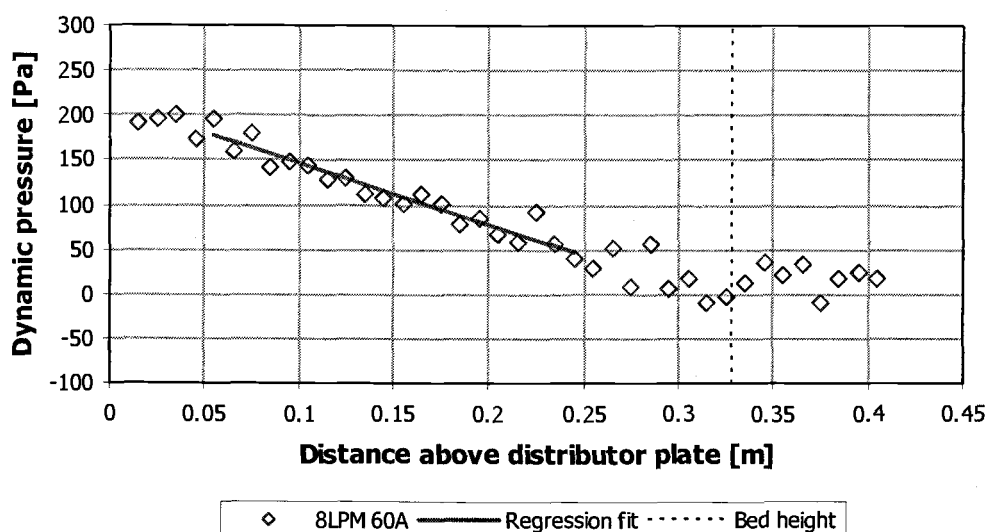


Figure D.35 Dynamic pressure data for $u_0 = 0.0287$ m/s and $B_0 = 15.3$ mT. The calculated voidage is $\varepsilon = 0.622$.

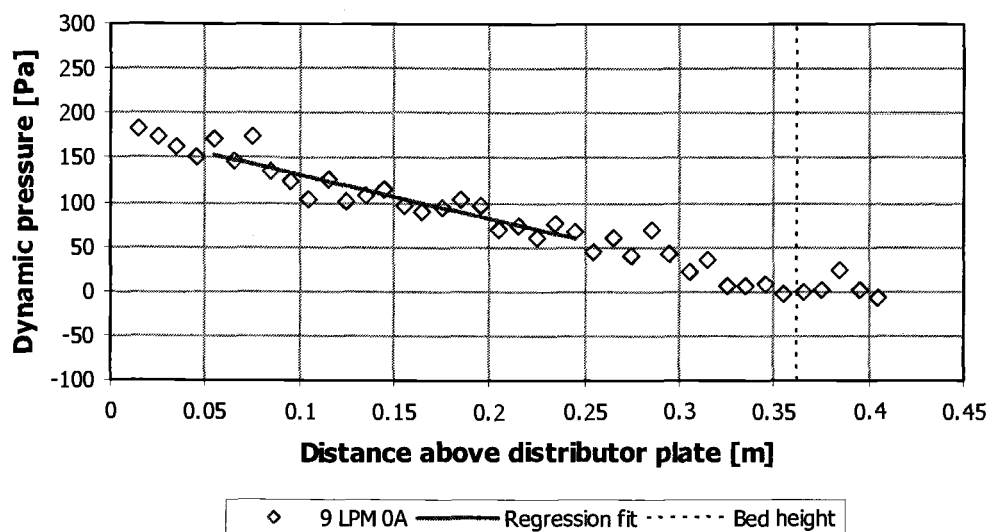


Figure D.36 Dynamic pressure data for $u_0 = 0.0328$ m/s and $B_0 = 0$. The calculated voidage is $\varepsilon = 0.727$.

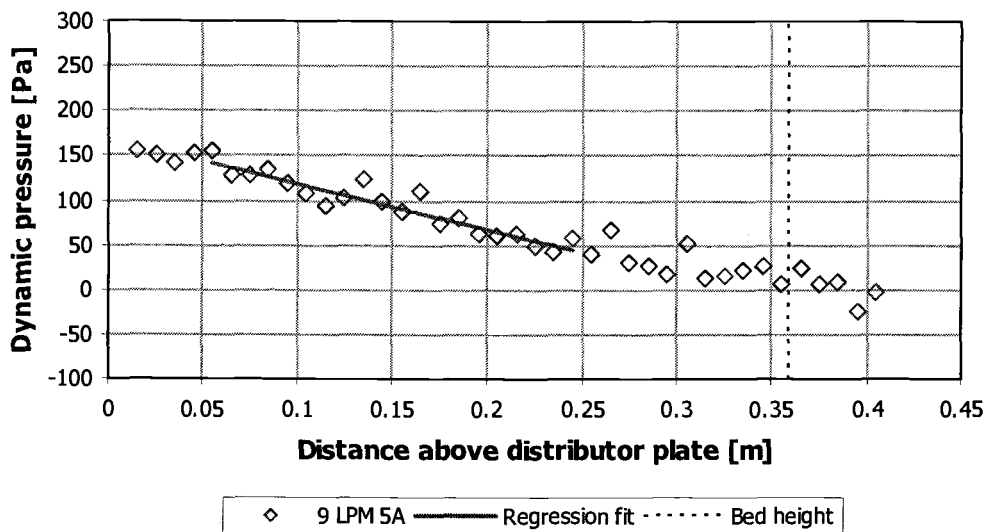


Figure D.37 Dynamic pressure data for $u_0 = 0.0328$ m/s and $B_0 = 1.28$ mT. The calculated voidage is $\varepsilon = 0.717$.

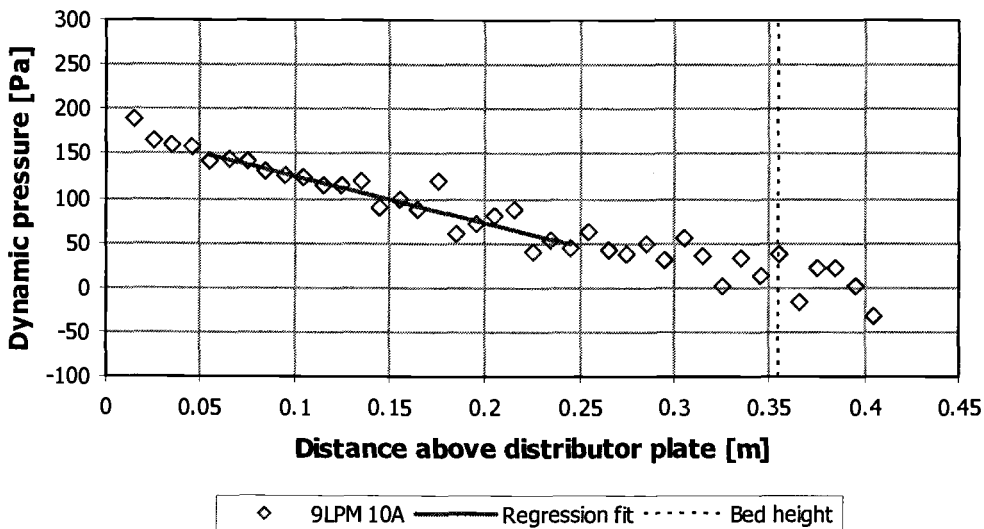


Figure D.38 Dynamic pressure data for $u_0 = 0.0328$ m/s and $B_0 = 2.56$ mT. The calculated voidage is $\varepsilon = 0.713$.

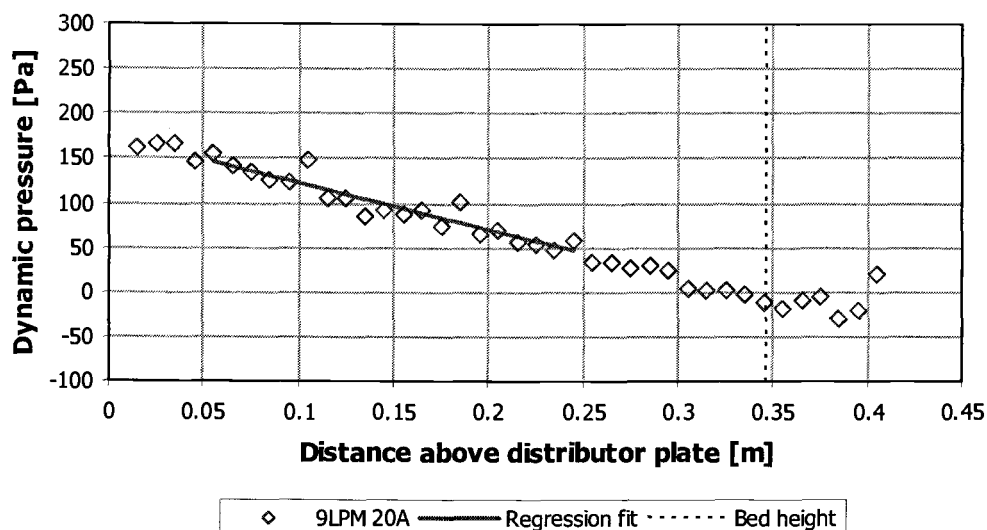


Figure D.39 Dynamic pressure data for $u_0 = 0.0328$ m/s and $B_0 = 5.11$ mT. The calculated voidage is $\varepsilon = 0.706$.

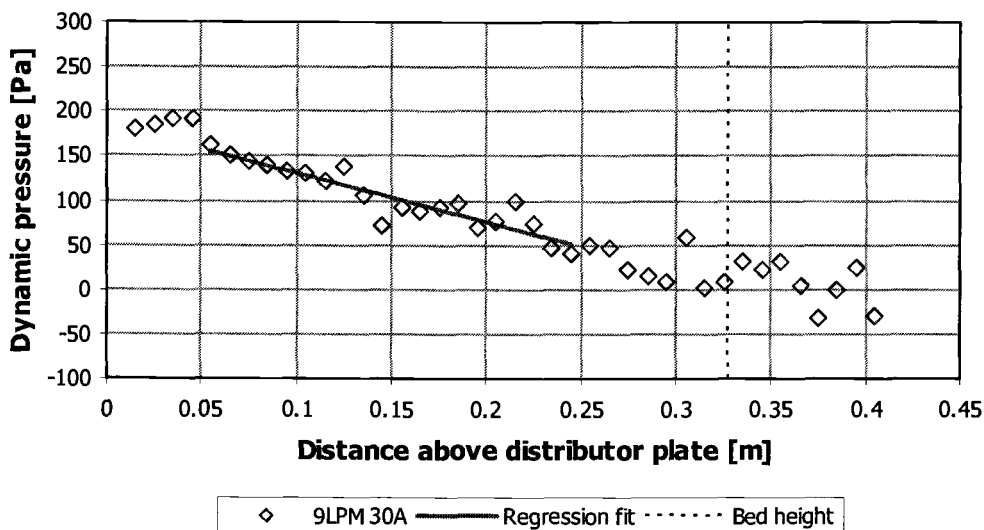


Figure D.40 Dynamic pressure data for $u_0 = 0.0328$ m/s and $B_0 = 7.67$ mT. The calculated voidage is $\varepsilon = 0.697$.

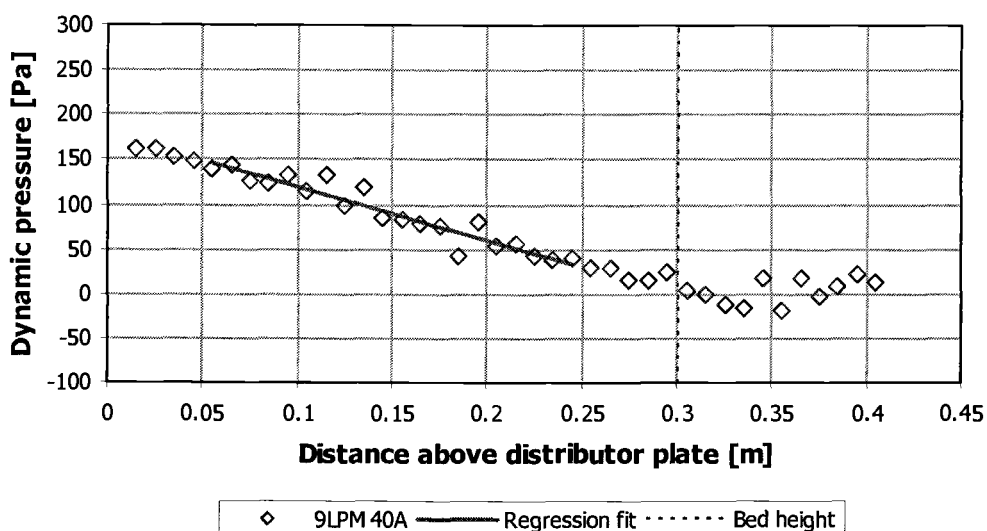


Figure D.41 Dynamic pressure data for $u_0 = 0.0328$ m/s and $B_0 = 10.2$ mT. The calculated voidage is $\varepsilon = 0.672$.

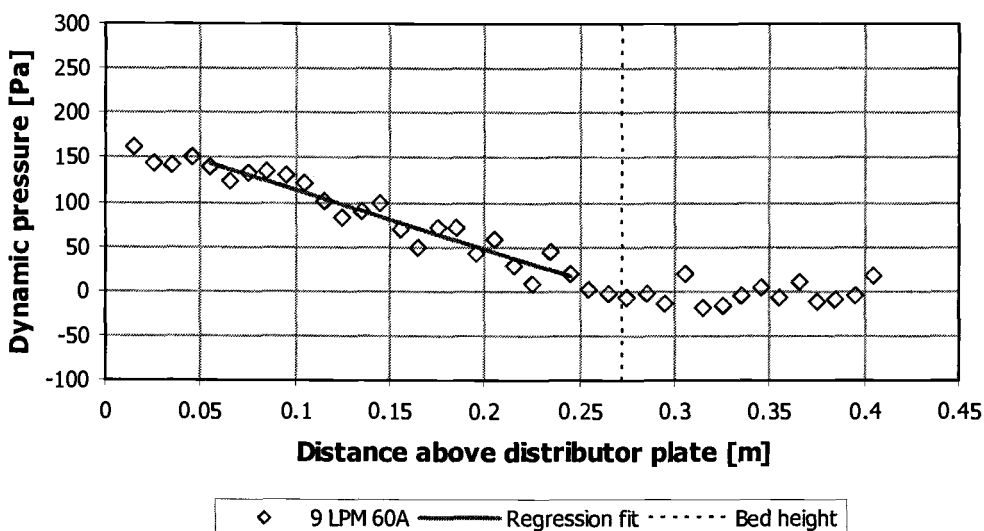


Figure D.42 Dynamic pressure data for $u_0 = 0.0328$ m/s and $B_0 = 15.3$ mT. The calculated voidage is $\varepsilon = 0.633$.

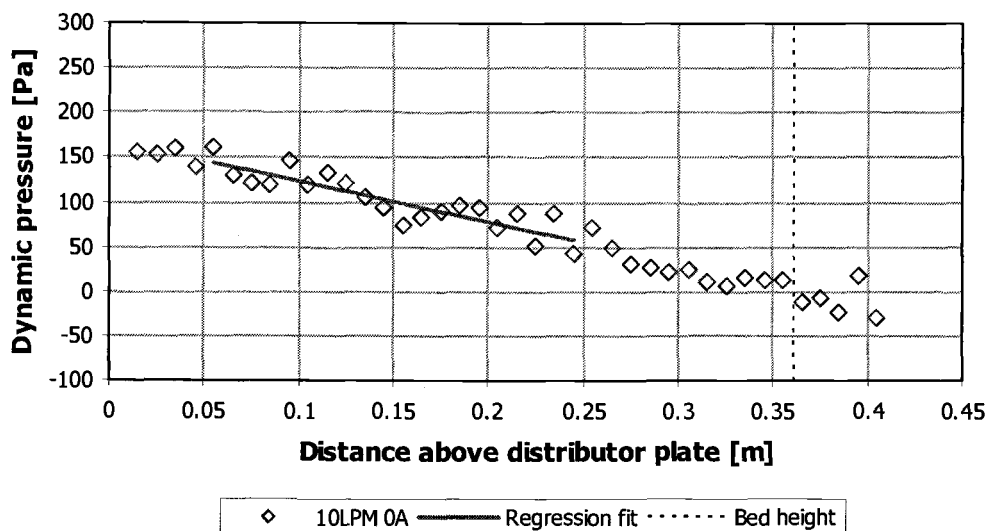


Figure D.43 Dynamic pressure data for $u_0 = 0.0370$ m/s and $B_0 = 0$. The calculated voidage is $\varepsilon = 0.751$.

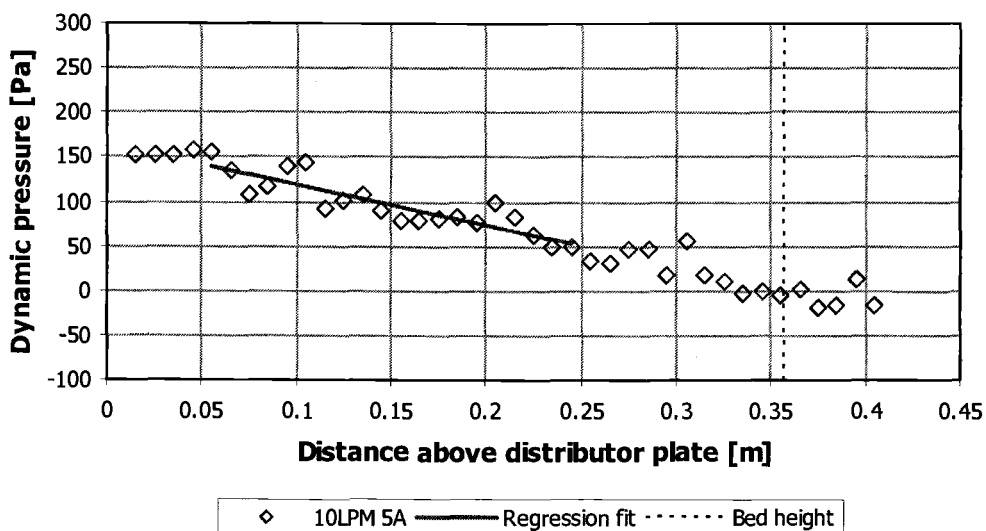


Figure D.44 Dynamic pressure data for $u_0 = 0.0370$ m/s and $B_0 = 1.28$ mT. The calculated voidage is $\varepsilon = 0.755$.

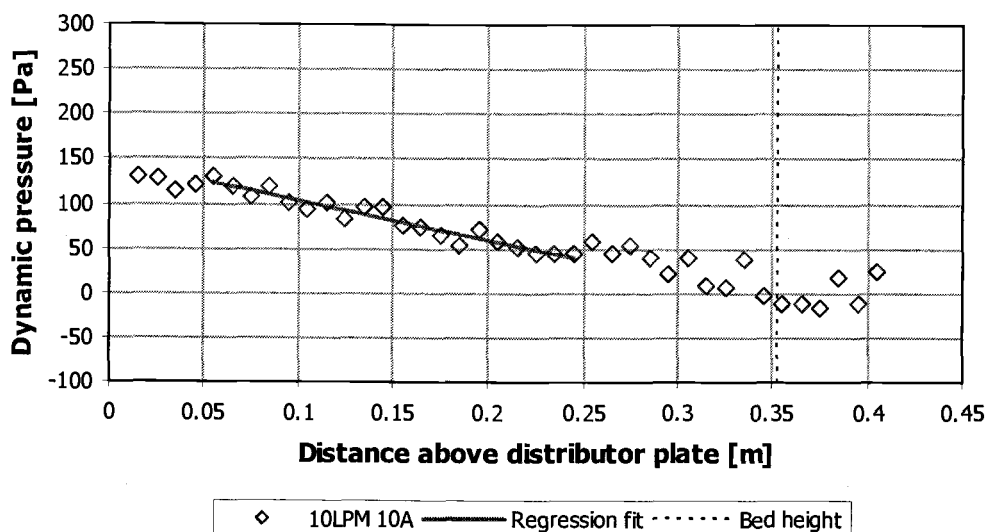


Figure D.45 Dynamic pressure data for $u_0 = 0.0370$ m/s and $B_0 = 2.56$ mT. The calculated voidage is $\varepsilon = 0.752$.

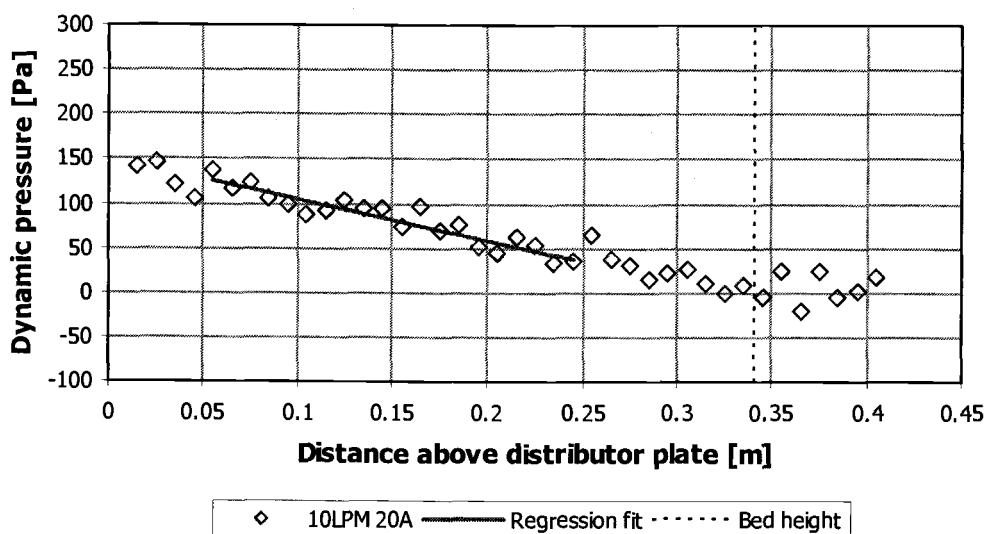


Figure D.46 Dynamic pressure data for $u_0 = 0.0370$ m/s and $B_0 = 5.11$ mT. The calculated voidage is $\varepsilon = 0.742$.

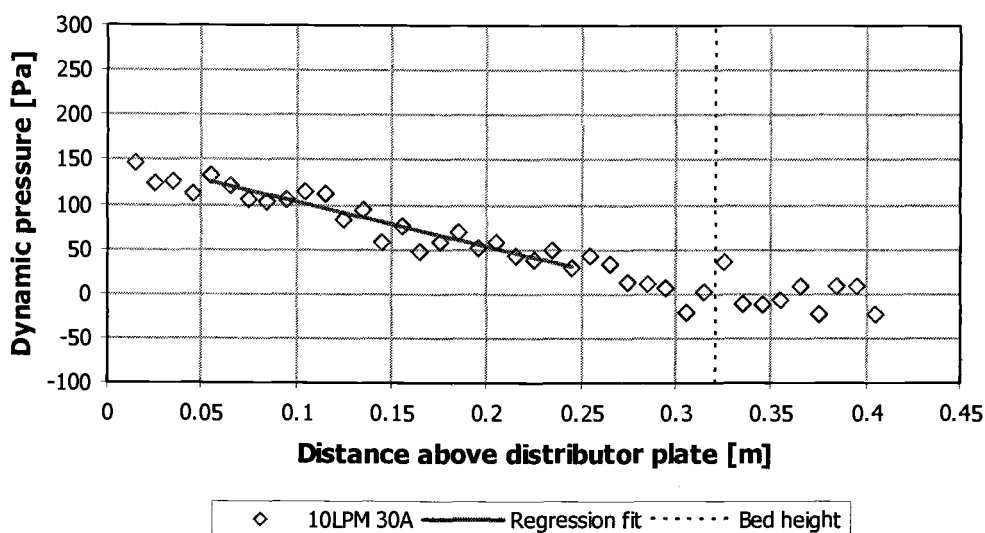


Figure D.47 Dynamic pressure data for $u_0 = 0.0370$ m/s and $B_0 = 7.67$ mT. The calculated voidage is $\varepsilon = 0.723$.

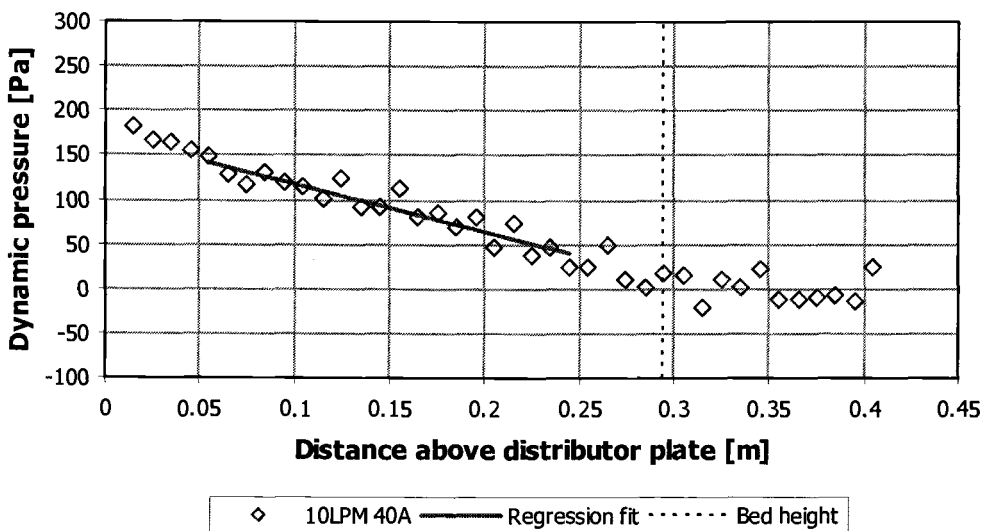


Figure D.48 Dynamic pressure data for $u_0 = 0.0370$ m/s and $B_0 = 10.2$ mT. The calculated voidage is $\varepsilon = 0.701$.

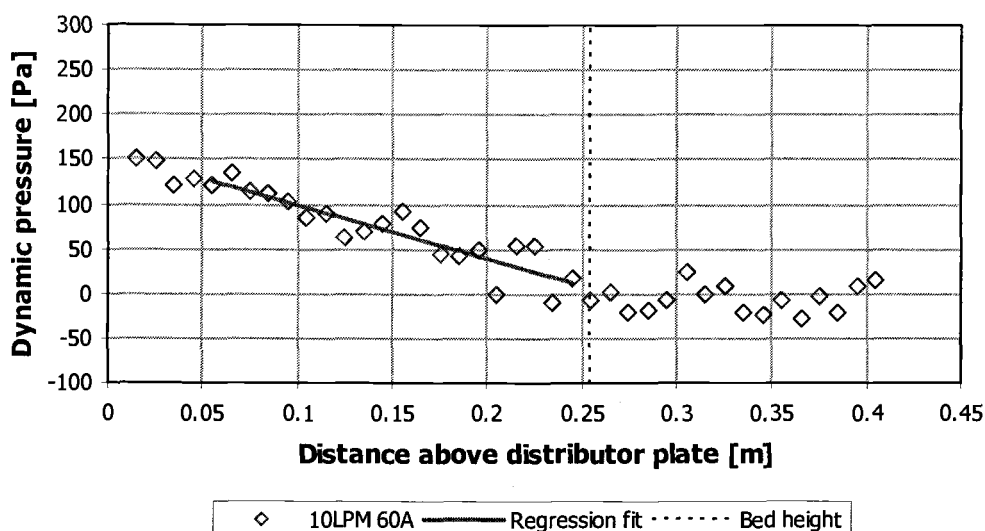


Figure D.49 Dynamic pressure data for $u_0 = 0.0370$ m/s and $B_0 = 15.3$ mT. The calculated voidage is $\varepsilon = 0.669$.

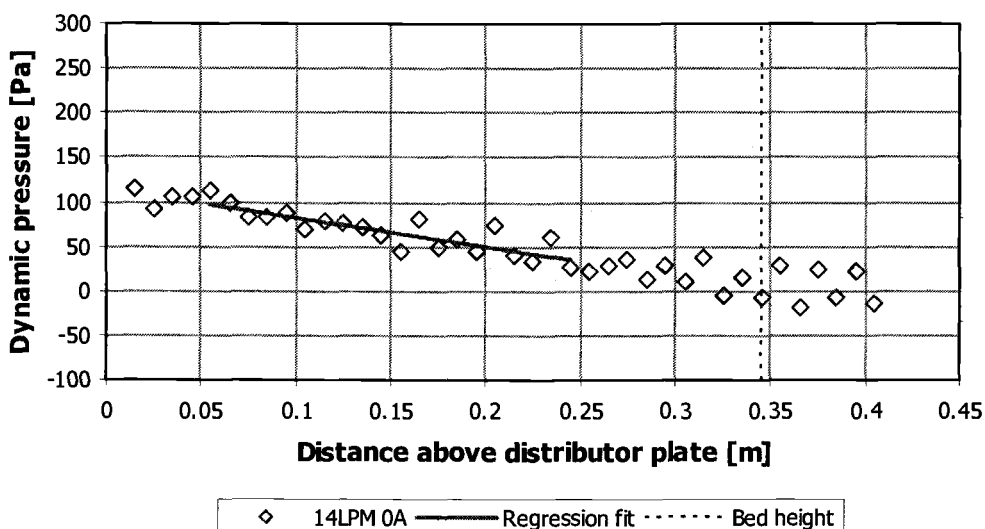


Figure D.50 Dynamic pressure data for $u_0 = 0.0482$ m/s and $B_0 = 0$. The calculated voidage is $\varepsilon = 0.824$.

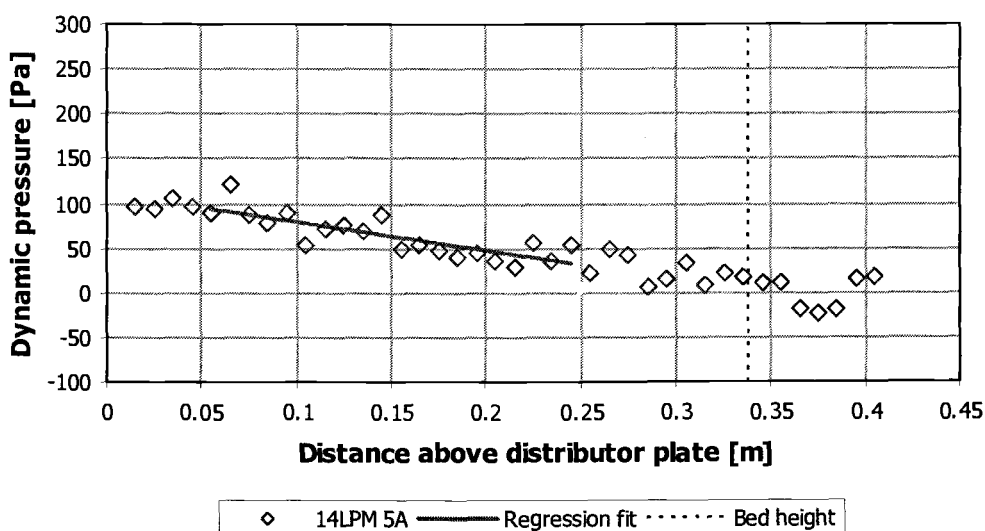


Figure D.51 Dynamic pressure data for $u_0 = 0.0482$ m/s and $B_0 = 1.28$ mT. The calculated voidage is $\varepsilon = 0.818$.

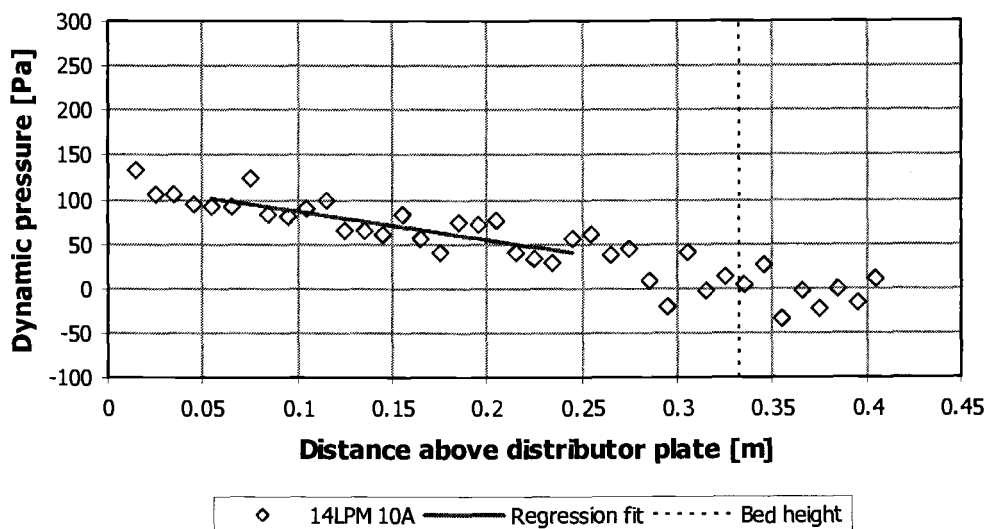


Figure D.52 Dynamic pressure data for $u_0 = 0.0482$ m/s and $B_0 = 2.56$ mT. The calculated voidage is $\varepsilon = 0.814$.

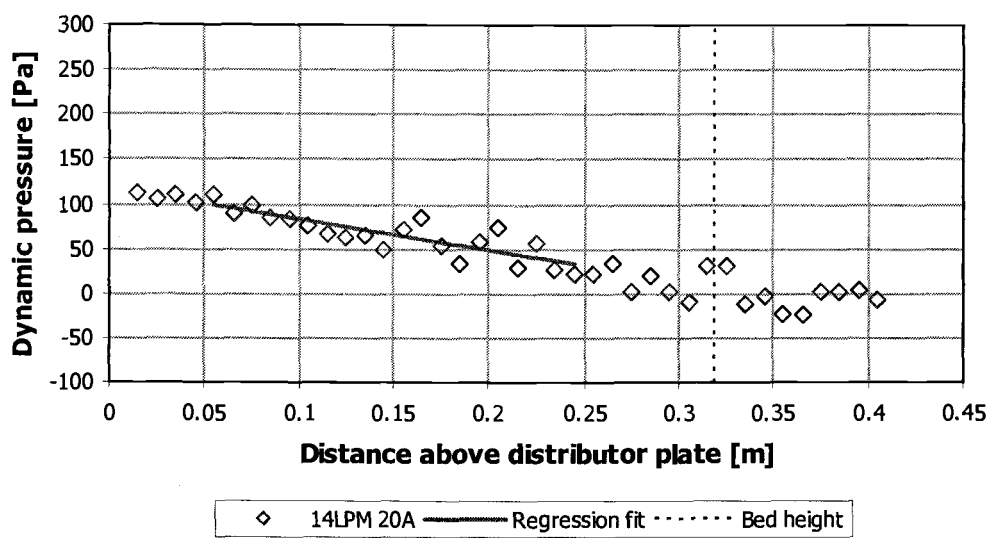


Figure D.53 Dynamic pressure data for $u_0 = 0.0482$ m/s and $B_0 = 5.11$ mT. The calculated voidage is $\varepsilon = 0.809$.

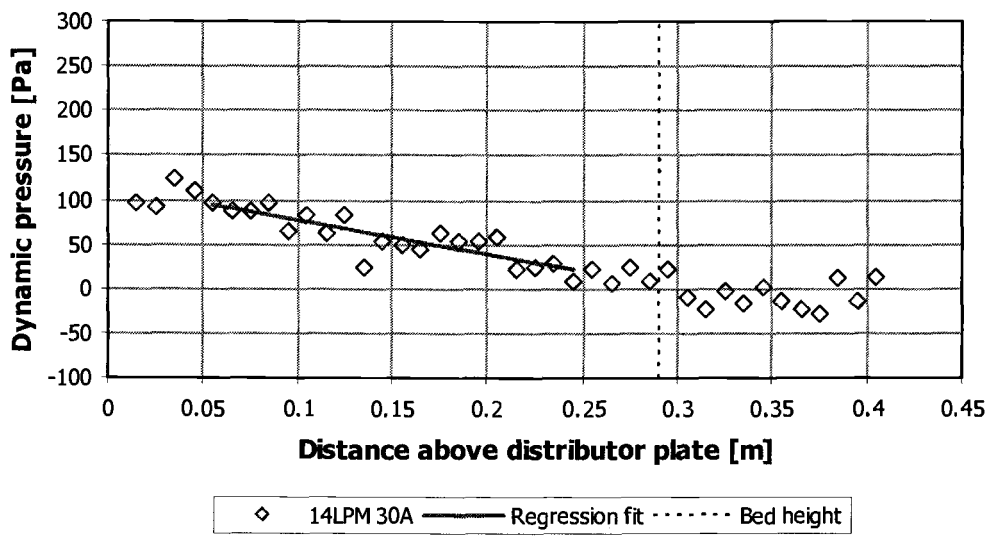


Figure D.54 Dynamic pressure data for $u_0 = 0.0482$ m/s and $B_0 = 7.67$ mT. The calculated voidage is $\varepsilon = 0.790$.

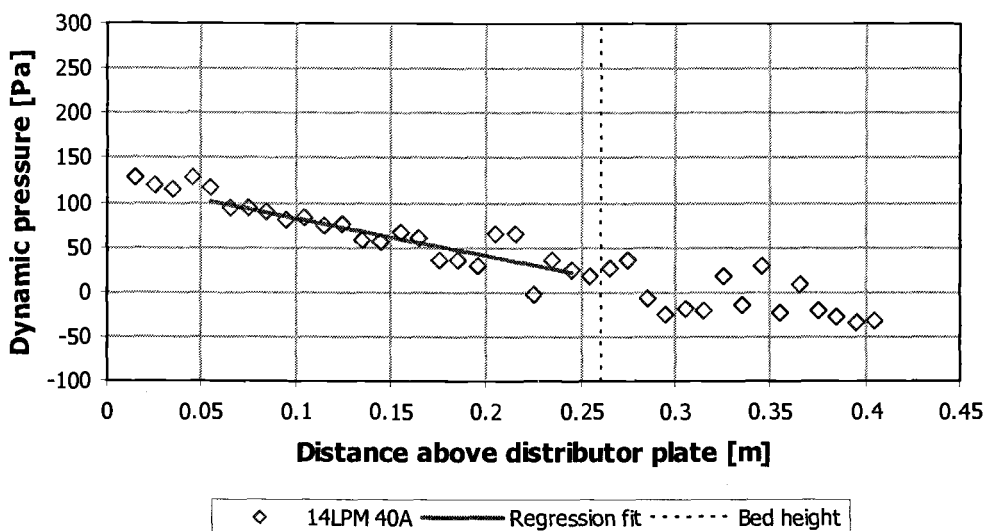


Figure D.55 Dynamic pressure data for $u_0 = 0.0482$ m/s and $B_0 = 10.2$ mT. The calculated voidage is $\varepsilon = 0.766$.

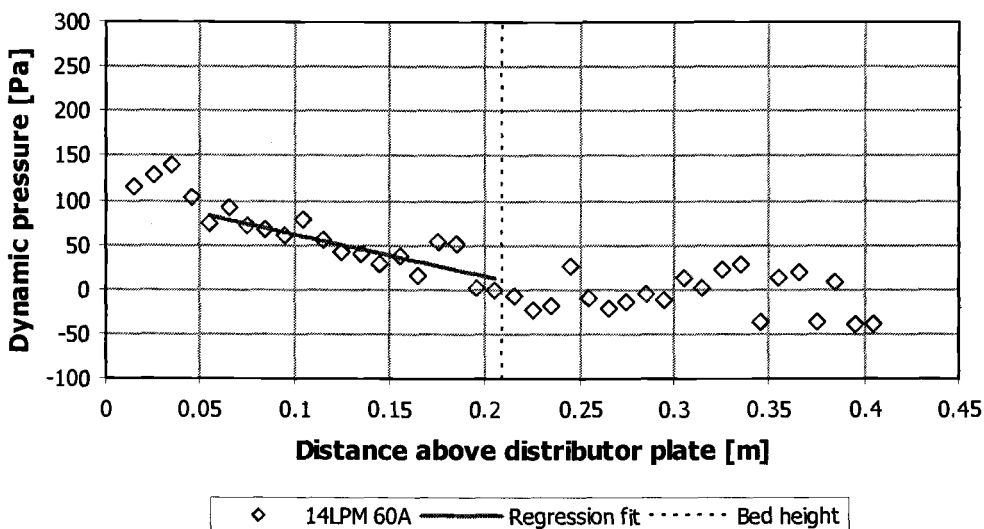


Figure D.56 Dynamic pressure data for $u_0 = 0.0482$ m/s and $B_0 = 15.3$ mT. The calculated voidage is $\varepsilon = 0.736$.

APPENDIX E

PARTICLE RADIAL DISTRIBUTION ANALYSIS

Picard: How can a geometric form disable a computer system?

Data: The shape is a paradox, sir. It cannot exist in real time or space.

— Star Trek The Next Generation,
“I Borg”

One possible tool for studying the degree of anisotropy in a fluidized bed is the radial distribution analysis. It describes how likely it is to find a neighboring particle at a given location around another particle. Since Discrete Particle Methods readily provide the location of all particles at any moment during the simulation, this technique can be applied without much difficulty.

From the simulation results, the region around any selected particle is divided into regions sectors of uniform Δr and $\Delta\theta$ ($0 \leq \phi < 2\pi$) based on a spherical coordinate system centered at the particle of interest, and with polar axis aligned with the magnetic field. For each neighboring particle within the given search distance, it is determined on which sector its center lies, and a counter is incremented for that sector (See Figure E.1)

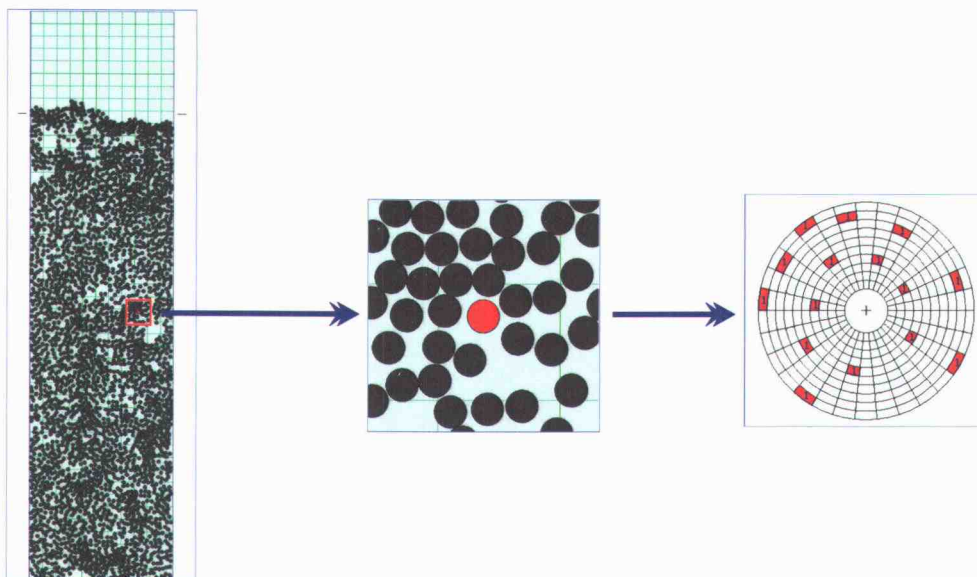


Figure E.1 Construction of a radial distribution map. The process is repeated for each particle in the frame (spatial average), for the same particle at different times (time average), or for all particles at all times (total average)

If the particles are randomly distributed, there is an equal probability for a neighbor to lie in any sector. The radial distribution map is therefore uniform. In the other extreme, if the particles form well defined structures, there will be a characteristic pattern (signature) in the radial map at particular distances. A mixture of such structures would show an intermediate signature.

Figure E.2 shows a preliminary analysis of the simulation data for the 8 LPM cases. Note the formation of a characteristic signature pattern at multiples of particle radius as the magnetic field is increased.

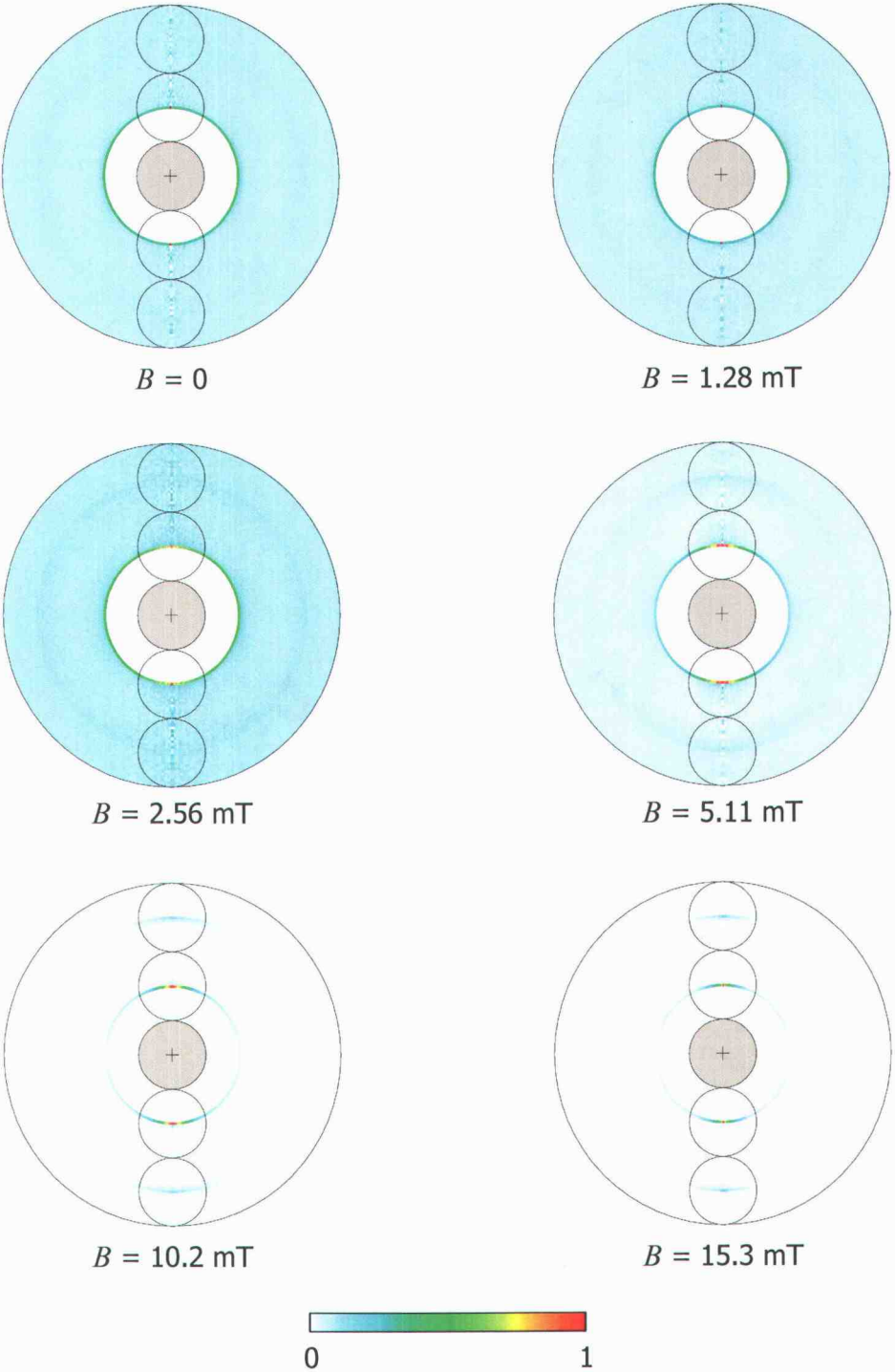


Figure E.2 Sample radial distribution maps from 8 LPM simulation cases.

This is a potentially useful way of describing (and possibly measuring) the degree of non-randomness in the distribution of particles within a fluidized bed. Future research in this area is recommended.

APPENDIX F

MATERIAL SAFETY DATA SHEETS

Riker: A cook is only as good as his ingredients.
— Star Trek The Next Generation,
"Time Squared"

F.1 Sodium alginate

Section 1 - Product and Company Information

Product Name ALGINIC ACID, SODIUM SALT
Product Number 180947
Brand ALDRICH
Company Sigma-Aldrich
Street Address 3050 Spruce Street
City, State, Zip, Country SAINT LOUIS MO 63103 US
Technical Phone: 314 771 5765
Emergency Phone: 414 273 3850 Ext. 5996
Fax: 800 325 5052

Section 2 - Composition/Information on Ingredient

Substance Name CAS # SARA 313
ALGINIC ACID, SODIUM SALT 9005-38-3 No
Synonyms Algin * Algin (polysaccharide) * Alginate KMF *
Algipon L-1168 * Amnucol * Antimigrant C 45 *
Cecalgine TBV * Cohasal-IH * Darid QH * Dariloid
QH * Duckalgin * Halltex * Kelco Gel LV *
Kelcosol * Kelgin * Kelgin F * Kelgin HV * Kelgin
LV * Kelgin XL * Kelgum * Kelset * Kelsize *
Keltex * Keltone * Algiline * Lamitex * Manucol *
Manucol DM * Manucol KMF * Manucol SS/LD2 *
Manugel F 331 * Manutex * Manutex F * Manutex RS
* Manutex RS 1 * Manutex RS-5 * Manutex SA/KP *
Manutex SH/LH * Meypralgin R/LV * Minus * Mosanon
* Nouralgine * OG 1 * Pectalgine * Proctin *
Protacell 8 * Protanal * Protatek * Snow algin H
* Snow algin L * Snow algin M * Sodium alginate *
Sodium polymannuronate * Stipine * Tagat * Tragaya
RTECS Number: AZ5820000

Section 3 - Hazards Identification

HMIS RATING
HEALTH: 0
FLAMMABILITY: 0
REACTIVITY: 0
NFPA RATING

HEALTH: 0

FLAMMABILITY: 0

REACTIVITY: 0

For additional information on toxicity, please refer to Section 11.

Section 4 - First Aid Measures

ORAL EXPOSURE

If swallowed, wash out mouth with water provided person is conscious. Call a physician.

INHALATION EXPOSURE

If inhaled, remove to fresh air. If breathing becomes difficult, call a physician.

DERMAL EXPOSURE

In case of contact, immediately wash skin with soap and copious amounts of water.

EYE EXPOSURE

In case of contact with eyes, flush with copious amounts of water for at least 15 minutes. Assure adequate flushing by separating the eyelids with fingers. Call a physician.

Section 5 - Fire Fighting Measures

FLASH POINT

N/A

AUTOIGNITION TEMP

N/A

FLAMMABILITY

N/A

EXTINGUISHING MEDIA

Suitable: Water spray. Carbon dioxide, dry chemical powder, or appropriate foam.

FIREFIGHTING

Protective Equipment: Wear self-contained breathing apparatus and protective clothing to prevent contact with skin and eyes.

Specific Hazard(s): Emits toxic fumes under fire conditions.

Section 6 - Accidental Release Measures

PROCEDURE(S) OF PERSONAL PRECAUTION(S)

Exercise appropriate precautions to minimize direct contact with skin or eyes and prevent inhalation of dust.

METHODS FOR CLEANING UP

Sweep up, place in a bag and hold for waste disposal. Avoid raising dust. Ventilate area and wash spill site after material pickup is complete.

Section 7 - Handling and Storage

HANDLING

User Exposure: Avoid inhalation. Avoid contact with eyes, skin, and clothing. Avoid prolonged or repeated exposure.

STORAGE

Suitable: Keep tightly closed.

Section 8 - Exposure Controls / PPE

ENGINEERING CONTROLS

Safety shower and eye bath. Mechanical exhaust required.

PERSONAL PROTECTIVE EQUIPMENT

Respiratory: Wear dust mask.
 Hand: Protective gloves.
 Eye: Chemical safety goggles.
 GENERAL HYGIENE MEASURES
 Wash thoroughly after handling.

Section 9 - Physical/Chemical Properties

Appearance Physical State: Solid
 Property Value At Temperature or Pressure
 Molecular Weight N/A
 pH 6 - 7.5
 BP/BP Range N/A
 MP/MP Range N/A
 Freezing Point N/A
 Vapor Pressure N/A
 Vapor Density N/A
 Saturated Vapor Conc. N/A
 SG/Density N/A
 Bulk Density N/A
 Odor Threshold N/A
 Volatile% N/A
 VOC Content N/A
 Water Content N/A
 Solvent Content N/A
 Evaporation Rate N/A
 Viscosity N/A
 Surface Tension N/A
 Partition Coefficient N/A
 Decomposition Temp. N/A
 Flash Point N/A
 Explosion Limits N/A
 Flammability N/A
 Autoignition Temp N/A
 Refractive Index N/A
 Optical Rotation N/A
 Miscellaneous Data N/A
 Solubility N/A
 N/A = not available

Section 10 - Stability and Reactivity

STABILITY

Stable: Stable.

Materials to Avoid: Strong oxidizing agents, Strong acids, Strong bases.

HAZARDOUS DECOMPOSITION PRODUCTS

Hazardous Decomposition Products: Carbon monoxide, Carbon dioxide.

HAZARDOUS POLYMERIZATION

Hazardous Polymerization: Will not occur

Section 11 - Toxicological Information

ROUTE OF EXPOSURE

Skin Contact: May cause skin irritation.

Skin Absorption: May be harmful if absorbed through the skin.

Eye Contact: May cause eye irritation.

Inhalation: May be harmful if inhaled. Material may be irritating to mucous membranes and upper respiratory tract.

Ingestion: May be harmful if swallowed.

SIGNS AND SYMPTOMS OF EXPOSURE

To the best of our knowledge, the chemical, physical, and toxicological properties have not been thoroughly investigated.

TOXICITY DATA

Oral

Rat

> 5000 mg/kg

LD50

Intravenous

Rat

1 GM/KG

LD50

Intraperitoneal

Cat

250 MG/KG

LD50

Intravenous

Rabbit

100 MG/KG

LD50

Section 12 - Ecological Information

No data available.

Section 13 - Disposal Considerations

APPROPRIATE METHOD OF DISPOSAL OF SUBSTANCE OR PREPARATION

Contact a licensed professional waste disposal service to dispose of this material. Dissolve or mix the material with a combustible solvent and burn in a chemical incinerator equipped with an afterburner and scrubber. Observe all federal, state, and local environmental regulations.

Section 14 - Transport Information

DOT

Proper Shipping Name: None

Non-Hazardous for Transport: This substance is considered to be non-hazardous for transport.

IATA

Non-Hazardous for Air Transport: Non-hazardous for air transport.

Section 15 - Regulatory Information

UNITED STATES REGULATORY INFORMATION

SARA LISTED: No

TSCA INVENTORY ITEM: Yes

CANADA REGULATORY INFORMATION

WHMIS Classification: This product has been classified in accordance with the hazard criteria of the CPR, and the MSDS contains all the information required by the CPR.

DSL: Yes

NDSL: No

Section 16 - Other Information

DISCLAIMER

For R&D use only. Not for drug, household or other uses.

WARRANTY

The above information is believed to be correct but does not purport to be all inclusive and shall be used only as a guide. The information in this document is based on the present state of our knowledge and is applicable to the product with regard to appropriate safety precautions. It does not represent any guarantee of the properties of the product. Sigma-Aldrich Inc., shall not be held liable for any damage resulting from handling or from contact with the above product. See reverse side of invoice or packing slip for additional terms and conditions of sale. Copyright 2005 Sigma-Aldrich Co. License granted to make unlimited paper copies for internal use only.

F.2 Calcium chloride

Section 1 - Product and Company Information

Product Name CALCIUM CHLORIDE DIHYDRATE USP
Product Number C8106
Brand SIGMA
Company Sigma-Aldrich
Street Address 3050 Spruce Street
City, State, Zip, Country SAINT LOUIS MO 63103 US
Technical Phone: 314 771 5765
Emergency Phone: 414 273 3850 Ext. 5996
Fax: 800 325 5052

Section 2 - Composition/Information on Ingredient

Substance Name CAS # SARA 313
CALCIUM CHLORIDE DIHYDRATE, USP 10035-04-8 No
Formula $\text{CaCl}_2 \cdot 2\text{H}_2\text{O}$
Synonyms Calcium dichloride dihydrate * CAL plus *
Replenisher (calcium)
RTECS Number: EV9810000

Section 3 - Hazards Identification

EMERGENCY OVERVIEW

Harmful.

Harmful if swallowed. Irritating to eyes, respiratory system and skin.

HMIS RATING

HEALTH: 1

FLAMMABILITY: 0

REACTIVITY: 0

NFPA RATING

HEALTH: 1

FLAMMABILITY: 0

REACTIVITY: 0

For additional information on toxicity, please refer to Section 11.

Section 4 - First Aid Measures**ORAL EXPOSURE**

If swallowed, wash out mouth with water provided person is conscious. Call a physician.

INHALATION EXPOSURE

If inhaled, remove to fresh air. If not breathing give artificial respiration. If breathing is difficult, give oxygen.

DERMAL EXPOSURE

In case of contact, immediately wash skin with soap and copious amounts of water.

EYE EXPOSURE

In case of contact, immediately flush eyes with copious amounts of water for at least 15 minutes.

Section 5 - Fire Fighting Measures**FLASH POINT**

N/A

AUTOIGNITION TEMP

N/A

FLAMMABILITY

N/A

EXTINGUISHING MEDIA

Suitable: Water spray. Carbon dioxide, dry chemical powder, or appropriate foam.

FIREFIGHTING

Protective Equipment: Wear self-contained breathing apparatus and protective clothing to prevent contact with skin and eyes.

Specific Hazard(s): Emits toxic fumes under fire conditions.

Section 6 - Accidental Release Measures**PROCEDURE(S) OF PERSONAL PRECAUTION(S)**

Wear respirator, chemical safety goggles, rubber boots, and heavy rubber gloves.

METHODS FOR CLEANING UP

Sweep up, place in a bag and hold for waste disposal. Avoid raising dust. Ventilate area and wash spill site after material pickup is complete.

Section 7 - Handling and Storage**HANDLING**

User Exposure: Do not breathe dust. Avoid contact with eyes, skin, and clothing. Avoid prolonged or repeated exposure.

STORAGE

Suitable: Keep tightly closed.

Section 8 - Exposure Controls / PPE**ENGINEERING CONTROLS**

Safety shower and eye bath. Mechanical exhaust required.

PERSONAL PROTECTIVE EQUIPMENT

Respiratory: Government approved respirator.

Hand: Compatible chemical-resistant gloves.

Eye: Chemical safety goggles.

GENERAL HYGIENE MEASURES

Wash thoroughly after handling.

Section 9 - Physical/Chemical Properties

Appearance Color: White

Form: Fine crystals

Property Value At Temperature or Pressure

Molecular Weight 147.02 AMU

pH 5 - 8

BP/BP Range N/A

MP/MP Range 176 °C

Freezing Point N/A

Vapor Pressure 0.01 mmHg 20 °C

Vapor Density N/A

Saturated Vapor Conc. N/A

SG/Density 1.85 g/cm³

Bulk Density N/A

Odor Threshold N/A

Volatile% N/A

VOC Content N/A

Water Content N/A

Solvent Content N/A

Evaporation Rate N/A

Viscosity N/A

Surface Tension N/A

Partition Coefficient N/A

Decomposition Temp. N/A

Flash Point N/A

Explosion Limits N/A

Flammability N/A

Autoignition Temp N/A

Refractive Index N/A

Optical Rotation N/A

Miscellaneous Data N/A

Solubility Solubility in Water: 1 M in H₂O, 20°C

complete, colorless

N/A = not available

Section 10 - Stability and Reactivity**STABILITY**

Stable: Stable.

Materials to Avoid: Strong oxidizing agents.

HAZARDOUS DECOMPOSITION PRODUCTS

Hazardous Decomposition Products: Hydrogen chloride gas, Calcium oxide.

HAZARDOUS POLYMERIZATION

Hazardous Polymerization: Will not occur

Section 11 - Toxicological Information**ROUTE OF EXPOSURE**

Skin Contact: Causes skin irritation.

Skin Absorption: May be harmful if absorbed through the skin.

Eye Contact: Causes eye irritation.

Inhalation: Material is irritating to mucous membranes and upper respiratory tract. May be harmful if inhaled.

Ingestion: Harmful if swallowed.

SIGNS AND SYMPTOMS OF EXPOSURE

To the best of our knowledge, the chemical, physical, and toxicological properties have not been thoroughly investigated.

TOXICITY DATA

Intraperitoneal

Mouse

20500 MG/KG

LD50

CHRONIC EXPOSURE - MUTAGEN

Species: Rat

Route: Oral

Dose: 500 UG/KG

Mutation test: Unscheduled DNA synthesis

Section 12 - Ecological Information

No data available.

Section 13 - Disposal Considerations

APPROPRIATE METHOD OF DISPOSAL OF SUBSTANCE OR PREPARATION

Contact a licensed professional waste disposal service to dispose of this material. Dissolve or mix the material with a combustible solvent and burn in a chemical incinerator equipped with an afterburner and scrubber. Observe all federal, state, and local environmental regulations.

Section 14 - Transport Information

DOT

Proper Shipping Name: None

Non-Hazardous for Transport: This substance is considered to be non-hazardous for transport.

IATA

Non-Hazardous for Air Transport: Non-hazardous for air transport.

Section 15 - Regulatory Information

EU ADDITIONAL CLASSIFICATION

Symbol of Danger: Xn

Indication of Danger: Harmful.

R: 22 36/37/38

Risk Statements: Harmful if swallowed. Irritating to eyes, respiratory system and skin.

S: 26 36

Safety Statements: In case of contact with eyes, rinse immediately with plenty of water and seek medical advice. Wear suitable protective clothing.

US CLASSIFICATION AND LABEL TEXT

Indication of Danger: Harmful.

Risk Statements: Harmful if swallowed. Irritating to eyes, respiratory system and skin.

Safety Statements: In case of contact with eyes, rinse immediately with plenty of water and seek medical advice. Wear suitable protective clothing.

UNITED STATES REGULATORY INFORMATION

SARA LISTED: No

CANADA REGULATORY INFORMATION

WHMIS Classification: This product has been classified in accordance with the hazard criteria of the CPR, and the MSDS contains all the information required by the CPR.

DSL: No

NDSL: No

Section 16 - Other Information**DISCLAIMER**

For R&D or manufacturing use. Not for prescription compound or other uses.

WARRANTY

The above information is believed to be correct but does not purport to be all inclusive and shall be used only as a guide. The information in this document is based on the present state of our knowledge and is applicable to the product with regard to appropriate safety precautions. It does not represent any guarantee of the properties of the product. Sigma-Aldrich Inc., shall not be held liable for any damage resulting from handling or from contact with the above product. See reverse side of invoice or packing slip for additional terms and conditions of sale. Copyright 2005 Sigma-Aldrich Co. License granted to make unlimited paper copies for internal use only.

F.3 Ferrite**Section 1 - Product and Company Information**

Product Name NICKEL ZINC IRON OXIDE,
NANOPOWDER, 99+%

Product Number 641669

Brand ALDRICH

Company Sigma-Aldrich

Street Address 3050 Spruce Street

City, State, Zip, Country SAINT LOUIS MO 63103 US

Technical Phone: 314 771 5765

Emergency Phone: 414 273 3850 Ext. 5996

Fax: 800 325 5052

Section 2 - Composition/Information on Ingredient

Substance Name CAS # SARA 313

NICKEL ZINC IRON OXIDE, 12645-50-0 No

NANOPOWDER, 99+%

Formula Fe₂NiO₃Zn

Synonyms zinc nickel iron oxide

RTECS Number: N07118000

Section 3 - Hazards Identification**EMERGENCY OVERVIEW**

Toxic.

Irritating to eyes, respiratory system and skin. May cause sensitization by skin contact. May cause cancer by inhalation. Calif. Prop. 65 carcinogen & reproductive hazard.

HMIS RATING

HEALTH: 3*

FLAMMABILITY: 0

REACTIVITY: 0

NFPA RATING

HEALTH: 3

FLAMMABILITY: 0

REACTIVITY: 0

*additional chronic hazards present.

For additional information on toxicity, please refer to Section 11.

Section 4 - First Aid Measures**ORAL EXPOSURE**

If swallowed, wash out mouth with water provided person is conscious. Call a physician.

INHALATION EXPOSURE

If inhaled, remove to fresh air. If breathing becomes difficult, call a physician.

DERMAL EXPOSURE

In case of contact, immediately wash skin with soap and copious amounts of water.

EYE EXPOSURE

In case of contact with eyes, flush with copious amounts of water for at least 15 minutes. Assure adequate flushing by separating the eyelids with fingers. Call a physician.

Section 5 - Fire Fighting Measures**FLASH POINT**

N/A

AUTOIGNITION TEMP

N/A

FLAMMABILITY

N/A

EXTINGUISHING MEDIA

Suitable: Water spray. Carbon dioxide, dry chemical powder, or appropriate foam.

FIREFIGHTING

Protective Equipment: Wear self-contained breathing apparatus and protective clothing to prevent contact with skin and eyes.

Specific Hazard(s): Emits toxic fumes under fire conditions.

Section 6 - Accidental Release Measures**PROCEDURE TO BE FOLLOWED IN CASE OF LEAK OR SPILL**

Evacuate area.

PROCEDURE(S) OF PERSONAL PRECAUTION(S)

Wear self-contained breathing apparatus, rubber boots, and heavy rubber gloves. Wear disposable coveralls and discard them after use.

METHODS FOR CLEANING UP

Sweep up, place in a bag and hold for waste disposal. Avoid raising dust. Ventilate area and wash spill site after material pickup is complete.

Section 7 - Handling and Storage**HANDLING**

User Exposure: Do not breathe dust. Do not get in eyes, on skin, on clothing. Avoid prolonged or repeated exposure.

STORAGE

Suitable: Keep tightly closed.

Section 8 - Exposure Controls / PPE**ENGINEERING CONTROLS**

Use only in a chemical fume hood. Safety shower and eye bath.

PERSONAL PROTECTIVE EQUIPMENT

Respiratory: Government approved respirator in nonventilated areas and/or for exposure above the TLV or PEL.

Hand: Compatible chemical-resistant gloves.

Eye: Chemical safety goggles.

GENERAL HYGIENE MEASURES

Wash contaminated clothing before reuse. Wash thoroughly after handling.

EXPOSURE LIMITS, RTECS

Country Source Type Value

USA ACGIH TWA 1 MG(NI)/M3

EXPOSURE LIMITS

Country Source Type Value

ACGIH TLV 1.5 mg/m3

Remarks: A5 ACGIH TLV 0.2 mg/m3

Remarks: A1 ACGIH TLV 0.1 mg/m3

Remarks: A4 (SOLUBLE COMPOUNDS)

USA PEL 1 mg/m3

Section 9 - Physical/Chemical Properties

Appearance Physical State: Solid

Color: Dark - brown Black

Form: Powder

Property Value At Temperature or Pressure

Molecular Weight 283.76 AMU

pH N/A

BP/BP Range N/A

MP/MP Range N/A

Freezing Point N/A

Vapor Pressure N/A

Vapor Density N/A

Saturated Vapor Conc. N/A

SG/Density 2.81 g/cm3 25 °C

Bulk Density N/A

Odor Threshold N/A

Volatile% N/A

VOC Content N/A

Water Content N/A

Solvent Content N/A

Evaporation Rate N/A

Viscosity N/A
 Surface Tension N/A
 Partition Coefficient N/A
 Decomposition Temp. N/A
 Flash Point N/A
 Explosion Limits N/A
 Flammability N/A
 Autoignition Temp N/A
 Refractive Index N/A
 Optical Rotation N/A
 Miscellaneous Data N/A
 Solubility Solubility in Water: Insoluble.
 N/A = not available

Section 10 - Stability and Reactivity

ALDRICH - 641669 www.sigma-aldrich.com Page 3

STABILITY

Stable: Stable.

Materials to Avoid: Strong oxidizing agents.

HAZARDOUS DECOMPOSITION PRODUCTS

Hazardous Decomposition Products: Metal oxides, Zinc oxide fumes may also form.

HAZARDOUS POLYMERIZATION

Hazardous Polymerization: Will not occur

Section 11 - Toxicological Information

ROUTE OF EXPOSURE

Skin Contact: May cause skin irritation.

Skin Absorption: May be harmful if absorbed through the skin.

Eye Contact: May cause eye irritation.

Inhalation: Material may be irritating to mucous membranes and upper respiratory tract. May be harmful if inhaled.

Ingestion: May be harmful if swallowed.

SENSITIZATION

Skin: May cause allergic skin reaction.

Sensitization: Possible sensitizer.

Skin: May cause skin sensitization

IRRITATION DATA

Skin

Remarks: Moderate irritation effect

CHRONIC EXPOSURE - CARCINOGEN

Result: May cause cancer by inhalation.

CHRONIC EXPOSURE - REPRODUCTIVE HAZARD

Species: Rat Rat

Dose: 560 UG/M3/24H 560 UG/M3/24H

Route of Application: Inhalation Inhalation

Exposure Time: (1-22D PREG) (1-22D PREG)

Result: Effects on Fertility: Pre-implantation mortality (e.g., reduction in number of implants per female; total number of implants per corpora lutea). Effects on Embryo or Fetus: Fetal death. Effects on Fertility: Pre-implantation mortality (e.g., reduction in number of implants per female; total number of implants per corpora lutea). Effects on Embryo or Fetus: Fetal death.

Species: Rat Rat

Dose: 750 UG/M3/24H 750 UG/M3/24H
 Route of Application: Inhalation Inhalation
 Exposure Time: (17W MALE) (17W MALE)
 Result: Paternal Effects: Spermatogenesis (including genetic material, sperm morphology, motility, and count). Paternal Effects: Spermatogenesis (including genetic material, sperm morphology, motility, and count).

Section 12 - Ecological Information

No data available.

Section 13 - Disposal Considerations

APPROPRIATE METHOD OF DISPOSAL OF SUBSTANCE OR PREPARATION
 Contact a licensed professional waste disposal service to dispose of this material. Observe all federal, state, and local environmental regulations.

Section 14 - Transport Information

DOT

Proper Shipping Name: None

Non-Hazardous for Transport: This substance is considered to be non-hazardous for transport.

IATA

Non-Hazardous for Air Transport: Non-hazardous for air transport.

Section 15 - Regulatory Information

EU ADDITIONAL CLASSIFICATION

Symbol of Danger: T

Indication of Danger: Toxic.

R: 36/37/38 43 49

Risk Statements: Irritating to eyes, respiratory system and skin. May cause sensitization by skin contact. May cause cancer by inhalation.

S: 26 36/37 45 53

Safety Statements: In case of contact with eyes, rinse immediately with plenty of water and seek medical advice. Wear suitable protective clothing and gloves. In case of accident or if you feel unwell, seek medical advice immediately (show the label where possible). Avoid exposure - obtain special instructions before use.

US CLASSIFICATION AND LABEL TEXT

Indication of Danger: Toxic.

Risk Statements: Irritating to eyes, respiratory system and skin. May cause sensitization by skin contact. May cause cancer by inhalation.

Safety Statements: In case of contact with eyes, rinse immediately with plenty of water and seek medical advice. Wear suitable protective clothing and gloves. In case of accident or if you feel unwell, seek medical advice immediately (show the label where possible). Avoid exposure - obtain special instructions before use.

US Statements: Calif. Prop. 65 carcinogen & reproductive hazard.

UNITED STATES REGULATORY INFORMATION

SARA LISTED: No

TSCA INVENTORY ITEM: Yes

CANADA REGULATORY INFORMATION

WHMIS Classification: This product has been classified in accordance with the hazard criteria of the CPR, and the MSDS contains all the information required by the CPR.

DSL: No

NDSL: Yes

Section 16 - Other Information

DISCLAIMER

For R&D use only. Not for drug, household or other uses.

WARRANTY

The above information is believed to be correct but does not purport to be all inclusive and shall be used only as a guide. The information in this document is based on the present state of our knowledge and is applicable to the product with regard to appropriate safety precautions. It does not represent any guarantee of the properties of the product. Sigma-Aldrich Inc., shall not be held liable for any damage resulting from handling or from contact with the above product. See reverse side of invoice or packing slip for additional terms and conditions of sale. Copyright 2005 Sigma-Aldrich Co. License granted to make unlimited paper copies for internal use only.

APPENDIX G

BIOGRAPHICAL NOTE

Picard: Someone once told me that time was a predator that stalks us all our lives. But I rather believe that time is a companion, that goes with us on the journey, reminds us to cherish every moment, because it'll never come again. What we leave behind is not as important as how we've lived it. After all, Number One, we are only mortal.

Riker: Speak for yourself, sir. I plan to live forever.

— Star Trek "Generations"

Carlos Francisco Cruz Fierro, fifth of five siblings, was born on September 8, 1976, in Mexico City. In 1983, his family moved to Durango, in Northern Mexico.

In 1994, he graduated from high school, earning the degree of Clinical Lab Technician, at Centro de Bachillerato Tecnológico, Industrial y de Servicios #130



Photo by Dr. Joaquin Pinto-Espinoza (2002)

(CBTis #130). Four years later, he obtained the Bachelor of Science degree in Chemical Engineering at Instituto Tecnológico de Durango (ITD). He also received the "José Gutiérrez Osornio" medal, the highest academic award given by ITD. From 1997 to 2000, he worked as half-time high school teacher of Physics and Computer Science, at Colegio Sor Juana Inés de la Cruz.

In 2000, he was granted a scholarship by the Mexican Government through Consejo Nacional de Ciencia y Tecnología (CONACyT) to pursue graduate studies abroad. In 2003, he obtained the Master in Science degree in Chemical Engineering, with a minor in Mathematics, at Oregon State University (OSU). At completion of his MS studies, he was awarded "Schulein Outstanding Graduate Student" by the Department of Chemical Engineering. In 2005 he earned the Doctor of Philosophy degree, with minors in Mathematics and Mechanical Engineering, also at OSU.

After five years living in Oregon, he returned to Durango to join the faculty of his Alma Mater, Instituto Tecnológico de Durango.